Practical Performance Criteria and Durability Prediction Modeling of Glass Fiber Reinforced Polymer (GFRP) Bars

by

Paulina Arczewska

A thesis
presented to the University of Waterloo
in fulfillment of the
thesis requirement for the degree of
Doctor of Philosophy
in
Civil Engineering

Waterloo, Ontario, Canada 2017

Examining Committee Members

The following served on the Examining Committee for this thesis. The decision of the Examining Committee is by majority vote.

External Examiner	MARK GREEN Professor
Supervisor(s)	MARIA ANNA POLAK Professor
Internal Member (s)	JEFFREY WEST Professor
	SCOTT WALBRIDGE Professor
Internal-external Member	ALEXANDER PENLIDIS Professor

Author’s Declaration

I hereby declare that I am the sole author of this thesis. This is a true copy of the thesis, including any required final revisions, as accepted by my examiners.

I understand that my thesis may be made electronically available to the public

Abstract

Glass fiber reinforced polymer (GFRP) bars are becoming a reasonable alternative to steel bars in reinforced concrete members as a method to address issues of corrosion and electromagnetic interference. This growing interest in GFRP reinforcement results in an increase in the types of products and their quantities in the market. GFRP bars are typically produced in an automated pultrusion process; however, when curved or bent bars are to be manufactured non-standardized production processes are adopted, which differ among manufacturers. This results in variability of the products, which raises concerns regarding quality and durability of the bars. Thus, to use GFRP bars more efficiently two fundamental technological barriers need to be resolved: material property and durability uncertainties.

Quality control (QC) and assurance (QA) testing is a proper way to check the properties of bars before using them in structures. In this thesis, an attempt was made to study the influence of GFRP bars geometrical and mechanical characteristics variability on standardized quality control tests (tensile, shear, flexure, and cure ratio tests). Bars from two different companies with two different diameters and three different surface finishes were included in this study. Based on obtained results it was postulated that variability of the currently available GFRP bars has an influence on testing procedures. As for e.g., surface finishing affects anchorage length for the tensile test, or cost of the shear test can directly depend on a number of bar sizes that need to be tested. Tests, investigated in this research program, were found to be impractical and inconvenient in a rutile use. Thus. adjustment of testing procedures is needed to improve QA and QC testing.

Subsequently, possible correlations between the bar properties were analyzed. Based on the research outcome the tensile-flexure correlation was found to be a great asset for quality control testing of GFRP bars. The study was performed with recognition of the composite bimodular properties in different states of stress (tension and compression) and the results were compared with standardized flexural strength determination protocols. A Weibull “Weakest Link Model” was utilized in the tensile-flexure strength correlation. Based on performed analysis it was found that correlation between tensile-flexure strength does exist and the flexure test potentially can be

used as a tensile strength prediction method for QA testing. The difference between the analytical value of the tensile strength, obtained by proposed methodology, and tensile strength measured directly from the test did not exceed five percent.

The second factor that partially impedes wider adaptation of GFRP bars is the absence of satisfactory life prediction models. Since GFRP bars are no longer used only as a longitudinal reinforcement, but also as stirrups in reinforced concrete structures, a model describing the deterioration of all properties is required. Thus, this research program is focused on the prediction capability of existing models to determine degradation of GFRP bar properties. An accelerated aging test (alkaline immersion) was introduced to study GFRP bars long-term performance. Specimens were kept in a highly alkaline solution (approximately 13 pH) under three temperatures: 50˚C, 60˚C, and 70˚C; for three different periods of time: 30, 90, and 150 days. Existing strength retention models were validated using the obtained data and durability of GFRP bar properties was investigated. Two from four introduced in this research program strength retention models were found to be proper estimations for the long-term behavior of GFRP bar properties. It was found that all properties of GFRP bars that directly depend on the bar cross-section area are characterized by a similar rate of degradation (tensile, shear strength). While the flexure strength degrades quicker. Also, smaller bar diameters are characterized by the higher speed of degradation than the bars with bigger diameters. In fact, degradation of GFRP bar properties depends on many factors, including the type of resin, fiber content or bar surface finishing. Thus, the durability of GFRP reinforcement is a complex problem that required further analysis. Discussion and comparison of results between different bar types are presented in this thesis.

Acknowledgements

I would like to place my deepest respects and gratitude to my supervisor Professor Maria Anna Polak for her valuable guidance, inspiration, and knowledge that she shared with me throughout this Ph.D. study.

Special thanks and respects to Professor Alexander Penlidis for his helpful suggestions and advices during completion of this thesis. Also, I would like to acknowledge Professor Jeffrey West, Professor Scott Walbridge, and Professor Mark Green for their time and valuable remarks as advisory committee members.

I would like to acknowledge the financial support from the Ministry of Transportation Ontario (MTO), Ontario Centre of Excellence (OCE), and Schoeck Canada Inc.

Manny thanks to all lab technicians: Richard Morrison, Douglas Hirst, and Rob Sluban that helped me with sample preparation, setting experiments and testing. I express my gratitude to Jessica Rossi, Victoria Tolton and Eleanor Clark for their help and kindness.

I would like to express my appreciation to Dr. Pouyan Sardashit and Dr. Dritan Topuzi for their support, help, and knowledge that they shared with me during my research.

I am particularly thankful for my colleagues Dr. Aikaterini Genikomsou, Dr. Georgios Balomenos, María José Rodríguez Roblero and Dr. Adam Wosatko who assisted me throughout versus stages of this research. Special thanks to Martin Krall, Joseph Stoner, and Shayan Sepiani.

Lastly, I would like to express my deepest thanks to my family who supported me during this important time in my life, encouraged me and gives me the confidence to reach my goals.

Dedication

"Family like branches on a tree, we all grow in different directions, yet our roots remain as one."

Anonymous

To my Family

Table of Contents

List of Figures

Chapter 1

Chapter 2

Chapter 3

Chapter 4

Chapter 5

Chapter 6

Chapter 7

List of Tables

Chapter 2

Chapter 3

Chapter 4

Chapter 5

Chapter 7

Chapter 1

INTRODUCTION

1.1 Overview

The decay of infrastructure is one of the significant challenges that the world is facing today. The cost of restoring and rehabilitating reinforced concrete (RC) structures is an important and growing issue. More than two-thirds of structures exposed to an aggressive environment like bridges, parking garages or marinas exhibit a significant concrete deterioration due to corrosion of embedded reinforcement (Zoghi 2013). The primary long-term degradation mechanism, in most of the cases, involves absorption, movement, and transport of dissolved harmful chemicals within the concrete, which leads to steel corrosion. Thus, a major component of infrastructure decay is the degradation of bridges and highways subjected to frequent contact with water, road salts and de-icing components (Fig. 1.1). To overcome the corrosion issue, new non-metallic reinforcement, fiber-reinforced polymer bars (FRP), have been introduced as a promising alternative to steel. FRP composites are common in many civil engineering applications in the form of bars or grids utilized as a concrete reinforcement for new constructions, profiles or whole structural elements in pedestrian bridges, or sheets used for repairs and rehabilitation. Composite reinforcement is one of the products that potentially can resolve structural decay issues for future generations.

Fig. 1.1 – Gardiner Expressway Toronto (2014)

Three main types of fiber reinforced bars (glass-GFRP, aramid-AFRP, and carbon-CFRP) are used nowadays as a concrete reinforcement. However, glass fiber reinforced polymer bars, due to a combination of relatively low cost (when compared to other composite materials) and good durability properties are more popular than its competitors. GFRP bars have already been utilized in several reinforced concrete structures; however, the variability of products that are currently available on the market, and inconsistency of their properties hinder industry's widespread adaptation of this new technology. To use GFRP bars more efficiently, standardized and easy to use material property determination procedures are needed.

The relative uncertainty about the lifetime performance of glass fiber reinforced polymer bars in their service environment also effectively limits material utilization. Thus, the widespread adaptation of GFRPs by the construction industry is partially impeded by the absence of satisfactory service life prediction models. The performance of GFRP bars under simulated field conditions has already been studied (Katsuki and Umoto 1995, Chen 2011, Beddow 2002, Purnel 2001) and several different long-term durability prediction models are available. However, since the GFRP bars are used not only as a tensile reinforcement in RC structures but also as shear stirrups and dowel bars for pavements, a model describing all typical properties of composite reinforcement with the same accuracy is required.

As a first step towards these goals, an attempt is made in this study to understand how the variability of geometrical and mechanical characteristics of currently available GFRP bars affects the results distained from standardized quality control tests. Subsequently, an investigation of the possible correlation between the bar properties is undertaken in this thesis. The second objective of this study is related to investigating existing deterioration models, their feasibility to describe different mechanical properties of composite reinforcement and to explaining possible discrepancies between deterioration of properties.

1.2 Objectives

This research program has been developed to study two fundamental technological barriers preventing GFRP bars widespread utilization, including an assessment of different possibilities to overcome these issues. The primary objectives were:

- investigation of GFRP bar tensile-flexure strength correlation, and

- evaluation of long-term GFRP bar properties.

Several secondary objectives, such as:

- performance assessment of quality control testing
- material dual moduli effect on flexural strength
- validation of long-term durability prediction models
- model development for flexure strength deterioration, and
- bar type, size, and surface finishing influence on the speed of degradation

were also established during the investigation processes.

1.3 Scope

Though many FRP composite materials are available on the market, only composite reinforcement used in the civil applications was considered in this study.

Among three major composite types (GFRP, AFRP, and CFRP) only glass fiber-reinforced polymer bars were used for this research.

The aim of this study is to evaluate and comment on existing quality control testing procedures and to identify another possible way to assess the tensile strength of GFRP bars.

The focus is not directed at developing a new GFRP service life prediction model, but the study is mainly intended to evaluate the feasibility of existing models to determine deterioration of GFRP bar properties.

1.4 Methodology

The overall objectives of this study were to identify the possible correlations between GFRP bar mechanical properties and to provide comprehensive information about bar long-term durability. The research project was divided into two sequential phases where the second phase was designed to utilize the findings obtained by the previous stage.

The purpose of phase 1 was to investigate the performance of each quality control test chosen for this research and to determine which correlation is the most beneficial for widespread adaptation of GFRP bars. An overview of the testing procedures, techniques, and methods, together with the

recorded outcomes were used to formulate a hypothesis that tensile-flexural strength correlation exists and can be a great asset to composite reinforcement quality control. At this stage, extensive attention was paid to the flexure test itself. Since the bending mechanism involves two different states of stress at the same time (tension and compression), a better understanding of this process was required. The influence of bimodularity of GFRP bars on the modulus of rupture was investigated. Subsequently, a Weibull "Weakest Link Model" and GFRP bar dual moduli theory were adapted into a tensile-flexure strength correlation. A methodology scheme is shown in Fig. 1.2.

Experimental results from phase 1 (short-term testing results) were utilized in phase 2 as a starting point for long-term durability prediction of GFRP reinforcement. Since the performance of RC structures depends on its field conditions, and monitoring of the structure in real life can take up to 100 years, it is not practical to wait such a long period to assess the service lifetime and performance of new construction materials. Therefore, an accelerated aging test was employed (alkaline immersion test) to study GFRP bar long-term performance. Existing strength retention models were validated using the obtained data. The durability of GFRP reinforcement was investigated using an adequate model that could describe deterioration of all bar properties. A schematic of phase 2 is shown in Fig. 1.3.

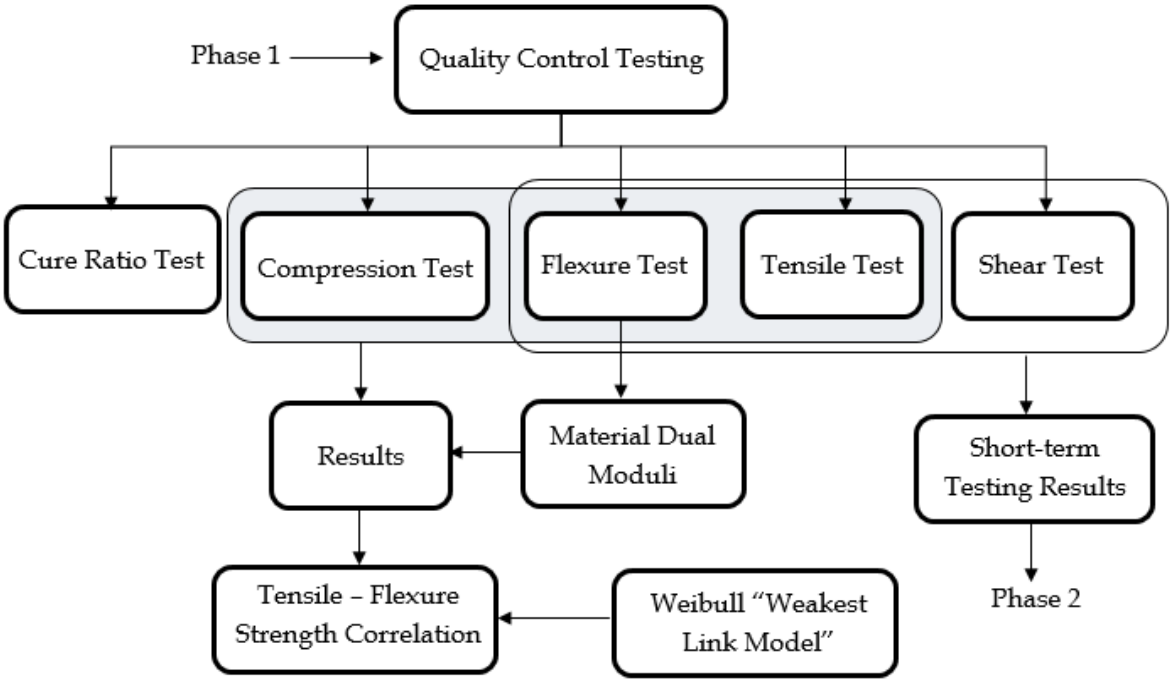

Fig. 1.2 – Phase 1 – methodology scheme

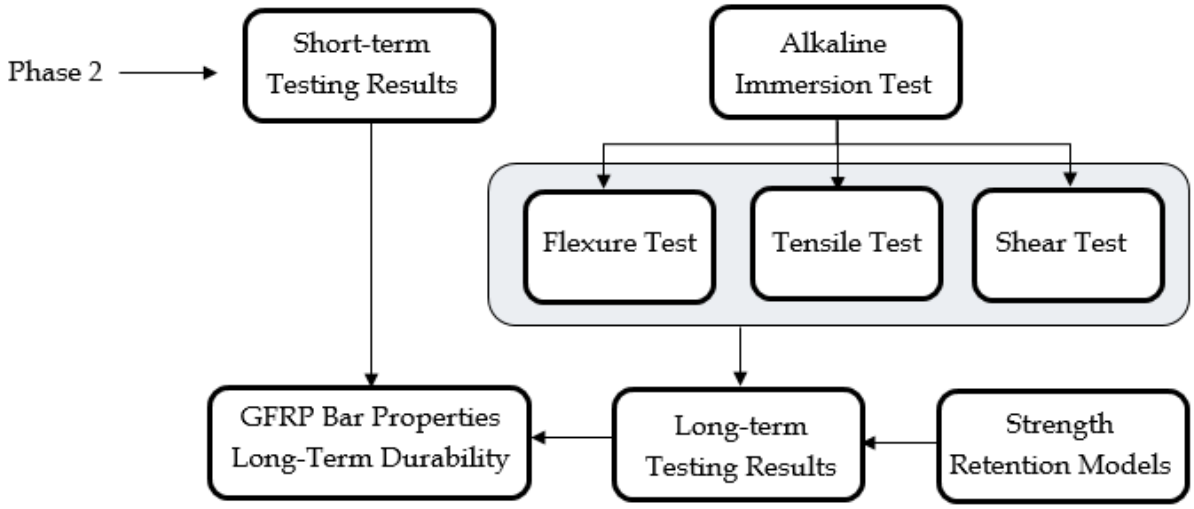

Fig. 1.3 – Phase 2 – methodology scheme

1.5 Thesis organization

This thesis consists of eight chapters and ten appendices. Chapter 1 presents an overview, scope, and the methodology that has been used to reach the outlined goals. Chapter 2 provides a detailed description of background information about FRP material and GFRP bars. It presents a literature review on quality control testing and bars durability. Chapter 3 describes material that was tested and gives an extensive explanation of the testing procedures used in this study. Chapter 4 contains an evaluation of the chosen quality control tests (tensile, shear, flexure, compression, and cure ratio tests) and presents the results obtained. Chapter 5 describes a tensile-flexure strength correlation procedure. Chapter 6 discusses the long-term strength prediction background information (Arrhenius relationship, diffusion models, and existing strength prediction models). Chapter 7 cites the findings from the alkaline immersion test, presents the validation of existing strength prediction models and provides the results for GFRP bar property deterioration. Chapter 8 contains the key findings and presents final comments and recommendations for future work. Appendices 1, 2 and 3 provide results from tensile, shear and flexural tests, respectively. Appendix 4 describes the procedure for effective volume determination for a rectangular cross-section rod. Appendix 5 provides results for Weibull modulus. Appendices 6, 7 and 8 contain results from the alkaline immersion test for tensile, shear and flexural strength degradation, respectively. Appendix 9 presents a procedure for prediction of shear and flexure long-term strength retention. Finally, appendix 10 provides a detailed description of model development for flexure strength degradation.

Chapter 2

BACKGROUND

2.1 Composite materials

A composite material (Latin: compositus-complex) can be described as a material that consists of at least two different components. These are combined with the intention to suppress the undesirable properties of bonded elements and form a composite with desirable parameters. In this composition, both materials preserve their unique mechanical and chemical identities. However, by the bond between components, a composite produces a combination of properties that cannot be achieved by any of combined elements acting alone. Composite anastomosis occurs at the macroscopic level. This means that any steel alloys, which are a composition of many ingredients on a microscopic scale, cannot be considered as a composite (German 2001).

The first known composite was used in the 13th century B.C. by Israelites who mixed mud with straws and used it in brick manufacturing. Development of modern composite materials was directly connected with inorganic fibers (glass, aramid, carbon, etc.), which gained wide interest due to their superior property combination. New fiber reinforced composites offer excellent mechanical and strength properties with light weight.

Composites consist of two phases. Matrix is the first phase, and it surrounds the second distributed phase called reinforcement. Composite characteristics are directly related to properties of these two phases and the volume percentage of each phase in a composite. Methods and direction of placing the reinforcement in a matrix, as well as the reinforcement shape, also have a significant influence on future composite properties. For primary classification of composites, researchers decided to use the reinforcement form, which leads to division into composites reinforced with particles, and fibers (or dispersion composites).

This research addresses only fiber reinforced composites, and the description herein is related only to this type.

2.1.1 Fiber reinforced composites

FRP composites contain reinforcing fibers embedded in a matrix. Major load-carrying elements are fibers while the surrounding matrix protects the fibers against damaging influences of environment, acts as a load transfer medium and keeps fibers in the desired configuration (Fig.2.1a). General classification of fibers includes three major groups: natural, regenerated and synthetic. First two types are rarely used on the market, and commercial expansion of composites is closely connected with the development of artificial fibers.

Fibers used for engineering purposes are various types of glass, aramid, and carbon fibers usually placed in a polymer resin (Glass FiberReinforced Polymer (GFRP), Aramid Fiber Reinforced Polymer (AFRP) or Carbon Fiber Reinforced Polymer (CFRP)). All fibers can be placed into a matrix either in continues bundles or short pieces, forming at the same time composites with different properties. Each of those materials presents different mechanical and physical properties, which should be taken into consideration during composite classification for a particular purpose. Utilization of other types of matrix such as steel or ceramic as well as other fibers such as boron, silicon carbide, and aluminum oxide is limited. Fiber reinforced composites are used in many fields for example for solving durability issues by using FRP internal reinforcement, or sheets used in rehabilitation or fully composite structure components (Fig. 2.1).

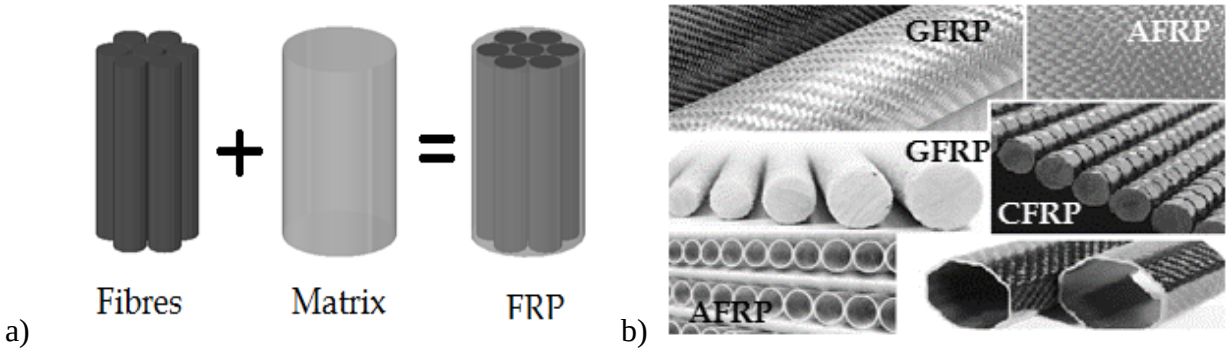

a) b)

Fig. 2.1 – a) FRP composite; b) different types of FRPs

2.2 Non-metallic reinforcement

Fiber Reinforced Polymer (FRP) bars as reinforcement for concrete have become available on the Canadian market over last the 15 years. Better than steel, FRPs durability properties contribute to bars utilization, but this is not their only advantage. FRP reinforcement exhibits electromagnetic

neutrality and significantly smaller (1/7 or 1/5 of steel reinforcement of equal diameter) weight, comparing to steel, decreases transportation related costs and helps with bar handling. Non-metallic bars are also characterized by outstanding tensile strength capacity in comparison to conventional and prestressed steel (Fig. 2.2). There are three different types of FRP bars commercially available on the market: GFRP, CFRP, and AFRP. However, recently Basalt Fiber Reinforced Polymer (BFRP) bars have been produced as a fourth alternative.

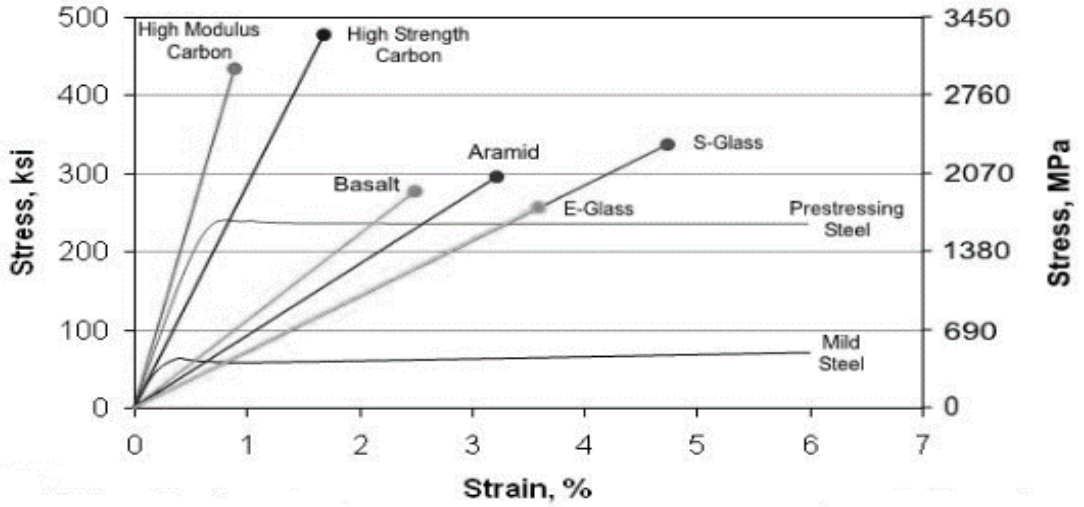

Fig. 2.2 – Comparison of FRP materials to steel (Prince Engineering/www.build-on-price.com)

2.2.1 GFRP bars

GFRP reinforcing bars are used in more applications than other composite materials, which is due to several different factors. Like all FRPs, GFRP bars offer a strength that is either comparable or greater than traditional metallic reinforcement used in civil engineering. Due to low density, strength-weight ratio, and modulus-weight ratio, GFRP bars are a practical solution for many structures such as bridges and parking garages. They are characterized by electromagnetic neutrality and high durability properties. However, in comparison with other FRP products, GFRP reinforcement has the lowest modulus of elasticity, and they are much more susceptible to the aggressive influence of alkaline environment. However, due to relatively low cost of production' GFRP bars are used much more often than other non-metallic reinforcement. GFRP bars are less expensive to manufacture when compared with corrosion-resistant steel alternatives such as stainless steel (Wenzlick 2007). Even if GFRP bars do not possess the most optimal properties, their performance is still acceptable. GFRPs reinforcing bars demonstrate good properties (strength and high durability) combined with a low price.

Glass fibers

Fibers of glass are produced by extruding molten glass through platinum alloy bushing, which can contain up to several thousand individual orifices. Glass molten mass is made by fusing silica with minerals, which contain the oxides needed to form a given composition. To avoid crystallization, the molten mass is rapidly cooled and subsequently formed into glass fibers in a process known as fiberization (Loewenstein 1993). The strength of glass filaments directly depends on any defects and flaws, commonly appearing at the surface of the fiber, what is primarily caused by abrasion. To prevent this process glass fibers are coated with binders (e.g., starch-oil), which can be easily removed (e.g., by heating) at the end of production.

Within glass categories, there are several types (Table 2.1). However, only a few are suitable for GFRP reinforcing manufacturing. Glass fibers can be divided into two groups: low-cost overall-purpose (E-glass) fibers and special purpose fibers (S-glass), whereas almost 90% of the market is dominated by E-glass. Each type of glass fiber has unique characteristics suitable for a particular application (Table 2.2). The primary component of the glass fibers is silica (SiO_2), which gives the glass fibers their strength. On the other hand, silica can be the biggest weakness as it is a highly reactive compound. E-glass corrodes quickly in acidic as well as alkaline environments.

Table 2.1 – Types of Glass fibers (Ehrenstein 2007)

Glass Designation	Type
E-Glass	Standard conventional glass type
S-Glass	High strength glass
C-Glass	Chemical resistant glass
ECR-Glass	Chemically resistant conventional glass
AR-Glass	Alkali resistant glass

Table 2.2 – Chemical composition of various glass types (Ehrenstein 2007)

	E-Glass	S-Glass	C-Glass	ECR-Glass	AR-Glass
Component %					
SiO_2	54	60	60-65	54-62	62
Al_2O_3	14-15	25	2-6	12-13	-
CaO	20-24	14	14	21	5-9
MgO	-	3	1-3	4.5	1-4
B_2O_3	6-9	<1	2-7	<0.1	<0.5
K_2O	<1	<1	8	0.6	-
Na_2O	-	-	-	-	
ZrO_2	-	-	-	-	17

Table 2.3 – Properties of various glass types (Ehrenstein 2007)

Properties					
Density (g/cm^3)	2.6	2.53	2.52	2.72	2.68
Tensile Strength (MPa)	3400	4400	2400	3440	3000
Modulus of Elasticity (MPa)	73000	86000	70000	7300	7300
Ultimate Strain (%)	<4.8	<4.6	<4.8	<4.8	<4.4
Thermal Coefficient (10^{-6}/ºC)	5.0	4.0	6.3	5.9	6.5
Softening Temperature (ºC)	850	980	750	880	770

Matrix

The matrix in composite materials fulfills four essential functions; it distributes the load between fibers, keeps fibers in place, protects fibers against the adverse environment and mechanical damaging (e.g., by abrasion). The matrix plays a significant role in the tensile load-carrying capacity of the composite material by uniformly distributing the load between the fibers. The matrix also has an influence on other properties such as compression (directly through the matrix compressive strength, and indirectly by preventing fiber buckling) and both interlaminar and in-plane shear.

Table 2. shows the list of polymeric matrix materials that have been used either commercially or in research. The attraction of polymers as a matrix can be easily explained by their low weight, with a density of little more than water. It can be used either in solution or molten, to impregnate the fibers at pressures and temperatures much lower than those which would be necessary for other materials.

Table 2.4 – Matrix materials (Mallick 2007)

Polymeric	**Thermoset polymers**	Polyesters, vinyl esters: commonly used in automotive, marine, chemical, and electrical applications Phenolics: used in bulk molding compounds Polyimides, polybenzimidazoles (PBI), polyphenyl quinoxaline (PPQ): for high-temperature aerospace applications (temperature range: 2508C–4008C) Cyanate ester
	Thermoplastic polymers	Nylons (such as nylon 6, nylon 6,6), thermoplastic polyesters (such as PET, PBT), polycarbonate (PC), polyacetals: used with discontinuous fibers in injection-molded articles Polyamide-imide (PAI), polyether ether ketone (PEEK), polysulfone (PSUL), polyphenylene sulphide (PPS), polyetherimide (PEI): suitable for moderately high-temperature applications with continuous fibers

Polymers consist of long chain molecules containing one or more repeating units of atoms, joined by strong covalent bonds. A polymeric material (also called plastic) is a collection of many polymer molecules of a similar chemical structure (but not of equal length). Polymers used as matrix materials can be divided into two groups, properties of which depend on their molecular structure. These are thermosetting and thermoplastic resins.

Thermoplastic polymers, which are more popular than other alternatives, are characterized by weak secondary bonds or intermolecular forces (van der Waals bonds and hydrogen bonds) holding in place individual molecules, which are not chemically connected (Fig. 2.3a). During heat application, those secondary bonds in a solid thermoplastic polymer can be broken, and the molecules can be moved relative to each other or flow to a new configuration if pressure is applied to them. During material cooling, the particles can be frozen in their new configuration and the secondary bonds are restored, forming a new solid shape. Thus, a thermoplastic polymer can be heat-softened, melted, and reshaped (or post-formed) as many times as desired. Due to high viscosity at the processing temperature, thermoplastic resins are challenging to use in composite manufacturing. However, the ability to thermal softening makes composite easy to repair or reform whenever it is needed. Typical properties of thermoplastic resins are shown in Table 2..

Table 2.5 – Thermoplastic matrix properties (Ceb-Fip bulletin 40 2007)

Property	Matrix		
	PEEK	PPS	PSUL
Density (kg/m^3)	1320	1360	1240
Tensile strength (MPa)	100	82.7	70.3
Longitudinal modulus (GPa)	3.24	3.3	2.48
Tensile elongation (%)	50	5	75
Poisson's ratio	0.4	0.37	0.37
Thermal expansion coefficient (10^{-6}/ºC)	47	49	56

Cross-links chemically join molecules in a thermoset polymer, forming a rigid, three-dimensional network structure (Fig. 2.3b). Once these cross-links are formed during the polymerization reaction (also called the curing reaction), the thermoset polymer cannot be melted by the application of heat. However, if the number of crosslinks is low, it may still be possible to soften the polymer at elevated temperatures. Thermoset resins have a relatively low initial viscosity, which allows for incorporation of high fiber volume into a composite. They are easy to produce and low in cost. Typical properties of thermosetting resins are shown in Table 2..

Table 2.6 – Thermoset matrix properties (Ceb-Fip bulletin 40 2007)

Property	Matrix		
	Polyester	Epoxy	Vinyl ester
Density (kg/m^3)	1200 – 1400	1200 – 1400	1150 – 1350
Tensile strength (MPa)	34.5 – 104	55 – 130	73 – 81
Longitudinal modulus (GPa)	2.1 – 3.45	2.75 – 4.1	3.0 – 3.5
Poisson's ratio	0.35 – 0.39	0.38 – 0.4	0.36 – 0.39
Thermal expansion coefficient (10^{-6}/ºC)	55 – 100	45 – 65	50 – 75
Moisture content (%)	0.15 – 0.6	0.08 – 0.15	0.14 – 0.3

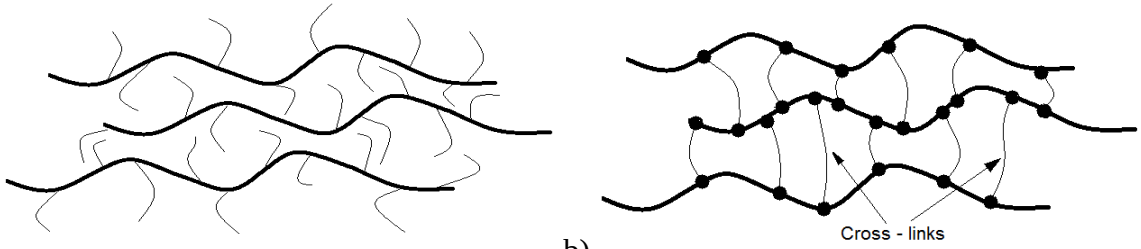

a) b)

Fig. 2.3 – Schematic representation of a) thermoplastic b) thermoset polymer (Mallick 2007)

2.2.2 GFRP bars manufacturing process

Straight bars

Pultrusion is a typical process used for manufacturing of constant cross-sectional profiles including GFRP reinforcing bars (Fig. 2.4 and Fig. 2.5). Low cost and full automatization of production attract manufacturers. Pultrusion of GFRP bars is based on a forming process, in which the glass fibers are passed through a resin bath where they are coated and pulled through a heated die. As the resin-impregnated fibers pass through the die, the polymer matrix hardens into the shape of the die, thus producing a structural component. Continuity of this process gives a great advantage for the production of various length production, which can be limited only by the transportation conditions.

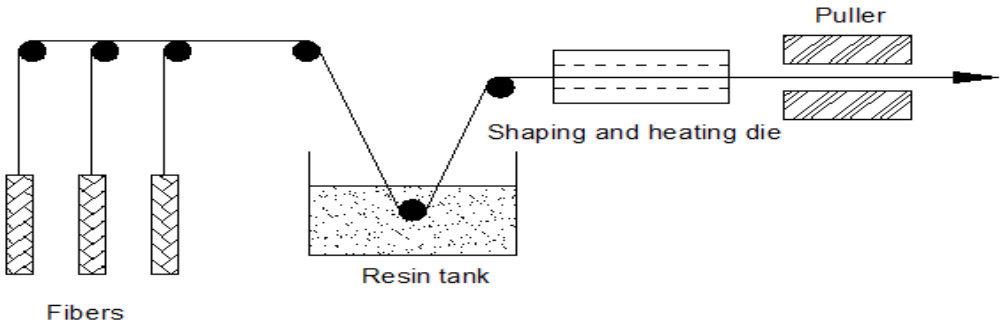

Fig. 2.4 – Schematic of GFRP manufacture process

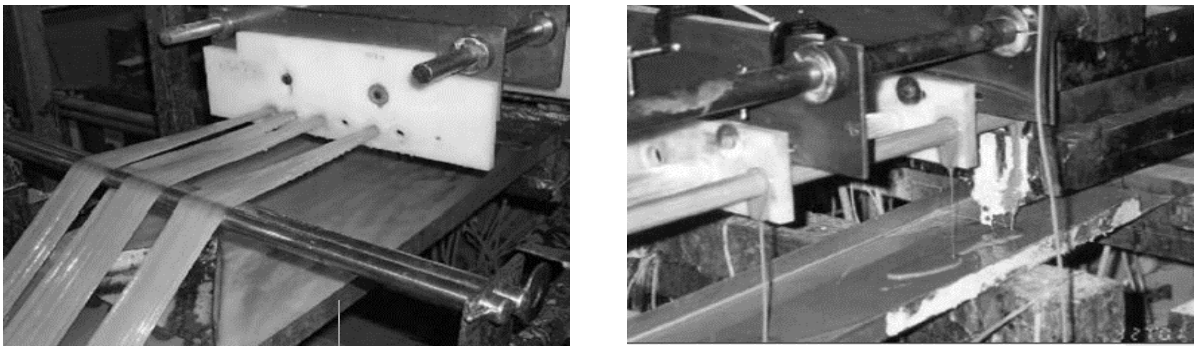

Fig. 2.5 – Pultrusion process (Benmokrane 2014)

Bent bars

In structural applications, curved bars are often used as shear reinforcement in the shape of stirrups or as bent hooks to reduce the development lengths of bars. Due to some of the GFRP bars material properties (thermosetting resin), bending a straight, already cured, bar is impossible. Thus, the bending process must be completed before curing. According to Maruyana (1993), there are two different types of bending processes. In the first method, the pre-pregs (resin-impregnated continuous fibers) are bent around metal bars of the required radius and heated for curing. During this process, the configuration of fibers at the bend becomes flattened, and consequently, the strength is reduced. The second method is based on bending FRP bars around semi-circular grooved metal molds with a radius equal to the bar diameter. This approach allows the cross section to remain circular and there is no flattening of the fibers, but due to compression of an internal portion of the bar at the curved section, the inner fibers are kinking. By containing the fibers around the bend, the cross-section is not deformed as the curing process is completed.

A different approach of rectangular cross-sectional stirrups was introduced by Duranovic et al. (1997). The stirrups are made by winding continuous glass fibers around a wooden mold producing a hollow rectangular section having a wall thickness of 4 mm. After removal of the wooden mold, the GFRP hollow section is cut into the desired stirrup width (10 mm). The cutting process causes discontinuity of several fibers and a consequent reduction of the active area of the stirrup. The loss of effective area is related to the angle at which the fibers are wound during the manufacturing process.

One of the newest production methods of bent bars has been described by Weber and Witt (2011). Plastic tubes filled with fibers and resin are bent to the desirable shape and then cured at high

temperature. As a result, due to compression stresses at the bent portion of the bar, the interior fibers are kinking. Due to intense competition between companies, information about the new manufacturing process of GFRP curved bars is not willingly shared, and it is hard to find in the available literature.

2.2.3 GFRP in Civil Engineering

Worldwide interest in GFRP as construction materials is directly connected with polymer resin development in the 1960s. Those resins, which can be cured at ambient temperatures, transformed GFRP manufacturing process into easier and more economical by using an open mold method. During the 1970s and early 1980s, GFRP composites appeared on construction sites as load bearing or semi-load bearing units between the structure's beams and columns. The structures that incorporated GFRP include Morpeth School in London, Mondial House on the north side of Thames at Blackfries (London) and American Express Building (Brighton). Since then, GFRP composites have started a new era in structural engineering, being formed in many different shapes and used in various fields.

Glass composites have a potential to replace steel reinforcement in environmentally exposed structures eliminating or reducing the durability issues. Fully composite structures or structures where glass fiber polymers constitute the majority of elements include small-scale bridges (Fig. 2.6 a), pedestrian platforms or parking garages stairwells. FRP materials are also successfully used in rehabilitation and strengthening of already existing structures in the form of sheets or plates (Fig. 2.6 b). GFRP internal reinforcing bars can be used to eliminate issues with structured aging and reinforced concrete deterioration (Fig. 2.6 c).

Significant resistance to corrosion makes composite reinforcing bars an attractive substitution for steel reinforcement, allowing for lower maintenance and repairing cost as well as a longer lifetime of structures. Moreover, the light weight of GFRP reinforcement potentially can have a great influence on dead load reduction. Those factors have a significant impact on successful utilization of GFRP bars in many bridges, marinas, parking garages or waterfront structures. Despite many advantages of GFRP reinforcing bars, simple substitution of steel with this material is not possible, due to mechanical property differences.

Fig. 2.6 – FRP applications – a) all GFRP composite bridge b) FRP strengthening sheets GFRP internal reinforcing bars (Zoghi 2013)

2.3. GFRP durability

Increased interest in GFRP materials has brought up concerns regarding their durability and long term properties. The durability of the material is defined as an ability to retain its original properties with time under load. In the case of reinforced concrete, durability means the capacity to resist cracking, chemical degradation (both concrete and reinforcement), wearing or aging. Per Benmokrane et al. (1998), the principal challenge for utilization of GFRPs in civil engineering applications is composite reinforcement capacity to maintain their structural performance in severe and constantly changing environmental conditions. During the last couple of years, a significant amount of research has been conducted regarding the investigation of different environmental conditions that have an impact on GFRP materials; moisture-solution, alkali, creep and relaxation, high temperatures, and fatigue. GFRP bar durability strongly depends on three major phases of a composite material, including fibers, matrix, and interface. Degradation of the composite can appear by deterioration in one or more of these phases. Thus, for a better understanding of GFRP bars durability, first, the degradation should be investigated.

2.3.1 Degradation mechanisms of GFRP bars

General degradation mechanisms in GFRP materials can be divided into two primary processes, involving non-linear viscoelastic-viscoplastic behavior and environmental degradation (Tuttle, 1996). Due to a major interest of this research and specification of the testing program, only the environmental degradation will be discussed in detail.

Load dependent degradation mechanisms

Fatigue and creep can be included to the load (stress) dependent degradation mechanisms, and are closely connected with matrix mechanical properties. The viscoelastic and viscoplastic behavior of the matrix influences the entire bar properties, making them time-sensitive. Fatigue is described as a failure of the material under cyclical loading, and as per the Uomoto (2001), FRPs may fracture. Fatigue of the GFRP reinforcement has not been fully understood since the majority of research performed has been focused on the fatigue behavior of FRP systems and reinforced concrete structure strengthened with FRP materials. In contrast to fatigue, creep can cause a failure or fracture of the FRP material under sustained load due to uneven stress distribution (Uomoto et al. 2001). According to Gonenc (2003), in several publications, researchers are investigating FRP creep behavior and rupture properties, but most of them provide the guidelines for future work instead of comprehensive knowledge about the long-term performance.

Interesting studies about GFRP bar degradation under sustained load have been performed by the Devalapura et al. (1997) and later by Benmokrane et al. (2002). These researchers have stated that the degradation of the composite reinforcement could be divided into three categories mainly depending on the sustained stress level. The first stage considers sufficiently low sustained load: from 25% to 30% of the ultimate strength of GFRP bar. In this stress interval, viscoelastic behavior of the resin releases the stresses and microcracking of the resin do not occur; then the degradation is mostly a diffusion dominated process. When the sustained stress level is higher than this threshold, the deterioration of the composite material is governed by matrix cracking propagation. Finally, when the stress is very high, the degradation of the material is mainly stress dominated, and the failure of the material occurs by rupture of the fibers.

Environmental degradation

It is worth mentioning that environmental deterioration of GFRP materials also depends on the loading conditions as described in the above paragraph. It can be stated that composite bar environmental resistance is inversely proportional to the stress level. However, steadily increasing stress eventually will change the degradation mechanism.

Matrix degradation

The environmental resistance of polymeric resins depends primarily on two factors: temperature of the environment and load conditions. The first factor is mainly responsible for the speed of diffusion, while the second one determines the matrix cracking. Environmental degradation of the resin can be divided into physical and chemical degradation.

Physical deterioration of the matrix can appear due to high temperature or moisture exposure. High temperatures, which are close to the glass transition temperature ($\boldsymbol{T_g}$) of the polymer, can cause a thermodynamic imbalance what leads to changes in mechanical properties of the material. On the other hand, moisture absorption causes matrix plasticization, which can be defined as reduction of mechanical properties and glass transition temperature. This process is mostly based on interruption of van der Waals bonds between the polymer chains (Bank et al. 1995).

Chemical degradation of the matrix is identified by a diffusion process, which causes matrix delamination, swelling and cracking with considerable reduction of modulus and strength at the same time. Many researchers (e.g., Benmokrane et al. 2002) state that the resin component plays a significant role in GFRP resistance to corrosion by protecting fibers against the damaging influence of pore water of the surrounding concrete. Chemical durability of thermosetting matrices is controlled mostly by the chemical nature of the polymer chain. According to Nkurunziza et al. (2005), vinyl ester epoxies have a great resistance to chemical attack. This phenomenon is due to the strong bond between carbon atoms, which form molecular chains. During exposure to OH^- or Cl^- ions, reactions do not affect the simple bond, which provides good durability. In the case of polyester resins, the prolonged exposure to OH^- or Cl^- ions involves a breakage of the bond between oxygen and carbon atoms (ester bonds) in the molecular chains, which can cause micro cracks, matrix fractures, and strength degradation, making polyester composites less durable. The reaction of the polymer chain with strong alkaline environments is shown in Eq.2.1 (Nkurunziza et al. 2005):

$$R-\underset{\underset{O}{\|}}{C}-O-R+OH \leftrightarrow R-\underset{\underset{OH}{|}}{\overset{\overset{O}{|}}{C}}-O-R \leftrightarrow R-\overset{\overset{O}{\|}}{C}-O+R-OH \tag{2.1}$$

Degradation of glass fibers

Composite bars reinforced with glass fibers are commonly used in engineering applications, due to their good mechanical properties and relatively low cost of production. Thus, it is important to understand the glass fiber behavior under different environmental conditions. It is widely known that glass fibers degrade in water, alkaline, acid and saline solution, but the most severe degradation occurs in the presence of alkaline environments. Since the concrete pore water is alkaline, this environment is most critical for the GFRP reinforcement.

Dissolution of glass in water environment

Per Charles (1959), degradation of glass fibers in water environment consists of four primary chemical processes. The first and the most important process is based on diffusion of the alkali ions out of the glass surface, also known as "leaching" process (Eq.2.2). The more alkali is added to the bulk of the glass, the more reactive glass becomes in moisture environment. From equation 2.2, the interruption between oxygen-sodium bond is noticeable, and the remaining oxygen atom captures a hydrogen ion H^+. This reaction causes additional surface stresses (Na^+ ion is larger than H^+ ion), what leads to crack formation. Moreover, a by-product of the reaction, silicon hydroxide, forms a gel layer on the fiber surface. In effect, the less dense layer of the gel accelerates the degradation process.

$$\begin{matrix} | & \uparrow & | \\ [-Si-O-Na] + H_2O \rightarrow & -SiOH & + OH^- \\ | & | & \end{matrix} \tag{2.2}$$

The other by-product, hydroxyl ion, plays an important role in the second reaction of dissolution process also known as etching (Eq.2.3). In this process, the hydroxyl ion breaks the Si – O – Si, forming SiO^-, which can dissociate another water molecule (Eq.2.4) and from SiOH, which constitutes the gel at the fiber surface.

$$\begin{matrix} | & | & | & | \\ [-Si-O-Si] + OH^- \rightarrow 2- & Si-OH & + & Si-O^- \\ | & | & | & | \end{matrix} \tag{2.3}$$

$$\begin{matrix} | & | \\ [-Si-O^-] + H_2O \rightarrow & -SiOH & + OH^- \\ | & | & \end{matrix} \tag{2.4}$$

From the above reaction, hydroxyl ions form, and the pH of the solution is increased. The last reaction (Eq.2.5) can also occur during the process of dissolution of the glass in water, but the occurrence of the first three reactions is much more likely.

$$\begin{matrix} | & | & | \\ [-Si-O-Si-] + H_2O \rightarrow 2-Si-OH \\ | & | & | \end{matrix} \quad (2.5)$$

Dissolution of glass in alkaline solution

Dissolution of glass fibers in alkaline solution is the same as Eq. 2.3. According to Gonenc (2003), it can be stated that eventually the degradation of fiberglass in water environment will evolve into an alkali attack since the chemicals from both processes are practically the same. However, due to immediate reactions in alkaline solution, the influence on bar durability is much more severe than moisture environment alone.

Parallel to the etching process, dissolution of calcium from the glass fiber occurs, also known as leaching of the calcium from the bulk of glass. This process is based on combining the calcium with water into a calcium hydroxide compound on the glass surface. This mixture will slow down the reaction, but the calcium hydroxide crystals growing on the glass surface will cause reduction of the fiber cross-section (Porter et al. 1998)

Dissolution of glass in salt environment

According to Porter (1999), the degradation process is similar to the alkaline attack with a much smaller rate of dissolution. The salt solution does not have a strong effect on the glass fiber until it exceeds nine pH of nine. Systematic studies by Wickert et al. (1999) showed: (1) a significant increase of soda-lime-silica glass in the dissolution rate with increasing NaCl concentration at the same time; (2) increased the amount of dissolved glass due to surface cracking and spalling. According to Charles (1959), dissolution of the soda-lime glass is very similar to alkaline silicates crystallization underwater attack. The second phenomenon is explained as the increment of the exposed area caused by the salt in the aqueous leachant. It results, in an increase of the amount of glass that dissolves within a given period.

Dissolution of glass in acids

Consideration of the acid influence on the GFRP interior reinforcement is not necessary since the concrete provides the high alkaline environment. However, investigation on glass degradation under acids is needed for GFRPs used as external reinforcement, such as cables or reinforcing sheets, when the composite can be affected by acid rain. This type of attack includes the "leaching" process, which is based on removing the alkali present in the bulk of glass by exchanging hydronium ions (H^+) in the acid with alkali in the glass (Eq.2.6 – Metcalfe et al. 1972). According to Adams (1984), the alkaline ions removed from the bulk enter the solution and attack the glass by etching again. In this sense, the moisture environment, which involves both leaching and etching, has the same influence on the glass fibers as the acid attack.

$$\begin{array}{c} | \quad \uparrow \quad | \\ [-Si-O-Na] + H^+ \rightarrow -SiOH + Na^+ \\ | \quad\quad | \end{array} \tag{2.6}$$

Degradation of interface

The interface defined as a heterogeneous region with a thickness of about one micrometer lies between fiber and matrix. Since the interface is at a critical location, where the transfer of stresses occurs, it should be characterized by good adhesion. Also, a strong interface is necessary to develop good composite properties. According to conducted research (Jayaraman et al. 1993), the interface should be characterized by:

- finite dimension or thickness
- elastic or inelastic response
- bond strength associated with adhesion to the fiber and matrix
- the degree of anisotropy
- elastic modulus, Poisson ratio, the coefficient of thermal expansion and cohesive strength

The interface is the weakest link most of the time and can degrade very easily. It can be damaged by delamination, interface debonding or matrix osmotic cracking (Bradshaw 1997). Degradation of the interface has an influence on short beam shear strength. However, according to Gentry (1998), the strength of the interface is important not only for interlaminar shear but also for the tensile strength of GFRP bars.

Due to complicated testing processes, the study of thermomechanical properties of the interface has not gained too much attention. However, modeling of the interface region has been investigated in the last couple of years. Due to "sizing" applied to the fiber surface to protect them from abrasion, physical models of the interface region became more complicated. "Sizing" contains three major elements: lubricant, wetting agent, and a coupling agent. It is well known that a coupling agent will form a strong bond between the fiber surface and polymer matrix through hydroxyl groups in the glass fibers (Ishida, 1983). This composition improves matrix-fiber adhesion. However, since the chemical bond of the coupling agent and fibers is more sensitive to the degradation, the coupling agent has the largest influence on interface properties (Schutte, 1994).

2.3.2 Durability studies on GFRP bars

The durability of GFRP reinforcing bars has been investigated under a variety of exposure conditions, different methodologies, and different material compositions. To simulate natural conditions different chemical environments have been used along with elevated temperatures which accelerate the aging process. Properties of GFRP bars are obtained before and after conditioning. It is important to mention that, due to differences in the manufacturing process and different composite components, the results from durability tests and their conclusions can be valid only for this one specific GFRP material.

Environmental effect on GFRP bar durability

GFRP bar durability has been studied in many different environments including acid, moist and salt environment, but due to the alkalinity of the pore water in concrete, more attention has been given to the high pH solution influence on GFRP lifetime. In general, the research on alkaline environment effects on GFRP reinforcement began in early 90's.

The first studies about pH effects on the GFRP composite were performed by Cowley and Robertson in 1991. The researchers investigated the influence of several solutions with different pH values (in the range from 7 to 11.5) on bar durability. The results of this test were estimated by the samples weight loss and showed that the degradation of bars immersed for four months in solution with variable pH and at elevated temperature (99°C) was similar to the continuous six-

month exposure to the solution with pH equal 9-9.5 at the same temperature. Researchers also noticed that increasing an exposure temperature will cause an increase in degradation rate as well. Similar research was performed by Mao et al. (2016). GFRP reinforcing bars were kept in the alkaline solution (approximately 13.62 pH) at 60˚C for 90 days. Bars show significant reduction of their tensile strength, which reached up to 30% of their ultimate capacity.

Besides the alkaline solution exposure effects on composite reinforcement, deterioration of GFRP bars directly embedded in concrete was investigated. Gooranorimi et al. (2017) studied the performance of GFRP bars exposed to concrete alkalinity after 15 years of service. Samples were retrieved from the bridge. Microscopic examination did not show any GFRP bars deterioration. There was no cross-sectional loss of the fibers, nor visible damage to the matrix or fiber-matrix interface. Energy dispersive x-ray spectroscopy analysis suggested no evidence of the chemical attack.

Effects of the marine environment on GFRP bar durability have been studied by Zayed (1991). Those bars were subjected to calcium hydroxide and sodium chloride solution, calcium hydroxyl solution and water at room and 40°C temperature. After 85 days of exposure time, the bars immersed in chemical solution lost 15% of their tensile strength, while the immersion in hot water caused 5% loss. Marine environment studies were also performed by Malvar et al. (2002). Results showed considerable deterioration of flexure and tensile strength in case of seawater exposure. Similar effects were observed in the event of salt fog exposure. Opposite results were obtained by Robert et al. (2013). Bars were embedded in concrete designate to simulate an aggressive alkaline environment of saturated concrete and kept in the saline solution at 23, 40 and 50˚C for 60, 120, 210 and 365 days. The change in the tensile strength even for high exposure temperatures (40 and 50˚C) was minor, and no significant microstructure changes were observed after 365 days of immersion in the saline solution at 50˚C.

Raham et al. (1998) performed experimental tests on GFRP bars exposed to varied aggressive environments and subjected to a stress equal to 30% of their ultimate strength at the same time. Bars had been tested at three different times of exposure: 45, 122 and 370 days, respectively. GFRP reinforcement exposed to the alkaline solution failed within the first month due to rapid diffusion of the hydrated hydroxyl ions.

Combined environmental conditions were studied by Micelli et al. (2001). GFRP reinforcement was subjected to four combined environmental cycles simulating eight years of structure lifetime in regions such as continental Europe or the central USA. Results of the test showed no influence on GFRP bar properties. Similar tests were repeated by Stone (2002), where the GFRP rods were studied in environmental cycles. This time, the strength (interlaminar shear) of samples was not affected by this type of conditioning.

Besides the solution exposure effects on GFRP reinforcing bars, degradation of composite due to ultraviolet rays was also studied by researchers. Exposure to ultraviolet radiation can occur in the case of external reinforcement, reinforcing sheets or simply material outdoor storing. According to Delre (1988), ultraviolet radiation caused degradation in a polymeric matrix. However, this deterioration occurs at the surface of the composite to a small depth. Studies performed by Yamaguchi (1998) proved this theory, while in the case of GFRP material after exposure to UV rays, deterioration of the matrix was not more than 0.6mm. Nevertheless, though the strength of glass fibers is not affected by UV directly, degradation of the resin system can allow chemicals to diffuse into the composite much quicker. Thus, UV effect is an important factor in overall durability of GFRP material. Umoto (2001) studied UV radiation influence on GFRP composite after three years of natural sun exposure. Composite bars experienced from 1 to 19% strength losses. Different research has been performed by Kato et al. (1997) where GFRP bars were exposed to UV with the intensity of 0.2MJ/m^2/hour in a temperature of 26°C. After 500 hours of exposure, GFRP materials lost 8% of their strength.

Recently, Yang et al. (2017) studied the influence of different curing temperatures on GFRP bars durability subjected to the aggressive environment. GFRP bars were cured in 20, 40, 60 and 80˚C, respectively, and cast in concrete cubes simulating the highly alkaline environment. The tensile strength of GFRP bars decreased with an increase of curing temperature.

Material effect on GFRP bar durability

The durability of GFRP material depends strongly on the durability of chosen components. Many factors have an influence on resin and fiber type, manufacturing process or chemistry of fibers. To improve GFRP bar durability, many studies evaluating the effects of resin/fiber types, fraction volume, surface treatment and manufacturing process have been done.

Resin type plays a major role in GFRP bar durability since it has a direct contact with the aggressive environment. Bank and Puterman (1997) performed a test on GFRP reinforcing bars with different types of resin. Specimens were embedded in concrete and placed in tap water at 80°C for 84 days. At the end of the test, samples from concrete-bar interface were taken for SEM (Scanning Electron Microscope) investigation. It was shown that parts of polyester resin experienced much more severe degradation than vinyl ester resin. Bakis (1998) performed similar studies. The researcher tested three different types of GFRP bars immersed for 28 days in a saturated solution of calcium hydroxide at a temperature of 80°C. Again, the vinyl ester rods were less affected by the aggressive environment than vinyl ester/ polyester blended resins (50% vinyl ester and 50% polyester; 20%vinyl ester and 80% polyester). Benmokrane et al. (2001) showed the superiority of vinyl ester resin to polyester resin in an alkaline environment, where vinyl ester resin type exhibited the highest resistance to alkaline environment, exceeding almost 12% more residual strength than polyester resin systems with the same type and amount of fibers. It can be noticed that more hydrophobic resins (vinyl esters) are more durable since the diffusion process is much slower than in the case of a polyester matrix. The most recent studies were performed by Brnmokrane et al. (2017). The durability of bars with three different resins glass-polyester, glass-vinyl-ester, and glass-epoxy were investigated. Bars were kept in a highly alkaline solution at 60˚C for up to 5000h (1000h, 2000h and 5000h). Both polyester and epoxy bars had similar flexure strength deterioration around 23-25% of ultimate capacity, respectively. While bars with vinyl-ester resin lost approximately 17% of ultimate flexure strength. The epoxy and vinyl-ester GFRP bars due to the higher fiber-resin bond strength exhibit lower reduction of flexure strength, flexure modulus of elasticity, and interlaminar shear.

Parallel to the investigation of resin durability, the chemical resistance of different types of glass fibers was also studied. According to the previously described deterioration mechanism of glass fibers, it can be stated that durability strongly depends on the composition of the glass bulk. The addition of alumina will improve glass fiber resistance to moisture but will decrease the resistance to alkaline solutions (Parera 1991). According to Yilmaz et al. (1991) and Tannous et al. (1999), the alkali resistance of glass can be improved by adding a trace amount of zirconium (ZrO_2). This type of glass fiber is called AR-Glass (alkaline resistance glass fiber). Dejke and Tepfer (2001) carried out an experimental study on durability of GFRP bars with a different type of glass fibers (E-glass and AR-glass). Reinforcing bars had been conditioned in three different environments

including concrete, an alkaline solution, and water at four different temperatures: 20, 40, 60 and 80°C. Contrary to their appearance, AR-Glass bars performed worse than E-Glass specimens in the interlaminar shear strength test, which had been used to evaluate bars deterioration. Also, Benmokrane et al. (2002) had been studied the alkaline resistance of bars reinforced with AR-Glass and E-Glass in alkaline solution. Bars had been exposed to the aggressive environment for 140 days at 22°C. Results showed 17% strength degradation of bars reinforced with E-glass, while the AR-Glass bars preserved the same strength.

2.4 What has been done – GFRP research literature review

2.4.1 Introduction

In traditional reinforced concrete structures, the alkalinity of the concrete should protect the steel bars against corrosion, and provide sufficient durability. Unfortunately, this mechanism usually stops working in strongly aggressive environments, where concrete carbonation or chloride ingress can occur. Steel corrosion creates a reduction of cross-sectional area of bars, the volume expansion of corrosion products increases internal stresses in concrete and leads to cracks, thus causing concrete splitting and rebar bonding problems. This phenomenon has become a primary issue for civil engineering these days.

Composite bars can be divided into three major groups: 1) conventional-flexural and transverse reinforcement, 2) dowel connectors in pavements and 3) pre-stressing tendons. Although GFRP is a new material, a substantial amount of research has already been conducted worldwide, to determine its mechanical properties. Canada, through the establishment of the Innovative Sensing of Intelligent Structure (ISIS) Canada network in 2001 has become a leading center of this research endeavor.

2.4.2 Tensile strength of bars

The research was done to improve tensile testing techniques that could be proposed for composite rods. It was quickly discovered that elements of the traditional tensile test method for steel (gripping of a rod) are not appropriate for the fiber reinforced materials. The difficulties are directly connected with the damage of the rods due to excessive gripping force, fracture out of the test length due to stress concentration and flexural forces (caused by specimen misalignment), yielding

or failure of the anchorages and slippage occurrence inside the anchorage elements used for testing (bond failure). In 1996 Bakis et al. proposed a gripping system for carrying out tensile strength testing of fiber reinforced rebars. The bar ends were roughened with sandpaper cleaned and embedded into conical steel anchors using the epoxy resin. A few years earlier, similar anchorage systems were proposed by Holte et al. (1993) and Erki and Rizkalla (1993) with a difference in the shape of the tube anchor. All those systems are based on force transition from epoxy to the bar by using bond strength between these materials. An alternative approach was proposed by Vijay, (2003) where researchers decided to use a split in half tube with the same diameter as a composite rod, sanded and coated with epoxy from inside. The tube was clamped to the rod until the resin was cured and placed into V grips. This system differs from the previous ones due to the indirect application of compressive stresses to the tested bar. Another research conducted by Castro and Carino (1998) and Nanni (1996) concentrated on the utilization of different tube fillers. In both test programs, the epoxy resin was substituted by a cement mortar or expansive grout. The effectiveness of this gripping method was shown for samples with at least 300 mm anchorage length. All of these tests influenced existing standards and testing regulations (CSA S806 Annex C, ASI 440-3R-04 B2 test method, ASTM D7205). In all types of testing, composite reinforcements demonstrate a significantly larger tensile strength than steel, with almost elastic behavior up to failure. The tensile test method became a standard test for any GFRP manufacturer and a part of quality assurance and control trials.

2.4.3 Shear and dowel action strength

GFRP bars can exhibit direct shear loading when are used as the reinforcement for elements that with construction joint. GFRP reinforcing bars are utilized as bridge barrier connections, stirrups, and dowels. Research in this area can be divided into two major types of reinforcement: stirrups as shear reinforcement in structures and dowel connectors for concrete pavements.

Joined concrete pavements are widely used in highways and roads. Dowel bars are placed along the joint transferring load on rods bearing on the surrounding concrete. Due to the extremely aggressive environment, steel dowels are often impractical resulting in steel degradation and concrete deterioration by cracking and splitting. Extensive research in this area was done at Iowa State University (Porter 2001) and the University of Manitoba (Eddie, Shalaby and Rizkalla 2001).

The researchers showed the usefulness of GFRP bars as dowel reinforcement. According to Rizkalla et al. (2001), the larger diameter of composite bars and lower elastic modulus of GFRP as opposed to steel bars, will reduce the bearing stress between the dowels and concrete support, and therefore reduce the dowel failure. However, use of GFRP bars as a shear reinforcement or dowels has not yet been explored enough to establish the rational method to predict the shear behavior and strength of bar.

Several studies were targeted to investigate the shear capacity of bars as a composite material property. Gentry (2011) described the ASTM D7617 standard test method for transverse shear strength and performed the test on three different types of GFRP. He states that this test is a significant addition to the body of test methods and specifications for FRP reinforcing bars. Furthermore, initial test results on bars immersed into alkaline solution show that the method can also be used for bar degradation investigations (Gentry 2011).

Research has also been done on the utilization of composite shear reinforcement in the form of stirrups or headed bars. Stirrups, which are usually located as an external reinforcement on flexural bars, are more susceptible to severe environmental effects than any other reinforcement in a structure. Furthermore, in many cases of composite bridge structures, shear reinforcement is extended outside of the beam to provide proper integration with the slab cast at the later stage. During this period, exposed reinforcement is extremely vulnerable to quick degradation. According to Shehata (1999), shear failure in GFRP reinforced concrete members can occur in two different ways: rupture of FRP stirrup or crushing the concrete in compression zone or the web. Because of GFRP non-ductile behavior, the rupture failure of stirrups occurs suddenly. The crushing of concrete failure mode occurs when the shear crack propagates toward the compression zone causing crushing of the concrete.

Bridge decks or slabs due to lack of shear reinforcement also may fail in direct shear or a combination of tension and shear. The flexural test was conducted in an experimental study, Michaluk et al. (1998), on the behavior of one-way concrete slabs reinforced with FRP bars. They found that one of their specimens failed due to GFRP bars shear rupture at a crack location. Thus, the direct shear strength of GFRP reinforcement may be a significant factor to consider in the design and requires further investigation.

2.4.4 Bending effects

Bending of GFRP bars in the form of stirrups or different bend configurations causes strength reduction. Therefore, stirrups have been evaluated by investigating the behavior of the bent. According to the one of the earliest studies carried on GFRP bent bars made by Miyate et al. (1989) and later research on FRP (Maruyama et al. 1993; Shehate et al. 2000; El-Sayed et al. 2007), bending composite bars to form stirrups significantly decreases the strength at the bent portion, reducing capacity of the whole stirrup by 40% - 60%. This phenomenon can be explained by the occurrence of several factors at the same time. Micro-scale single fiber investigations (Hull 1981) (Fig. 2.7) show that the sharp bends result in large deformations and crashing fibers.

The other reason for the weakening of the strength of the GFRP bent bars is found in the manufacturing process. Bent bars fabrication became much more challenging than the production of the straight bars and caused many issues, especially with uniform fibers distribution along the bent portion. Despite a lot of production developments and innovations, none of the new techniques can prevent this kinking effect (Fig. 2.8). While the outermost fibers are stretched and keep their “straight” form, the innermost fibers start “waving” to maintain their length inside the smaller circumference of the bend. This phenomenon effectively decreases GFRP bar capacity.

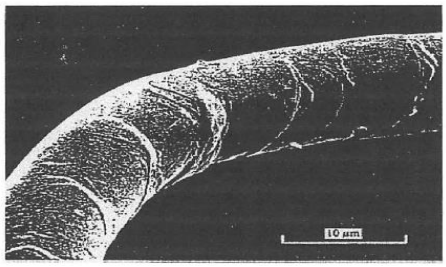

Fig. 2.7 – Bent fiber in microscopic scale (Hull 1981)

The fact that GFRP rods demonstrate much lower strength in a perpendicular direction to the fibers than in parallel direction is also very important. In the case of bent bars, in addition to the normal stress parallel to the fibers, the stirrups resist lateral load due to bearing against concrete (Fig. 2.9), which also has a significant influence on bent bar strength reduction.

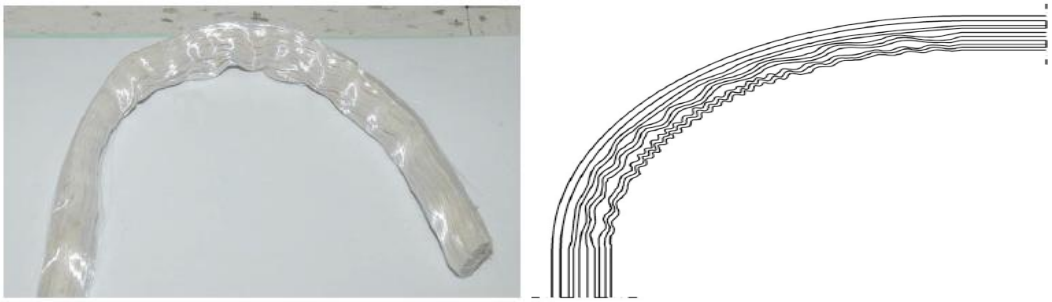

Fig. 2.8 – Fibers kinking effect (Ahmed 2010)

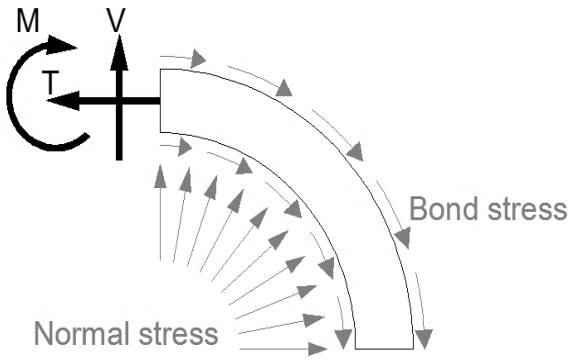

Fig. 2.9 – Stresses at the location of the bend

Chapter 3

RESEARCH PROGRAM

3.1 Introduction

The major interest of this experimental program is focused on two primary issues preventing composite reinforcement wider utilization. These include lack of effective and efficient (in terms of time and cost) evaluation methods of GFRP bars performance and lack of knowledge about material long-term behavior. Thus, the presented research program has been divided into two main sections.

Critical evaluation of four basic quality control tests for GFRP bars, used for tensile, shear, compression, and flexural properties investigation, is included in the first phase of this research. Based on obtained information recommendations for quality control tests modifications and tests procedure improvement was made. Subsequently, any possible correlation between tests was investigated. Obtained information from short-term testing (data) was used as a starting point for durability studies.

The second phase of presented research includes investigation of composite long-term behavior and bars durability. For this purpose, the accelerating aging test (alkaline immersion test) was used, and four most common deterioration models were investigated. Described in Chapter 6 durability prediction models were evaluated based on data obtained from a durability test, and possible improvements to the existing strength prediction models were considered.

This chapter consists of detailed information about composite materials that were tested and standardized testing procedures. Four basic tests (tensile, shear, flexure, compression) with the addition of a cure ratio test were applied to investigate bars short-term properties as well as were used as durability indicators in deterioration studies.

3.2 Choice of specimens

The specimens for this research were provided by two companies, which operate in Canada. For the purpose of this document, to ensure confidentiality of both producers, they were named

Company I and Company II, respectively. All specimens were straight bars; however, some bars were produced in the straight bar manufacturing process (pultrusion), and some were obtained from a straight portion of bent bars (Fig. 3.1). Two different bar diameters were used: #4 and #5 bars for Company I and 12 and 16 mm bars for Company II. Where #4 and #5 bars are considered as an equivalent of 12mm and 16mm bars in Imperial notation. In addition to typical bars, both manufacturers produced for this research a special set of smooth surfaced bars for shear and flexure tests as a control specimen. According to the producers, the smooth bars have the same mechanical properties as the straight bars, but with a slight difference in bar diameter. For simplification, the following name convention has been introduced:

Company I:	**Company II**
• Smooth Surface Bar (SSB-I)	• Smooth Surface Bar (SSB-II)
• Straight Bar (sand coated) (SB-I)	• Straight Bar (ribbed) (SB-II)
• the straight portion of Bent Bar (BB-I)	• the straight portion of Bent Bar (BB-II)

a) 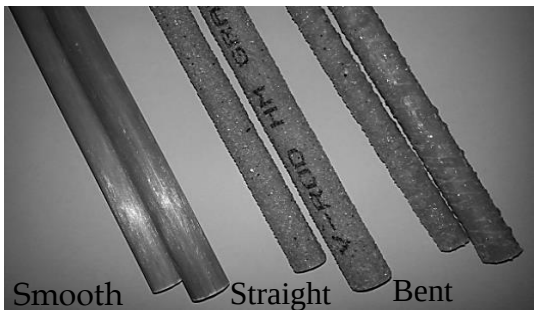

b) 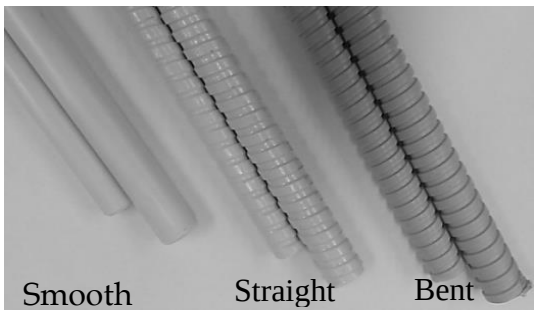

Fig. 3.1 – Straight and bent bars a) – Company I b) company II

GFRP straight bars are made in the fully automated pultrusion process. Pulling bars through a heated die assures the shape correctness (precise bar diameter) and fibers straight and parallel configuration (Fig. 3.2). Bent bars, on the other hand, are manufactured in the custom-made system. An individual for each company manufacture process of bent bars, brought many issues with fibers misalignment, waving and bars proper shape.

Fig. 3.2 – Cross – section of the straight bar

According to Weber and Witt (2011), the production process of the bent bars should satisfy the following conditions: hold all fibers in place during the bending process; achieve comparable to the straight bars bond behavior and mechanical properties, and use simple tools and machines. To fulfill those requirements producer from Company II uses corrugated pipe filled with fibers and resin. After the pipe is bent to the desirable shape, a bar is cured. Fibers inside the bent portion are no longer held in a parallel configuration. To avoid external stress indication (stretching of outer fibers) the outside fibers are kept "straight," what leads to compression of the inside fibers, and fibers buckling. Regardless of all the differences in the production process, all companies face a problem of fibers kinking effect (Fig.3.3 a), which due to different than pultrussion manufacturing, occurs not only at the bent but also at the straight portions of a bar (Fig.3.3 b).

All bars nominal characteristics specified by suppliers are shown in Table 3.1. Due to differences in specimen preparation for each test, further details will be provided with specific test information. For all tests, the effective bar diameter was taken as an interior bar diameter. Measured diameters and corresponding cross-section areas are reported in Table 3.2.

Table 3.1 – Nominal physical and mechanical properties of GFRP bars used

Manufacture properties of GFRP bars					
Straight bars					
Properties	**Company I**		**Company II**		**units**
Size	#4	#5	M12	M16	
Nominal bar diameter	12.7	15.875	12	16	mm
Nominal cross - section area	126.7	197.9	113	201	mm^2
Tensile strain	2	1.89	2.61	2.61	%
Nominal tensile strength	1312	1184	1000	1000	MPa
Modulus of elasticity	65.6	62.6	60	60	GPa
Glass fiber content (by weight)	83	83	>85	>85	%
Bent bars					
Properties	**Company I**		**Company II**		**units**
Size	#4	#5	M12	M16	
Nominal bar diameter	12.7	15.875	12	16	mm
Nominal tensile strength straight portion	560	580	1000	900	MPa
Nominal tensile strength bent portion	238	230	700	550	MPa
Modulus of elasticity	41.9	43.4	>50	>50	GPa

a) 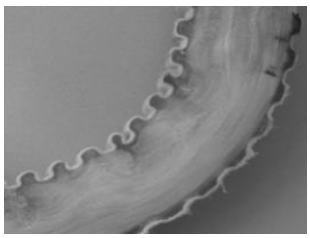 b) 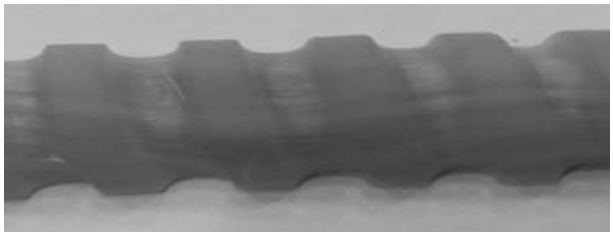

Fig. 3.3 – Cross-section of the bent bar a) bent portion; b) straight portion

Table 3.2 – GFRP bars diameter and cross-section area

Properties		**Company I**		**Company II**	
Size		#4	#5	M12	M16
Measured bar diameter [mm]	**SSB**	14	18	13.2	18
	SB	14	18	12	16
	BB	12	16	12	16
Measured cross - section area [mm^2]	**SSB**	153.85	254.35	143.07	254.36
	SB	153.85	254.35	113.09	200.95
	BB	113.09	200.95	113.06	200.95

The following methods were used in determining geometrical properties. The CSA S806 Annex A standard was used for determination of smooth surfaced bar (SSB) cross-sectional areas from both companies. This method determines the bar diameter based on the total volume of the bar immersed in water. The diameters were determined from the cross-sectional areas assuming circular bars. It was considered necessary to obtain the cross-sectional areas that are effective in carrying stresses. Therefore, for the other bars, the following methods were used. For straight bars (SB) from Company I, with a sand coating, the cross-sectional area was taken as the same as for equivalent smooth bars as sand coating does not contribute to carrying longitudinal stresses. For bent bars from Company I, the diameter was measured at several points using a caliper with precision to three significant digits, and the mean value was calculated. For straight bars (SB) from Company II, which have grooves cut into the bar surface, the bar diameters were measured inside the grooves. Cross-sectional areas were determined from these diameters assuming circular bars. For the diameter of bent bars from Company II was obtained the same way as straight bars (SB).

3.3 Laboratory test procedures

In this section tests procedures and methodologies are described in accordance with the four main standards: 1) CSA-S807-10 “Specification for fiber-reinforced polymers”; 2) CSA-S806-12 “Design and construction of building structures with fiber-reinforced polymers”; 3) ACI 440.3R-

04, and 4) ASTM. ACI and ASTM procedures are used in this research as additional information supplementing Canadian regulations.

3.3.1 Longitudinal tensile properties and modulus of elasticity test method

Tensile test procedure specified by three major standards, CSA S806 (Annex C), ACI-440.3R-0.4 (B.2) and ASTM (D 7205/D 7205M), determines the longitudinal strength, elongation properties of fibers reinforced polymers, modulus of elasticity, and the stress-strain relationship curve.

Apparatus

The test should be conducted on a machine with either load or displacement rate control. A specimen should be attached to the testing machine by an anchorage device (tubes), which prevents crushing of the sample ends. Both CSA and ASTM standards present the preferable anchorage systems (Fig. 3.5). There are also acceptable alternative anchoring methods, but they should satisfy the following conditions: load transmission should be devoid of any eccentricity or torsion; failure should not appear under the grips; no alteration (mechanical or chemical) should be applied to the effective length of a sample.

ASTM recommendations for the anchorage dimensions have been shown in Table 3.3. It has been noticed that specified values depend on bar diameter, but the protocol does not include any information about how they were obtained. In contrast to the ASTM, Canadian standard CSA S806 determines a relationship between anchorage length and bar ultimate capacity, which is specified as $f_u A/350$, but not less than 250mm (f_u – ultimate tensile strength, A – cross-section area of a specimen). Moreover, the tube thickness should not be less than 5mm and inside diameter it, should be greater than the bar diameter from 10 to 14mm. The above anchors are not recommended for specimens with tensile capacity greater than 400 kN. Both standards recommend using polymer resin, 1:1 mixture of resin and sand, or an expansive cement as tube filler. The anchor's attachment to the testing machine can be realised in several ways (Fig. 3.). However, the most popular is the grip attachment. The grips should transfer lateral load through the anchorage to the sample in such a way as to prevent the slippage between grip face and anchor.

Table 3.3 – Anchorage tube dimensions per ASTM D7205/D7205M

Type of FRP bar	Bar diameter [mm]	Steel tube [mm] diameter	Steel tube min. length [mm]
GFRP	6.4 – 9.5	35	300
GFRP	13 – 16	42	380
GFRP	19 – 29	48	460
GFRP	32	75	800
CFRP	9.5	35	460

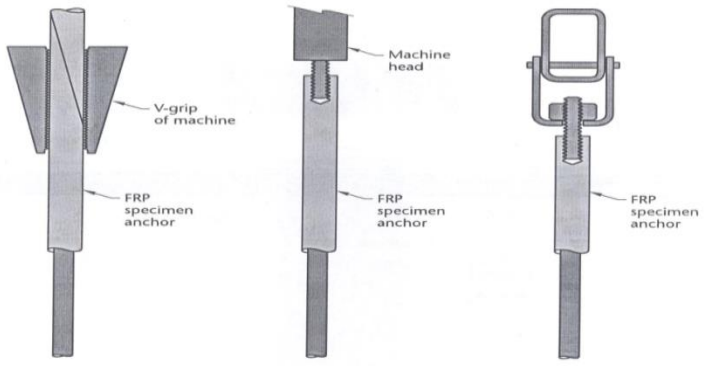

Fig. 3.4 – Attachment of anchor to the testing machine per the CSA S806

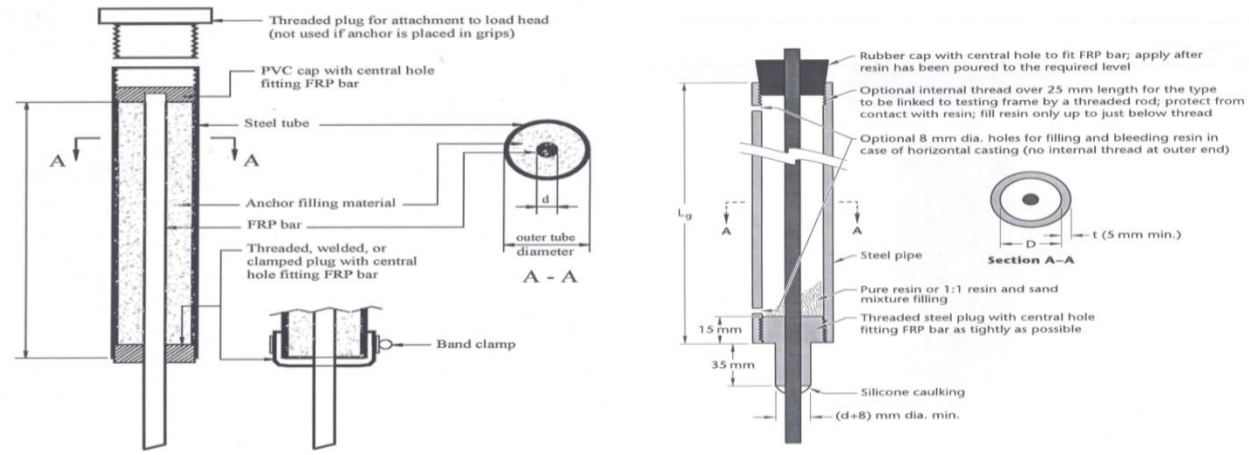

a) b)

Fig. 3.5 – Anchorage system referring to the a) ASTM b) CSA

During the test, both strain and elongation should be recorded. Per the ASTM standard, any strain measuring device can be used, as long as the attachment of this device will not damage the bar. In the case of a braided, twisted or indented bar, the surface should be smoothed by using an epoxy resin to provide a suitable bonding surface.

Sampling

According to the referenced standards, a minimum of 5 bars for each bar size should be used. However, CSA S807 standard states that if the mechanical, physical and durability properties are determined for qualification testing, there should be at least eight samples for each size of the bar for each manufacturer. The total length of a sample should consist of a free length and two lengths of anchoring sections. The free length should not be less than 40 times the effective bar diameter (ASTM, CSA, and ACI) or 380 mm (ASTM).

Procedure

Specimens shall be mounted in the testing machine, such as to avoid bending or torsion. The strain measurements shall be done in the middle part of the bar between the grips. The rate of load (strain) shall be constant during the test, and it should be selected that way that the failure appears between 1 to 10 min. The CSA standard defines the applying stressing rate of 250 to 500 MPa per minute. The strain measuring devices should be detached from the sample when the bar reaches at least 50% of the ultimate strength (ACI) or 75% of the ultimate strength (CSA), respectively. If any sample fails partially or entirely inside the grips, the test result should be neglected.

Calculations

According to all mentioned standards, the tensile strength (F_{tu}) shall be obtained by dividing the highest recorded load (P_{max}) by the area (A) of bar cross-section:

$$F_{tu} = \frac{P_{max}}{A} \tag{3.1}$$

Tensile stress at ith data point (ASTM)

$$\sigma_i = \frac{P_i}{A} \tag{3.2}$$

where: $\sigma_i -$ tensile stress at i – th data point [MPa]; $P_i -$ force at i – th data point [N]; $A -$ cross – section area of the bar [mm^2]

ASTM defines the tensile strain, which can be obtained from the indicated displacement.

$$\varepsilon_i = \frac{\delta_i}{Lg} \tag{3.3}$$

where: $\varepsilon_i -$tensile strain and i – th data point [mm/mm] $\delta_i -$ extensometer displacement at i – th data point, $Lg -$extensometer gage length

The tensile modulus of elasticity is calculated as a linear regression from the two data points (ASTM and CSA from 25 to 50% of the tensile strength of the bar and according to the ACI-440.3R-04 standards from 20 to 50%). It can be calculated from:

$$E = \frac{1000(P_1 - P_2)}{(\varepsilon_1 - \varepsilon_2)A} \tag{3.4}$$

where: E – modulus of elasticity[MPa]; A –cross-section area of the bar [mm^2]; $P_1 and\ \varepsilon_1$ – load and strain at approximately 50% of the ultimate tensile capacity [N]; $P_2 and\ \varepsilon_2$ – load and strain, respectively, at approximately 20% of the ultimate tensile capacity [N]

3.3.2 Test method for shear properties of FRP rods

To determine FRP bar shear strength several laboratory tests methods were developed. Shear test procedures are specified by CSA S806 (Annex L) ACI-440.3R-0.4 (B.4) and ASTM (D 4475; D 7617/D7617M). Those methods are considered for developing transverse shear strength of fiber reinforced polymer smooth, texture bars or prestressed tendons. Force is applied directly to the sample by a double shear device.

Apparatus

The testing machine should have either load or displacement rate control and provide measurements of loading accurately to 1% throughout the test. The shear testing device (Fig. 3.) should consist of two bar holds two bottom blades, and guides, which are used to create a distance between the bottom blades. These parts are connected by two threaded rods.

Fig. 3.6 – Shear test device

Sampling and test specimens

The test specimen should be representative of the tested batch and should not be subjected to any processing. Cutting off the specimen should be performed without any influence on the bar testing area. The specimen should be straight without any imperfections and a bent portion. Any specimen deformation, heating, outdoor exposure to ultraviolet light or any condition, which can change sample properties should be avoided. The minimum number of specimens should constitute of at least 5 bars for each bar size. However, CSA S807 standard states that if the mechanical, physical and durability properties are determined for qualification testing, there should be at least eight samples for each size of the bar for each manufacturer. Different standards define the different length of a specimen. The CSA standards state that the specimen shall be no longer than 300 mm without specifying the minimum value. The ACI standard in B.4 test method specifies the total length of specimen exactly 300 mm, while the ASTM gives 225 mm for the sample length.

Procedure

The specimen shall be placed in the shear testing device centrally. No gap is allowed between the contact surface of the loading device and bar surface to avoid the impact effect at the beginning of loading. According to the ACI and CSA standards, the load rate (stress) shall be of 30 to 60 MPa per minute. According to the ACI standard, the failure load shall be measured with the precision to the three significant digits. Loading can decrease, and the stiffness of the specimen may change at the failure onset due to delay in the formation of the second failure face. The loading should be continued until the second failure face forms or the force has dropped to 70%of the observed peak force.

Calculations

Transverse shear strength shall be computed as (ASTM, CSA, ACI):

$$\tau_u = \frac{P_s}{2A} \tag{3.5}$$

where: τ_u – transverse shear strength [MPa]; P_s – maximum failure force [N]; A – cross-section area of the bar [mm^2]

3.3.3 Flexural properties of FRP pultruded plastic rods

Canadian standard CSA S807-10 specifies that flexural properties test method should be conducted in accordance with the ASTM D4476-09. A specimen is tested like a simple beam using three point bending until failure or reaching 5% of maximum fiber strain. Semicircular cross section of a sample was chosen to avoid premature compression failure, and allow for the maximum axial stress of external fibers to occur.

Apparatus

The machine should be properly calibrated to operate at a constant rate of 3 mm/min and should be equipped with the deflection measuring device. For proper holding of the specimen, the additional fixture should be used (Fig. 3.7).

Sampling and test specimen

The ASTM standard does not specify the minimum number of samples but suggests using at least five specimens to develop efficient statistical values. The length of the sample should be 16 to 24 times of specimen thickness plus at least 20% of the support span to allow a minimum 10% overhang at the supports. The specimen should be cut into two parts from the bar in a way that each part should be less than half of the bar cross section (Fig. 3.8).

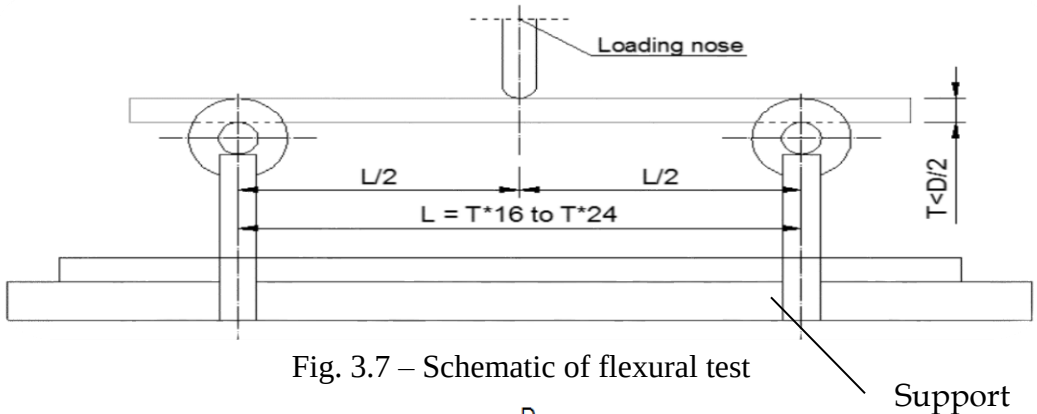

Fig. 3.7 – Schematic of flexural test

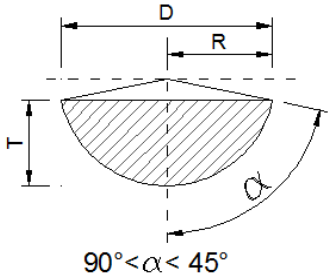

Fig. 3.8 – Flexural test specimen

Procedure

The test should be conducted as a simple 3 – point bending with the displacement control rate 3 mm per minute for the specimen with D/2 between 6.35 mm to 9.52 mm and 6mm per min for samples with D/2 between 9.52 mm to 12.7 mm.

Calculations

Maximum fiber stress

$$S = \frac{P*L*C}{4I} \tag{3.6}$$

where: $S-$ stress in the outer fibers at midspan [MPa]; $P-$ load at a given point on the load deflection curve [N]; $L-$ support span [mm]; $I-$ moment of inertia [mm^4] $C-$distance from centroid to extremities

Modulus of elasticity

$$E_b = \frac{P*L^3}{48*I*Y} \tag{3.7}$$

where: E_b-modulus of elasticity in bending [MPa]; $P-$ load at a given point on the load deflection curve [N]; $L-$ support span [mm]; $I-$ moment of inertia [mm^4]

Maximum strain

$$\varepsilon = \frac{12*C*Y}{L^2} \tag{3.8}$$

where: $\varepsilon-$maximum strain in outer fibers [mm/mm]; $Y-$ maximum deflection at chosen load [m]; $C-$distance from centroid to extremities; $L-$ support span [mm]

3.3.4 Compression test for FRP rods

According to the CSA S807-10, the compression properties of GFRP bar should be determined by a procedure described in the ASTM D695-10 or ASTM D3410/D3410M-03. Compression test method provides a standardized method of obtaining data for research, development, quality control, acceptance or rejection of specification.

Apparatus

For both methodologies, the test can be conducted by using any machine capable of controlling a constant rate of crosshead movement. It shall be constructed that such as loading is axial and

applied through surfaces that are flat within 0.025 mm and parallel to each other in a plane normal to vertical loading axis.

Sampling and test specimens

The standard test specimen, according to the first ASTM protocol, should be in the form of a cylinder or prism, whose length is twice its principal width or diameter. For the rod samples, the test specimen should have the same diameter as the bar has. The second methodology has a different approach for specimen preparation. Tested samples should be attached to the machine by the anchorage device, which indirectly indicates uniformly distributed stress to the sample. For both methods, a minimum of 5 specimens should be tested.

Procedure

The test specimen should be measured with an accuracy of 0.01 mm at several points along the length. The specimen should be placed on the surface of a compression tool or into the grips, taking care to align the center line of its long axis with the center line of the plunger and to ensure that the ends of the specimen are parallel with the surface of compression tool. The standard speed of testing shall be 1.3 ± 0.3 mm per minute.

Calculations

Compressive strength should be calculated as a division of maximum compressive load carried by the specimen and minimum of cross-sectional area of this sample. Modulus of elasticity should be calculated by drawing a tangent to the initial linear portion of the load-deformation curve, selecting any points on the straight line portion, and dividing the compressive stress represented by this point by the corresponding strain, measured from the point that extended tangent line intersects the strain axis.

3.3.5 Test method for alkali resistance of FRP rods

The alkali resistance of FRP bars test procedure is described by three standards CSA S806 Annex M, ACI 440.3R B.6, and ASTM D7705/D7705M. This method is based on immersion of FRP bars into alkali environment (with or without sustained tensile stress) and testing them in tension. ACI and ASTM present three different procedures to be conducted at a temperature of 60ºC. CSA gives

only two procedures specified such as method B and C. Each procedure defines different loading conditions.

Procedure A is based on immersing FRP bar in alkali environment without any tensile load. The control parameters of the test are pH, the temperature of alkali solution, and immersion time. According to the ASTM standard, four sets of the specimen should be used, each set for a different period: 1, 2, 3 and 6 months. CSA recommends only 3 different time periods including only 1, 3 and 6 months. After the immersion time, bars should be tested in tension.

Apparatus

This test should be conducted in a special environmental chamber capable of heating the alkaline solution to 60ºC and able to maintain the required temperature within ±3ºC.

Sampling and test specimens

The test specimen should be representative of the tested batch, and any processing beyond manufacturing is not allowed. Each specimen consists of three bars from each manufacture and bar diameter. The bar ends and the ends of transverse elements of grids should be coated with epoxy resin to avoid infiltration of the solution via those cuts. Resin should be cured completely before immersion.

Alkali solution requirements

The alkali solution should have the same composition as the pore solution found in concrete. It should contain 118.5g of $Ca(OH)_2$, 0.9g of NaOH and 4.2g of KOH in 1 L of deionized water. The solution shall have an initial pH between 12.6 and 13.0.

Procedure

The pH of the alkali solution shall be recorded before and after the test. In addition to the test, the value of pH should be measured every 5 days. An7y changes to the sample surface should be recorded (the color, surface condition and change of shape). Optionally, the specimen can be cut and polished, and the condition of the bar can be defined under a microscope. Before the test, the specimen should be dried and weighed (using procedure D of ASTM D5229/D5229M), this is the initial mass W_0. After conditioning, the specimen should be washed and paper dried and then

immediately weighed (W_1). After that, the specimen should be placed in the tensile machine and tested in tension within 24 h after removal from the conditioning.

Calculations

Retention of tensile capacity:

$$R_{et} = \frac{F_{tu1}}{F_{tu0}} * 100 \quad (3.9)$$

where: R_{et} – tensile capacity retention [%]; F_{tu0} – tensile capacity before conditioning [N]; F_{tu1} – tensile capacity after conditioning [N]

3.3.6 Cure ratio test for FRP bars by DSC

The method for FRP bar cure ratio determination is described in CSA S807 Annex A standard. This test method uses differential scanning calorimeter (DSC). To obtain the FRP cure ratio, the following is needed:

- the resin matrix content;
- the enthalpy of polymerization of the resin mixture;
- the residual enthalpy of polymerization of the material.

Apparatus

Primary apparatus used in this test is a differential scanning calorimeter (DSC). DSC measurement includes heating the specimen with the temperature rate of 10ºC/min and 20ºC/min and automatically recording differential heat flow.

Sampling and test specimen

A test specimen should be kept indoor at a room temperature. The specimen should be taken from the center of the rod, due to the possibility of less curing in the core of a bar. The sample shall be cut using diamond blade saw equipment. The special care should be taken to avoid heating the sample during cutting. The minimum amount of specimen used should not consist of less than three samples.

Procedure

The CSA standard describes three basic steps for determining the cure ratio:

1. Determination of the resin matrix content of the material by weight. If it is provided by the manufacturer or if it was determined in previous tests this step can be omitted.

According to the CSA, the resin matrix content of glass FRP bars can be determined by one of two methods: thermogravimetry (TGA) or ignition loss. Before sampling of the material, any coating shall be discarded, and the sample should be representative of the core of the FRP rod.

The thermogravimetry method procedure is as follows:

The sample should weigh between 20 and 75 mg. The weight loss (W_m) should be measured at 550ºC. The calculated resin content should be corrected by adding the weight ratio (W_f) of inorganic fillers found in the material (data from the manufacture of the FRP rods). Then the resin matrix content (W_r) should be calculated using the equation:

$$W_r = W_m + W_f \tag{3.10}$$

If the FRP material is free from the inorganic filler, then $W_r = W_m$

The ignition loss method procedure is as follows:
The initial weight of the sample should be measured (P_t) to an accuracy of ±1%, and specimen should be heated to between 500ºC to 600ºC for 30 min or until all carbonaceous material has disappeared. Subsequently, the specimen shall be cooled to room temperature in a desiccator. The fibers shall be washed with acetone to remove particles from the surface of the fibers. This step should be repeated until the fibers bath in clear acetone. After the fibers are cleaned, they should be evaporated in an oven set to 70ºC before weighing the specimen (P_f) to an accuracy of ±1%. The resin matrix content (W_r) should be calculated with the following equation:

$$W_r = 100 - \frac{P_f}{P_t} \tag{3.11}$$

2. Determination of the enthalpy of the resin matrix of the FRP material. If it is provided by the manufacturer or if it was determined in previous tests the step can be omitted.

Using a balance capable of weighing to an accuracy of ±1 mg, a sample of 5 to10 mg of the liquid resin matrix used in FRP material shall be weighed, in a clear metal pan that is hermetically sealed. The pan should be placed onto an appropriate heating element of the calorimeter. The calorimeter

heating should be set up between 10ºC/min and 20ºC/min. To highlight the heat flow baseline, it should be chosen that the start and stop temperatures are before and after the exothermal reaction corresponding to cross - linking. The purging gas (nitrogen) should be set up between 50 ml/min and 80 ml/min. Subsequently, the cycle should be recorded. The resin matrix enthalpy should be calculated (ΔH_{total} (J/g)). As the beginning and end of the exothermic reaction, the researchers should choose the start and stop temperatures of integration, defined as a deviation from the baseline of the heat flow.

3. Determination of the residual enthalpy of polymerization of the material.

The sample of the specimens (P_s) shall be 5 to 75 mg to an accuracy of ±1 mg. The new weight of the resin matrix (P_r) should be calculated:

$$P_r = P_s * W_r \tag{3.12}$$

where: W_r is the resin matrix content; P_r should be used as an input in the interface of the calorimeter

The sample should be placed into a calorimeter, and the same procedure should be repeated as for the determination of enthalpy of polymerization. By using the analysis of the calorimeter interface, the resin enthalpy of polymerization of the specimen (ΔH_R (J/g)) should be calculated.

Calculations

The cure ratio is calculated as:

$$C\ (\%) = \frac{\Delta Htotal - \Delta HR}{\Delta Htotal} * 100 \tag{3.13}$$

where: $C(\%)$ − cure ratio [%]; $\Delta Htotal$ −enthalpy of polymerization of the resin matrix [J/g]; ΔHR − residual enthalpy of polymerization of the specimen [J/g]

Chapter 4

PROPERTIES OF GFRP BARS BASED ON STANDARD QUALITY CONTROL TESTS

4.1 Introduction

This chapter presents research work on mechanical testing of GFRP bars. In addition, cure ratio tests are presented. Efficient testing and rational evaluation of the obtained results allow for quality assessment of reinforcing bars, which in turn promotes wider and more confident utilization of these products in construction. In this work, short-term testing is described, and the recorded obtained results are evaluated in terms of information obtained on strength, stiffness, and bar's quality (durability). Five basic tests (tensile, shear, flexure, compression, and cure ratio) were performed and evaluated for bars from the same manufacturing batches. The information provided should help in the selection of proper testing procedures, adequate sample preparation and interpretation of results. It should be noted, that the long-term goal of this research program is the development of quality assessment testing protocols for GFRP bars that would be fast, and provide objective information on quality and strength.

Even though the most common manufacturing process for GFRP is pultrusion, GFRP bar production procedures can yield bars of variable quality in terms of material properties and bar geometry. Moreover, GFRP bars are often produced in a bent configuration. The manufacturing procedures of bent bars are unique for each manufacturer, and thus the quality of the resulting products is difficult to assess (Weber and Witt 2011). Several testing protocols have been implemented to ensure product quality. First, a manufacturer must do product qualification testing to place the product on the market. Quality control testing is a standard protocol for all manufacturers that must be performed for every product lot that will be placed in construction. In Canada, these tests are based on [3] CSA S807-10 and include the tests specified in Table 1.

Systematic research on quality control tests started in the early 1990s. Holte et al. 1993, Erik and Rizkalla 1993, and Bakis 1996 were among the first researchers who proposed several testing

procedures. Those developed methodologies are still in use, not only as property indicators but also as part of other more complicated tests: creep-rupture, or fatigue (Nkurunziza et al. 2005). Some testing methodologies have been evaluated (e.g., shear test, Gentry 2011), or modified to suit specific needs (Adimi et al. 2000). The testing procedures for GFRP bars are comprehensive; however, with many different products available in the market nowadays (different diameters and material compositions), routine testing of the bars is becoming increasingly complex. Therefore, improvements leading to simpler and faster, yet rational, testing protocols for quality control and assurance testing are needed.

Table 4.1 – Quality control test per Ministry of Transportation Ontario

Property	Standard for Test
Cross section area	CSA S806, Annex A
Longitudinal tensile strength for straight bars and straight portion of the bent bars	CSA S806, Annex C; ASTM D7205
Longitudinal tensile modulus and ultimate elongation for straight bars and straight portion of bent bars	CSA S806, Annex C; ASTM D7205
Transverse shear strength	CSA S806, Annex L; ASTM D7617
Longitudinal tensile strength of FRP bent bars at bend location	ACI 440.3R-B.5 or B12, ASTM D7914
Fiber content	ASTM D3171; E1131; D2584
Void content	ASTM D2734; ASTM D5117
Water absorption at 50° for straight bars, straight portion and curved portion of bent bars and grids	ASTM D570
Cure ratio for straight bars, straight portion and curved portion of bent bars and grids	CSA S807; ASTM D5028
Wet glass transition temperature	ASTM D3418; ASTM E1640

4.2 Quality control and qualification testing

In general quality control and qualification tests are the same standardized methodologies designed for both short and long-term property assessment. The difference between those two definitions is recognized as a purpose for which tests should be performed. Based on information that is needed the quality control tests can be limited to those procedures that give the most important properties (e.g., tensile and shear strength, moisture absorption or durability). In effect, evaluation of material performance is made accordingly to the information obtained from these tests. The quality control testing should be carried out recurrently as routine inspections. On the other hand, qualification testing is performed mostly for new products, or if any changes were introduced to the material or

production process. Qualification testing consists all tests specified by the standard regulations (CSA S807-10) that were used for material characterization, including all mechanical, physical and durability properties.

While the qualification testing should be performed in detail without any cost or time limitation, the quality control testing usually should be done quickly; the test should be relatively easy to perform and considering a frequent repeatability should not be costly. This part of research is aimed to investigate a performance of four basic testing procedures (tensile, shear, flexure strength estimation and cure ratio test) used daily as a quality control tests. In addition, compression strength investigation methods were studied. Tests were evaluated accordingly to constantly changing mechanical and physical characteristics of the material. Detailed descriptions of tested material and the test itself are available in a previous chapter.

4.2.1 Tensile test

Testing procedure

Tensile tests were performed according to Annex C of CSA S806-12. The test method determines longitudinal strength, elongation properties, modulus of elasticity, and the stress-strain curve. According to the standard, a specimen should be attached to the testing machine by an anchorage device, which assures pure tensile stress. The anchorage system was chosen based on prescribed requirements, as presented in Fig. 4.1a. Specimens were tested using a MTS testing machine with total capacity of 500kN (Fig 4.1b)

The test was conducted on a 500kN machine with a load control rate of 300MPa/min. In effect, different load rates were applied to bars of different diameters:
Company I

- 76kN/min for 18mm bars
- 46kN/min for 14mm bars

Company II

- 60kN/min for 16mm bars
- 34kN/min for 12mm bars

a)

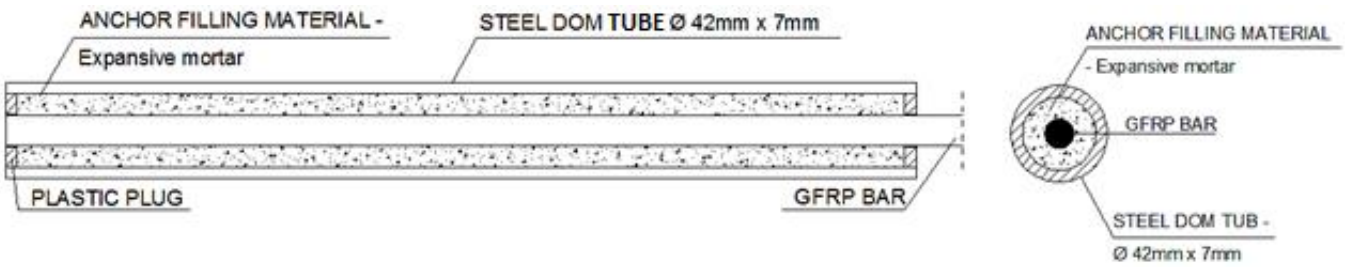

b)

Fig. 4.1 – a) Anchorage system for tensile test specimen, b) tension test in progress

Specimens were divided into two groups: straight bars (SB) and straight portions of bent bars (BB). Eight samples of the BB specimens were tested for each diameter to check for consistency. In the case of the straight bars, the test consisted of five bars for each diameter. Specimen lengths were 40 times the bar diameter plus twice the anchorage length, as shown in Table 4.2. Bars were cast into steel tubes using expansive mortar (Fig. 4.2).

Table 4.2 – Tensile test specimen dimensions

Bar type	Effective diameter	Free length	Anchorage length	Total length
SB (1–5)	12/14 mm	480/560 mm	380 mm	1250/1320 mm
SB (6–10)	16/18 mm	640/720 mm	380 mm	1400/1480 mm
BB (1–8)	12 mm	480 mm	380 mm	1250 mm
BB (9–16)	16 mm	640 mm	380 mm	1400 mm

a) 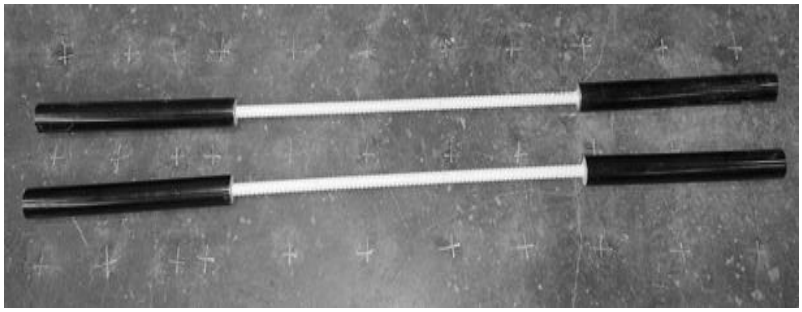 b) 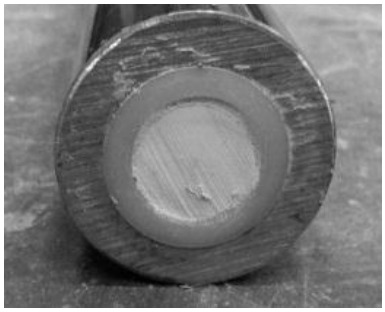

Fig. 4.2 – Tensile test specimen M16 bar – length 1400mm a) overall view, b) end view

The load and the displacement of the bar were recorded during the test. The load cell of the test frame recorded the loads. The displacements were measured using an extensometer with a 145mm gage length, mounted in the middle of the bar, and these displacements were subsequently used for strain calculations. The extensometer was detached from the samples at approximately 75% of the ultimate bar strength to avoid damaging the device at failure. Displacements of the crosshead of the test machine were recorded until failure of the bars.

Results and discussion

Results from the tensile tests are available for the bars from company II only. For Company I, pre-testing was conducted using the standard anchorage length (ASTM D7205 – 380mm). The samples failed by debonding of the DOM tubes from the bar (Fig. 7). The test was then repeated with larger anchorage lengths, 430 and 480mm, respectively. However, the same failure occurred. Several attempts to modify the anchorage type for sand coated specimens were tried, including using epoxy tube fillers or splitting the tube in half to provide semi-direct pressure from the grips. Further investigation of the issue revealed that a minimum of 630 mm of anchorage length for the #5 bars and 510 mm for the #4 bars was needed (anchorage length used by the manufacturer). This would increase the required total length of the specimens from 1480 mm (the sample length that we had available) to 1980 mm for the #5 bars; and from 1320 mm (available length) to 1580 mm for the #4 bars. The available test samples and equipment did not allow to proceed with tensile testing for Company I specimens, and it was decided that only samples from Company II would be tested in tension.

a) 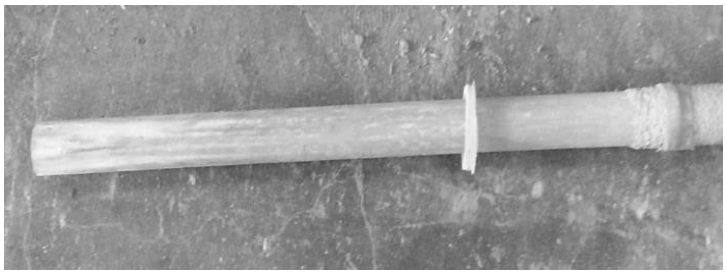 b) 

Fig. 4.3 – Company I bars' anchorage failure a) bar view, b) tube view

Test results include the tensile strength of a bar, calculated as a maximum force recorded at failure divided by the bar effective cross-section area (eq.3.1), the stress-strain relationship where strains were obtained from the displacement transducer attached to the middle section of the bars and stresses obtained from the load cell on the test machine and the measured cross-sectional area, and finally the modulus of elasticity obtained from the stress-strain relationship (eq.3.4). Graphical interpretations of all results are available in Appendix 1. Note that stress-strain curves are only shown until approximately 75% of ultimate strength as the displacement transducer was removed at this stage. Table 4.3 presents an overview of the obtained values for maximum tensile strength and modulus of elasticity. The maximum (break) mean tensile forces for straight bars (SB) bars were 138.3kN and 255.2kN for M12 and M16, respectively. For bent bars (BB), the mean maximum forces were 144.8kN and 261.6kN for M12 and M16, respectively. All specimens did show linear elastic behavior to breakage without any ductility, with a sudden failure. The failure of SB bars occurred by a brittle burst of the bar and fiber delamination (Fig.4.4 a), while the plastic tube of the BB bars kept the fibers in place (Fig.4.4 b). All samples have similar moduli of elasticity for the same bar type, with slightly larger modulus for SB bars. This can be due to a greater amount of glass fibers in straight bars SB (75% by volume) than in BB bars (60% by volume). This also has an influence on the displacements, with the BB bars having a larger total elongation of 4-5%, while maximum elongation for the SB bars does not exceed 3.5%. Since all bars showed very similar behavior, results from just one representative bar diameter are shown in Fig. 4.5 and Fig. 4.6.

a)  b) 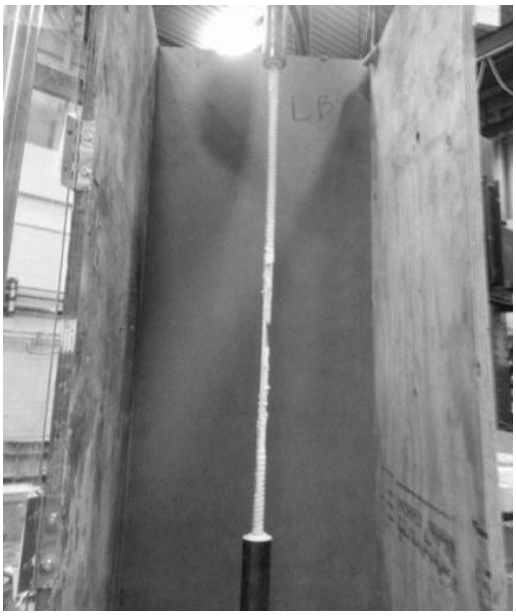

Fig. 4.4 – Specimen failure a) SB bar, b) BB bar

Table 4.3 – Tensile test results

Straight bars (SB) properties							
Sample	M12			Sample	M16		
	Ultimate capacity [kN]	Tensile strength [MPa]	Modulus of elasticity [GPa]		Ultimate capacity [kN]	Tensile strength [MPa]	Modulus of elasticity [GPa]
mean	139	1223	62	mean	255	1270	63
s.d	4	32	3.4	s.d	4	56	1
cov	0.03		0.05	cov	0.04		0.02
Straight portion of the bent bars (BB) properties							
Sample	M12			Sample	M16		
	Ultimate capacity [kN]	Tensile strength [MPa]	Modulus of elasticity [GPa]		Ultimate capacity [kN]	Tensile strength [MPa]	Modulus of elasticity [GPa]
mean	145	1280	55	mean	262	1302	54
s.d	13	109	3	s.d	16	102	1
cov	0.09		0.05	cov	0.08		0.02

a)

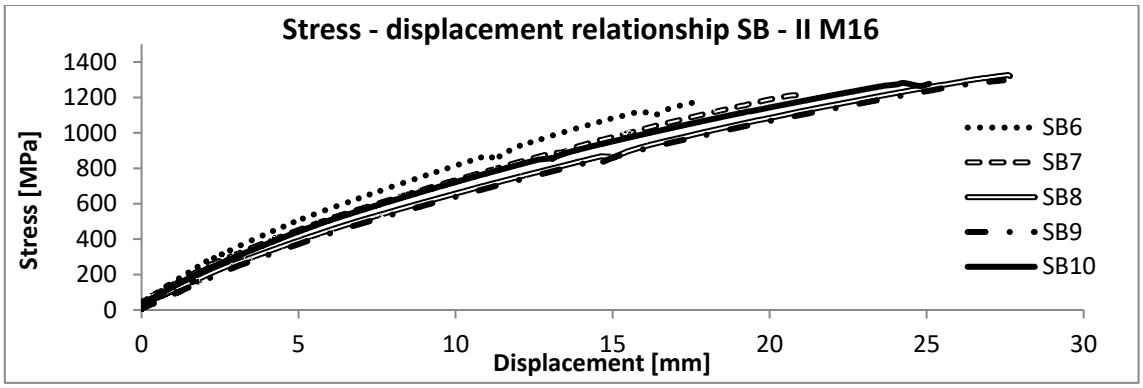

b)

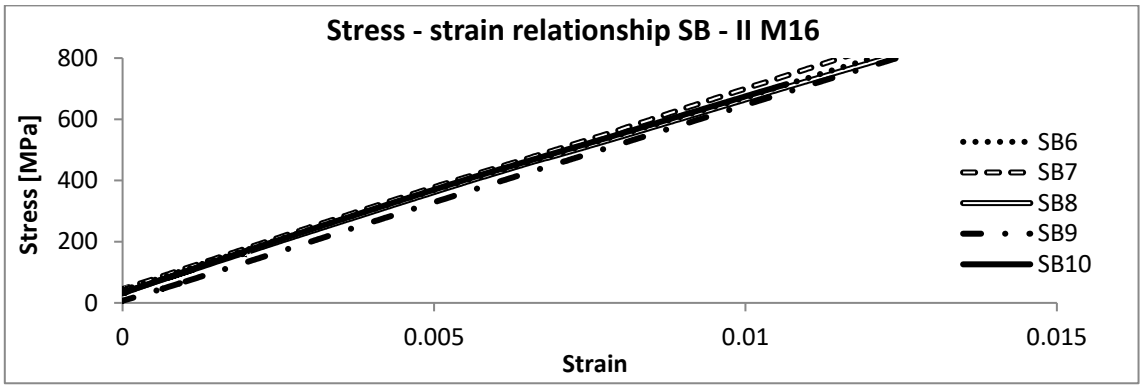

Fig. 4.4 – a) Stress-displacement and b) stress-strain relationship

a)

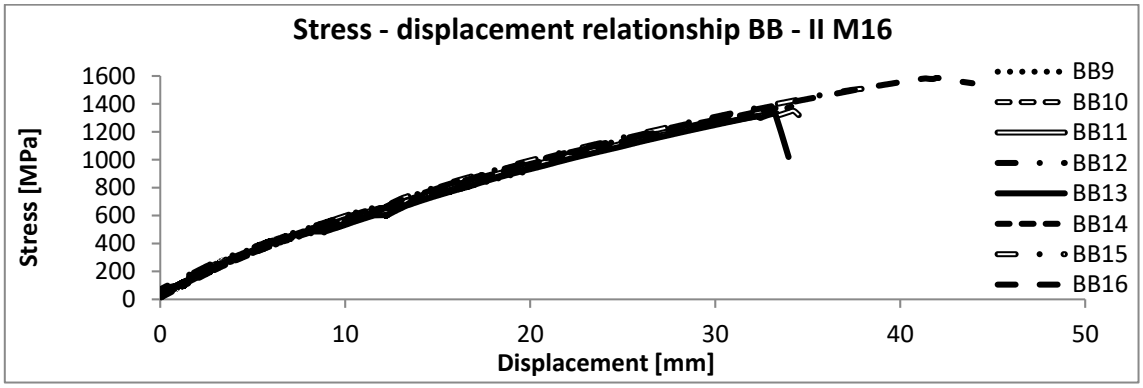

b)

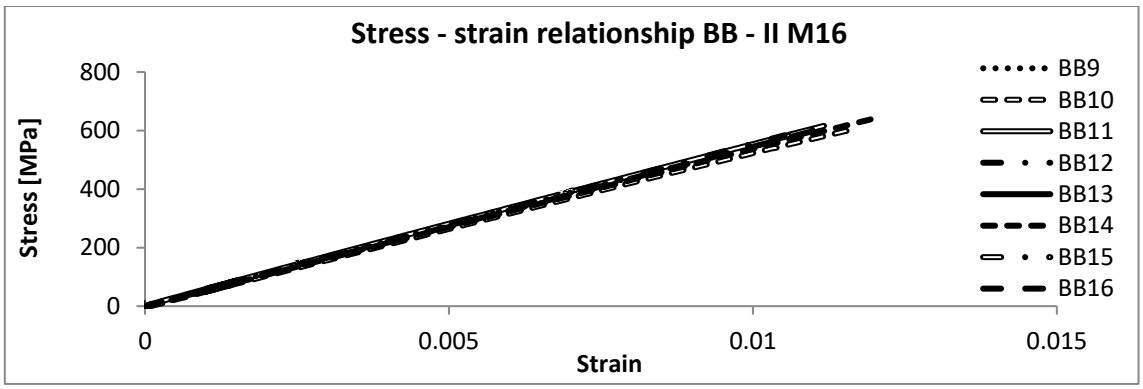

Fig. 4.5 – a) Stress-displacement and b) stress-strain relationship

4.2.2 Shear test

Testing procedure

Shear tests were performed according to Annex L of CSA S806-12; the test method has been designed to determine transverse shear strength. Three different types of bars from both manufacturers were used in these tests: smooth surface bars (SSB) as control specimens, straight bars (SB), and straight portions of bent bars (BB). Specimens were divided into 6 sets per bar type and diameter, and each set consisted of 8 samples. All specimens were 300 mm long. Double shear was applied to each specimen using a special shear test device (Fig. 4), with a 45 MPa/min load control rate. Due to different bar diameters, the load control rate varied for each bar size as shown in Table 4.4.

Table 4.4 – Test load rates

Company I				Company II			
Load rate	SSB and SB	#4	14	SSB	12M	13	kN/min
Load rate		#5	23		16M	23	kN/min
Load rate	BB	#4	10	SB and BB	12M	10	kN/min
Load rate		#5	18		16M	18	kN/min

The shear test device consists of 1) two bar holders, 2) two bottom blades specific for the outside diameter of each bar, and 3) guides used to create distance between the bottom blades. The shear load is applied to the bar by the upper blade attached to the machine load cell. For each bar diameter, a separate set of blades was manufactured.

a)  b) 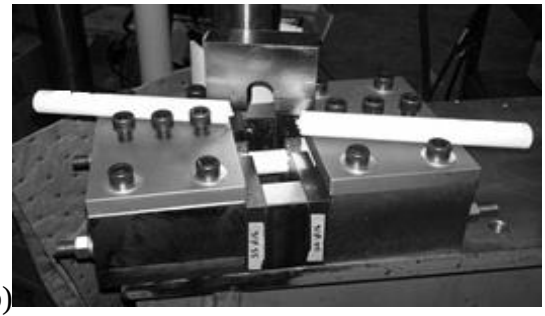

Fig. 4.6 – Shear test device with a sample a) before testing, b) after testing

Results and discussion

The primary test result is the transverse shear stress, calculated as half of the peak failure load divided by the cross-section area (effective cross-section area reported in Table 3.2). The graphical interpretation of the test can be shown in both: stress-displacement and stress-strain configurations. Different failure modes can be observed in these tests; when both planes fail at the same time (Fig. 4.7 a), and when one plane fails after the other (Fig. 4.7 b). The results are shown in Table 4.5 for

strength and table 4.6 for shear modulus. Graphical interpretations of all results are available in Appendix 2.

a)

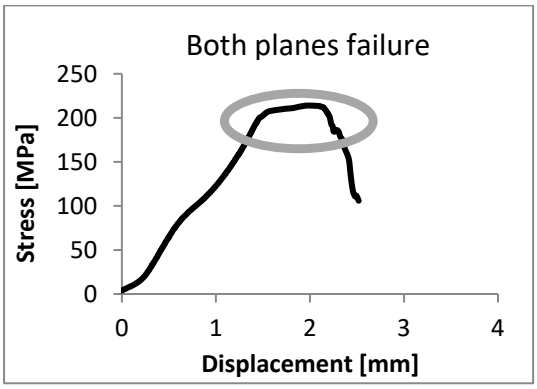

b)

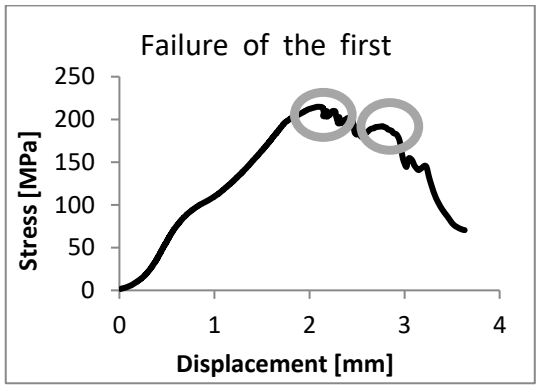

Fig. 4.7 – Shear failure modes a) double shearing b) one plane shearing before another

To further analyze the response of bars in shear tests, stress-strain relationships were calculated as the stress versus strain (displacement of the blade divided by the diameter of the bar), and the comparison of the most typical curves for each type of bar is shown in Fig. 4.8a for Company I, and Fig. 4.8b for Company II.

a)

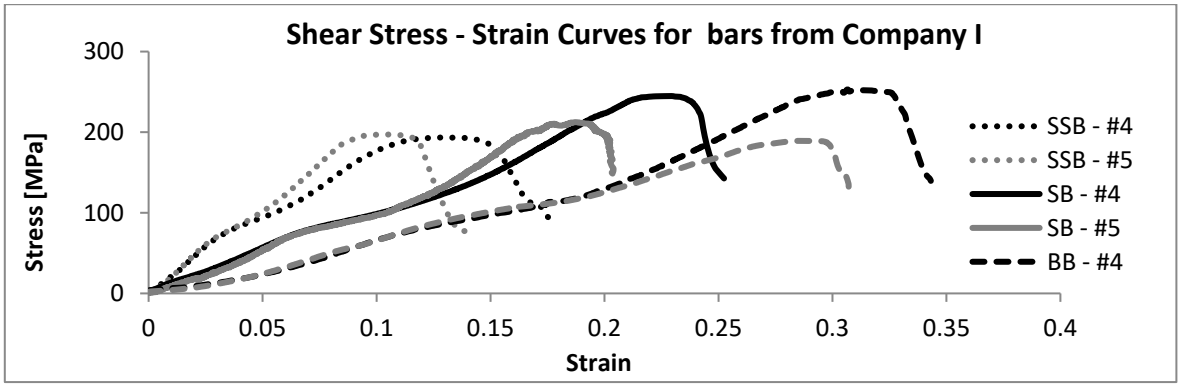

b)

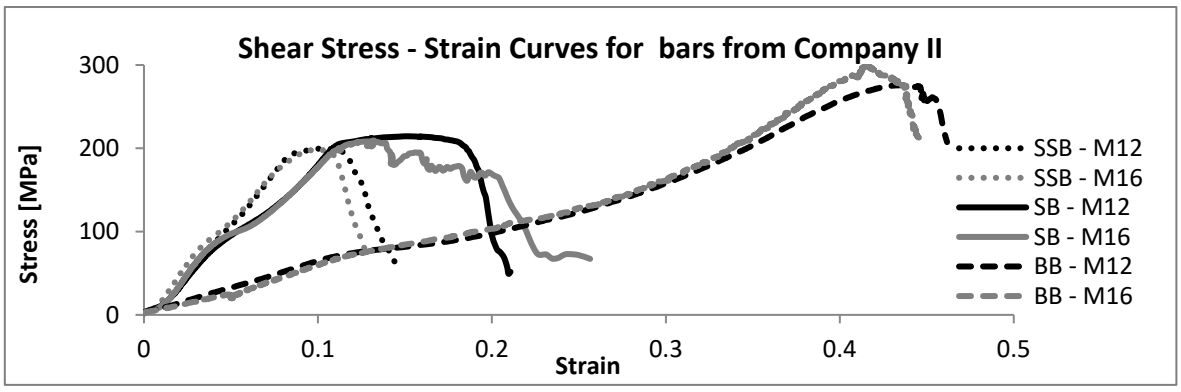

Fig. 4.8 – Shear Stress-strain curves a) Company I b) Company II

Table 4.5 – Shear strength test results

Company I				
Sample	Smooth bars (SSB)			
	#4		#5	
	Shear Strength [MPa]	Ultimate capacity [kN]	Shear Strength [MPa]	Ultimate capacity [kN]
mean	195	60	192	98
s.d.	1.7	6	12	5.8
cov	0.01		0.06	
Sample	Sand coated bars (SB)			
	#4		#5	
	Shear Strength [MPa]	Ultimate capacity [kN]	Shear Strength [MPa]	Ultimate capacity [kN]
mean	242	74	214	109
s.d.	24	7.4	5	3.3
cov	0.1		0.03	
Sample	Bent bars (BB)			
	#4		#5	
	Shear Strength [MPa]	Ultimate capacity [kN]	Shear Strength [MPa]	Ultimate capacity [kN]
mean	247	56	191	77
s.d.	7	1.7	10	4
cov	0.03		0.05	
Company II				
Sample	Smooth bars (SSB)			
	M12		M16	
	Shear Strength [MPa]	Ultimate capacity [kN]	Shear Strength [MPa]	Ultimate capacity [kN]
mean	197	56	194	99
s.d.	5.7	1.7	5.7	3
cov	0.03		0.03	
Sample	Ribbed bars (SB)			
	M12		M16	
	Shear Strength [MPa]	Ultimate capacity [kN]	Shear Strength [MPa]	Ultimate capacity [kN]
mean	221	50	210	84
s.d.	10.7	2.5	17	6.7
cov	0.05		0.08	
Sample	Bent bars (BB)			
	M12		M16	
	Shear Strength [MPa]	Ultimate capacity [kN]	Shear Strength [MPa]	Ultimate capacity [kN]
mean	289	65	280	112
s.d.	18	4	22	9
cov	0.06		0.08	

The larger bars have smaller shear strength. The influence of different bar finishing is visible for shear moduli, where the largest moduli were obtained for smooth surface bars. BB bars from

Company II show the highest shear strength with the biggest maximum strain. It is probably caused by the polyethylene sleeve, which covers these bent bars. Examination of the curves in Figure 4.8 shows that shear modulus is stress dependent. Also, there is a definite initial stiffness, followed by a plateau, and then the second stiffness region. This behavior was observed for all tested bars.

The shear modulus was calculated as a secant, separately for two regions: the first before a plateau, and the second after the plateau (Fig. 4.9). The shear moduli for SSB bars are similar for both regions (for both companies), with slightly smaller values for H2. In the case of the SB bars, samples from Company II show the same behavior as SSB samples, while SB bars from Company I show smaller H1 moduli. The smallest shear modulus was obtained for BB bars from both companies, with H2 slightly larger (except for BB #5).

Table 4.6 – Shear modulus test results [GPa]

	Company I				Company II			
Sample	Smooth bars (SSB)				Smooth bars (SSB)			
	#4		#5		M12		M16	
	H1	H2	H1	H2	H1	H2	H1	H2
mean	2.5	2.2	2.6	2.4	2.6	2.6	2.7	2.5
s.d.	0.16	0.13	0.2	0.09	0.12	0.14	0.09	0.04
cov	0.06	0.06	0.08	0.04	0.05	0.05	0.03	0.02
Sample	Sand coated (SB)				Ribbed bars (SB)			
	#4		#5		M12		M16	
	H1	H2	H1	H2	H1	H2	H1	H2
mean	1.2	1.7	1.3	2	2.3	2.1	2.3	2.1
s.d.	0.04	0.13	0.09	0.12	0.06	0.12	0.06	0.07
cov	0.03	0.7	0.06	0.06	0.02	0.05	0.02	0.03
Sample	Bent bars (BB)				Bent bars (BB)			
	#4		#5		M12		M16	
	H1	H2	H1	H2	H1	H2	H1	H2
mean	0.9	1.3	0.95	0.9	0.6	1	0.7	1.2
s.d.	0.06	0.11	0.13	0.12	0.05	0.07	0.07	0.08
cov	0.07	0.09	0.14	0.13	0.06	0.05	0.08	0.05

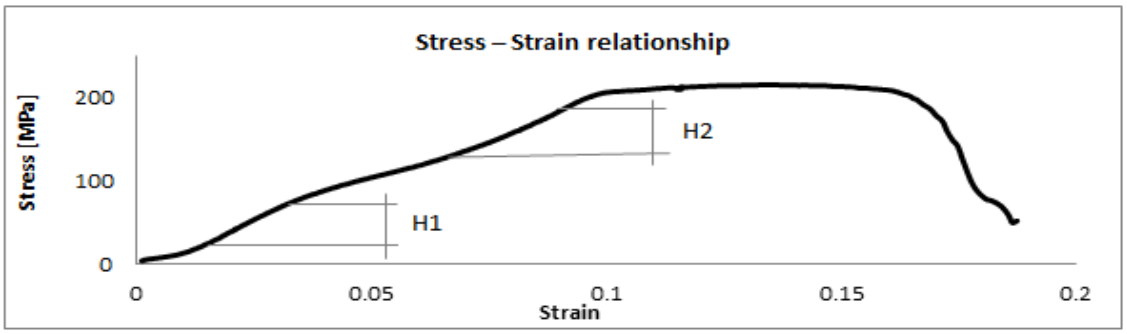

Fig. 4.9 – Shear modulus – calculation concept

4.2.3 Flexure test

Testing procedure

Canadian standard CSA S807-10 specifies that the flexure properties test method should be conducted according to ASTM D4476-09. The test method determines the longitudinal strength of outer fibers (rupture modulus, eq. 3.6), modulus of elasticity (eq. 3.7) and the stress-strain relationship. In the method, the specimen is tested like a simple beam with three-point bending until failure or until fiber strain reaches 5%. The tests were conducted using a 3mm/min displacement rate. Sample dimensions depended on the bar diameter and are shown in Table 4.7. The shape of the semicircular cross-section shown in Fig. 4.10 a) was created by water-jet cutting along the bar length, and resulted in moderate variations in dimensions; thickness of all samples was measured before testing. The use of a semi-circular cross-section eliminates premature compression shear. The test consisted of 5 samples for each type of bar, for both manufacturers (SSB, SB, BB). A fixture was made to properly hold specimens. It consists of a base with two supports and special roll holders unique to each bar diameter (Fig. 4.10b).

Table 4.7 – Flexure test specimen dimensions

	Bar type	Bar size	Φ [mm]*	T [mm]	α°	Total length [mm]
Company I	SSB	#4	14	6 – 6.6	82 – 87	150
	SSB	#5	18	7.6 – 8.3	81 – 86	180
	SB	#4	14	6.1 – 66	82 – 87	150
	SB	#5	18	7.6 – 8.4	82 – 86	180
	BB	#4	12	5.2 – 6	82 – 90	150
	BB	#5	16	7.2 – 8.3	85 – 90	180
Company II	SSB	M12	13.5	2.5 – 7	88 – 90	150
	SSB	M16	18	7.8 – 8.7	80 - 85	180
	SB	M12	12	4.8 – 5.8	78 – 87	120
	SB	M16	16	6.6 – 6.9	80-82	150
	BB	M12	12	4.2 – 5.5	72 - 85	150
	BB	M16	16	6.2 – 6.9	77 – 82	180

a) 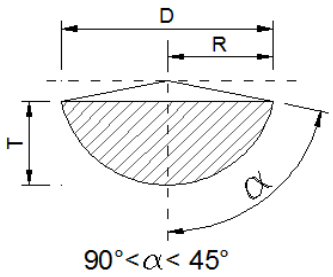

b) 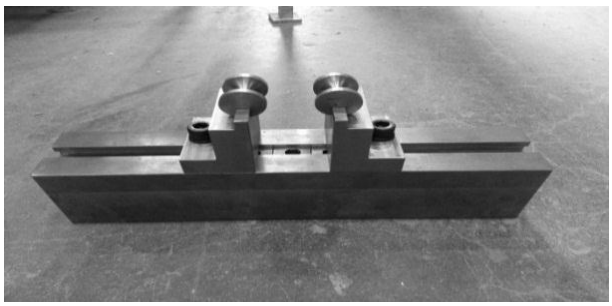

Fig. 4.10 – a) Specimen cross-section, b) Flexure test device

Results and discussion

The results from the flexure test were the tensile strength of the external fibers (modulus of rupture) and the modulus of elasticity in bending (Table 4.8). All tested specimens failed by the desired tensile rupture of the external fibers (Fig.4.11). Stress-strain curves have been developed from recorded data. Due to high similarity only results for two bar diameters are shown below (Fig.4.12 for Company I-bar #5 and Fig.4.13, for Company II-bar M16). Graphical interpretations of all results are available in Appendix 3. It should be noted that consistent with the standard CSA S806, the strains and moduli were calculated assuming the same stiffness in tension and compression.

a) 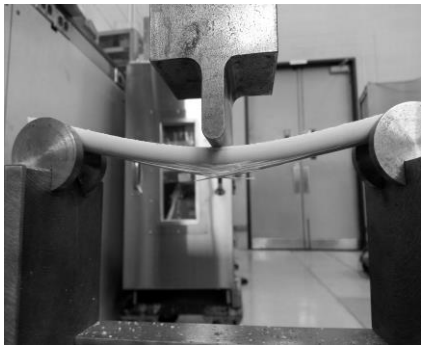 b) 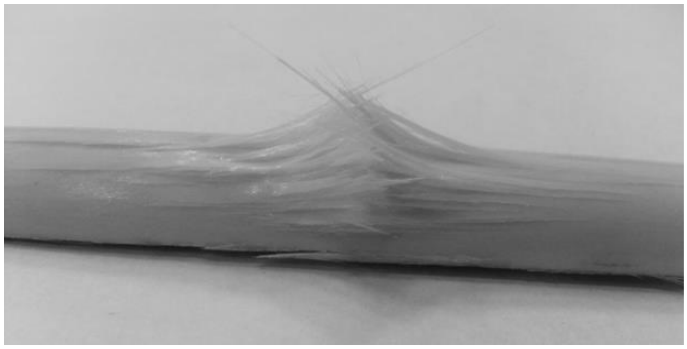

Fig. 4.11 – a) Test in progress b) failure mode of specimens tested in flexure

Rupture moduli (tensile strength in bending) of bars with a smaller diameter, for all cases, are larger or at least equal (BB bars from Company II and SSB bars from Company I) to the moduli of bars with a larger diameter. This apparent size effect is linked with fewer imperfections in smaller bars and the shear lag effect. Finally, comparing Company II results from the flexure test with the values obtained from the direct tension, it can be noticed that the modulus of elasticity values for the same type of bars are similar: around 65GPa for SB bars and around 55GPa for BB bars. The tensile strength from bending (of the outer fibers) is higher than the strength from the direct tensile test. It is likely caused by testing a much smaller area in the case of flexure test than in the direct tension test; the imperfections in the bar cross-section influence the direct tensile strength much more than the flexure test results. This is a well-known phenomenon for brittle materials (Laws 1982). This also shows the potential of using flexure test for the estimation of the FRP tensile strength (similarly as it is done for concrete). Investigation of tensile-flexure strength correlation is explored in detail in Chapter 5.

Table 4.8 – Flexure test results

Company I					
Smooth surface bar (SSB) properties					
Sample	#4		Sample	#5	
	Strength [MPa]	Modulus of elasticity [GPa]		Strength [MPa]	Modulus of elasticity [GPa]
mean	1687	56.8	mean	1544	54.3
s.d	46	1.5	s.d	56	1
cov	0.02	0.03	cov	0.03	0.02
Straight bars (SB) properties					
Sample	#4		Sample	#5	
	Strength [MPa]	Modulus of elasticity [GPa]		Strength [MPa]	Modulus of elasticity [GPa]
mean	1646	51	mean	1510	47
s.d	42	0.7	s.d	42	2.2
cov	0.03	0.01	cov	0.03	0.04
Straight portion of the bent bars (BB) properties					
Sample	#4		Sample	#5	
	Strength [MPa]	Modulus of elasticity [GPa]		Strength [MPa]	Modulus of elasticity [GPa]
mean	1557	60	mean	1403	47
s.d	54	2	s.d	49	1
cov	0.03	0.03	cov	0.03	0.02
Company II					
Smooth surface bar (SSB) properties					
Sample	M12		Sample	M16	
	Strength [MPa]	Modulus of elasticity [GPa]		Strength [MPa]	Modulus of elasticity [GPa]
mean	1757	66	mean	1763	60
s.d	80	0.9	s.d	46	0.1
cov	0.04	0.01	cov	0.02	0.002
Straight bars (SB) properties					
Sample	M12		Sample	M16	
	Strength [MPa]	Modulus of elasticity [GPa]		Strength [MPa]	Modulus of elasticity [GPa]
mean	1920	67	mean	1835	64
s.d	105	3	s.d	85	2
cov	0.05	0.05	cov	0.04	0.03
Straight portion of the bent bars (BB) properties					
Sample	M12		Sample	M16	
	Strength [MPa]	Modulus of elasticity [GPa]		Strength [MPa]	Modulus of elasticity [GPa]
mean	1684	66	mean	1572	65
s.d	82	4	s.d	165	5
cov	0.05	0.07	cov	0.1	0.08

a)

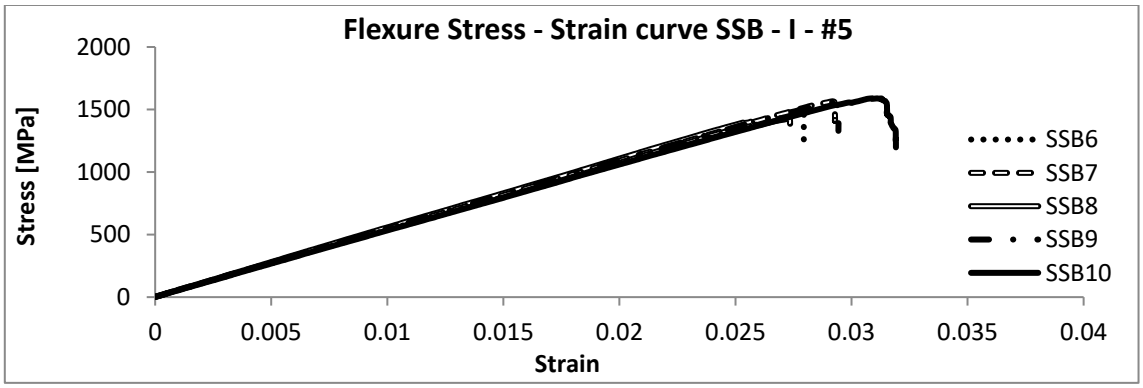

b)

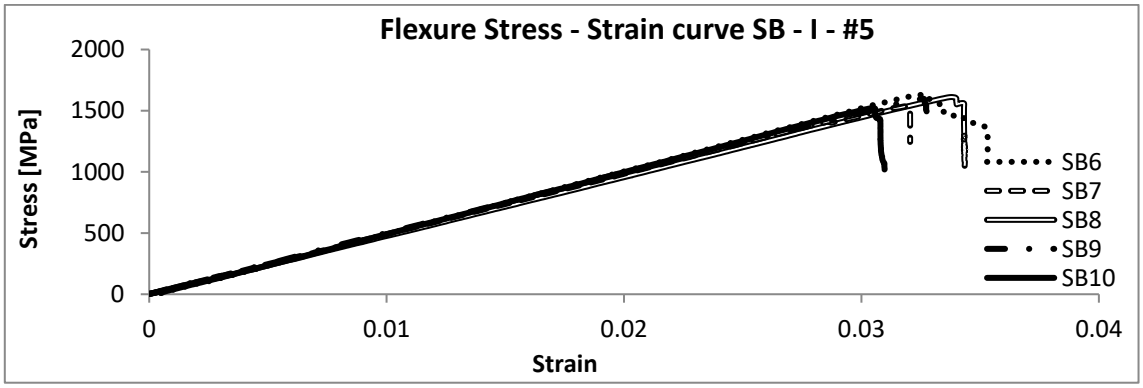

c)

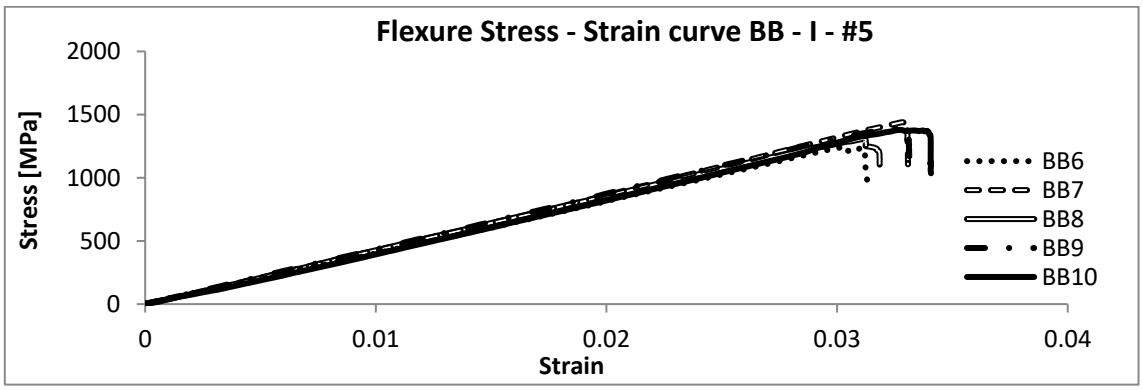

Fig. 4.12 – Stress-strain relationship in flexure for a) SSB b) SB c) BB #5 bars Company I

a)

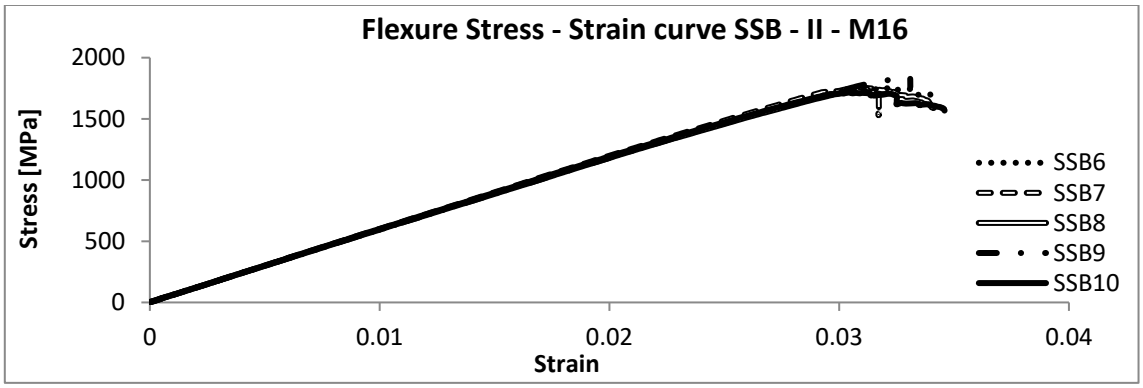

b)

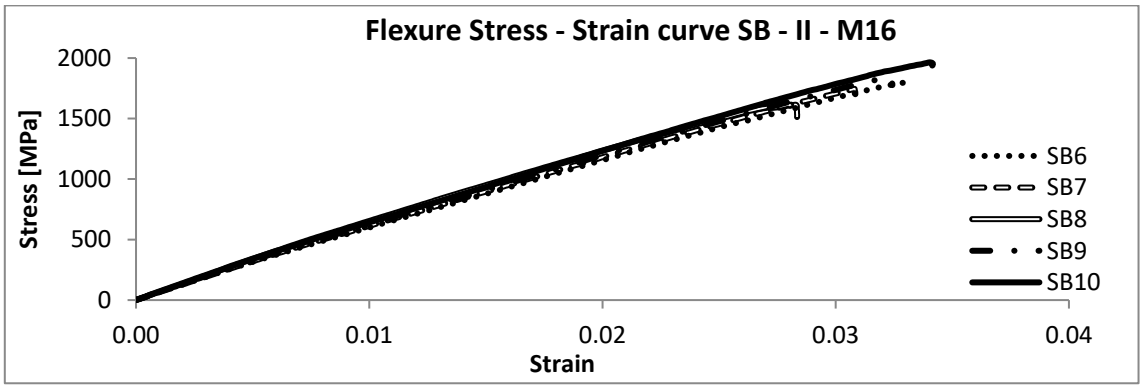

c)

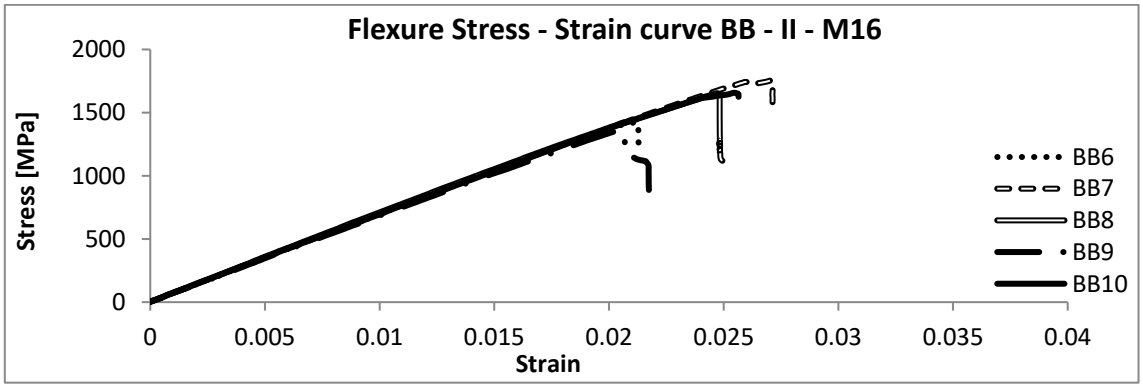

Fig. 4.13 – Stress-strain relationship in flexure for a) SSB b) SB c) BB M16 bars Company II

4.2.4 Compression test

Testing procedure

Two methodologies were used for compression testing; the first one was based on Canadian standard CSA S807-10 that specifies compression properties of GFRP bars should be determined by the procedure described in ASTM D695-10. This test method determines the compression strength, compression modulus of elasticity and stress-strain curve. Two different types of bars from both manufacturers were used in this test: SB and BB bars. The specimen length was chosen as twice the bar diameter. In effect, bars with different diameters had different lengths (Table 4.9).

Five samples for each bar type and each diameter were tested. To achieve perfect parallel plane alignment between both ends of a bar and the compression platens, diamond blade cutting and additional smoothing of the sample surface was applied (Fig. 4.15a). Specimens were tested in a 500 kN machine with the displacement rate control equal to 1.3 mm/min.

The second methodology is based on the ASTM D3410/D3410M-03 protocol. One type (SB-bars) and one size of the specimen (M12 and #4) were tested from each company. Similar to the tensile test, compression samples have to be attached to the testing machine by an anchorage device, which applies a uniform compression stress at the middle of a sample. For this purpose, 125 mm long DOM (Drawn Over Mandrel) tubes were chosen (Fig. 4.15b). The sample length should be chosen short enough to be free from buckling, but long enough to allow stress decay to uniform uniaxial compression and minimize the Poisson restraint influence due to anchorage. In effect, specimens with a total length of 335 mm for Company I and 325 mm for Company II were cast into steel tubes using an epoxy resin (Fig.4.14). The load, displacement (readings from the testing machine) and strain (from strain gauges) at the middle of the bar were recorded during the test. Specimens were tested in a 500 kN machine with a displacement rate control equal to 0.5 mm per minute.

Table 4.9 – Compression test specimen dimensions

Bar type	Bar size	Φ [mm]	length [mm]	Bar type	Bar size	Φ [mm]	length [mm]
Company I				Company II			
SB	#4	14	28	SB	M12	12	24
SB	#5	18	36	SB	M16	16	32
BB	#4	12	24	BB	M12	12	24
BB	#5	16	32	BB	M16	16	32

a) 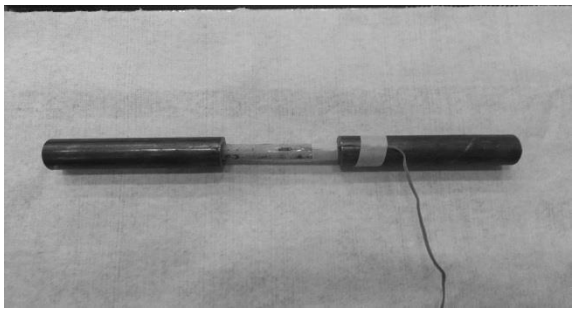 b) 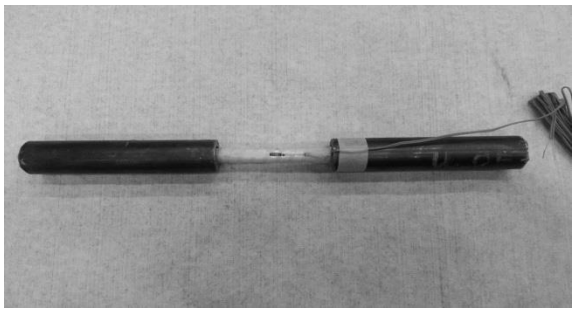

Fig. 4.14 – Compression sample for ASTM D3410-03 a) Company I b) Company II

a) 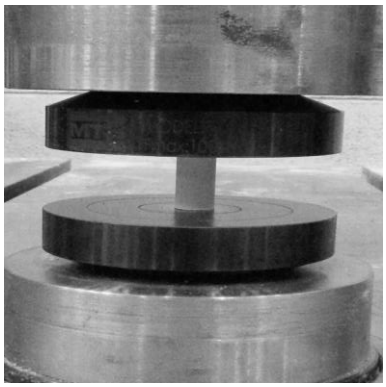 b) 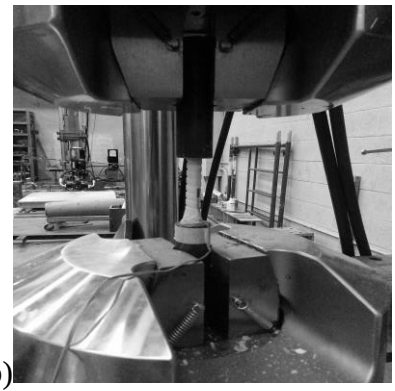

Fig. 4.15 – Compression test in progress a) ASTM D695-10 b) ASTM D3410-03

Results and discussion

The results from the compression test were compression strength, modulus of elasticity in compression and stress-strain relationship. The test methodology has an influence on the obtained compression moduli of elasticity. For the first test method (ASTM D695-10), the obtained average modulus value was 20 GPa for both types of bars (SB, BB) for Company I, 20 GPa for Company II SB bars and 10 GPa for Company II BB bars. Eksani (1993) reported much higher moduli in compression for GFRP bars. To investigate this further, the samples were modified. Previous samples were prepared by diamond blade cutting, which assures the accuracy of sample dimensions within 0.1 mm. The second set of samples was additionally smoothed by a lathe, and the variability of the dimensions was measured within 0.01 mm. Only of SB bars from both companies were tested. The test results for modulus of elasticity values did change (average of 30 GPa for Company I and 28 GPa for Company II), but they were still smaller than values published in the literature (about 40% less).

The compression strength measured during the test, seems to be accurate (compered to the previus findings Eksani (1993)) and consistent with values around 50% - 60% of the tensile strength. Compression strength slightly decreased for the second set of (smooth) specimens. The test results are shown in Table 4.10 for the diamond (blade) cut specimens and in Table 4.11 for the additionally smoothened samples.

Considering that the previous test method produced results dependent on the smoothness of the end surfaces of the compression specimens, a second method was employed (ASTM D3410/D3410M), which requires specimen casting into steel tubes for testing. Only one bar type (SB bars) and one bar size (M12 and #4) were used. The vobtained values are shown in Table 4.12.

The compression moduli of elasticity obtained by the second method are higher than those from the previous approach; 45 GPa for Company I and 56 GPa for Company II. This phenomenon is caused primarily by the imperfections of the sample surfaces used for the first methodology. Even after additional smoothing of the samples, the stress was not distributed evenly on the sample surface, and modulus of elasticity in compression was decreased by the additional crashing of the surface imperfections. The compressive strength of the samples obtained from this testing is similar to the strength obtained using the previously described method, which is faster and simpler. Thus, if only compression strength needs to be obtained the first procedure can be employed.

Table 4.10 – Compression test results – diamond cut specimen

Company I							
Properties of straight bars (SB)							
Sample	#4			Sample	#5		
	Strength [MPa]	Ultimate capacity [kN]	Modulus of elasticity [GPa]		Strength [MPa]	Ultimate capacity [kN]	Modulus of elasticity [GPa]
mean	690	105	21	mean	670	170	19
s.d	33	5.2	1	s.d	52	13.6	1.8
cov	0.05		0.05	cov	0.08		0.1
Properties of bent bars (BB)							
Sample	#4			Sample	#5		
	Strength [MPa]	Ultimate capacity [kN]	Modulus of elasticity [GPa]		Strength [MPa]	Ultimate capacity [kN]	Modulus of elasticity [GPa]
mean	676	76	19	mean	661	132	21
s.d	70	7.6	2	s.d	37	7.9	3
cov	0.1		0.11	cov	0.06		0.14
Company II							
Properties of straight bars (SB)							
Sample	M12			Sample	M16		
	Strength [MPa]	Ultimate capacity [kN]	Modulus of elasticity [GPa]		Strength [MPa]	Ultimate capacity [kN]	Modulus of elasticity [GPa]
mean	840	95	19	mean	817	164	20
s.d	73	8.5	0.9	s.d	51	9.8	1.5
cov	0.09		0.05	cov	0.06		0.08
Properties of bent bars (BB)							
Sample	M12			Sample	M16		
	Strength [MPa]	Ultimate capacity [kN]	Modulus of elasticity [GPa]		Strength [MPa]	Ultimate capacity [kN]	Modulus of elasticity [GPa]
mean	530	60	11	mean	480	96	10
s.d	60	6.6	0.8	s.d	25	4.8	0.8
cov	0.11		0.07	cov	0.05		0.08

Table 4.11 – Compression test results – smoothen specimen

Company I							
Properties of straight bars (SB)							
Sample	#4			Sample	#5		
	Strength [MPa]	Ultimate capacity [kN]	Modulus of elasticity [GPa]		Strength [MPa]	Ultimate capacity [kN]	Modulus of elasticity [GPa]
mean	660	101	30	mean	650	165	30
s.d	60	9.1	2.4	s.d	45	11.6	2.7
cov	0.09		0.08	cov	0.07		0.09
Company II							
Properties of [straight] bars (SB)							
Sample	M12			Sample	M16		
	Strength [MPa]	Ultimate capacity [kN]	Modulus of elasticity [GPa]		Strength [MPa]	Ultimate capacity [kN]	Modulus of elasticity [GPa]
mean	780	88	26	mean	762	153	30
s.d	52	6.2	1.3	s.d	43	9.2	2.4
cov	0.07		0.05	cov	0.06		0.08

Table 4.12 – Compression test results – alternative methodology

Company I				Company II			
Properties of straight bars (SB)							
Sample	#4			Sample	M12		
	Strength [MPa]	Ultimate capacity [kN]	Modulus of elasticity [GPa]		Strength [MPa]	Ultimate capacity [kN]	Modulus of elasticity [GPa]
mean	720	110	45	mean	880	99	53
s.d	36	5.5	2	s.d	17	2	1
cov	0.05		0.04	cov	0.02		0.02

4.2.5 Cure ratio test

Testing procedure

The cure ratio test was performed per CSA S807 Annex A. This test contains three different steps: determination of the matrix content, obtained by Thermogravimetric Analysis (TGA); determination of the enthalpy of the resin (ΔH_{total}), obtained by Differential Scanning Calorimetry (DSC); and determination of the residual enthalpy of polymerization (ΔH_R), obtained by DSC. The first two steps of the procedure can be omitted if appropriate information is provided by a manufacturer. Subsequently, the cure ratio can be calculated directly from the equation 3.13.

Due to complications with the procurement of resin matrix samples (curing during shipping) and with other confidential information from manufacturers, only one type of bars (BB bars) from

Company II were tested. However, an extensive analysis was made using samples from different spots on the bar cross-section area, to highlight typical needs and pitfalls of the test.

Results and discussion

The cure ratio of a GFRP bar was obtained for a curved bar (BB) from company II. It should be noted that such detailed analysis as described below is only possible if the resin is supplied by the manufacturer (which was the case described herein). Otherwise, enthalpy of polymerization should be taken from the information provided by the manufacturer. Also, the fiber content is usually not assessed independently and taken from the manufacturer information.

Herein the analysis was performed in three different steps. The first step is the matrix content evaluation, and Thermogravimetric Analysis (TGA) methodology was chosen for its determination. This test is based on the measurement of the mass loss of material as a function of temperature. 20-75 mg samples were taken from different parts of the GFRP bar cross-section and heated at a uniform rate increasing from room temperature to 550ºC. Subsequently, the plot of the mass change versus temperature was obtained (Fig. 4.16). Independent replicates on different parts of the bar cross-section give a spectrum of the resin content distribution along the bar radius. The value of the resin matrix content at the bar core was calculated as W_r = 15%.

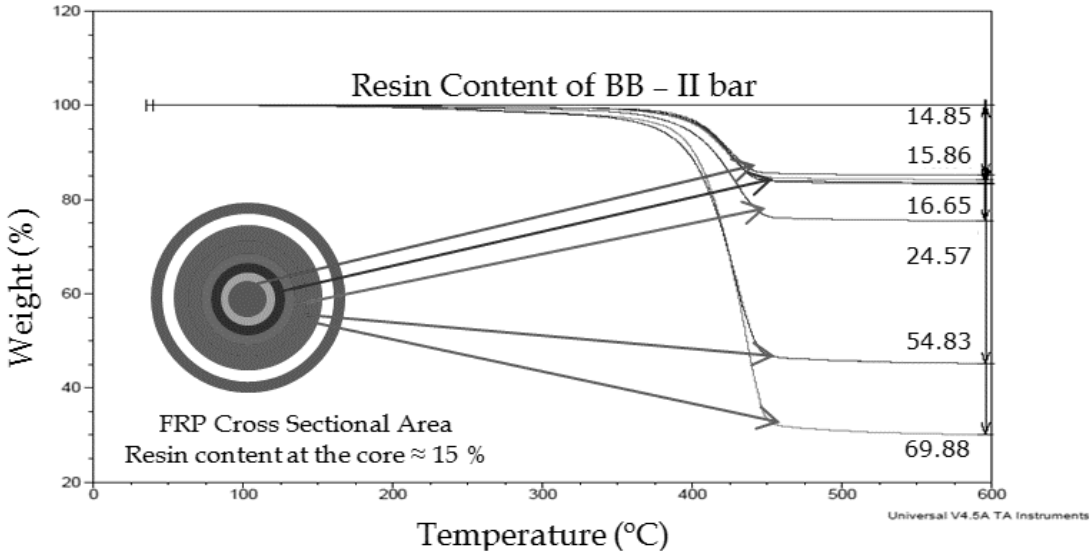

Fig. 4.16 – Mass change plot for BB bars from Company II

The second step of the cure ratio test is the determination of the enthalpy of polymerization (ΔH_{total}) of the resin. This was done via Differential Scanning Calorimetry (DSC). DSC can measure the

heat into or out of the sample relative to a reference and heats/cools the sample with a linear/modulating ramp. Samples of 2-4 mgs of the liquid resin provided by the bar manufacturer were used in this test. The specimens were placed into the inert environment (nitrogen) and heated at the rate of 10 to 20 ºC per minute. As a result of this test, heat flow versus temperature curves were collected (again, independently replicated in order to gain more confidence in the results). The mean value obtained was ΔH_{total} = 248 (J/g). Finally, determination of the residual enthalpy (ΔHR) of polymerization of the bar is the last step of the cure ratio procedure (still from the DSC step). Samples from different parts of the bar cross-section were used. The weight of the samples varied between 5-75 mg. Two typical graphs of heat flow versus temperature are shown Fig. 4.17 as a result of this test. The mean value for samples taken from the bar core was obtained as ΔHR = 40 (J/g), while for samples collected from the outer parts of the bar ΔHR = 0.

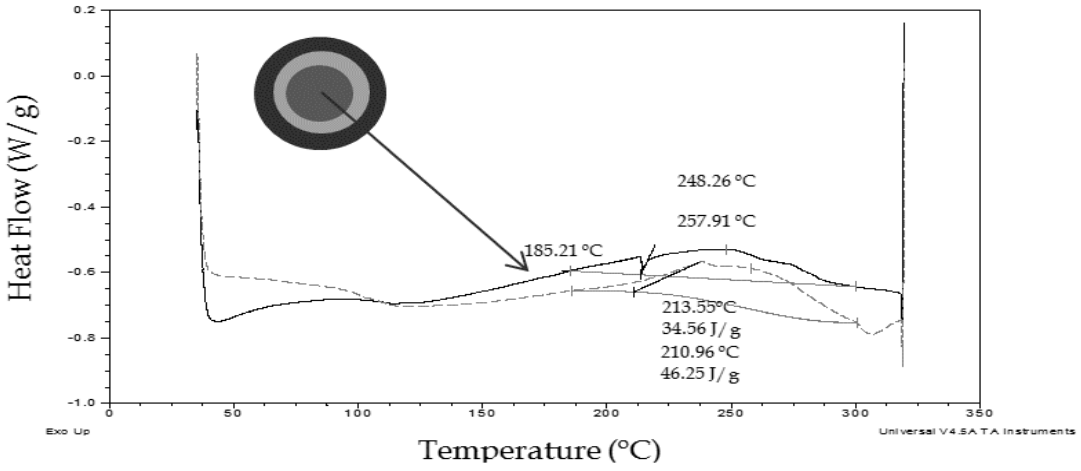

a)

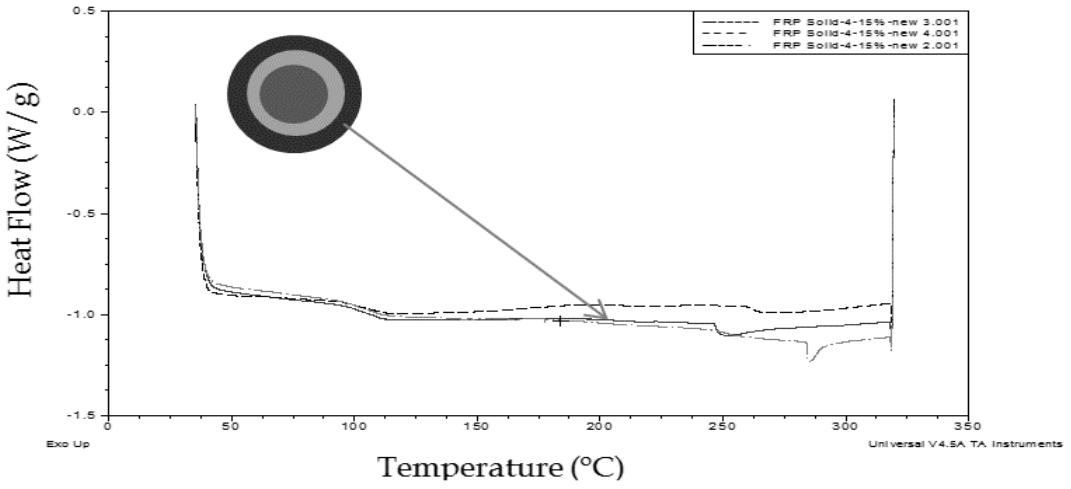

b)

Fig. 4.17 – a) Residual enthalpy of polymerization of the bar core, b) – Residual enthalpy of polymerization of the outer parts of the bar

Using the information obtained, the cure ratio of the BB bars from Company II was calculated (Eq. 3). Since the test results depend on the location of the sample taken from the bar (ΔH_R= 0-40), the cure ratio value varies between 84-100% going from inner to outer locations in the bar cross-section, respectively.

4.3 Comments and recommendations

4.3.1 Summary of test evaluation

The described testing procedures are among the specified test methods (ASTM and CSA) for quality assurance and control of new products. The overall objective of this study was to identify potential issues associated with large variability of physical and mechanical properties of GFRP bars currently available in the Canadian market. No similar research was previously performed. The primary concern is future recommendations for quality assurance testing (done for the batch delivered on site) which should include tests that are fast and relatively easy to perform. The provided information can help with the selection of appropriate procedures, test preparation, parameters, and implementation. This research program can be used as a guideline for other researchers to design the successful testing procedure. It describes common issues associated with each test and possible solutions.

The tensile test is one of the most important and most frequently used tests for investigation of GFRP bar properties. It gives information on bar tensile strength, modulus of elasticity, elongation, and stress-strain behavior. If properly done, the test is precise. However, the procedure is not simple for either specimen preparation or testing itself. Due to the high tensile strength of the GFRP bars (more than 1000 MPa), a high capacity machine has to be used (500 kN), even for small diameters used in this work. The specimen preparation includes choosing an adequate anchorage type (DOM tubes and their length), specimen casting into the anchorage tubes (48 hours are needed for curing expansive grout), constant re-ordering of the materials (storing an expansive mortar is not recommended due to short expiration date), and preparing for the anchorage system (providing adequate roughness between tube and expanding grout, and manufacturing of plastic plugs used for the centering of the specimens). The ASTM recommended standard anchorage length (380 mm) appear to be inadequate for the tested bars with a sand coated surface. The CSA 806-12 also provides guidelines for anchorage length, calculated as an expected ultimate tensile

strength times the bar area, divided by 350 (but not less than 250 mm). This formula suggests an increased (as compared to ASTM) anchorage length. It gives 577 mm for the #4 bars, and 860 mm for the #5 bars. Such long anchorage plus the test section make the specimens very long and impractical (the # 4 specimen is 1634 mm long, and # 5 is 2360 mm). The length of the specimens increases proportionally to the bar diameter, where samples for 20 and 25 mm bars can reach even 3 m of length (Fig.4.18). Such specimens are long and cumbersome, and they require special equipment with adequate testing span. The tensile test, although essential for product specification testing, is rather impractical even for routine quality control testing and for quality assurance testing.

Fig. 4.18 – Tensile test sample for 25 mm bar diameter from Company I
(Sherbrook University – Benmokrane 2014)

The shear test provides information about the GFRP bar's shear strength, the shear stress-strain behavior, and the shear stiffness. Specimen preparation and testing are quick. The test needs to be performed using a special shear testing device designed and manufactured per the standards (Annex L of CSA S806-12; ASTM D7617M). For each bar diameter, a separate set of blades needs to be manufactured. This can be impractical considering the variety of bars currently manufactured. The question that needs to be addressed is what type of information on specimen's quality is obtained during shear testing. The testing action is not consistent with transverse loading on bars in real members like dowel action- the test blade simply cuts through a bar. However, this test can be a source of information on the quality of the resin, fiber content or resin-fiber interface. The stress-strain curve (see Fig. 4.10) can be divided into three different regions, where two of them (H1 and H2) have relatively constant shear moduli. The third region, between H1 and H2,

can represent a delamination process. It seems reasonable to assume that the first region H1 describes properties of the resin (before failure of the interface), while the second region H2 represents properties of the fibers (after the failure of the interface). The justification of this hypothesis can be found in the similarities between the shear modulus values of SB and SSB bars (both bar types are made from the same resin with the same fiber content), and at the same time in differences between these two types and BB bars, which are made with a different resin and a different fiber content (especially noticeable for bars from Company I). The shear moduli could be related to the quality of the resin, resin-fiber interface, and fiber content. The introduction of shear moduli (H1 and H2) and further analysis of these parameters can lead to identification bars of poor quality. As observed the BB bars from both companies are characterized by the lower shear moduli, which can indicate lower quality of resin or smaller fiber ration. In fact, both mentioned variables are present in BB bars from both companies. Further work in the area should be done for proper interpretation of shear testing results.

An interesting observation can be made by analyzing tensile and shear tests. The tensile strength of BB is similar (or sometimes higher) that the strength of SB. It should be noted that straight portions of BB were tested herein. What these results indicate is that the tensile testing might, in fact, not reflect the actual quality of the bars. Bent bars (BB), even if manufactured is a very rational manner, are not likely to have higher quality than their straight bar (SB) counterparts, which are manufactured using pultrusion. This can be however seen in the analysis of shear test results. The stiffness moduli H1 and H2 for BB are smaller than for SB, indicating lower quality of resin and less perfect bond between the fibers and the matrix.

The flexure test is a relatively simple, the test gives information on the tensile strength of the outer fibers (modulus of rupture) and the tensile modulus of elasticity. The test can be considered as precise and accurate. A special testing device needs to be manufactured for flexural testing, with additional support rollers made for each bar diameter. The specimen preparation requires cutting the bars longitudinally. The main appeal of this test is that it is easy and quick to perform and the results provide information on tensile properties which are essential for GFRP bars used as concrete reinforcement. Investigation of tensile-flexure strength correlation is explored in detail in Chapter 5.

The test results show that the tensile strength obtained from the flexure test is higher than the tensile strength obtained from direct tension (see Table 8). However, the stiffness obtained from the flexural testing is comparable to tensile stiffness. This phenomenon is well known for brittle materials and connected with the way the loading is applied to the samples. In the case of direct tensile test whole sample volume is stressed in tension. In this loading condition possibility that large size flaw will initiate the sample rupture is higher than in the case of flexure test, were just a small portion of a sample is stressed in tension. In bending possibility of large flaw occurrence in an area of maximum stress is lower. It should be noted that the complete analysis of the stress-strain relationship of the semicircular bar in bending, with dual moduli in tension and compression, will also allow for an estimation of the compression modulus of elasticity.

Compression is not a standard test for quality control and assurance; however, in this work, it was performed to assess its significance and to aid in future work on linking flexural and tensile testing. Two standardized methodologies were used (ASTM D695-10 and ASTM D3410/D3410M). In the first method, the compression stiffness results appeared sensitive to the quality of surface finishing. This is likely due to the steel platens crushing the initial specimen surface imperfections, before compressing the sample. The second methodology requires casting bars into steel tubes. It gives higher compressive stiffness than the first tests, but similar strength. Due to the indirect load application (anchorage device) to the specimen during testing, sample preparation is time-consuming and involves additional costs (tubes and epoxy resin). The first compression test (ASTM D695-10) does not require special sample preparation, and it is fast. By comparing this test with the second test (ASTM D3410/D3410M), it can be stated that it is a quicker and simpler method for compression strength evaluation. The second test can be recommended for detailed investigation of the compression properties of FRP bars, including compression stiffness.

It is worth noting that compression strength and stiffness of GFRP bars is relatively high as compared to tensile properties. It is approximately 70-80% of the tensile strength and stiffness. At present, GFRP concrete reinforcement in compression is not accounted for in member strength calculations (e.g., CSA S806-12). In reality, a compression GFRP reinforcements do contribute to the strength of reinforced concrete members.

The cure ratio test is one of the standardized testing procedures for quality control and qualification testing. Due to problems with obtaining resin samples (usually proprietary information), the test is

not straightforward and almost impossible to perform outside the producer's testing facility. Also, as was shown (see Fig. 4.16 and 4.17), the results are dependent on the location of where the sample was taken.

4.3.2 Conclusions

GFRP bars from two different companies were used in this research to evaluate standardized testing protocols. Bars were tested using five methodologies for obtaining tensile, shear, flexure and compression properties, and cure ratio information. The variety of tested products (two different types of bars from two different companies) allowed the evaluation of the testing procedures in terms of practicality, cost, and aid in interpretation of the results. The following concluding remarks can be offered:

- The tensile test requires considerable lengths of the specimen, and this makes the testing often impractical for routine screening. However, this test is essential for testing for product qualification. The information obtained is of tensile strength and durability of the bars cannot be assessed from these results.
- The shear test is easy to conduct and provides information on the shear strength, the resin quality, the fiber content and the resin-fiber interface. The problem is the variability of the bar diameters available on the market and the fact that the current device requires separate blades precisely made for each bar diameter. New designs of the testing device leading to methodology unification should be considered.
- The flexure test is easy and fast. This test provides information on the tensile strength of the outer fibers and the moduli of elasticity in tension and compression. After developing an adequate relationship between the direct tension and the modulus of rupture, this test could prove to be a promising alternative for the tensile test for quality assurance testing.
- Compression testing was conducted using two methods (ASTM D695-10 and ASTM D3410/D3410M). The first method is faster, provides good estimates on compression strength but yields low stiffness. The second approach allows for the proper determination of both strength and stiffness. The compressive strength and stiffness of the GFRP bars is about 70-80% of the equivalent tensile properties.

- The cure ratio test is rather inconvenient to perform outside of manufacturer testing facilities since the second step of the test can only be done if properties of the resin are known, or the liquid resin sample is provided. Both requirements are difficult to satisfy due to patent and confidentiality issues or shipping problems (resin curing during transportation). The test gives adequate information about the cure ratio.

Chapter 5

ANALYSIS OF RELATIONSHIP BETWEEN TENSION TEST AND FLEXURE TEST STRENGTH RESULTS

5.1. Introduction

Essential properties for GFRP bars are the modulus of elasticity and the tensile capacity obtained by a direct tensile test. As described in the previous chapter, the tensile test procedure is not simple for either sample preparation or testing itself. The first research aimed to develop a procedure for tensile properties determination started in the early 90s (Erki and Rizkalla 1993, Nanni (1996), Carino (1998)), and some test improvements were proposed a few years later (Vijay, 2003). However, none of these new developments can eliminate the most problematic aspects of a direct tension test such as the relatively high cost of sample preparation, excessive sample length or need of the high capacity testing machine.

Conversely, flexural testing of composite reinforcements is relatively easy and quick. Samples are small even for large bar diameters of 20-25mm, the test can be performed on low capacity testing machines (there is no need for more capacity than 15 kN), preparation is limited only to cutting the sample in the longitudinal direction, and the test itself does not require an excessive amount of time. For example, a sample preparation for the tensile test can take up to 3 days (including curing time required for expansive mortar), while the sample preparation for the flexure day shouldn't take more than few hours. The flexure test can be used for establishing the tensile strength of the bars; however, the results need to be calibrated to account for differences in comparison to direct tension, test setup (e.g., mean value of the GFRP bars tensile capacity is approximately 30% smaller than modulus of rupture). Using flexural testing material characterization and quality control could be achieved at low cost.

This Chapter is aimed at investigation of the correlation between the direct tension and the flexure tests. Such relationship could allow wider utilization of the flexural test as a method for determining properties of GFRP bars in tension. Since the test is relatively simple, this would lead

to wider use of GFRP reinforcements in Civil Engineering applications. In the first stage of research, the focus was on the flexure test itself, mechanisms occurring due to bending and the correctness of the obtained results. Current standardized testing procedures (ASTM D447) and corresponding calculations for rupture modulus assume the same tensile and compressive stiffness of a GFRP bar. Ignoring the difference in material tensile and compressive stiffness introduces an error in the results. In this research, the bi-modularity of a composite material is introduced in the flexural calculations. The magnitude of the error due to the assumption of constant stiffness is small, and it is evaluated in this work. Subsequently, using a Weibull "weakest link model" for material flaws distribution, a proper correlation between tensile and flexure test results is investigated.

5.2. Material dual modulus

Classical linear theory of elasticity assumes that a material has the same elastic properties in tension and compression. However, this is only a simplified interpretation which does not account for material nonlinearities. In fact, many materials, e.g., concrete, plastics, ceramics, graphite and several composites (especially Fiber Reinforced Polymers (FRP)) have exhibited a different behavior in tension and compression. Thus, both the elastic modulus and strength of FRP composites in the principal direction of these orthotropic materials are different for tensile and compression loading. This characteristic is one of many that distinguishes composite reinforcements from steel and makes them harder to analyze. There is no clear pattern which allows for classification of composite materials to only one category. A higher modulus of elasticity can occur in tensile stress (as it is in GFRPs, where compression modulus is 20% smaller than tensile) in one composite material as likely as in compression stresses in the other (boron/epoxy fiber reinforced materials, where compression moduli is 20% higher than tensile) (Jones 1978). Also, the magnitude of the difference between tensile and compression properties is not always similar to the same composite type; the carbon fiber reinforced materials have from two (2) to five (5) higher times tensile modulus than compression. There is no clear explanation for the difference between tensile and compression behavior; there could be many reasons that contribute to this phenomenon. However, some speculations have already had made. Per Jones (1977), it depends on the fiber-matrix ratio of stiffness, where fibers can tend to contact and hence stiffen material

when tensile stress is applied, or fibers buckle when compression stress is applied, which can cause material weakening.

The elastic theory of different moduli has been studied by Jones (1977), Medri (1982), and Ambartsumyan (1986). Researchers proposed a bi-linear stress-strain relationship (Fig.5.1), which simplified actual material behavior. In fact, a nonlinear transition exists between the tension and compression linear portions of the stress-strain curve. This simplification can cause problems for stresses close to zero, but it is justified for most practical cases where the analysis is about failure stresses like in this research.

Even though GFRP reinforcing bars can certainly be classified as dual modulus materials, and during bending both states of stress (tensile and compression) are present in the material, the ASTM standard D447 does not account for this material characteristic in calculations for bending capacity. This simplification of material properties can lead to underestimation of rupture modulus. None of the previously mentioned issues of proposed simplification for composite bi-linear behavior affects the further analysis in this research. Thus, dual modulus stress-strain relationship proposed by Jones and Ambarstsumyan was adaped for flexural strength determination. Using this approach, an investigation of dual modulus influence on bending properties of GFRP bars was undertaken in this chapter.

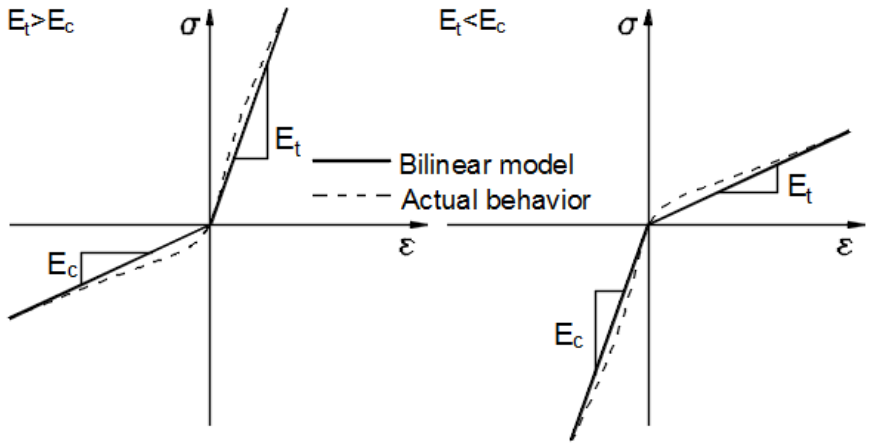

Fig. 5.1 – Comparison of actual stress-strain behavior with the bilinear model

5.2.1. Three-point bending test – modified approach

To determine the influence of GFRP dual modulus on bending properties, the idea of dual modulus of elasticity was introduced to the three basic equations: equilibrium of forces (eq.5.1), equilibrium

of moments (eq.5.2), and linearity of strains (eq. 5.3 – eq.5.4) (Beer et al. 2012). Distribution of stresses and strains along the specimen cross-section is sown on Fig.5.2.

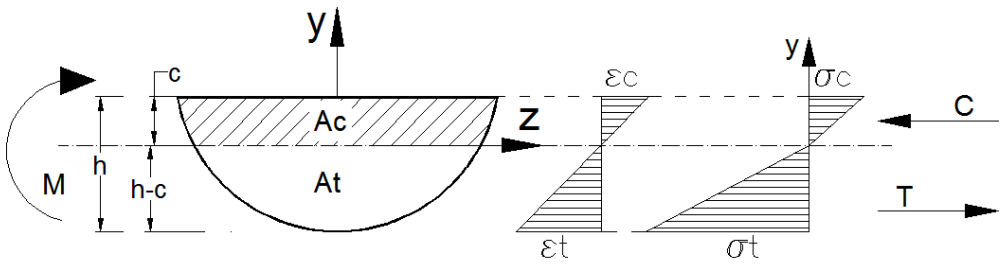

Fig. 5.2 – Distribution of stresses and strains along the cross-section due to bending

$$\int_{A_t} \sigma_t dA + \int_{A_c} \sigma_c dA = 0 \tag{5.1}$$

$$\int_{A_t} -y\sigma_t dA + \int_{A_c} -y\sigma_c dA = M \tag{5.2}$$

$$\frac{\varepsilon_c}{c} = \frac{\varepsilon_t}{(h-c)} \tag{5.3}$$

$$\frac{\sigma_c}{E_c * c} = \frac{\sigma_t}{E_t * (h-c)} \tag{5.4}$$

where: σ_t - tensile stress (rupture modulus), σ_c - compression stress, E_t-tensile modulus, E_c - compression modulus, c-height of compression stress block, (h-c) height of tension stress block, ε_t - tensile strains, ε_c - compression strains

The stiffness moduli in compression E_c and tension E_t, are taken as in Tables 3.1, 4.3 and 4.12, and they are:

for Company I E_c = 45GPa and E_t = 65.6GPa (#4)/62.6GPa (#5),

for Company II E_c = 53GPa and E_t = 62GPa (M12)/63GPa (M16).

Considering the known failure moments M and the cross-sectional areas, the calculations of the moduli of rupture are shown in Table 5.1.

Table 5.1 – Rupture modulus – modified results

	Company I		Company II	
	Flexural Strength (Modulus of Rupture) [MPa]			
Sample Size	#4	#5	M12	M16
Mean	1818	1653	2010	1923
Standard deviation	47	46	111	79
Coefficient of variation	0.026	0.028	0.055	0.04
Results from ASTM D447	1646	1510	1920	1835
* Relative error %	9.5	8.6	4.4	4.6

* Relative error – percentage difference between results from modified method and standardized procedure (ASTM D447)

Comparing these results with values obtained directly from the flexure test (Table 4.8), it can be noticed that modulus of rupture is higher for the modified procedure than in the case of the ASTM standard. The position of neutral axis depend on differences between moduli and it shifts toward section with a higher modulus of elasticity. Therefore, due to change of the stress-block geometry (position of neutral axis) and the fact that the system needs to be in equilibrium (Eq.5.1 and Eq.5.2), the calculated tensile strength of the outer fibers increases (when compared with results from the ASTM D447 standard).

In the case of GFRP bars, the difference between modified and unmodified modulus of rupture is small and does not exceed 10%. However, this relative error depends on the difference between moduli. Larger difference between moduli leads to higher discrepancies between flexural strengths obtained by the standard formulations and modified methodologies. Influence of different ratios of tensile and compression moduli on material properties is presented on Fig.5.3 and Fig.5.4. The curves are normalized and represent analysis done for the semicircular cross section.

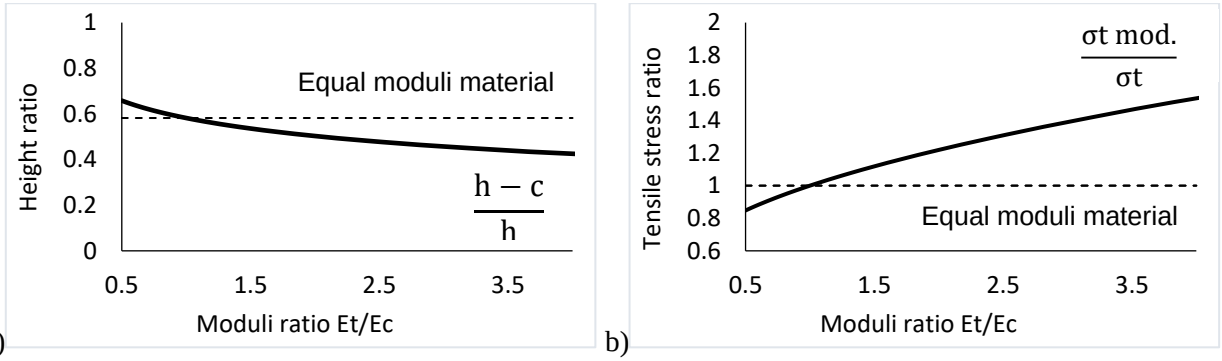

a) b)

Fig. 5.3 – Effect of modular ratio on a) shift of neutral plane and b) tensile strength

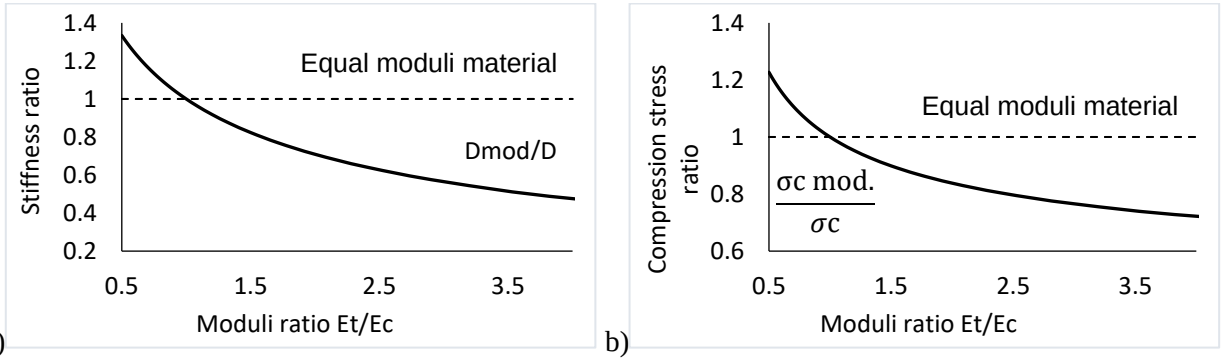

a) b)

Fig. 5.4 – Effect of modular ratio on a) stiffness and b) compression stress

*σtmod, σcmod – modified flexural stress and compression stress due to bending, Dmod – modified stiffness, σc – compression stress, σt – tensile stress, Et – modulus of elasticity in tension, Ec – modulus of elasticity in compression

5.3. Tensile strength vs. modulus of rupture

For an ideal linear material, free from any defects, the tensile strength measured from a direct tensile test and that calculated from bending should be equal, without any influence of "size effect." However, in reality, this is usually not the case, and the materials show a distribution of tensile strengths, which depends on the size of the tested specimen and method of load application, which influences the zone in tension. Thus, an adjustment needs to be made for the effect of the non-uniform application of stresses due to bending and sample size.

One of the first research performed on brittle cracking (Griffith 1920) assumes that crack extension in brittle materials occurs when there is sufficient elastic strain energy near a growing crack to form two new surfaces. Other research (Irwin 1956) associated crack extension with an energy release rate KI_c (resistance to crack grow). Based on the Irwin approach the strength prediction relates the crack extension to the size (c) of pre-existing cracks within a material (Eq.5.5).

$$\sigma_f = \frac{K_{Ic}}{y\sqrt{c}} \tag{5.5}$$

where: σ_f – fracture stress, K_{Ic} - resistance to crack grown, and y (dimensionless) stress intensity factor, c flaw size

Flaws, which depend on material composition, size, and processing, are distributed through the material volume. It can be seen from Equation 5.5 that a smaller strength is associated with larger flaw sizes. Thus, the failure is strongly associated with the largest flaw or in other words with a "weakest link."

5.3.1. Weibull "Weakest Link" model

The Weibull weakest link model assumes that the "largest flaws" are primarily responsible for the sample's failure. The statistical model attempts to determine the strength of brittle materials. The method accounts for specimen size, a scatter of failure strength (number of flaws) and a distribution of applied stresses. The theory assumes two basic criteria of fracture: the flaw size and the magnitude of normal stresses. It is assumed that the material failure can be fully described by three material properties: the zero strength (σ_u), the flaw density exponent (m), and a scale parameter (σ_o). In other words, the probability of failure P of a material that has Weibull distribution of flaws throughout its volume V can be described by:

$$P = 1 - \exp\left(\int \emptyset(\sigma) dv\right) \tag{5.6}$$

$\emptyset(\sigma)$ is a function expressing the strength properties of the material

$$\emptyset(\sigma) = \left(\frac{\sigma - \sigma_u}{\sigma_o}\right)^m \tag{5.7}$$

where: σ – is applied stress, m – shape parameter (Weibull modulus) constant related to the flaw size distribution, σ_u – stress below which no failure occurs (usually assumed to be 0), σ_o – normalizing factor (the scale parameter)

Substituting Equation 5.7 into Equation 5.6:

$$P = \begin{cases} 1 - \exp\left(-\int_V \left(\frac{\sigma - \sigma_u}{\sigma_o}\right)^m dV\right) => 1 - e^{-\beta};\ \sigma \geq \sigma_u \\ 0 \qquad\qquad\qquad\qquad\qquad\qquad\qquad\quad ;\ \sigma < \sigma_u \end{cases} \tag{5.8}$$

where:

$$\beta = \int_V \left(\frac{\sigma - \sigma_u}{\sigma_o}\right)^m dV \tag{5.9}$$

Assuming that the Weibull distribution of material strength can be used to calculate the probability of failure when a uniform tensile stress (direct tensile test) or nonuniform stress (bending test) is applied over a sample volume that is in tension (V_t – sample volume that is stressed in tension for the direct tensile stress σ_t and V_b – sample volume that is stressed in tension for the tensile stress due to bending σ_b, one can obtain the following forms:

- for direct tensile stress (σ_t)

$$P = 1 - \exp\left(-\int_{Vt} \left(\frac{\sigma_t - \sigma_u}{\sigma_o}\right)^m dV_t\right) \tag{5.10}$$

- for tensile stress due to bending (σ_b)

$$P = 1 - \exp\left(-\int_{Vb} \left(\frac{\sigma_b - \sigma_u}{\sigma_o}\right)^m dV_b\right) \tag{5.11}$$

Taking into consideration the fact that probability of failure of the same material, which has the same distribution of flaws, should be the same for the sample subjected to the direct tension stress and the sample subjected to the tensile stress due to bending, Equations 5.10 and 5.11 lead to:

$$1 - \exp\left(-\int_{Vt}\left(\frac{\sigma_t - \sigma_u}{\sigma_o}\right)^m dV_t\right) = 1 - \exp\left(-\int_{Vb}\left(\frac{\sigma_b - \sigma_u}{\sigma_o}\right)^m dV_b\right) \tag{5.12}$$

$$\int_{Vt}\left(\frac{\sigma_t - \sigma_u}{\sigma_o}\right)^m dV_t = \int_{Vb}\left(\frac{\sigma_b - \sigma_u}{\sigma o}\right)^m dV_b \tag{5.13}$$

In the case of direct tension, the stress is applied uniformly along the sample length and the cross-section, and the integration over the sample volume (left side of Equation 5.13) yields (Laws 1982):

$$\int_{Vt}\left(\frac{\sigma_t - \sigma_u}{\sigma_o}\right)^m dV_t = V_t\left(\frac{\sigma_t}{\sigma_o}\right)^m \tag{5.14}$$

For the tensile stress due to bending, the integration needs to be done over the tension volume that must be determined considering a distribution of stress along the sample cross-section area and along the length, which is dependent on the shape of the bending moment diagram along the sample's length. Research on this topic was done by Weil et al. (1964) for many different bending options (bending moment diagram along the beam) for the case of a rectangular cross-section. Considering the case of three-point bending, as per ASTM D447, the right part of the Equation 5.13 can be written:

$$\int_{Vb}\left(\frac{\sigma_b - \sigma_u}{\sigma_o}\right)^m dV_b = V_b\left(\frac{\sigma_b}{\sigma_o}\right)^m \frac{1}{2(m+1)^2} \tag{5.15}$$

Which, after combining with Equation 5.14 leads to:

$$V_t\left(\frac{\sigma_t}{\sigma_o}\right)^m = V_b\left(\frac{\sigma_b}{\sigma_o}\right)^m \frac{1}{2(m+1)^2} \tag{5.16}$$

The ratio of stress in direct tension to tensile stress due to bending can be expressed as:

$$\frac{\sigma_b}{\sigma_t} = \left(\frac{V_t\ 2(m+1)^2}{V_b}\right)^{\frac{1}{m}} \tag{5.17}$$

Simplifying Equation 5.17:

$$\frac{\sigma_b}{\sigma_t} = \left(\frac{V_{Et}}{V_{Eb}}\right)^{\frac{1}{m}} \tag{5.18}$$

where: $V_{Et} = V_t$ and $V_{Eb} = \frac{V_b}{2(m+1)^2}$ are effective volumes in direct tension and bending, respectively.

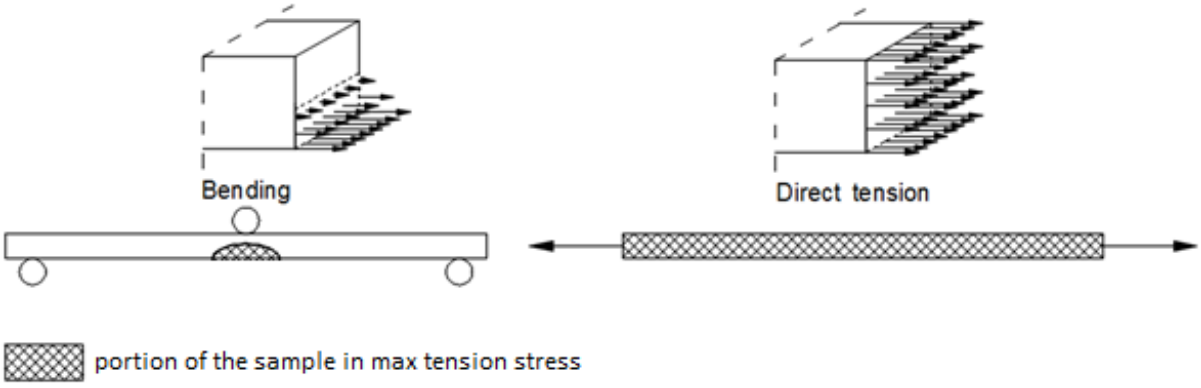

Fig. 5.5 – Effective volumes in direct tension and three-point bending for rectangular cross-section

In the simple case of direct uniform tension, the effective volume V_{Et} is assumed to be the specimen volume V ($V_{Et} = V_t = V$).

In other loading cases, like bending, the effective volume is smaller than the total volume of the sample or the sample volume stressed in tension ($V_{Eb} < V_b < V$).

The relation between these V and V_{Eb} is expressed as (Weil et al. 1964):

$$V_{Eb} = kV \tag{5.19}$$

where: k – is a loading factor and V is the total volume

For a rectangular cross-section specimen under three-point bending, $k = \frac{1}{2(m+1)^2}$ and the effective volume is $V_{Eb} = \frac{V}{2(m+1)^2}$. The concept is illustrated in Figure 5.5.

5.3.2. Effective volume for semi-circular cross-section

For a three-point bending test (ASTM D447), tensile stress is changing not only along the sample height but also along the sample length with respect to the shape of the bending moment diagram. (Fig.5.6). Thus, to determine the effective volume of the sample subjected to three-point bending, an integration needs to be done over the portion of the specimen that is stressed in tension, what includes both stress gradients: tensile stress block and bending moment.

A general equation for effective volume, in this case, will look like:

$$V_{Eb} = \int_{Vb} \left(\frac{\sigma_b - \sigma_u}{\sigma_o}\right)^m dV_b = \int_{Vb} \left(\frac{\sigma_b}{\sigma_{max}}\right)^m dV_b \tag{5.20}$$

Where: $\sigma_u = 0$ and $\sigma_o = \sigma_{max}$, σ_{max} – is a maximum tensile stress due to three-point bending.

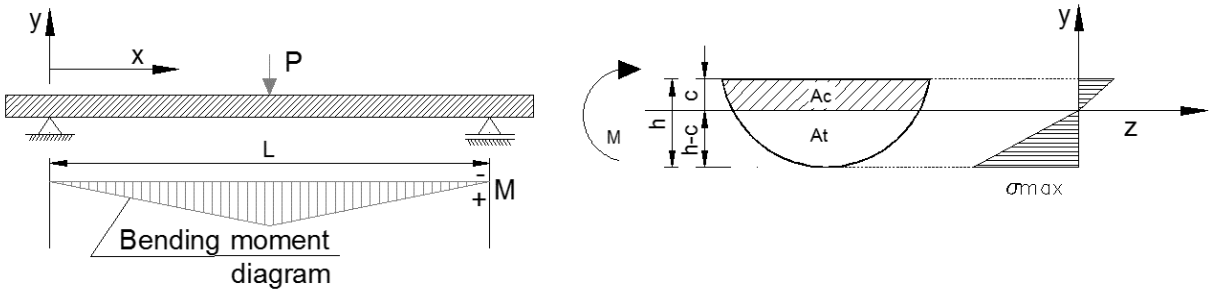

Fig. 5.6 – Bending moment diagram and stress distribution in the sample due to bending.

Referring to Fig. 5.6 the tensile stress varies linearly with distance x. Thus the stress change along the sample length can be written as:

$$\sigma_b = \left(\frac{x}{\frac{L}{2}}\right)\sigma_{max} = \left(\frac{2x}{L}\right)\sigma_{max} \tag{5.21}$$

Where $x \in \left(0, \frac{L}{2}\right)$ due to the symmetry of the bending moment diagram

Assuming that the tensile stress varies linearly with the height of the cross section the stress distribution function can be determined as:

$$\sigma_b = -\left(\frac{y}{h-c}\right)\sigma_{max} \tag{5.22}$$

where $y \in (-(h-c), 0)$

Applying both equations (Eq. 5.21 and Eq. 5.22) to the general formula (Eq.20) for the effective volume in three-point bending:

$$V_{Eb} = 2\int_{Vb}\left(\frac{-\left(\frac{y}{h-c}\right)\left(\frac{2x}{L}\right)\sigma max}{\sigma max}\right)^{m} dV_b = -2\int_{Vb}\left(\left(\frac{y}{h-c}\right)\left(\frac{2x}{L}\right)\right)^{m} dV_b \qquad (5.23)$$

With proper integral limits (See Fig 5.6), and excluding all constants from the integral Equation 5.23 takes a form:

$$V_{Eb} = \frac{-2^{m+1}}{\left((h-c)*L\right)^{m}}\int_{0}^{L/2}\int_{0}^{-(h-c)}\int_{-\sqrt{R^2-(y-(R-(h-c))^2}}^{\sqrt{R^2-(y-(R-(h-c))^2}} y^m x^m \, dzdydx \qquad (5.24)$$

For a better understanding of the described procedure, the determination of effective volume for a rectangular rod is presented in Appendix 4.

Due to the complex form of Equation 5.24, all further calculations for determination of the effective volume for semi-circular cross-sectioned samples, tested in three-point bending, were carried out in MathCAD. Results are reported in Tables 5.5 and 5.6 for Company I and Tables 5.7 and 5.8 for Company II, respectively. However, before the calculations for effective volume can be performed, the Weibull modulus (shape parameter m) needs to be determined.

5.3.3. Weibull modulus

Weibull modulus, also known as a shape parameter (dimensionless), describes the flaw distribution in a material. The higher the Weibull modulus is, the more uniform material that is tested. This can be interpreted that higher shape parameter defines material with uniform defects evenly distributed along the sample volume or surface.

The Weibull modulus can easily be established from the Weibull strength distribution graph. To establish such a graph, results from three-point bending tests are needed. It is recommended that a sufficient number of tests will be needed to determine the flaw distribution parameter. The optimum amount of test specimens depends on many variables, including material and testing cost, previous knowledge about material parameters (if large scatter of results is expected) and the desired precision of results. In this research, five samples were tested for each bar diameter and each bar type. The first step to obtain the Weibull graph is putting the recorded flexural data in

ascending order (e.g., the second column in Table 5.2). The natural logarithm of the stress is computed and shown in the third column. Next, to each data point, a probability of failure (Eq. 5.25) is provided. It is reasonable to estimate that the highest tensile strength measured during the test will have the higher probability of failure.

$$Pf = \frac{i - 0.5}{n} \tag{5.25}$$

where: i – is the ith data point and n is the total number of the data points.

Subsequently, the double logarithm is taken of the expression $\left(\frac{1}{1-Pf}\right)$, shown in last column of Table 5.2 The double logarithm of the expression mentioned above is established from the Weibull distribution weakest link model. To get the Weibull graph, the natural logarithm of strengths need to be plotted on the x axis and $\ln\left(ln\left(\frac{1}{1-Pf}\right)\right)$ on the y axis. Finally, a trend line needs to be fitted through the data. The slope of the line is the Weibull modulus, m. To interpret the importance of bi-modular effect (in flexure analysis) on the correlation between tensile and flexure test, both results (from modified and unmodified methods) are presented below. Due to the method's repeatability, just one example of the data table and the corresponding Weibull graph are shown below. Additional results are available in Appendix 5.

Table 5.2 – Dataset for unmodified results for #4 bar for Company I

Unmodified results for #4				
i	Strength [Mpa]	x=ln(strength)	Pf=(i-0.5)/n	Y = lnln[1/(1-Pf)]
1	1569.6	7.358576089	0.1	-2.250367327
2	1623.13	7.392111663	0.3	-1.030930433
3	1645.98	7.40609123	0.5	-0.366512921
4	1651.23	7.409275744	0.7	0.185626759
5	1700.37	7.438601153	0.9	0.834032445

Table 5.3 – Dataset for modified results for #4 bar for Company I

Modified results for #4				
i	Strength [Mpa]	x=ln(strength)	Pf=(i-0.5)/n	Y = lnln[1/(1-Pf)]
1	1741.6	7.46255951	0.1	-2.250367327
2	1800.84	7.496008502	0.3	-1.030930433
3	1826.62	7.510222544	0.5	-0.366512921
4	1832.4	7.513381862	0.7	0.185626759
5	1886.61	7.542536847	0.9	0.834032445

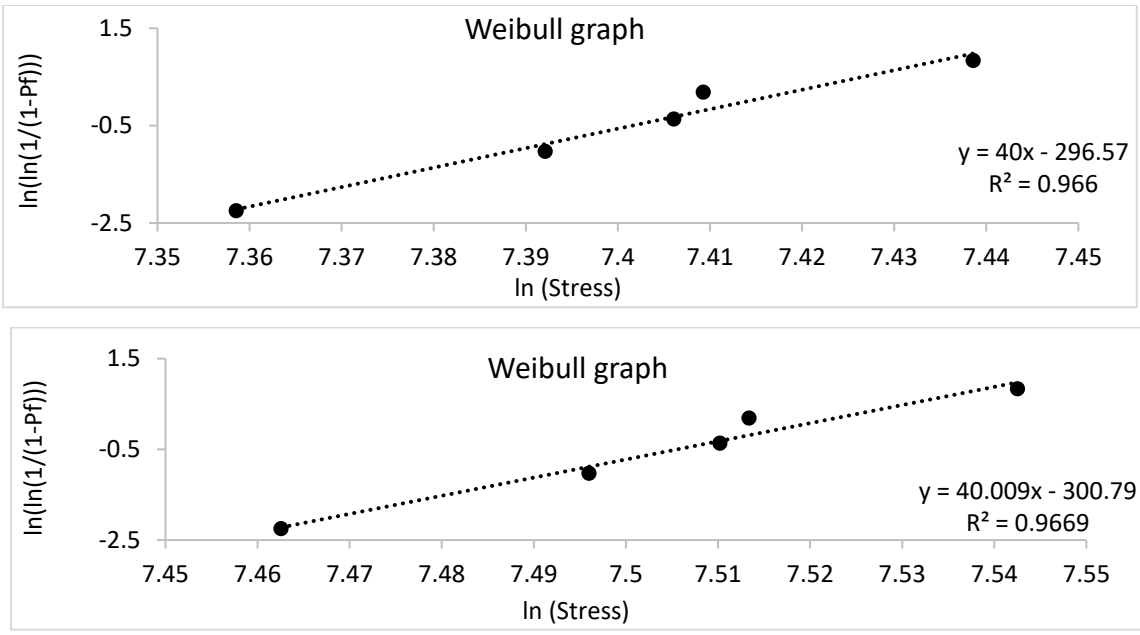

Fig. 5.7 – Weibull graph for a) unmodified and b) modified results for #4 bar from Company I.

It can be noticed (Fig.5.7) that the Weibull modulus m is independent of methodology (constant or bi-moduli analysis) used for the determination of flexural strength. This observation is correct since modification of flexural capacity changes the calculated tensile strength with a constant ratio, which does not interfere with strength distribution (see Table 4.8 and 5.1, where the coefficient of variation stays the same for both methodologies). Values of different Weibull moduli for various bar sizes and types are reported in Table 5.4.

Table 5.4 – Weibull modulus

	Company I		Company II	
Bar size	#4	#5	M12	M16
m	40	36	21	24

5.3.4. Correlation between tensile strength due to bending and direct tensile strength

Using information obtained from the section 5.3.3 (Weibull modulus, m), the effective volume of the semi-circular cross-sectional samples was calculated from Equation 5.24. Results are available in Tables 5.5, 5.6, 5.7 and 5.8 for unmodified and modified methodologies for prediction the modulus of rupture. Also, reported in Tables 5.5-5.8 are the tensile stress ratios (tensile stress of the outer fibers due to bending vs. tensile stress from direct tension) calculated from equation 5.18. Experimental tensile stress ratios are also presented for comparison. Note that direct tension

strengths for Company I were taken from the manufacturer's data (as explained before in this chapter). Direct tension test results for Company II and bending test results for both companies s were measured in this research.

Table 5.5 – Tensile-flexure stress correlation (unmodified) for Company I

SB #4					
Sample	σ_t	V_{Et} in tension [mm^2]	σ_b - not modified	V_{Eb} in bending for m=40 [mm^2]	$\sigma_b/\sigma_t = (V_{Et} / V_{Eb})^{1/m}$
mean	1312	86161.6	1638	0.536	1.349
s.d.			42.5	0.026	0.002
c.o.v.			0.03	0.048	0.001
Tensile stress ratio (σ_b / σ_t) directly from tests				1.25	
SB #5					
Sample	σ_t	V_{Et} in tension [mm^2]	σ_b - not modified	V_{Eb} in bending for m=36 [mm^2]	$\sigma_b/\sigma_t = (V_{Et} / V_{Eb})^{1/m}$
mean	1184	183124.8	1510	1.338	1.389
s.d.			42.22	0.077	0.002
c.o.v.			0.03	0.057	0.002
Tensile stress ratio (σ_b / σ_t) directly from tests				1.28	

Table 5.6 – Tensile-flexure stress correlation (modified) for Company I

SB #4					
Sample	σ_t	V_{Et} in tension [mm^2]	σ_b - modified	V_{Eb} in bending for m=40 [mm^2]	$\sigma_b/\sigma_t = (V_{Et} / V_{Eb})^{1/m}$
mean	1312	86161.6	1817.61	0.476	1.353
s.d.			47.16	0.021	0.001
c.o.v.			0.03	0.043	0.001
Tensile stress ratio (σ_b / σ_t) directly from tests				1.39	
SB #5					
Sample	σ_t	V_{Et} in tension [mm^2]	σ_b - modified	V_{Eb} in bending for m=36 [mm^2]	$\sigma_b/\sigma_t = (V_{Et} / V_{Eb})^{1/m}$
mean	1184	183124.8	1653	1.212	1.393
s.d.			46	0.072	0.002
c.o.v.			0.03	0.059	0.002
Tensile stress ratio (σ_b / σ_t) directly from tests				1.40	

Table 5.7 – Tensile-flexure stress correlation (unmodified) for Company II

SB M12					
Sample	σ_t	V_{Et} in tension [mm^2]	σ_b - not modified	V_{Eb} in bending for m=21 [mm^2]	$\sigma_b/\sigma_t = (V_{Et} / V_{Eb})^{1/m}$
mean	1222.98	54259.20	1920	1.356	1.657
S.d.	93.24		91	0.226	0.013
C.o.V	0.08		0.05	0.166	0.008
Tensile stress ratio (σ_b / σ_t) directly from tests				1.57	
SB M16					
Sample	σ_t	V_{Et} in tension [mm^2]	σ_b - not modified	V_{Eb} in bending for m=24 [mm^2]	$\sigma_b/\sigma_t = (V_{Et} / V_{Eb})^{1/m}$
mean	1269.98	128614.40	1835	2.172	1.581
S.d.	50.48		122	0.039	0.001
C.o.V	0.04		0.07	0.018	0.001
Tensile stress ratio (σ_b / σ_t) directly from tests				1.45	

Table 5.8 – Tensile-flexure stress correlation (modified) for Company II

SB M12					
Sample	σ_t	V_{Et} in tension [mm^2]	σ_b - modified	V_{Eb} in bending for m=21 [mm^2]	$\sigma_b/\sigma_t = (V_{Et} / V_{Eb})^{1/m}$
mean	1222.98	54259.20	2010	1.280	1.662
S.d.	93.24		111	0.177	0.011
C.o.V	0.08		0.05	0.138	0.007
Tensile stress ratio (σ_b / σ_t) directly from tests				1.64	
SB M16					
Sample	σ_t	V_{Et} in tension [mm^2]	σ_b - modified	V_{Eb} in bending for m=24 [mm^2]	$\sigma_b/\sigma_t = (V_{Et} / V_{Eb})^{1/m}$
mean	1269.98	128614.40	1923	2.082	1.584
S.d.	50.48		79	0.052	0.002
C.o.V	0.04		0.04	0.025	0.001
Tensile stress ratio (σ_b / σ_t) directly from tests				1.51	

* σ_t – tensile stress from direct tension test, σ_b – tensile stress of the outer fibers due to bending (modulus of rupture) directly from the bending test (per ASTM D447 and for modified methodology, respectively), V_{Et} – effective volume in direct tension test, V_{Eb} – effective volume in flexure test

For a better understanding of the results a relative error (percentage value of the difference between values) for the results obtained from correlation and results obtained directly from tests is presented in Table 5.9 for Company I and Table 5.10 for Company II.

Table 5.9 – Relative error for tensile-flexure strength correlation for Company I

Sample	Unmodified ASTM 447			Modified method		
	Tensile stress ratio calculated σ_b/σ_t	Tensile stress ratio from tests σ_b/σ_t	Error [%]	Tensile stress ratio calculated σ_b/σ_t	Tensile stress ratio from tests σ_b/σ_t	Error [%]
#4	1.35	1.25	8	1.35	1.39	2.8
#5	1.39	1.28	8.6	1.39	1.40	0.7

Table 5.10 – Relative error for tensile-flexure strength correlation for Company II

Sample	Unmodified ASTM 447			Modified method		
	Tensile stress ratio calculated σ_b/σ_t	Tensile stress ratio from tests σ_b/σ_t	Error [%]	Tensile stress ratio calculated σ_b/σ_t	Tensile stress ratio from tests σ_b/σ_t	Error [%]
M12	1.66	1.57	5.7	1.66	1.64	1
M16	1.58	1.45	8.9	1.58	1.51	4

It can be noticed that the error in both cases for modified and unmodified methodology is relatively small (does not exceed 10%) when compared with results obtained directly from tests. This suggests that the correlation between the tensile test and the flexural test does exist for GFRP bars, and the methodology presented in this chapter has the potential for practical applications of this type of testing for a simpler and faster, yet reliable determination of tensile strength.

5.4. Concluding remarks

The tensile strength of composite reinforcements used for RC structures is the most valuable property. Bars tensile characteristics should be established not only for new products entering the market but also whenever reinforcements are used in construction to ensure their quality. A straightforward and efficient method for tensile testing would be an improvement in quality assurance of these bars. Research presented in this chapter shows that the flexure test can be a rational alternative for determination of tensile strength. Flexure test is relatively easy to perform and does not involve excessive time or financial and technical resources. It can be used in small technical facilities on a daily basis as a quality control test.

Based on the obtained results it can be concluded that dual moduli of the material do not have a significant influence on the final correlation results and the simpler calculation as per ASTM 477 can be considered acceptable for correlation between rupture moduli and tensile strength for GFRP bars with similar stiffness in tension and compression. However, for products with large differences between tensile and compression moduli, bimodular characteristic of the material should be considered. In the case of a significant difference in moduli, approximately 30% and larger, a dual modulus should be included in the calculations. The omission of a large difference between modulus of elasticity in tension and compression will lead to a significant calculation error for tensile-flexure strength correlation. Detailed analysis of the material, dual moduli should be undertaken for new products or whenever a change is introduced to the material production line.

The Weibull "weakest link" model proves to be a proper methodology for obtaining a correlation between the tensile strength from direct tension and modulus of rupture from flexure. It allows establishing the distribution of flaws of the materials, based on flexure test only. This correlation is then used to calculate the ratio between direct tension and bending test results for tensile strength. The procedure considers the difference between both testing protocols, namely a different load application (stress distribution along specimen) and flaws distribution in the material. The Weibull model recognizes that both the flaw distribution and the stress distribution are indicators of failure. In other words, certain favorable circumstances need to occur to trigger sample rupture: the largest flaw needs to be present in this portion of a sample where the largest stress is applied. This interpretation of the method is an explanation why small values of the effective volume are calculated from the flexure test, where a maximum stress occurs in a limited area of the specimen due to the character of load application during the three-point bending test. It is expected that in the case of other load applications, e.g., four-point bending test, the effective volume in bending will be much larger. In addition, application of the four-point bending test will induce a larger area of uniformly distributed bending moment. In effect, the larger portion of the sample will be stressed in the same maximum tensile stress reflecting more effectively the flaws distribution along the sample volume.

This research clearly demonstrates that a correlation between the strength of the bar from a direct tension test and the tensile strength of the bar from a flexure test does exist and can be established

using information from the manufacturer and results from a rather straightforward bending test. It is recognized that some information (material properties like modulus of elasticity in tension) needs to be provided for the proposed calculations. However, there is no need for performing an additional direct tension test if proper information is available from manufacturer, as was done in this research in case of bars from Company I. It should be mentioned, however, that information on modulus of elasticity could potentially be eliminated by considering the measured deflection in the bending test.

Direct tensile testing must remain a primary test for establishing tensile strength, stiffness and the stress-strain relationship of GFRP bars. However, a faster, simpler, and cheaper flexure test is shown to have the potential to be an efficient method for determining tensile strength and stiffness of GFRP bars via the proposed correlation in this chapter.

Chapter 6

DURABILITY PREDICTIONS

6.1. Introduction

The major interest of GFRP reinforcement in Civil Engineering applications is mostly driven by the fact that composite bars do not exhibit conventional corrosion. However, GFRP bars can lose their strength with time in certain environments. Despite, the fact that GFRP reinforcement has already been used in several structural applications, they still are considered a new material, and lack of long-term performance data effectively prevents wider utilization of bars. In effect, design guidelines for GFRP bars recommend high load and resistance factors and low allowable sustained stress levels. These conservative restrictions can prevent engineers from taking a full advantage of GFRP bars properties. Therefore, there is the need for a new and effective tests methods and models that can predict long-term durability performance of GFRP bars.

6.2. Accelerated test

Since long-term (75 to 100 years) performance data for GFRP material is not available, accelerated tests are used to predict GFRP material durability in practice. According to Bank et al. (1995), the accelerated test methodology is divided into two basic parts. The first part consists of a test procedure that is used to monitor the material property change, and the second part includes a description of the analytical or statistical model used for prediction of the long-term behavior. The testing procedure is usually based on simple mechanical tests conducted on conditioned samples at different time intervals. There are several tests that can be chosen, but for GFRP reinforcing bars the most commonly used are tensile, short beam shear and flexure tests. The selected tests should characterize properties that are significant for designers and represent the material over its service live, and should be efficient (Bank et al. 2002). After choosing the type of test, the failure mode of the material should be studied. Good understanding of failure mechanisms is crucial since various types failure during the test will lead to confusion and incorrect prediction.

Accelerated tests shorten the duration of degradation by accelerating factors and use the short-term measurements to predict the long-term behavior or service lifetime. In all accelerated tests, an acceleration factor should be chosen. Typical accelerating factors are mechanical load, voltage, temperature, weathering and the use of high concentrations of chemical environments (Nelson, 1990). In some cases, dual accelerating factors can be employed (as load and temperature), but this involves more complex test methodology and is not commonly used. Since the degradation rate of GFRP materials depends mostly on diffusion and chemical reactions, it is reasonable to use an elevated temperature as an accelerating factor, which will speed up the diffusion process. However, due to the possibility of changing degradation mechanism to another one, which GFRP bars in field conditions may not experience, the accelerating temperature should be chosen wisely. According to Benmokrane et al. (2002), the temperature of 60 ºC is adequate as an elevated temperature for an alkaline exposure. This temperature will increase the degradation process, and since it is below the matrix glass transition temperature, it will not change bar properties and it will not cause the formation of additional degradation mechanisms. The second part of accelerated testing has been described further in this section.

6.3. Background to modeling

To predict the long-term behavior or service lifetime of a material using results from accelerated tests, statistical or analytical models must be employed. Models used commonly for prediction of FRP material degradation are based on three general assumptions (Nelson 1990):

- Degradation is not reversible; material performance is getting worse with time.
- Most of the time just one model is used for prediction of the degradation process. If degradation has changed, a different model should be applied.
- Deterioration of a material at time zero (any previous imperfections or strength losses due to other factors such as UV exposure) is negligible.

The second assumption is the most important. It employs the need of implication of several different prediction models to describe a complex problem of FRP material degradation. Although some models combine several factors and different degradation mechanisms, they are too complicated for routine use, and if they cannot be used effectively on a daily basis, then the methodology is useless.

In the following, the theoretical background to time-temperature shift (Arrhenius model) and modeling diffusion are presented.

6.3.1. Arrhenius model – temperature shift

There are several models proposed in the published literature. Among existing degradation formulas described as a function of temperature, the most popular are the one based on the Arrhenius relationship (Gonenc, 2003). The Arrhenius equation was developed in 1899 by the Swedish chemist Svante Arrhenius, who combined the concept of activation energy and the Boltzmann distribution law. Originally, the Arrhenius model was developed for gasses in which the chemical reactions were observed to proceed more rapidly at higher temperature. Using the Arrhenius relationship, the natural aging behavior can be established by extrapolation of accelerated degradation data. However, this model can be used when the temperature is the only significant accelerating factor, and chemical or diffusion reactions are the dominant degradation processes. The Arrhenius equation takes the form (Nelson 1990):

$$k = Aexp\left(\frac{-E_a}{RT}\right) \tag{6.1}$$

Where: $k -$ the Arrhenius degradation rate constant; $E_a -$ the activation energy of the phenomenon; $R -$ universal gas constant (8.3145 J/K/mol); $T -$ temperature in K; $A -$ constant base on test conditions

Analyzing the Arrhenius relationship (neglecting, for now, the constant A), it can be noticed that it is an exponential decay law, where a magnitude of the degradation rate "decays" as a function of the exponent$\left(\frac{-E_a}{RT}\right)$. This means that high temperature and low activation energy give larger degradation rates, and thus speed up the degradation phenomenon (Fig.6.1 and Fig.6.2).

a)

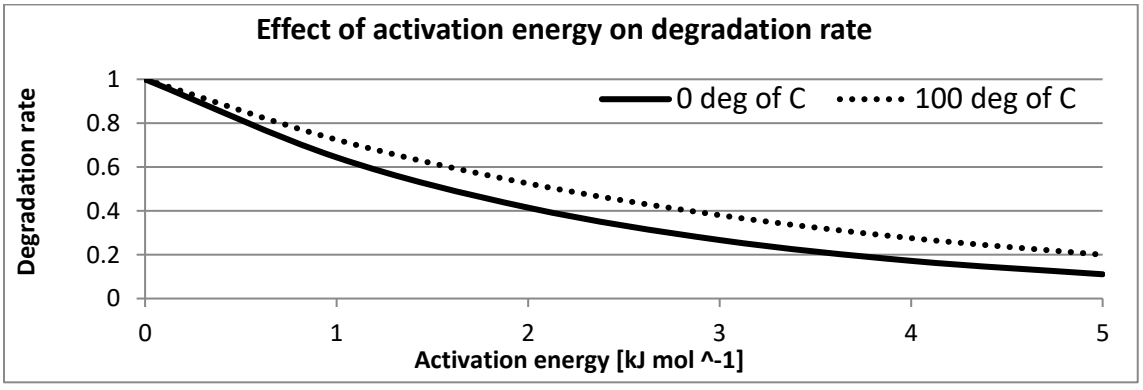

b)

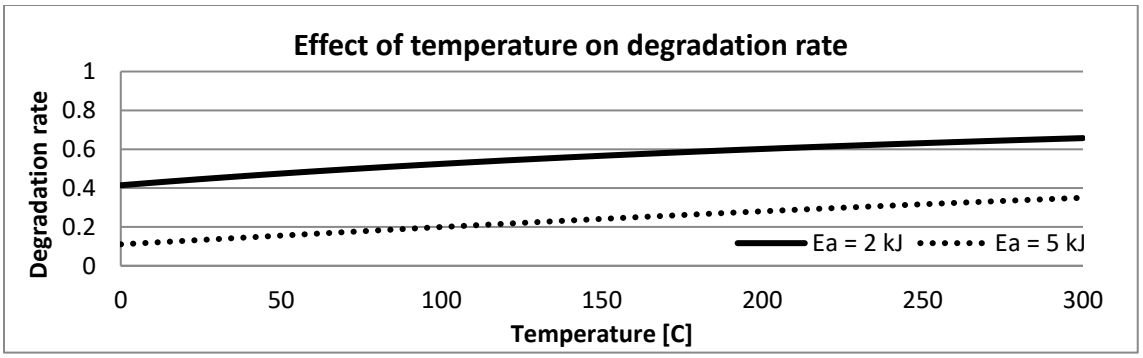

Fig. 6.1 – a) Effect of activation energy on degradation rate; b) effect of temperature on degradation rate (logarithmic)

The Arrhenius equation can be expressed in a non-exponential form which is often more convenient to use and easier to interpret graphically. Taking the natural logarithm of both sides of Eq. 6.1 yields the following straight line equation:

$$\ln(k) = \ln(A) - \left(\frac{E_a}{RT}\right) \tag{6.2}$$

If the logarithmic reaction rate is plotted against inverse of temperature as shown in Fig.6.2-b (Arrhenius Plot), the slope of the line will be $\left(\frac{-E_a}{R}\right)$ and the intercept on the vertical axis will be the constant $\ln(A)$.

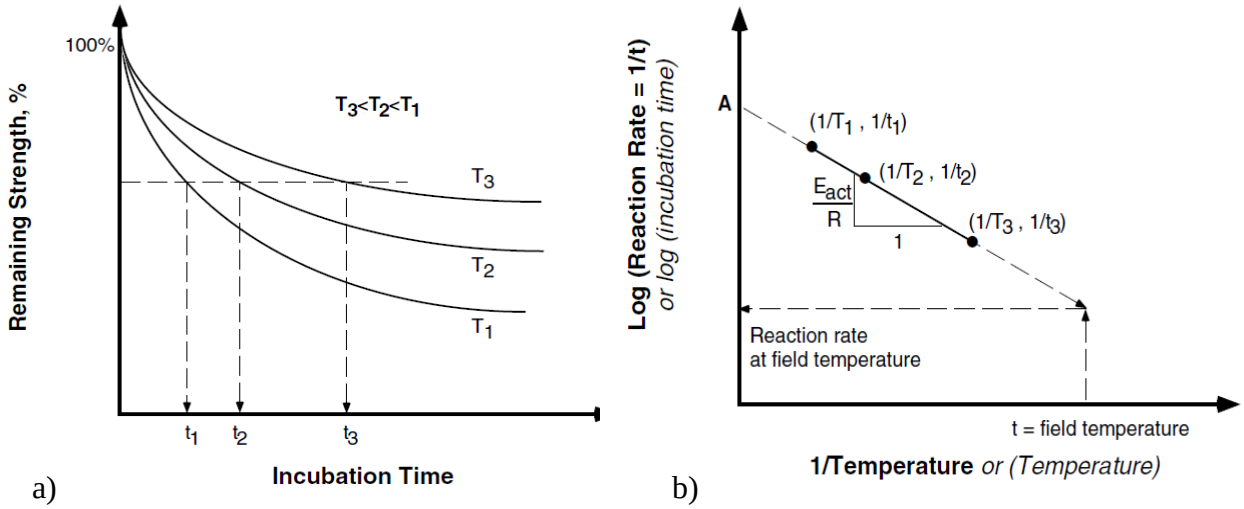

Fig. 6.2 – The Arrhenius Model a) change in measuring property via time for different incubation temperature b) Arrhenius Plot (Iskander 2002)

Since the plot of logarithmic degradation rate versus 1/T yields a straight line, it is often convenient to calculate the activation energy from an experiment at only two temperatures:

$$lnk_2 - lnk_1 = \left(lnA - \left(\frac{Ea}{RT_2}\right)\right) - \left(lnA - \left(\frac{Ea}{RT_1}\right)\right) = \frac{Ea}{R}\left(\frac{1}{T_1} - \frac{1}{T_2}\right) \quad (6.3)$$

Solving the expression for activation energy:

$$Ea = \frac{Rln\left(\frac{k_2}{k_1}\right)}{\frac{1}{T_1} - \frac{1}{T_2}} \quad (6.4)$$

However, avoiding the third temperature (third data point) can lead to miscalculation of activation energy, and generate a substantial error.

It is important to realize that relationship 6.1 is based on a simple view that failure is due to chemical reaction or diffusion. The specimen is assumed to fail when the same critical amount of chemical has reacted or diffused. It can be explained by:

Critical amount = rate x time to failure

Equivalently:

Time to failure = critical amount/rate

This suggests that nominal time (τ) to failure is inversely proportional to rate (Eq. 6.1). This yields the Arrhenius life relationship (Nelson 1990):

$$\tau = Aexp\left(\frac{E_a}{RT}\right) \quad (6.5)$$

Similar to equation 6.1, nominal time to failure is expressed by an exponential function dependent on activation energy and temperature, but contrary to degradation rate time to failure, this takes a form of exponential growth law. Caring the same investigation as for degradation rate (neglecting, for now, constant A), it can be noticed that high activation energy and low-temperature favor longer lifetime of a material (Fig.6.3).

a)

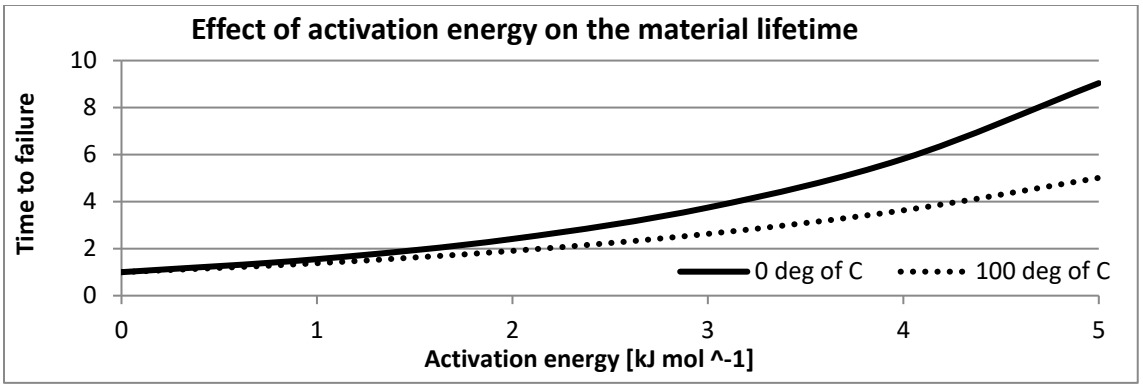

b)

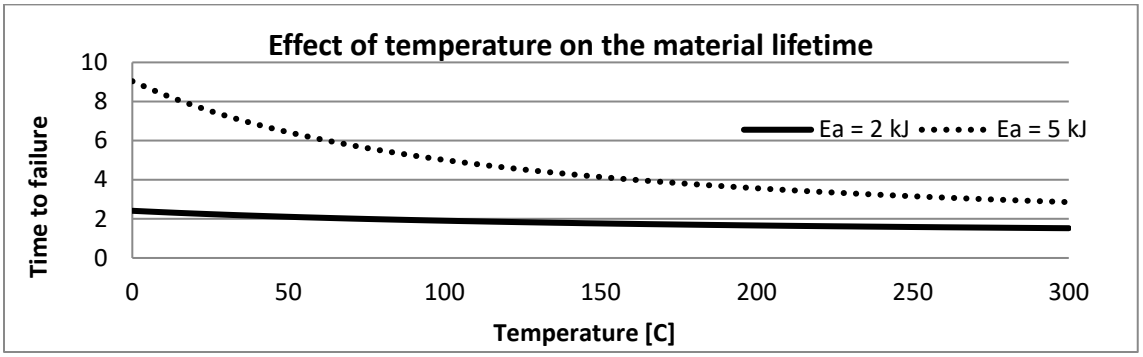

Fig. 6.3 – a) Effect of activation energy on the material lifetime b) effect of temperature on material lifetime (logarithmic)

The pre-exponential factor A (also called "frequency factor") has been neglected in the previous investigation because it does not interact directly with temperature and activation energy in the Arrhenius relationship. However, since A multiplies the exponential term, it contributes to the value of the degradation rate. Constant A combines two factors: collision frequency, which is the total number of collisions between reactants per unit volume per unit time, and orientation factor, which is the fraction of collisions that have proper orientation.

To relate the degradation in the accelerated environment (lifetime τ' and temperature T') to the one under service conditions (lifetime τ and temperature T), the acceleration factor AF for this model can be written:

$$AF = \frac{\tau}{\tau'} = \frac{\frac{c}{k}}{\frac{c}{k'}} = \frac{k'}{k} = \frac{Aexp\left(-\frac{Ea}{RT'}\right)}{Aexp\left(-\frac{Ea}{RT}\right)} = \exp\left(\left(\frac{Ea}{R}\right)\left(\frac{1}{T} - \frac{1}{T'}\right)\right) \tag{6.6}$$

Where: $k-$ the Arrhenius degradation rate; E_a- the activation energy of the chemical reaction; $R-$ universal gas constant (8.3145 J/K/mol); $c-$ critical amount of diffusion; $A-$ constant of the test conditions and product failure

Based on research conducted by Pilkington Brothers LTD and Iowa State University (ISU), a relation between the bath temperature (the temperature used in accelerated aging) and the number of estimated natural aging days per day in the bath was developed as (Litherland et al., 1981, Aindow et al., 1984 and Porter, 1999):

$$AF = \frac{N}{C} = 0.183e^{0.052(T)} \tag{6.7}$$

where: $N-$ the prediction age in natural days; $C-$ the number of exposure days in bath at temperature T (ºF);

However, this equation relates accelerated aging time with natural aging days in water. Moreover, it was evaluated for United Kingdom climate with a mean annual temperature (MAT) of 50.72 ºF (10.4 ºC). To make a prediction of aging days in other climates, another equation for the acceleration factor was proposed (Aindow et al. 1984):

$$AF = 2.986 * 10^{-19} * e^{13.783X} \tag{6.8}$$

The term of "X" in equation 6.8 is calculated as:

$$X = \frac{1000}{50^\circ C + (MAT - 10.4^\circ C) + 273} \tag{6.9}$$

There are several limitations for the Arrhenius Model application. First, the Arrhenius relationship cannot be used with degradation mechanisms changing over time. Only one chemical degradation mode must be dominant in the degradation mechanism. Second, the conditioning of material at elevated temperatures must not alter the way by which the material would degrade under its service conditions. The third difficulty is the fact that this process does not account for the influence of mechanical loading or other environmental factors that may exist in many actual service conditions. Therefore, accelerated test results may not represent the situation of the FRPs in their real environment. Applied mechanical loads in addition to harsh environments will probably make the degradation occur at a higher rate by opening up micro-cracks that allow the diffusion of water and other chemicals into the composite. The fourth limitation is the fact that the degradation rate shown in Eq.6.2 ignores the effect of geometry of the material on its durability characteristics.

6.3.2. Modeling of diffusion.

A GFRP reinforcement is usually subjected to a low-stress level. Therefore the degradation of this material is diffusion dominated in most cases. Diffusion can be described as a net transfer of a substance from a region of high concentration to a region of low concentration. Two general models have been developed to describe chemical diffusion through a resin matrix: 1) single free-phase and 2) Langmuir two-phase model. Both of these models are based on the Fick's Law of Diffusion (Crank, 1975), which states that the driving force for this process is a concentration gradient of the absorbent.

Fick's First Law of Diffusion

Fick's first law of diffusion (steady state of diffusion) relates the diffusion flux with the concentration field, by postulating that flux goes from the region of high concentration to a region of low concentration, with a magnitude that is proportional to the concentration gradient. For Fick's First law, the concentration gradient $\left(\frac{dc}{dx}\right)$is constant with time and diffusion occurs in one dimension. Flux can be described as a transportation of particles (dm) through some area (A) per unit time(dt). Fick's first low of diffusion, as it applies to one-dimensional transport, is given by:

$$\frac{dm}{A * dt} = J = -D\frac{dc}{dx} \tag{6.10}$$

where: $J -$ flux in one dimension; $D -$ diffusion coefficient; $c -$ concentration of the solution; $x -$direction of flux

Mathematics behind Fick's First Law of Diffusion

Analyzing the one-dimensional case of diffusion in a solid (Fig.6.4), where the transfer of interstitials atoms flow from high to low concentration, the likelihood of an atom jump from one plain to another $(1 \rightarrow 2)$takes the form:

$$\vec{J} = \frac{1}{6}\Gamma n_1 \tag{6.11}$$

where: $J -$ flux, $\Gamma -$ sucesful jump frequency, n_1 $-$number of atoms per unit area in plane 1. The 1/6 coefficient is for one dimensional jump in one direction (Mehrer 2007)

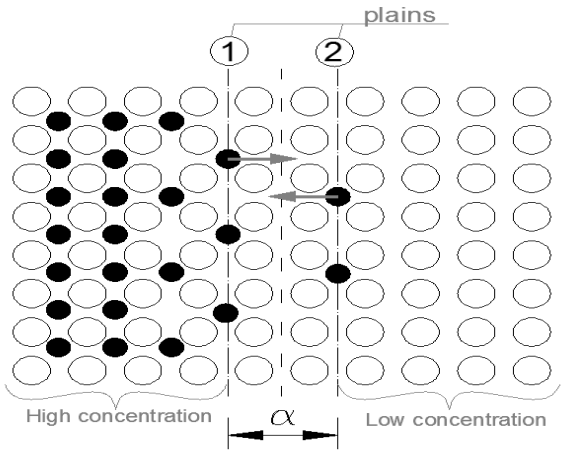

Fig. 6.4 – One-dimensional diffusion (Mehrer 2007)

Since the jump can occur from plane 1 into plane 2, the likelihood of jump occurring from plane 2 into plain 1 is the same:

$$\overleftarrow{J} = \frac{1}{6}\Gamma n_2 \tag{6.12}$$

where: n_2 −number of atoms per unit area in plane 2.

Therefore, the net flux will take a form:

$$J = \vec{J} - \overleftarrow{J} = \frac{1}{6}\Gamma(n_1 - n_2) \tag{6.13}$$

Transferring the area concentration into normal concentration per unit line (α)

$$C_1 = \frac{n_1}{\alpha} \quad and \quad C_2 = \frac{n_2}{\alpha} \rightarrow \quad n_1 - n_2 = \alpha(C_1 - C_2) \tag{6.14}$$

$$J = \frac{1}{6}\Gamma\alpha(C_1 - C_2) \tag{6.15}$$

Considering:

$$C_1 - C_2 = -\alpha\left(\frac{\Delta c}{\Delta x}\right) \tag{6.16}$$

The flux takes the final form of:

$$J = -\frac{1}{6}\Gamma\alpha^2\left(\frac{\Delta c}{\Delta x}\right) \tag{6.17}$$

and, for small distances:

$$J = -\frac{1}{6}\Gamma\alpha^2\left(\frac{dc}{dx}\right) \tag{6.18}$$

Where: $\frac{1}{6}\Gamma\alpha^2$ − diffusion coefficient D

Successful jump frequency

Considering the case of a single interstitial atom in a host environment, it can be said that since that atom is in a vibration motion, it has an intention to jump to another free space. A number of these jumps can be described by the successful jump frequency:

$$\Gamma = \begin{Bmatrix} vibration \\ frequency \end{Bmatrix} * \begin{Bmatrix} number\ of \\ places\ to\ jump \end{Bmatrix} * \begin{Bmatrix} eought \\ energy \end{Bmatrix}$$

$$\Gamma = \nu Z e^{\left(-\frac{Ea}{RT}\right)} \tag{6.19}$$

Where: Γ – successful jump frequency; ν – vibration frequency; Z – coordination factor; E_a – the activation energy

Concentration gradient

As mentioned earlier the concentration gradient for Fick's First law of diffusion is constant with time, what gives a linear relationship between concentration and distance (Fig.6.5).

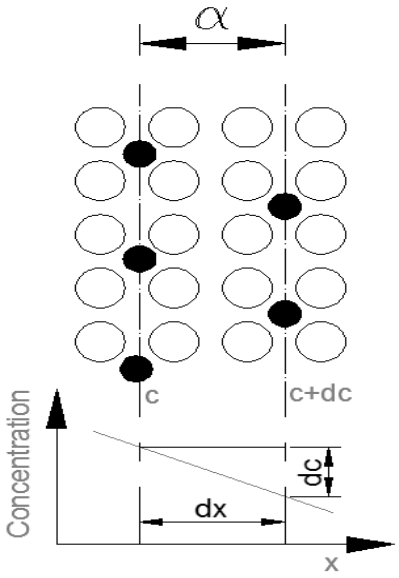

Fig. 6.5 – Concentration and distance relationship in case of Fick's First law (Mehrer 2007)

Fick's Second Law of Diffusion

Fick's second law of diffusion applies to cases where the concentration gradient (dc/dx) is not constant with time, which means that the relationship between concentration and distance over which concentration changes is no longer linear and flux is not constant (Fig.6.6).

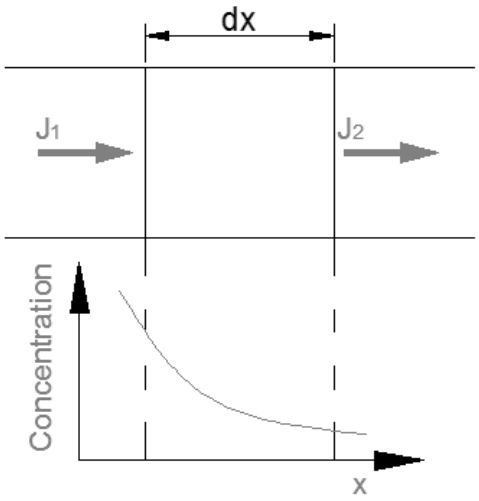

Fig. 6.6 – Concentration and distance relationship in case of Fick's Second law (Mehrer 2007)

$$flux\ in\ J_1 \neq flux\ out\ J_2$$

$$J_1 = -D\left(\frac{dc}{dx}\right)_1 \ ; \ J_2 = -D\left(\left(\frac{dc}{dx}\right)_1 + dx\left(\frac{d^2c}{dx^2}\right)\right) \tag{6.20}$$

The difference between J_1 and J_2 gives the change of the concentration as a function of time

$$dcdx = (flux\ in - flux\ out)dt$$

Hence, Fick's Second Law can be written for one-dimensional diffusion as:

$$\frac{dc}{dt} = D\ \frac{d^2c}{dx^2} \tag{6.21}$$

For three – dimensional diffusion:

$$\frac{dc}{dt} = D\left(\frac{d^2c}{dx^2} + \frac{d^2c}{dy^2} + \frac{d^2c}{dz^2}\right) \tag{6.22}$$

where: $D -$ diffusion coefficient; $c -$ concentration of the solution; $x, y, z -$direction of flux; $t -$ time;

The first law is obtained by reducing the previous equation to one-dimensional flow for the case of no change in concentration with time.

$$\frac{dc}{dt} = 0 \tag{6.23}$$

For 1 – D, the first law can be shown:

$$D\ \frac{d^2c}{dx^2} = 0; \frac{dc}{dx} = constant; c = c_0 + c_1 x \tag{6.24}$$

Free Phase Model

In many systems, e.g., diffusion of organic vapors in a polymer, the diffusion coefficient depends on the diffusing substance concentration, and D varies from point to point. Then the eq.6.22 can be written:

$$\frac{dc}{dt} = \frac{d}{dx}\left(D\frac{dc}{dx}\right) + \frac{d}{dy}\left(D\frac{dc}{dy}\right) + \frac{d}{dz}\left(D\frac{dc}{dz}\right) \tag{6.25}$$

In Cylindrical coordinates ($x = cos\theta; y = rsin\theta$) or for an element of a cylinder volume of sides $dr, rd\theta, dz$, the above equation will transform into:

$$\frac{dc}{dt} = \frac{1}{r}\left(\frac{d}{dr}\left(rD\frac{dc}{dr}\right) + \frac{d}{d\theta}\left(\frac{D}{r}\frac{dc}{d\theta}\right) + \frac{d}{dz}\left(rD\frac{dc}{dz}\right)\right) \tag{6.26}$$

Finally assuming that the cylinder is efficiently long and everywhere diffusion occurs radially, concentration then is a function of radius r and time t, and the diffusion equation 6.26 takes the form:

$$\frac{dc}{dx} = \frac{1}{r} * \frac{d}{dr}\left(r * D * \frac{dc}{dr}\right) \tag{6.27}$$

where: $D -$ mass diffusion coefficient (mm^2/min); $c -$ ion concentration (mol/l) at a distance 'r' (mm) measured in the direction normal to the surface; $r -$ the distance from the central axis of the cylinder; $t -$ exposure time (min)

The mass diffusion coefficient D can be obtained by a moisture absorption test. Crank (1975) gives the solution for eq. 6.27 as:

$$\frac{M}{M_m} = \frac{4*\sqrt{t}}{\sqrt{\pi}} * \left(\frac{\sqrt{D}}{r}\right) \tag{6.28}$$

where: $M_m -$Saturated moisture content; $M -$moisture content at time, t.

In the above equation, the M_m value is reached after a long period. For a sufficiently short period from eq. 6.28 for two different times during moisture absorption, the following can be obtained:

$$D = \frac{\pi * r^2}{16} * \left(\frac{M_2 - M_1}{M_m}\right)^2 * \left(\frac{1}{\sqrt{t_2} - \sqrt{t_1}}\right)^2 \quad (6.29)$$

where: M_1 and M_2 – moisture contents at time t_1 and t_2

For experimental purposes, the moisture content of FRP specimens, M, is calculated as a percentage of the weight gain:

$$M = \frac{W - W_d}{W_d} * 100 \quad (6.30)$$

where: W –wet weight; W_d –dry weight of the specimen

The initial part of the M (%) vs. $\sqrt{t}$ the relationship is linear if the nature of the diffusion is Fickian. This linear relationship can be seen in Eq.6.28. After a period of time, which is dependent on the type of fibers, matrix material, temperature, and type of solution, the curve should level off towards an asymptotic value corresponding to M_m as shown in Fig. 6.7. After an extended period of time ($t > t_m$), which is also dependent on the same aforementioned factors, a non-linear increase in M with respect to $\sqrt{t}$ occurs, indicating non-Fickian diffusion due to fiber degradation and matrix fracturing. Fickian and Non-Fickian stages are shown in Fig 6.7. The non-linear behavior can easily be seen after t_m (time at which maximum Fickian saturation is achieved).

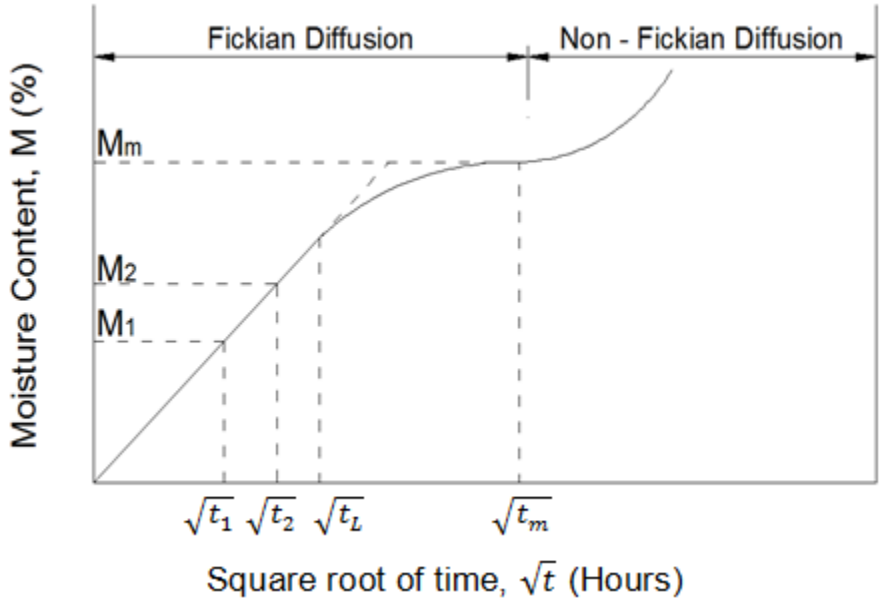

Fig. 6.7 – Different stages of moisture absorption (Tannous et al. 1998)

Langmuir Two-Phase Diffusion Model

As indicated earlier, the Langmuir Model is also based on Fickian diffusion and was developed to model the non-linear Fickian moisture absorption range between times t_L and t_m (Fig.6.7). This model has also been used to determine the diffusivity and weight gain in composites when exposed to temperature and humidity. It can be defined by following two parameters (a and b) that can be obtained experimentally (Tannous et al.1998). In the two-phase diffusion model, for a sufficiently small exposure time, eq. 6.28 can be written:

$$\frac{M}{M_m} = \left(\frac{b}{a+b}\right) * \frac{4 * \sqrt{t}}{\sqrt{\pi}} * \left(\frac{\sqrt{D}}{r}\right) \tag{6.31}$$

For longer time periods (t_L<t<t_m) Eq.3.31 can be written as:

$$\frac{M}{M_m} = 1 - \left(\frac{b}{a+b}\right) * e^{-b*t} \tag{6.32}$$

where: a −the time rate of moisture absorption (%/hours); b −the time rate of moisture desorption (%/hours).

It is very important to note that free-phase (6.25) and Langmuir models (6.31) converge to the same moisture level (M_m). The only difference between them is that the second (6.31) one simulates the transition region ($\sqrt{t_L}$<$\sqrt{t}$<$\sqrt{t_m}$) better than the first one. Both of these models cannot be used after $\sqrt{t_m}$.

6.4. Long-term strength prediction models

Currently, there is no universally agreed prediction model for the long-term behavior of GFRP materials. Among existing models, those that correlate time of accelerated aging (simulated aggressive environment) to real time under the service conditions using the Arrhenius concept, are the most popular, and they describe the degradation rate as a function of temperature. In the following sections, four typical types of prediction models for GFRP materials are discussed.

Model #1

According to Katsuki and Uomoto (1995), free-phase and two-phase diffusion models were employed to predict the losses of tensile strength in this degradation formula. Katsuki and Uomoto assumed the tensile strength of composite reinforcement after alkaline solutions exposure could be predicted using the hypothesis that GFRP bars deteriorate due to the alkaline attack on the glass fibers (Fig.6.8). They specified that the matrix and fibers in the depth of the damaged zone "x" are ineffective in transferring a tensile force and the tensile strength of an undamaged zone is the same as that of a bar before exposure to the aggressive environment. In simple mechanics, the authors assumed that a ratio of the initial strength (σ_0) and strength after immersion ($\sigma_0{}'$) is directly proportional to the ratio of the initial bar area (A_0) and undamaged area (A_1) of the bar after alkaline attack.

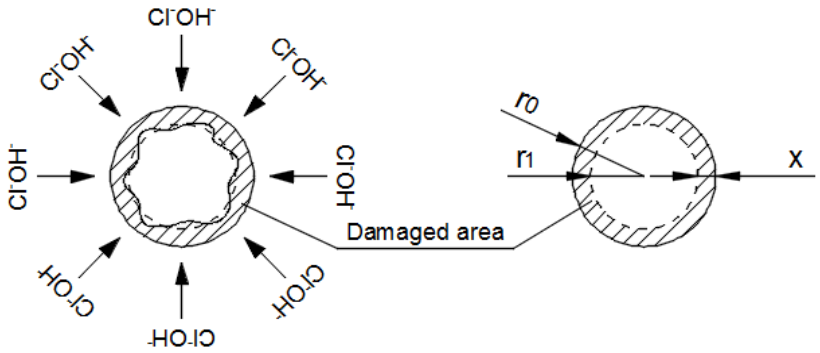

Fig. 6.8 – Diffusion of free ions into GFRP bar (Katsuki and Uomoto, 1995)

$$\frac{\sigma_0{}'}{\sigma_0} = \frac{A_1}{A_0} \rightarrow \sigma_0' = \frac{A_1}{A_0} * \sigma_0 \tag{6.33}$$

Expending eq. 6.33 using r_0, r_1 and x, the residual tensile strength of a bar can be predicted from:

$$\sigma_0' = \frac{{r_1}^2 * \pi}{{r_0}^2 * \pi} * \sigma_0 = \left(\frac{r_0 - x}{r_0}\right)^2 * \sigma_0 = \left(1 - \frac{x}{r_0}\right)^2 * \sigma_0 \tag{6.34}$$

Assuming σ_0 is equal to 100%, the strength retention equation can be written as:

$$Y = 100\left(1 - \frac{x}{r_0}\right)^2 \tag{6.35}$$

where: Y −property retention

Subsequently, they observed and measured the depth of penetration of the alkaline solution into the bars with an Electron Probe Microscope Analyzer, and proposed the use of the following expression to compute the depth of penetration:

$$x = \sqrt{2Dct} \tag{6.36}$$

where: c −alkaline concentration; t − time; D −the mass diffusion coefficient;

In most cases, the diffusion coefficient D is obtained through measuring of moisture absorption and Fick's law. The Arrhenius equation can be applied to the determination of diffusion coefficient to correlate it with accelerated and ambient temperature:

$$D = D_0 * \exp\left(\frac{\Delta H}{RT}\right) \tag{6.37}$$

where: ΔH −activation energy of diffusion; T – temperature in K; R − universal gas constant (8.3145 J/K/mol); D_0 – diffusion constant

Model limitations:

- The affected area of FRP bar is completely degraded, though it can still carry some amount of load
- It is not possible to apply the model to specimens exposed to water because the solution concentration is required in the prediction procedure
- Measurement of moisture absorption is a difficult task. During the degradation of GFRP, by-products of a chemical reaction are leaching out as voids and defects of a bar are filled with solution. Therefore, the weight change may not accurately represent moisture absorption.

Model #2

The second type of prediction model was presented by Bank et al. (2003). This type of model is based on Arrhenius relation, and the relationship between residual strength and time is assumed as:

$$Y = a\log(t) + b \tag{6.38}$$

where: Y is the property retention (%), t is exposure time, a and b are constants. Described model was developed to obtain the strength of glass fiber - reinforced concrete (GRC) and was

successfully applied to data of ten years (Litherland et al. 1981). This is also the most often used prediction model for all FRP materials. However, there is no hypothesis concerning the degradation mechanism and it is only a phenomenological representation of the data. As well, the strength approaches infinity at time zero, based on the assumed relationship. When this method was applied to GFRP bar test results, researchers (Gonenc, 2001) found that the "Arrhenius plots" were not parallel to each other. Thus, it can be stated that the mechanism of degradation has changed with the exposure time, which is against the fundamental assumptions of the Arrhenius relationship.

Model #3

Similar to the second model, the third model was developed for GRC (Beddow 2002, Purnel 2001), with the degradation mechanism assumed to be stress corrosion of glass fibers. The authors assumed that fiber strength loss is not a result of gross fiber corrosion (loss of section as it was presented in model 1), but most likely is governed by the stress correlated expansion of fiber defects. It is known that flaws will be introduced into the fiber surface during fiber handling, packaging, and bar manufacturing. Since fiber strength is closely related to the maximum flaw size it is reasonable to assume (given the lack of gross corrosion) that enlargement of these flaws is the cause of weakening. As a possible mechanism causing flaws, the authors presented a static fatigue and adapted version of this model was used to describe the relationship of strength retention and exposure time.

$$Y = 1/\sqrt{1 + gt} \tag{6.39}$$

where: Y −property retention; t − time; g − temperature function, stress, and solution concentration obtained by:

$$g = g_T g_0 \exp\left(-\frac{E_a}{RT}\right) \tag{6.40}$$

where: g_T −function of temperature; g_0 − account for pH and initial state of fibers

According to Chen 2007, the major limitation of this model is mainly associated with g_T term, which as function of exposure temperature was not explained by authors (Beddow 2002, Purnel 2001). Also, when the activation energy was calculated using equation 6.40, the effect of this factor was ignored in Beddow et al. (2002) without any explanation (i.e., the g_0 term in the equation 6.40 was neglected):

$$\ln(g_2) = \ln(g_1) - \frac{E_a}{RT}\left(\frac{1}{T_1} - \frac{1}{T_2}\right) + \ln\left(\frac{g_{T1}}{g_{T2}}\right) \quad (6.41)$$

where: g_1, g_2, g_{T1}, g_{T2} −values corresponding to temperatures of T_1 and T_2

Model #4

The last model proposed by Chen and Davalos (2011) is based on following equation 6.42 and the assumption that the whole GFRP bar can be considered as a glass fiber.

$$f = \beta t^{\alpha} \quad (6.42)$$

where: f −is the rate of change; β − constant of rate; t − time; α −material constant

This equation is commonly used to describe the rate of changes in the material properties with time (Prian, Barkatt, 1999). In some degradation processes, same changes of the microstructure of the material, for example, cracking, occur, and the degradation rate has a superlinear relationship with time ($\alpha > 0$). In this case the constant-rate degradation, α will be equal to zero. For example the glass dissolution in basic solutions has a constant rate. For degradations where protective layers are formed, the degradation rate has a sublinear dependence on time. To formulate the prediction model for GFRP bars, it is assumed that unaffected cross sectional area is proportional to the the ultimate tensile load capacity of the GFRP bars. Therefore, from equation 6.42, the tensile capacity retention (%) of bars vs. time can be defined as:

$$Y = 100\left(1 - \frac{\int_0^t f\,dt}{r_0}\right)^2 = 100\left(1 - \frac{\beta t^{\alpha+1}}{(\alpha+1)r_0}\right)^2 = 100(1 - jt^{\alpha+1})^2 \quad (6.43)$$

$$j = \frac{\beta}{(\alpha+1)r_0}$$

where: Y −property retention; r_0 −radius of total cross section; t − time; j − temperature factor

It can be found that if $\alpha = -0.5$, eq. 6.43 become an equivalent to equation eq.6.35, which is the prediction equation based on moisture absorption. But by using eq. 6.43, the difficult task of moisture absorption test does not have to be carried out and the strength retention of specimens exposed to water can also be predicted. According to Chen and Davalos, since the factors j and α can be determined for each specific condition, this equation can be used more widely and most likely provides more accurate predictions.

Chapter 7

GFRP BAR DETERIORATION

7.1 Introduction

The influence of the environment on composite bar properties is of great interest in the effective design of structures with nonmetallic reinforcements. Degradation of the composite as a result of exposure to an aggressive environment may result in loss of strength of the reinforcing fibers caused by stress corrosion, fiber-matrix debonding or moisture absorption and polymer degradation. The focus of this chapter is directed into GFRP bar durability and strength prediction models. Using an accelerated aging test (alkaline immersion test) deterioration of basic mechanical properties of GFRP bars (tensile, shear, and flexure strength) was studied. Subsequently, strength degradation data obtained from the test were used for evaluation of existing durability models (as described in Chapter 6) and validation of the new strength prediction method for flexural capacity deterioration.

7.2 Accelerated aging test

The alkaline immersion test has been chosen as an accelerated aging test. Testing methodology used in this research followed the CSA S806-12 standard Annex M, supplemented by information included in ASTM D7705/D7705M protocol. Due to the extensive limitation of an allowable sustained stress level for GFRP bars in service, a temperature was chosen as the only accelerating factor. The alkaline environment designed in proportions of 118.5 g of $Ca(OH)_2$, 0.9 g of NaOH and 4.2 g of KOH in 1 L of deionized water, was considered as an equivalent of the concrete environment. Investigation of GFRP bar properties deterioration has been done at 60° C. Subsequently, data obtained from this temperature were supplemented by two additional tests performed at 50° and 70°C. The total duration of the alkaline immersion test for one temperature was 5 months with three different periods of bars conditioning: 1, 3 and 5 months, respectively. To evaluate the durability performance of GFRP bars in this study, tensile, shear, and flexure tests have been chosen as durability indicators. After each immersion period, bars were taken out ofthe

alkaline environment and individual property retention was investigated. The change in these properties provided information about the rate of bar deterioration and material lifetime.

Since the determination of tensile properties appeared to be inefficient in terms of time and cost (Chapter 4), a decision was made to limit the investigation of tensile strength deterioration only to the one type of GFRP bars (straight bars-SB). Also, due to an excessive number of tests only one temperature (60°C) was chosen to study flexural and shear material deterioration for all three bar types: smooth surface bars (SSB), straight bars (SB), and the straight portion of the bent bar (BB). Since smooth surface bars were produced just as a control specimen and are not typically available on the market, they were excluded from testing at the two other temperatures (50°C and 70°C). Tables 7.1 and 7.2 contain information for Company I and Tables 7.3, 7.4 and 7.5 for Company II, respectively. In total, 660 tests were performed.

Results for GFRP bar property deterioration are shown below after 150 days of immersion in an highly alkaline solution (approximately 13 pH) for tensile test: Company II (Table 7.6, Fig 7.1), shear test: Company I (Table 7.7, Fig 7.2) and Company II (Table 7.8, Fig 7.3), and flexure test: Company I (Table 7.9, Fig 7.4) and Company II (Table 7.10, Fig. 7.5).

All results for the alkaline immersion tests are available in Appendix 6, 7 and 8 for tensile, shear and flexure strength deterioration, respectively. Based on the results from the alkaline immersion tests it can be noticed that the high pH solution has an adverse influence on GFRP bar properties, and the speed of property deterioration increases with the increase of temperature. Thus, it can be stated that temperature and alkaline environment are adequate accelerating factors for GFRP bars. For all tests, the highest degradation rate was observed at 70˚C and the lowest at 50˚C. Thus, the Arrhenius concept should be applicable to determine GFRP bar long-term properties. It was observed, that after 150d of alkaline immersion all types of bars from both companies experienced significant tensile, shear, and flexure strength losses.

In the case of the tensile and shear test, the bars with the smaller diameter deteriorate faster than the bigger diameter bars. This is a common observation for all bar types and tests when the strength directly depends on the bar diameter (tensile and shear capacity). This observation is governed by the ratio of the “degraded” (zone attacked by the alkaline solution) to the “undegraded” (untacked zone) area of the bar, which is higher for bars with the smaller diameter. A similar tendency can be noticed for the flexure test. In addition, it was observed that the BB bars deterioration is quicker

than deterioration of the straight (SB) or smooth (SSB) bars. Quicker degradation of BB bars was noticed for all investigated properties (tensile, shear and flexure strength). This observation is reasonable since the bent bars are characterized by the different type of resin (apparently resin of a lower quality) than SB or SSB bars and smaller fiber- matrix ratio.

Influence of different bar finishing on the degradation speed was analyzed for the temperature of 60˚C for shear and flexure tests. In the case of the shear test, SB and BB bars from Company I and SB and SSB bars from Company II are characterized by a similar degradation rate, while the SSB bars from Company I degraded quicker and BB bars from Company II degraded slower than the other bar types from the same company. This observation shows that the type of the bar finishing has an influence on the degradation rate. In the case of SB and BB bars from Company I, the additional sand coating protects bars and slows the bar deterioration. Similarly, the polyethylene sleeve on BB bars from Company II also slows down the deterioration. Different bar surface finishing seems to have a little or no influence on the deterioration of the modulus of rupture (strength in bending), where no significate difference was observed between deterioration of bars with different surface finishing.

Table 7.1 – Test information for Company I – shear test

Shear test																		
Test Temperature (°C)	50																	
Bar type	SB						BB											
Bar size	#4			#5			#4			#5								
Immersion period (months)	1	3	5	1	3	5	1	3	5	1	3	5						
# of specimens	3	3	3	3	3	3	3	3	3	3	3	3						
Test Temperature (°C)	60																	
Bar type	SB						BB						SSB					
Bar size	#4			#5			#4			#5			#4			#5		
Immersion period (months)	1	3	5	1	3	5	1	3	5	1	3	5	1	3	5	1	3	5
# of specimens	3	3	3	3	3	3	3	3	3	3	3	3	3	3	3	3	3	3
Test Temperature (°C)	70																	
Bar type	SB						BB											
Bar size	#4			#5			#4			#5								
Immersion period (months)	1	3	5	1	3	5	1	3	5	1	3	5						
# of specimens	3	3	3	3	3	3	3	3	3	3	3	3						

Table 7.2 – Test information for Company I – flexure test

Flexure test																		
Test Temperature (°C)	50																	
Bar type	SB						BB											
Bar size	#4			#5			#4			#5								
Immersion period (months)	1	3	5	1	3	5	1	3	5	1	3	5						
# of specimens	4	4	4	4	4	4	4	4	4	4	4	4						
Test Temperature (°C)	60																	
Bar type	SB						BB						SSB					
Bar size	#4			#5			#4			#5			#4			#5		
Immersion period (months)	1	3	5	1	3	5	1	3	5	1	3	5	1	3	5	1	3	5
# of specimens	4	4	4	4	4	4	4	4	4	4	4	4	4	4	4	4	4	4
Test Temperature (°C)	70																	
Bar type	SB						BB											
Bar size	#4			#5			#4			#5								
Immersion period (months)	1	3	5	1	3	5	1	3	5	1	3	5						
# of specimens	4	4	4	4	4	4	4	4	4	4	4	4						

Table 7.3 – Test information for Company II – shear test

Shear test																		
Test Temperature (°C)	50																	
Bar type	SB						BB											
Bar size	12M			16M			12M			16M								
Immersion period (months)	1	3	5	1	3	5	1	3	5	1	3	5						
# of specimens	3	3	3	3	3	3	3	3	3	3	3	3						
Test Temperature (°C)	60																	
Bar type	SB						BB						SSB					
Bar size	12M			16M			12M			16M			12M			16M		
Immersion period (months)	1	3	5	1	3	5	1	3	5	1	3	5	1	3	5	1	3	5
# of specimens	3	3	3	3	3	3	3	3	3	3	3	3	3	3	3	3	3	3
Test Temperature (°C)	70																	
Bar type	SB						BB											
Bar size	12M			16M			12M			16M								
Immersion period (months)	1	3	5	1	3	5	1	3	5	1	3	5						
# of specimens	3	3	3	3	3	3	3	3	3	3	3	3						

Table 7.4 – Test information for Company II – flexure test

Flexure test																		
Test Temperature (°C)	50																	
Bar type	SB						BB											
Bar size	12M			16M			12M			16M								
Immersion period (months)	1	3	5	1	3	5	1	3	5	1	3	5						
# of specimens	4	4	4	4	4	4	4	4	4	4	4	4						
Test Temperature (°C)	60																	
Bar type	SB						BB						SSB					
Bar size	12M			16M			12M			16M			12M			16M		
Immersion period (months)	1	3	5	1	3	5	1	3	5	1	3	5	1	3	5	1	3	5
# of specimens	4	4	4	4	4	4	4	4	4	4	4	4	4	4	4	4	4	4
Test Temperature (°C)	70																	
Bar type	SB						BB											
Bar size	12M			16M			12M			16M								
Immersion period (months)	1	3	5	1	3	5	1	3	5	1	3	5						
# of specimens	4	4	4	4	4	4	4	4	4	4	4	4						

Table 7.5 – Test information for Company II – tensile test

Tensile test									
Test Temperature (°C)	50								
Bar type	SB								
Bar size	12M			16M					
Immersion period (months)	1	3	5	1	3	5			
# of specimens	4	4	4	4	4	4			
Test Temperature (°C)	60								
Bar type	SB								
Bar size	12M			16M					
Immersion period (months)	1	3	5	1	3	5			
# of specimens	4	4	4	4	4	4			
Test Temperature (°C)	70								
Bar type	SB								
Bar size	12M			16M					
Immersion period (months)	1	3	5	1	3	5			
# of specimens	4	4	4	4	4	4			

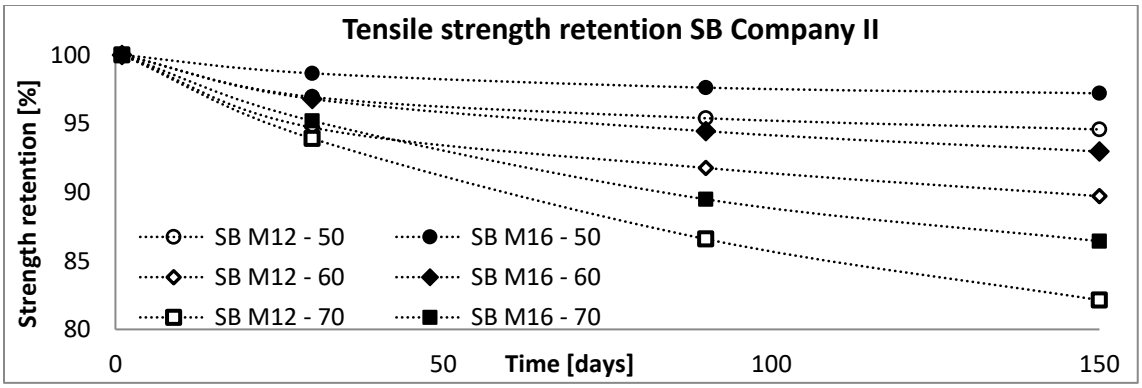

Fig. 7.1 – Tensile strength retention

Table 7.6 – Tensile strength deterioration for SB bars from Company II

Temp.		**Ultimate capacity [kN]**				**Strength degradation [MPa]**				**Strength retention [%]**			
	Time [days]	**0**	**30**	**90**	**150**	**0**	**30**	**90**	**150**	**0**	**30**	**90**	**150**
50 °C	SB M12	138	134	131	130	1223	1186	1167	1157	100	96.9	95.4	94.6
	SB M16	255	252	249	248	1270	1253	1240	1235	100	98.7	97.6	97.2
	Time [days]	**0**	**30**	**90**	**150**	**0**	**30**	**90**	**150**	**0**	**30**	**90**	**150**
60 °C	SB M12	138	131	127	124	1223	1158	1122	1097	100	94.7	91.8	89.7
	SB M16	255	247	241	237	1270	1229	1199	1181	100	96.8	94.4	93
	Time [days]	**0**	**30**	**90**	**150**	**0**	**30**	**90**	**150**	**0**	**30**	**90**	**150**
70 °C	SB M12	138	130	120	113	1223	1148	1059	1004	100	93.9	86.6	82.1
	SB M16	255	243	228	220	1270	1209	1136	1098	100	95.2	89.5	86.4

a)

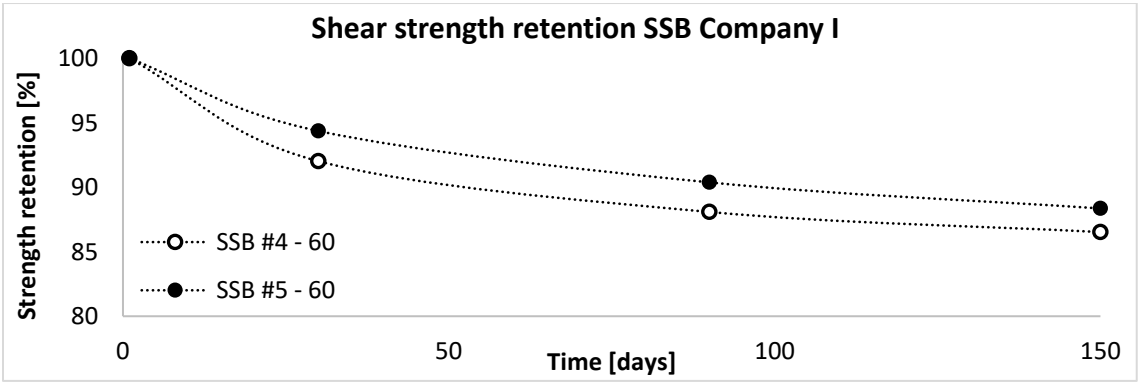

b)

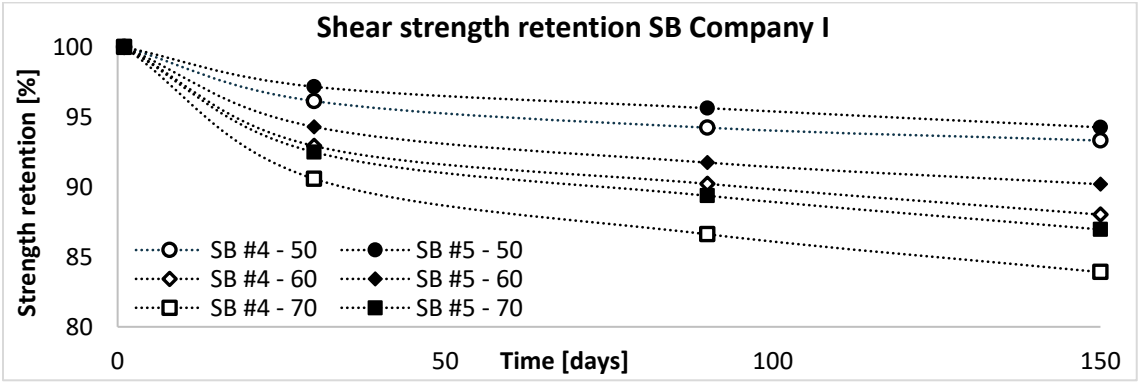

c)

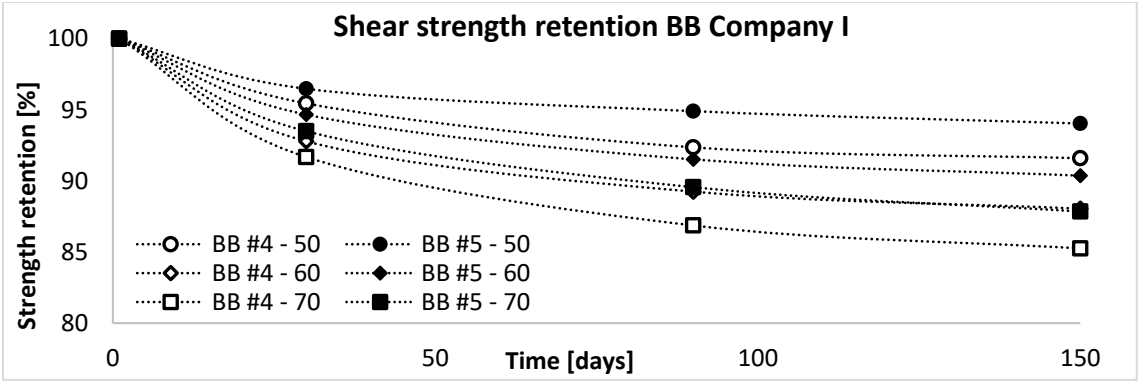

Fig. 7.2 – Shear strength retention – Company I for a) SSB, b) SB c) BB bars

Table 7.7 – Shear strength deterioration for bars from Company I

Temp.		**Ultimate capacity [kN]**				**Strength degradation [MPa]**				**Strength retention [%]**			
	Time [days]	**0**	**30**	**90**	**150**	**0**	**30**	**90**	**150**	**0**	**30**	**90**	**150**
50 °C	SB #4	74	71	70	69	242	232	227	225	100	90.6	86.6	83.9
	SB #5	109	106	104	102	214	208	205	202	100	92.5	89.4	87.0
	BB #4	56	53	52	51	247	235	228	226	100	91.7	86.9	85.3
	BB #5	77	74	73	72	191	184	181	179	100	93.5	89.6	87.9
60 °C	**Time [days]**	**0**	**30**	**90**	**150**	**0**	**30**	**90**	**150**	**0**	**30**	**90**	**150**
	SSB #4	60	55	53	52	195	180	171	168	100	92.0	88.1	86.5
	SSB #5	98	92	89	87	192	182	174	170	100	94.4	90.4	88.4
	SB #4	74	69	67	65	242	225	218	212	100	92.9	90.2	88.0
	SB #5	109	103	100	98	214	202	197	193	100	94.3	91.7	90.2
	BB #4	56	52	50	49	247	229	220	217	100	92.8	89.2	88.0
	BB #5	77	72	70	69	191	180	174	172	100	94.7	91.5	90.4
70 °C	**Time [days]**	**0**	**30**	**90**	**150**	**0**	**30**	**90**	**150**	**0**	**30**	**90**	**150**
	SB #4	74	67	64	62	242	219	209	203	100	96.1	94.2	93.3
	SB #5	109	101	97	95	214	198	192	186	100	97.2	95.6	94.3
	BB #4	56	51	48	47	247	226	214	210	100	95.4	92.4	91.6
	BB #5	77	71	68	67	191	178	170	167	100	96.5	95.5	94.0

a)

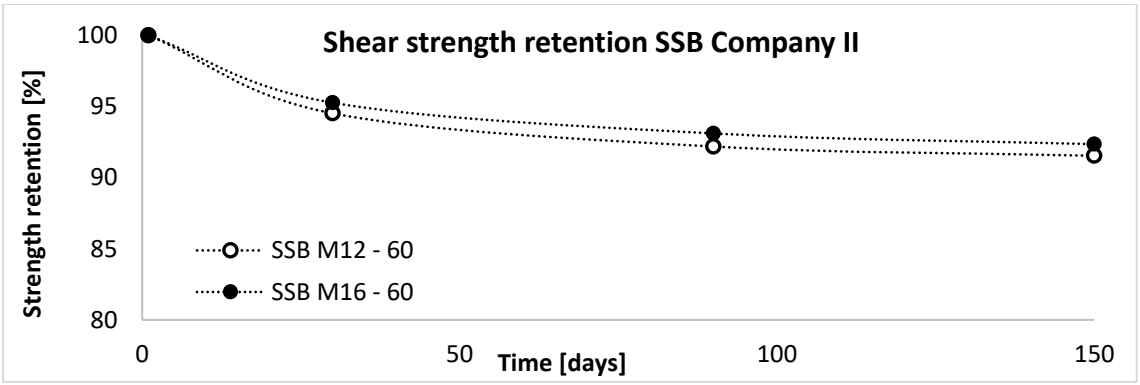

b)

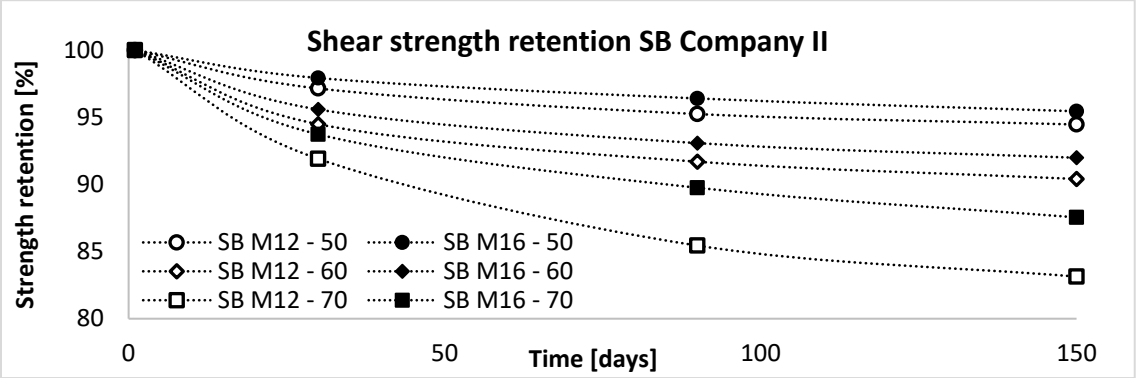

c)

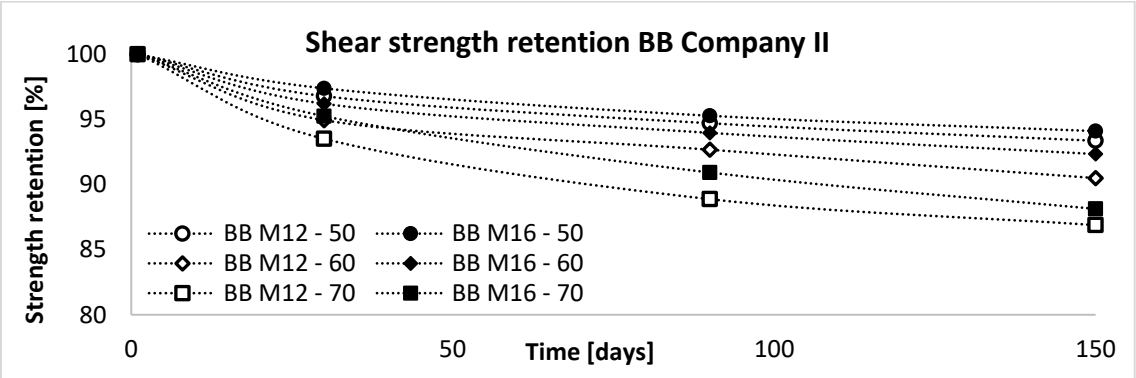

Fig. 7.3 – Shear strength retention – Company II for a) SSB, b) SB c) BB bars

Table 7.8 – Shear strength deterioration for bars from Company II

Temp.		**Ultimate capacity [kN]**				**Strength degradation [MPa]**				**Strength retention [%]**			
	Time [days]	**0**	**30**	**90**	**30**	**0**	**30**	**90**	**150**	**0**	**30**	**90**	**150**
50 °C	SB M12	50	48.5	47.5	47	221	214	210	208	100	91.9	85.4	83.1
	SB M16	84	83	81.5	81	210	206	203	201	100	93.7	89.8	87.5
	BB M12	65	63	62	61	289	280	274	270	100	93.5	88.9	86.9
	BB M16	112	110	108	106	280	273	267	264	100	95.2	90.9	88.1
60 °C	**Time [days]**	**0**	**30**	**90**	**30**	**0**	**30**	**90**	**150**	**0**	**30**	**90**	**150**
	SSB M12	56	49	48.3	48	197	187	182	180	100	94.5	92.2	91.5
	SSB M16	99	94	92	91	194	185	180	179	100	95.3	93.1	92.4
	SB M12	50	47	46	45	221	208	202	199	100	94.5	91.7	90.4
	SB M16	84	81	79	78	210	201	196	193	100	95.6	93.1	92.0
	BB M12	65	62	61	60	289	275	268	262	100	94.9	92.7	90.5
	BB M16	112	109	106	104	280	270	264	259	100	96.2	94.0	92.3
70 °C	**Time [days]**	**0**	**30**	**90**	**30**	**0**	**30**	**90**	**150**	**0**	**30**	**90**	**150**
	SB M12	50	46	43	41	221	203	188	183	100	97.1	95.2	94.5
	SB M16	84	79	76	74	210	197	189	184	100	97.9	96.4	95.5
	BB M12	65	61	58	57	289	270	257	251	100	96.8	94.7	93.4
	BB M16	112	107	102	99	280	267	255	247	100	97.4	95.3	94.1

Table 7.9 – Flexural strength deterioration for bars from Company I

Temp.		Strength degradation [MPa]				Strength retention [%]			
	Time [days]	**0**	**30**	**90**	**150**	**0**	**30**	**90**	**150**
50 °C	SB #4	1646	1564	1482	1455	100	95.0	90.0	88.4
	SB #5	1510	1457	1410	1349	100	96.5	93.3	89.3
	BB #4	1557	1454	1398	1367	100	93.4	89.8	87.8
	BB #5	1403	1316	1264	1245	100	93.8	90.1	88.8
	Time [days]	**0**	**30**	**90**	**150**	**0**	**30**	**90**	**150**
60 °C	SSB #4	1687	1527	1463	1427	100	90.53	86.77	84.62
	SSB #5	1544	1410	1356	1329	100	91.33	87.83	86.05
	SB #4	1646	1478	1409	1352	100	89.8	85.6	82.1
	SB #5	1510	1396	1302	1257	100	92.5	86.2	83.2
	BB #4	1557	1423	1338	1288	100	91.4	85.9	82.7
	BB #5	1403	1286	1225	1194	100	91.7	87.3	85.1
	Time [days]	**0**	**30**	**90**	**150**	**0**	**30**	**90**	**150**
70 °C	SB #4	1646	1396	1295	1222	100	84.8	78.7	74.2
	SB #5	1510	1329	1221	1166	100	88.0	80.8	77.2
	BB #4	1557	1356	1259	1204	100	87.1	80.8	77.3
	BB #5	1403	1235	1169	1125	100	88.0	83.3	80.2

a)

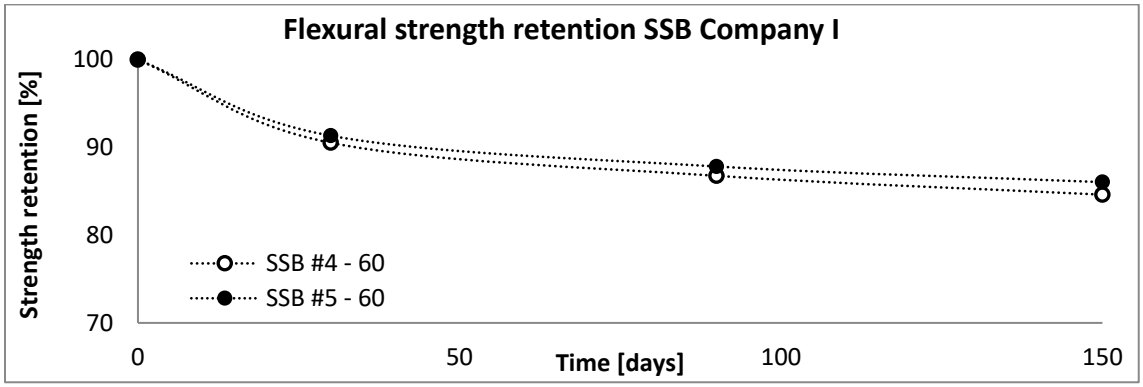

b)

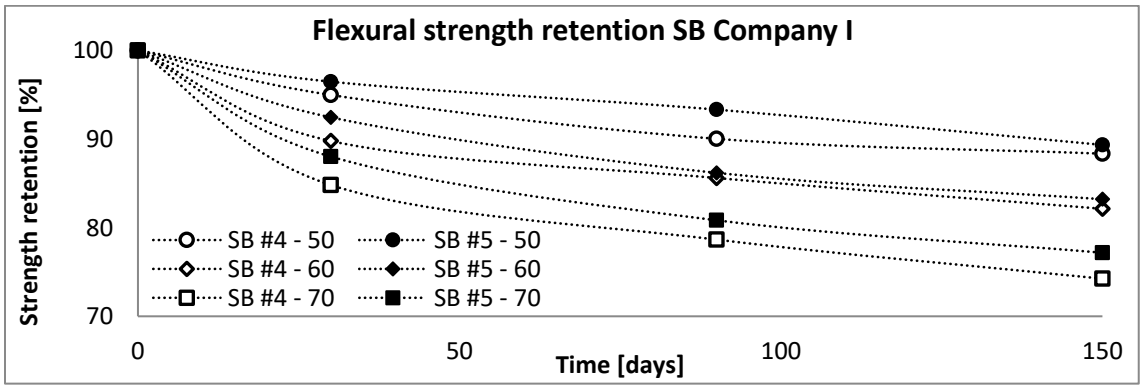

c)

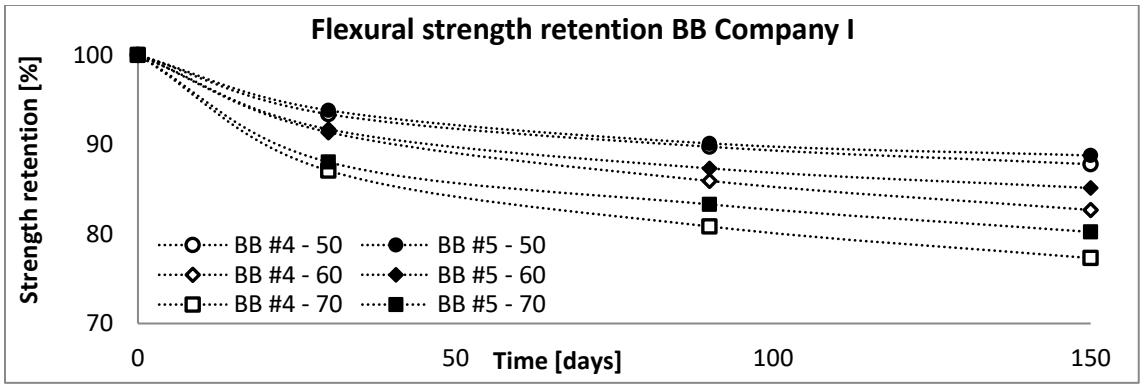

Fig. 7.4 – Flexural strength retention – Company I for a) SSB, b) SB c) BB bars

Table 7.10 – Flexural strength deterioration for bars from Company II

Temp.		**Strength degradation [MPa]**				**Strength retention [%]**			
	Time [days]	**0**	**30**	**90**	**150**	**0**	**30**	**90**	**150**
50 °C	SB M12	1927	1851	1818	1779	100	96.1	94.4	92.3
	SB M16	1836	1791	1756	1725	100	97.5	95.7	94.0
	BB M12	1684	1603	1564	1517	100	95.2	92.9	90.1
	BB M16	1572	1523	1476	1444	100	96.9	93.9	91.8
60 °C	**Time [days]**	**0**	**30**	**90**	**150**	**0**	**30**	**90**	**150**
	SSB M12	1757	1658	1605	1580	100	94.3	91.3	89.9
	SSB M16	1763	1658	1593	1570	100	94.0	90.3	89.0
	SB M12	1927	1796	1709	1665	100	93.2	88.7	86.4
	SB M16	1836	1737	1672	1648	100	94.6	91.1	89.8
	BB M12	1684	1573	1499	1431	100	93.4	89.0	84.9
	BB M16	1572	1485	1432	1395	100	94.4	91.1	88.7
70 °C	**Time [days]**	**0**	**30**	**90**	**150**	**0**	**30**	**90**	**150**
	SB M12	1927	1720	1607	1518	100	89.3	83.4	78.8
	SB M16	1836	1666	1553	1490	100	90.8	84.6	81.2
	BB M12	1684	1497	1359	1316	100	88.9	80.7	78.2
	BB M16	1572	1429	1317	1272	100	90.9	83.8	80.9

a)

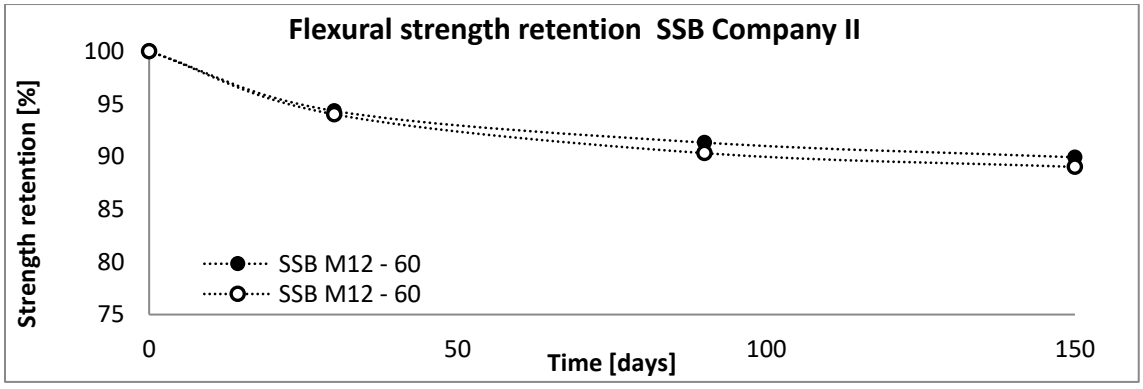

b)

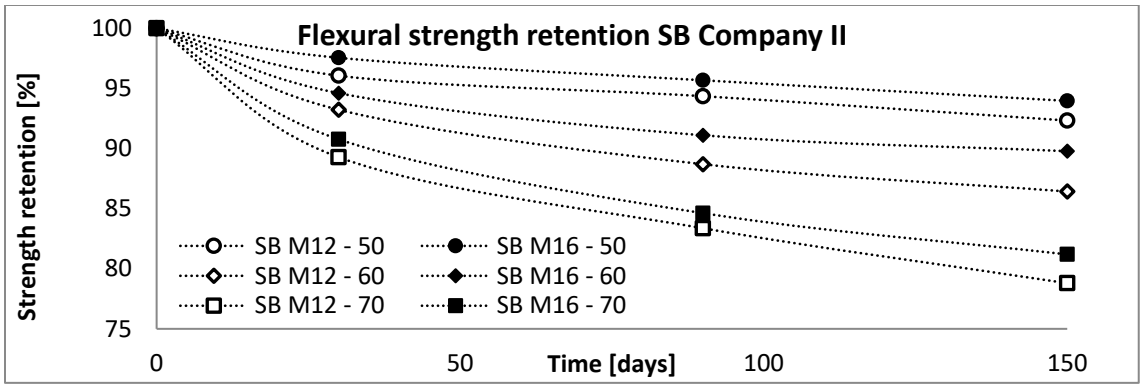

c)

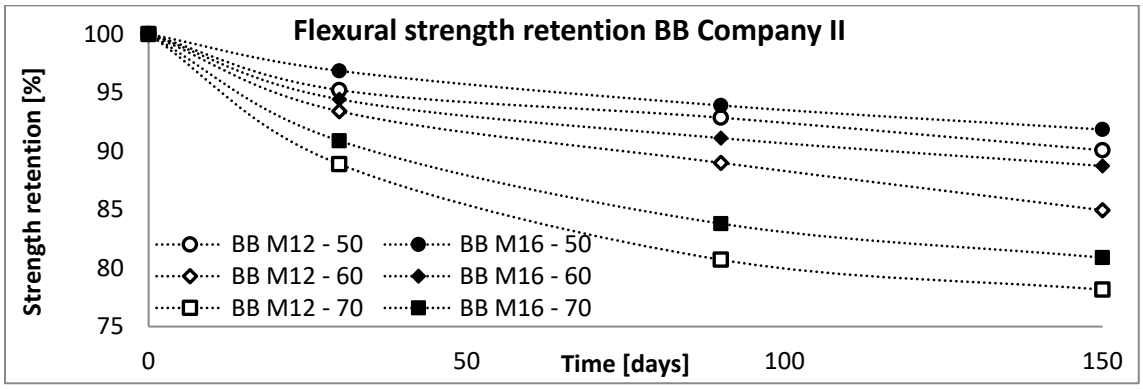

Fig. 7.5 – Flexural strength retention – Company II for a) SSB, b) SB c) BB bars

7.3 Evaluation of the existing strength prediction models

The test results presented in section 7.2 represent only bar property deterioration after an alkaline immersion test with a maximum duration of 150 days. To predict GFRP bar long-term performance from these results, an appropriate strength prediction model should be employed. However, there are several different prediction models proposed for the durability of the composite in the published literature (Katsuli and Umoto 1995, Bank et al. 2003, Beddow 2002, etc.), and each of them can lead to a different outcome. In this section, the available strength prediction models, described in Chapter 6, are evaluated using the tensile test results of this study. It is assumed there is just one major deterioration mechanism, which is time and temperature independent, and the degradation rate is temperature sensitive.

7.3.1 Durability prediction procedure and models evaluation

Based on the findings presented in section 6.4, the durability prediction Model#4 was chosen as an example to describe the general durability prediction procedure. Subsequently, using the same concept the remaining strength prediction models were analyzed and evaluated.

Model #4

- **Step 1**

The first step in a strength prediction procedure is developing a proper correlation between tensile strength retention (the percentage of residual strength over original tensile strength) obtained through the alkaline immersion test with the chosen model (eq. 6.43). However, because the strength prediction Model # 4 directly depends on the rate of change (f) in the material properties with time (eq. 6.42) before any actions for durability prediction can be undertaken, all parameters describing the rate of change (β and α) need to be determined.

Parameter "α" is a material constant and depends on the material ability to resist an aggressive environment. As observed in the alkaline immersion test results (Fig.7.1-Fig.7.5) and as described in section 2.3 and 6.4, the degradation rate for GFRP bars is characterized by a sublinear dependence on time. Thus, the material parameter α was selected as - 0.5.

The temperature factor "j" introduced in equation 6.43 is, in fact, a combination of the integration product directly correlated with the constant rate "β", and the radius of the bar. Thus, equation 6.43 takes the form (Eq. 7.2):

$$Y = 100\left(1 - \frac{\int_0^t f dt}{r_0}\right)^2 = 100\left(1 - \frac{\beta t^{-0.5+1}}{(-0.5+1)r_0}\right)^2 = 100\left(1 - \frac{2\beta t^{0.5}}{r_0}\right)^2 \quad (7.2)$$

Taking a closer look at the first part of the equation 7.2 it can be noticed that the integral over the rate of change (f) is equivalent to the penetration depth "x" described in model number 1 and the rate constant "β" represents a speed of penetration [mm/s]. Since the literature (Davalos and Chen (2011)) on Model #4 did not provide any explanation for parameter "β", it was determined by curve fitting to the data points obtained from the alkaline immersion test, with a coefficient of correlation greater than 0.8. Both the rate parameter "β" and the correlation coefficient for three different temperatures (50˚C, 60˚C, and 70˚C) are reported in Table 7.11.

Table 7.11 – Rate constant "β"

Temperature	β[mm/s]	R^2 for M12	R^2 for M16
50˚C	7.87 * (10^{-8})	0.83	0.82
60˚C	1.562 * (10^{-7})	0.97	0.93
70˚C	2.315 * (10^{-7})	0.89	0.92

Results obtained for parameter "β" show a strong influence of the temperature on the speed of penetration. Moreover, the rate parameter exhibits the same characteristics as a mass diffusion coefficient D, thus the Arrhenius relationship should be applicable to describe the correlation between the speed of penetration and temperature:

$$\beta = \beta_0 \exp\left(\frac{\Delta H}{RT}\right) \tag{7.3}$$

Where: β – speed of penetration; β_0 – constant; R – universal gas constant (8.3145 J/K/mol); T – temperature in K; ΔH –activation energy

Thus, the Arrhenius plot can be used to verify the obtained values of parameter "β" by curve fitting as per Fig. 7.6. A high coefficient of determination (0.98) for the regression line proves that the speeds of penetration were obtained correctly.

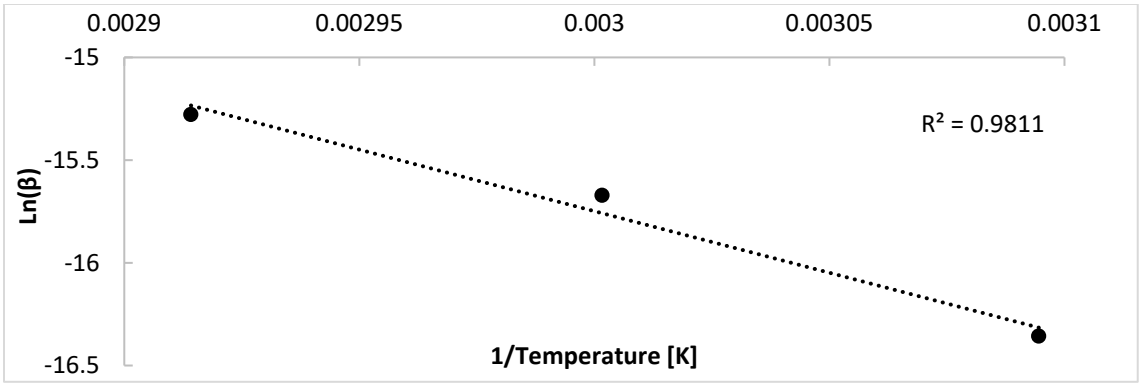

Fig. 7.6 – Arrhenius plot for rate parameter "β"

Subsequently, the tensile strength retention curvatures calculated directly from equation 7.2 were plotted in Fig.7.7 with the obtained test data. Because the standard error of the regression for all curvatures is less than 1.5, hence the strength retention models obtained from Model #4 represent the data with sufficient accuracy and can be used for further investigation.

a)

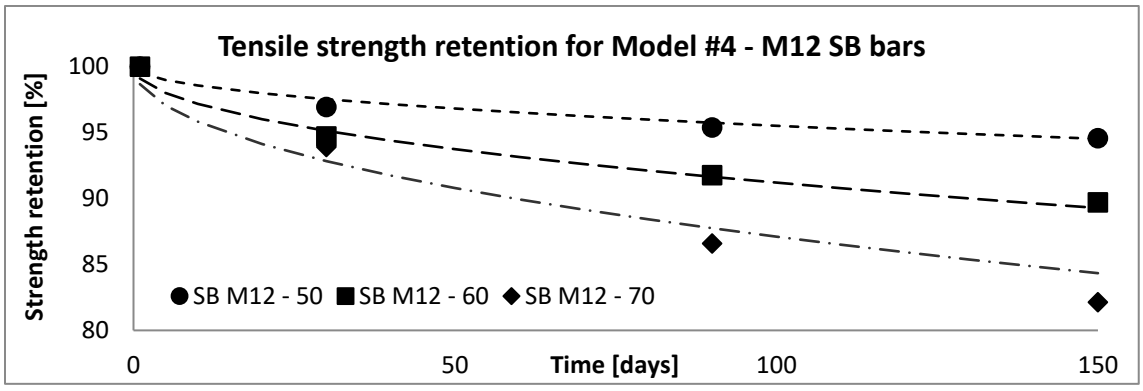

b)

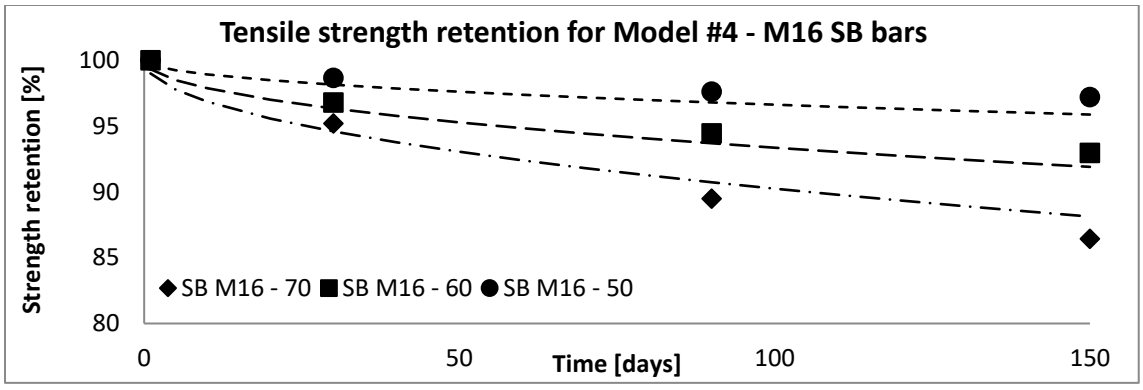

Fig. 7.7 – Tensile strength retention a) SB M12, b) SB M6 bars

- **Step 2**

The time to reach a specific strength retention (Table 7.12) at different temperatures can be approximately calculated through equation (7.2) after a proper transformation:

$$t = \left(\frac{1 - \sqrt{\frac{Y}{100}} * r_0}{2\beta} \right)^2 \tag{7.4}$$

A visual interpretation of the procedure for 95% retention of M12 bars is shown in Fig. 7.8.

Table 7.12 – Required time in alkaline solution bath to reach specific tensile strength retention

Retention	SB M12 - 50	SB M12 - 60	SB M12 - 70	SB M16 - 50	SB M16 - 60	SB M16 - 70
	Time to reach specific retention [days]					
95	124.79	31.66	14.43	221.84	56.29	25.65
85	1185.55	300.80	137.05	2107.65	534.75	243.64
75	3493.57	886.38	403.86	6210.79	1575.79	717.97

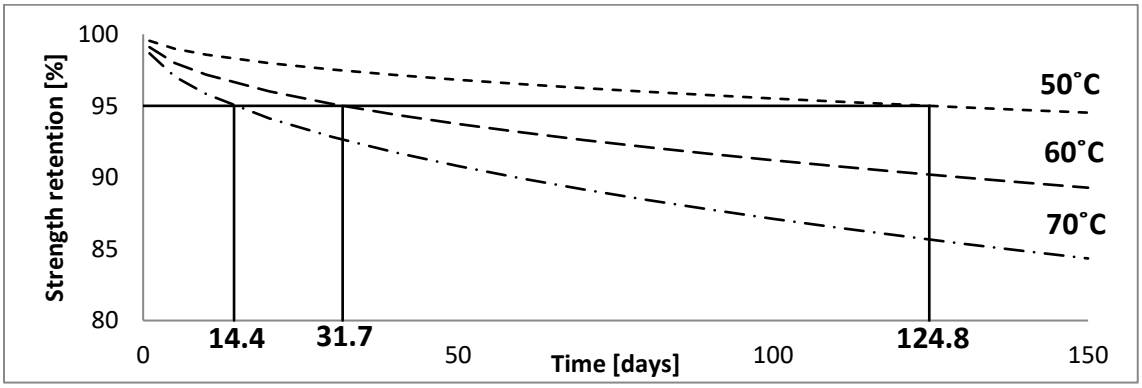

Fig. 7.8 – Required time in alkaline solution bath for M12 bars to reach 95% tensile strength retention for 50˚C, 60˚C, and 70˚C, respectively.

- **Step 3**

The next step is to use the data obtained from the GFRP bar strength retention in the Arrhenius relationship. Analyzing equations 6.1 and 6.5 (Chapter 6) it can be found that the degradation rate can be expressed as the inverse of time needed for a material property to reach a given retention value.

From equation 6.2, it can be further observed that the logarithm of inverse time is a linear function with slope of $\left(\frac{E_a}{R}\right)$. The Arrhenius plot of the logarithm of reaction rate vs the inverse of immersion temperature (in K) is shown on Fig.7.9.

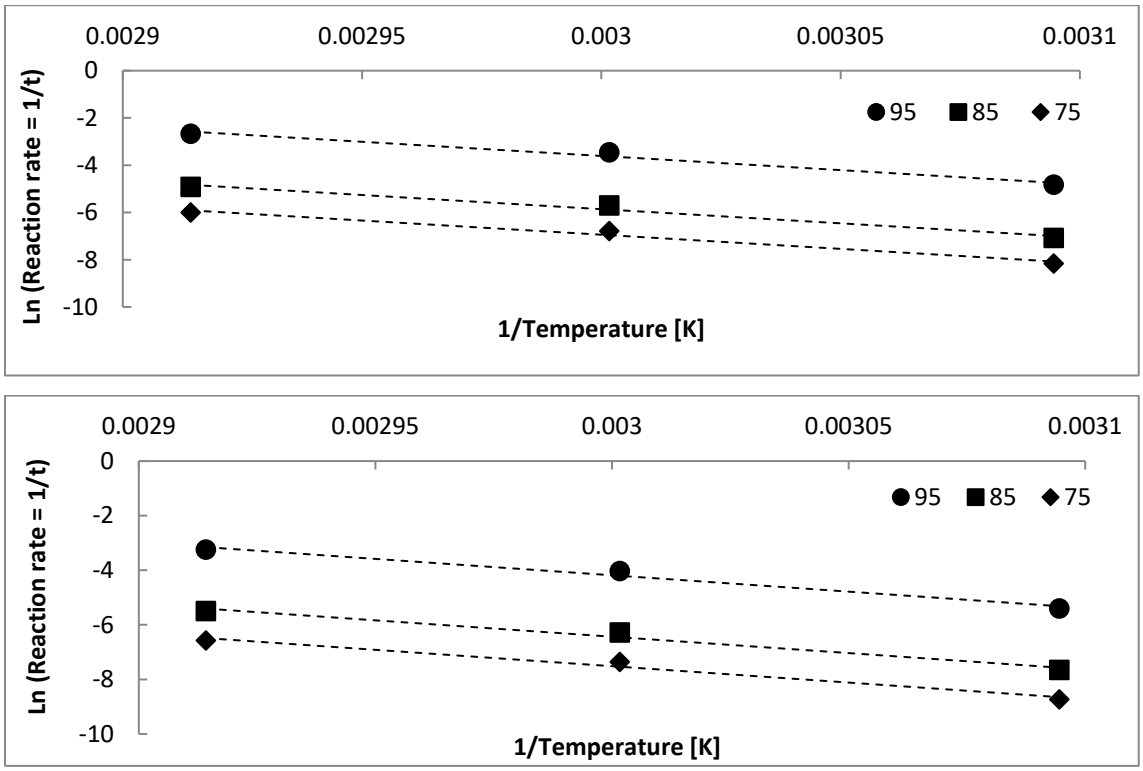

Fig. 7.9 – Arrhenius plot for a) M12 and b) M16 bars

Analyzing Fig. 7.9 it can be noticed that the regression lines in the Arrhenius plots for different strength retentions are nearly parallel to each other. The calculated coefficient of determination (R^2) for all regression lines is close to 1 (Table. 7.13), and the slopes of the lines are equal to $\left(\frac{E_a}{R}\right)$. This implies that the Arrhenius model can be used to describe the degradation rate of the GFRP bars, as the degradation mechanism in Model #4 does not seems to change with temperature or time during the alkaline immersion. Thus, Model #4 can be successfully used to describe the GFRP bar long-term durability.

Table 7.13 – Slope $\left(\frac{E_a}{R}\right)$ and correlation coefficient

Temperature	$\left(\frac{E_a}{R}\right)$ for M12	R^2 for M12	$\left(\frac{E_a}{R}\right)$ for M16	R^2 for M16
50˚C	11962	0.98	11962	0.98
60˚C	11963	0.98	11962	0.98
70˚C	11962	0.98	11961	0.98

- **Step 4**

Subsequently, after the activation energy is known, the acceleration factor (AF) for the alkaline immersion test at three different temperatures can be obtained from previously obtained Arrhenius plots (i.e., see Fig 7.9) by using equation 6.6. Since the fitted lines in the Arrhenius plots (Fig. 7.9) are nearly parallel to each other, the calculated acceleration factor is constant for all strength retention values (95%, 85%, 75%). The acceleration factor values for all three temperatures related to 20˚C are listed in Table 7.14.

Table 7.14 – Acceleration Factors

Temperature	AF
50˚C	44
60˚C	134
70˚C	382

- **Step 5**

Finally, once the AF values for 50˚C, 60˚C, and 70˚C were obtained, the long-term durability can be predicted by multiplying the times of exposure at 50˚C, 60˚C, and 70˚C by the corresponding AF values (Table 7.14). Master curves (Fig. 7.11) for tensile strength retention for two bar diameters M12 and M16 versus exposure time at 20˚C were obtained from eq. 7.2 with the material parameter α equal to -0.5 and the speed of penetration $\beta = 1.22*10^{-8}$. The rate parameter "β" was determined using the Arrhenius relationship established previously (eq. 7.3 and Fig. 7.6). Visualization of this process is shown in Fig. 7.10.

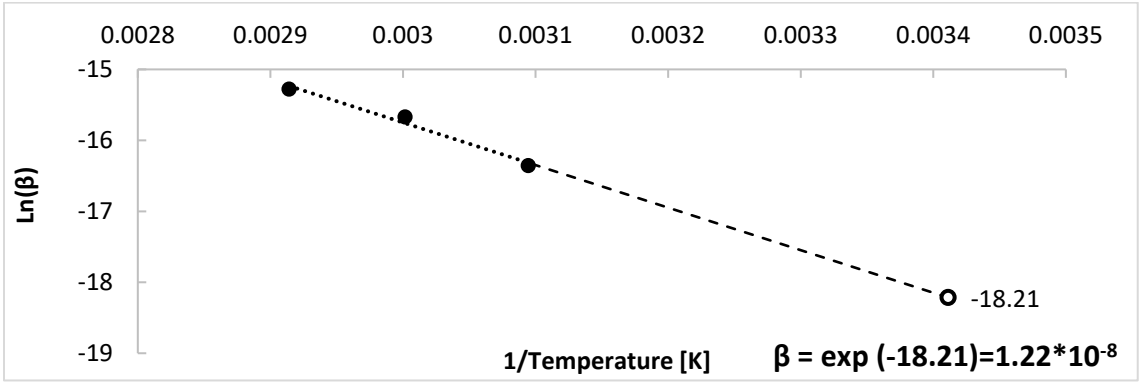

Fig. 7.10 – Arrhenius plot for rate parameter "β"

Table 7.15 – Long-term tensile strength retention

Tensile strength retention			
Time in Bath	Time in Construction	SB M12 [%]	SB M16 [%]
[days]	[years]	50˚C	
30	3.6	96.94	98.66
90	10.9	95.38	97.62
150	18.2	94.57	97.2
[days]	[years]	60˚C	
30	11	94.71	96.8
90	33.1	91.76	94.44
150	55.2	89.71	92.96
[days]	[years]	70˚C	
30	31.4	93.9	95.2
90	94.3	86.58	89.48
150	157.1	82.48	86.43

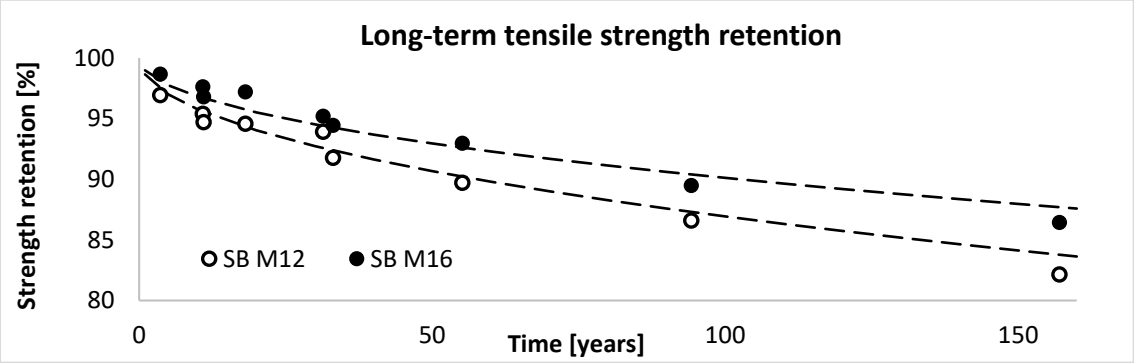

Fig. 7.11 – Long-term tensile strength retention at 20˚C for Model #4

The standard error of the regression for both master curves in Fig. 7.11 representing long-term tensile strength retention (eq. 7.2) is less than 1. Thus, it can be stated that durability Model #4 can be considered as a satisfactory prediction for the long-term property behaviour. The master curves from Fig. 7.11 can be used to predict tensile strength retention for any exposure time at 20˚C. For example, at year 100, SB M12 bars will lose 13%, and SB M16 10% of their original capacity (eq. 7.4). Using the presented methodology, the master curves can be established for any temperature by calculating new accelerating factors (eq. 6.6).

Model #1

In the case of Model #1 before any actions for long-term durability predictions can be undertaken, the mass diffusion coefficient (D) needs to be determined. This is due to the direct relationship between the strength retention model and depth of the "damaged zone" x (depth of solution penetration). In most cases, the diffusion coefficient is obtained through moisture absorption tests.

The test was performed according to the ASTM D570 as specified in CSA S 807-10 and the mass diffusion coefficients for four different temperatures is reported in Table 7.16.

Table 7.16 – Mass diffusion coefficients

Temperature	D [mm^2/s]
20 ˚C	$2.315 * (10^{-11})$
50˚C	$1.099 * (10^{-9})$
60˚C	$3.472 * (10^{-9})$
70˚C	$9.838 * (10^{-9})$

Due to fact that bars were kept in a highly alkaline solution, the concentration of 1 was used to obtain the depth of penetration. Graphical visualization of damaged zone x (eq. 6.36) for three different temperatures (50˚C, 60˚C, and 70˚C) after 150-days of immersion is shown in Fig. 7.12.

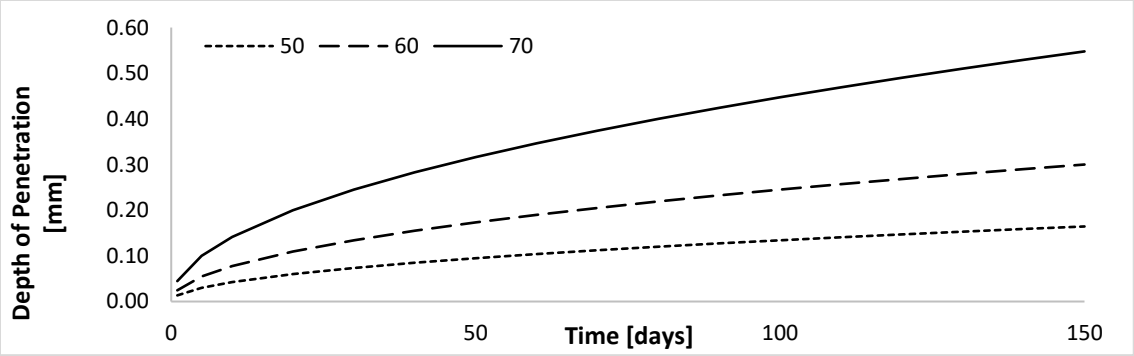

Fig. 7.12 – Penetration depth of alkaline solution at three different temperatures

- **<u>Step 1</u>**

The tensile strength retention curves calculated directly from equation 6.35 were plotted in Fig.7.13 with the obtained test data. All correlation coefficients for strength retention curves with a respect to the obtained data points are reported in Table 7.17. Because all standard errors of the regression are less than 1.35 it can be stated that the durability prediction Model #1 represents data with sufficient accuracy, and can be used for further investigation.

a)

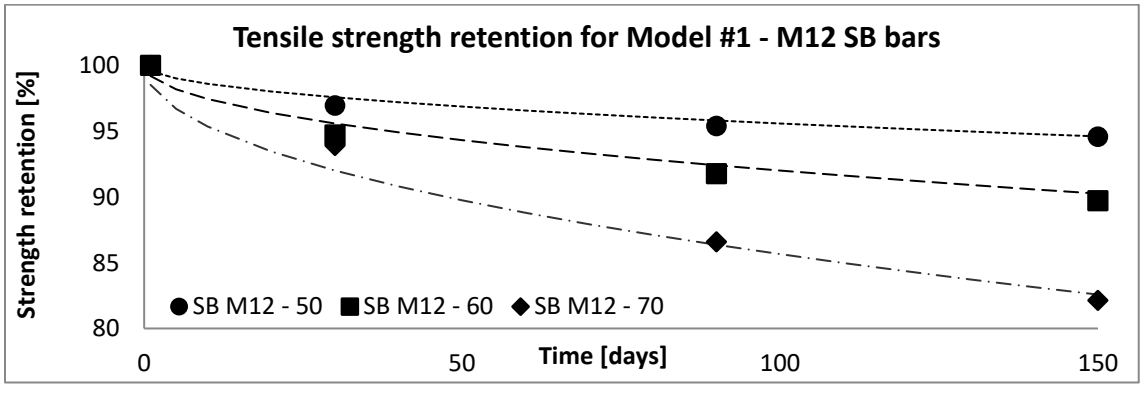

b) 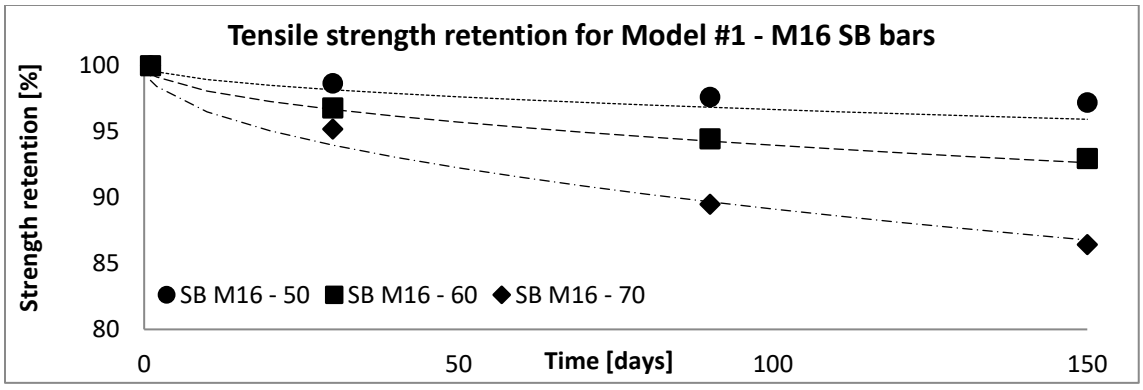

Fig. 7.13 – Tensile strength retention a) SB M12, b) SB M6 bars

Table 7.17 – Coefficient of correlation (R^2)

	M12	M16
Temperature	R^2	R^2
50˚C	0.85	0.81
60˚C	0.88	0.99
70˚C	0.92	0.95

- **Step 2**

The time to reach a specific strength retention (Table 7.18) at different temperatures can be approximately calculated through equation (6.35) after a proper transformation (eq. 7.5):

$$t = \frac{\left(\left(1 - \sqrt{\frac{Y}{100}}\right) * r_0\right)^2}{2Dc} \tag{7.5}$$

Where: Y – strength retention; r_0 −bar radius; c −alkaline concentration; t − time; D − mass diffusion coefficient;

Table 7.18 – Required time in alkaline solution bath to reach specific tensile strength retention

Retention	SB M12 - 50	SB M12 - 60	SB M12 - 70	SB M16 - 50	SB M16 - 60	SB M16 - 70
	Time to reach specific retention [days]					
95	121.5	38.5	13.6	216	68	24
85	1154.1	365.5	129.0	2052	650	229
75	3400.9	1077.0	380.1	6046	1915	676

- **Step 3**

Subsequently, the data obtained from the GFRP bars strength retention was used in the Arrhenius relationship (Arrhenius plot Fig 7.14). It can be noticed that the straight lines in the Arrhenius plots for different strength retentions are nearly parallel to each other and the calculated coefficient of determination for all regression lines is close to 1. This suggests that the Arrhenius mechanism can

be used to describe the degradation rate of GFRP bars, as the degradation process described by Model #1 does not change with temperature or time during the alkaline immersion.

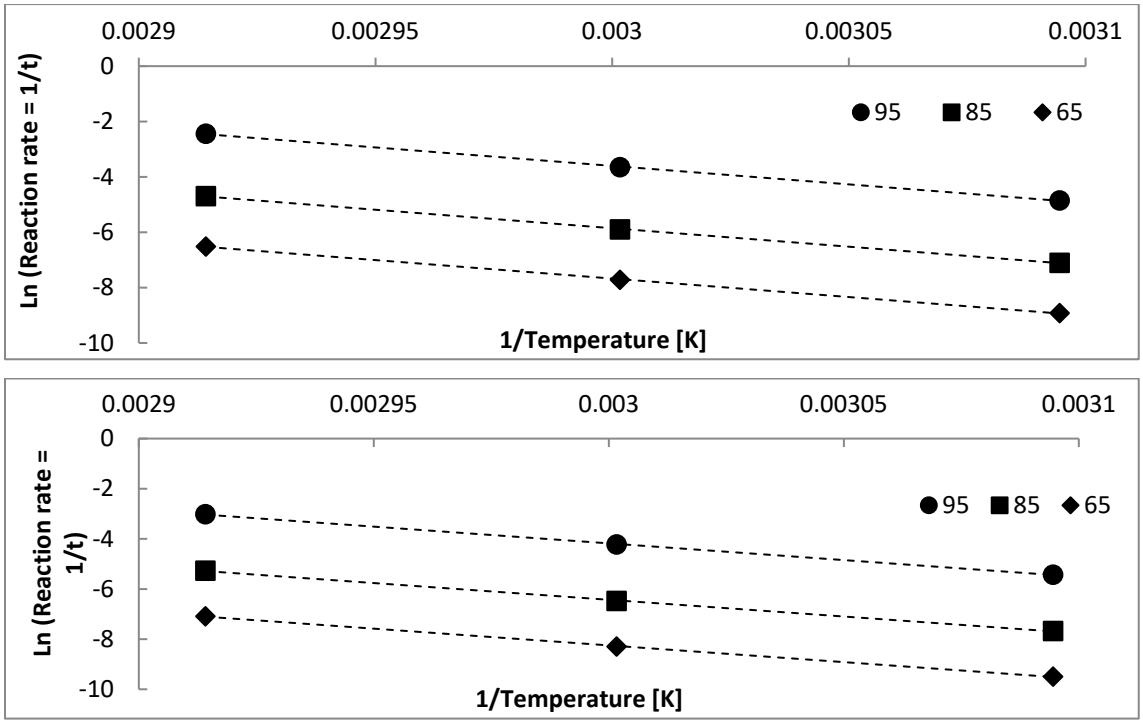

Fig. 7.14 – Arrhenius plot for a) M12 and b) M16 bars

The regression coefficients $\left(\frac{E_a}{R}\right)$ for the Arrhenius plots and correlation coefficients for three different temperatures 50 ˚C, 60 ˚C and 70˚C are listed in Table 7.19.

Table 7.19 – Regression coefficient $\left(\frac{E_a}{R}\right)$ and correlation coefficient

Temperature	$\left(\frac{E_a}{R}\right)$ for M12	R^2 for M12	$\left(\frac{E_a}{R}\right)$ for M16	R^2 for M16
50˚C	12149	0.99	12150	0.99
60˚C	12150	0.99	12150	0.99
70˚C	12149	0.99	12149	0.99

- **<u>Step 4</u>**

The acceleration factor values for all three temperatures with respect to the reference temperature of 20˚C are shown in Table 7.20.

Table 7.20 – Acceleration Factors

Temperature	AF
50˚C	46
60˚C	145
70˚C	419

- **Step 5**

Master curves were obtained directly from equation 6.35 with the mass diffusion coefficient equal to 2.315 * (10^{-11}) [mm^2/s] (Fig. 7.15)

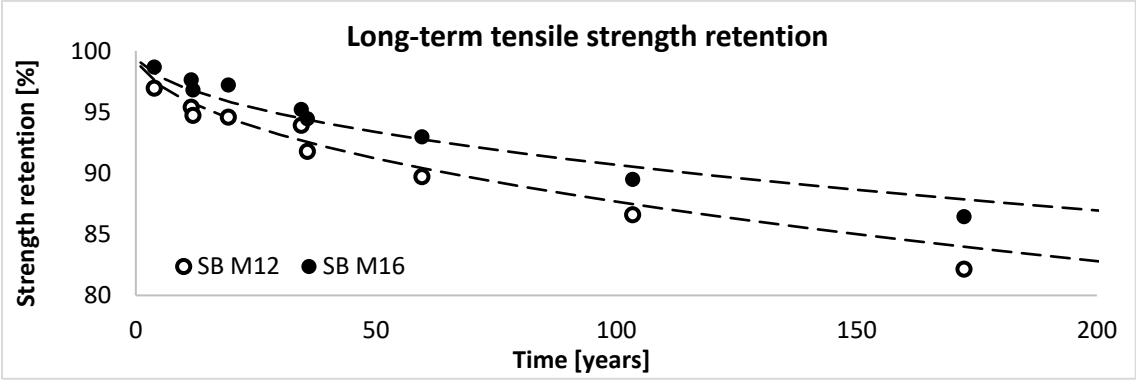

Fig. 7.15 – Long-term tensile strength retention at 20˚C for Model #1

The standard error of the regression for both master curves in Fig. 7.15 representing long-term tensile strength retention (eq. 6.35) are below 1. The master curves can be used to predict tensile strength retention for any exposure time at 20˚C. For example, at year 100 SB M12 bars will lose 12% and SB M16 9% of their original capacity (eq. 7.5).

Model #2

As described in section 6.4, model # 2 is one of the most commonly used models for long-term durability prediction.

- **Step 1**

Tensile strength retention data obtained by the alkaline immersion test was used to determine the best fitting curves (Fig.7.16). Model equations representing GFRP bar deterioration in three different temperatures and standard errors of regression (S) are summarized in Table 7.21. All regression lines have the standard error of the regression below 1.

a)

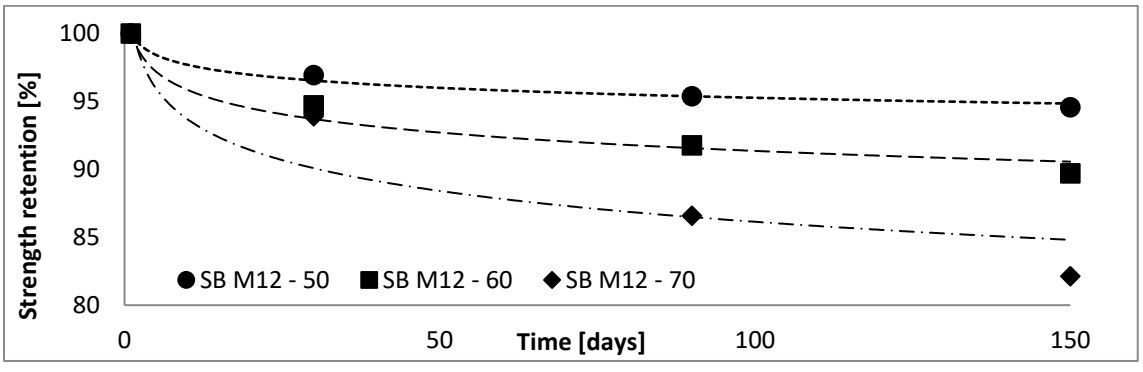

b)

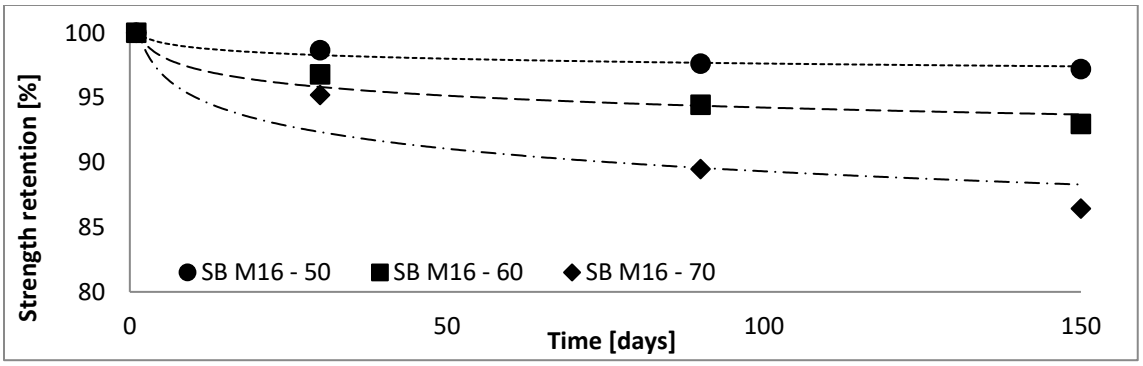

Fig. 7.16 – Tensile strength retention a) SB M12, b) SB M6 bars

Table 7.21 – Model equations for three different temperatures and coefficient of determination

	M12		M16	
Temperature	Model equation	S	Model equation	S
50˚C	$y = -1.054\ln(t) + 100.13$	0.96	$y = -0.54\ln(t) + 100.12$	0.99
60˚C	$y = -1.95\ln(t) + 100.34$	0.82	$y = -1.323\ln(t) + 100.32$	0.85
70˚C	$y = -3.278\ln(t) + 101.24$	0.84	$y = -2.519\ln(t) + 100.91$	0.89

- **Step 2**

The time to reach a specific strength retention (Table 7.22) at different temperatures can be approximately calculated through the equations of Table 7.18.

Table 7.22 – Required time in alkaline solution bath to reach specific tensile strength retention

Retention	SB M12 - 50	SB M12 - 60	SB M12 - 70	SB M16 - 50	SB M16 - 60	SB M16 - 70
	Time to reach specific retention [days]					
95	129.9	15.4	6.7	13114.6	55.7	10.4
85	1714854	2608.8	141.7	1.446E+12	106910	553
75	22629150197	440150	2995	1.594E+20	204959303	29314

- **Step 3**

Subsequently, the data obtained from the GFRP bar strength retention was used in the Arrhenius relationship (Arrhenius plot Fig 7.17). It can be noticed that the regression lines are not parallel to each other, which indicates that Model #2 used to describe material deterioration is not adequate and can be time or temperature dependent (change in the alkaline immersion bath during the exposure time). Regardless of the good correlation between model equations and recorded data (R^2 more than 0.87) provided in Table 7.18, model number 2 cannot be used for further GFRP long-term durability prediction since it can lead to incorrect results.

a)

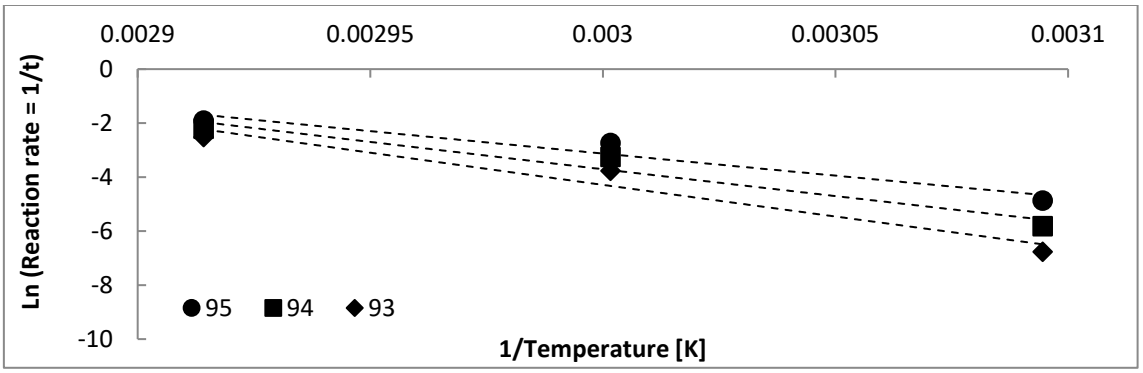

b)

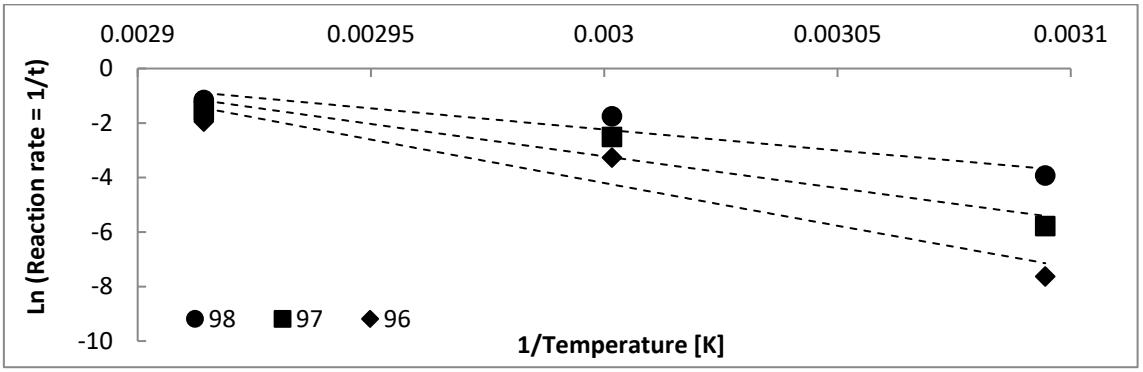

Fig. 7.17 – Arrhenius plot for a) M12 and b) M16 bars

Model #3

Model #3 was excluded from further analysis for the long-term durability prediction process, due to the lack of information about some of the model parameters and incompatibility between the testing program and model principles.

According to Purnel (2001), the strength deterioration of the fiberglass is mostly driven by stress corrosion. The strength of the glass fibers is mainly governed by the size and distribution of the surface flaws and the stress concentration presented at the tips of pre-existing flaws increases constantly causing expansion of the flaw. The speed of the process can be increased by an increase in temperature. Thus, the time to failure can be described as a thermally activated process depending on glass composition, environment pH, stress level and temperature.

Due to the specifications of the chosen alkaline immersion tests, no external stress was applied to the samples during the bath conditioning, which is in contradiction of the presented above principles of Model 3. Moreover, Beddow (2002), Purnel (2001) intentionally excluded an influence of exposure temperature on the Arrhenius relationship, during the determination of the activation energy of the deterioration process, without any further explanation.

7.3.2 Concluding remarks

Lack of extensive knowledge about the durability of GFRP bars, among other (creep and rupture), prevents the wider utilization of bars. Several conservative prescriptions, as high load and resistance factors and low design stress, preclude taking full advantage of GFRP bar properties. Thus, a better understanding of long-term durability can influence the use of composite reinforcement. The objective of Chapter 7 is to validate existing strength prediction models. Four existing durability models were evaluated in the previous section using short term results from the alkaline immersion test.

Based on the results of this Chapter 7, it was observed that the most commonly used deterioration model for FRP reinforcement (Model #2) is not appropriate. The simple logarithmic definition of the strength retention does not reflect the complexity of the degradation mechanics. Not parallel regression lines in the Arrhenius plots (Fig. 7.17) indicate that the deterioration process has changed during the exposure time and the procedure for long-term durability prediction can no longer be used. Results obtained by this model can carry a significant error, especially if the long-term strength retention is investigated.

The prediction procedure based on the model #1 and #4 using the Arrhenius relationship was successfully applied to the short-term alkaline immersion test results of this study. However, even if the long-term strength prediction procedure was accurate and efficient for both models, certain discrepancies between the results can be observed. Model #4 is characterized by the more conservative approach where 10% of the strength deterioration is noticeable after 57 years for M12 and 102 years for M16, respectively, while in Model #1it is noticeable after 65 years for M12 and 115 years for M16 bars. Discrepancies within 12% can be considered as acceptable, however, it is worth mentioning that models built on different principles lead to different results and usage of one model instead of another is mostly driven by engineering judgment.

Due to the complexity of the degradation mechanism, no degradation model has been proposed to simulate exactly the deterioration of GFRP bars in alkaline media. The accelerated test method and prediction procedure based on Model #4 and Model #1 described in this study can be a good option to assess the long-term durability performance of composite reinforcements. However, it should be noted that it is just an approximation and further investigation in this field should be

undertaken. The results indicate that increasing the number of exposure temperatures and using longer exposure duration in accelerated tests can lead to more precise predictions.

7.4 GFRP bar properties durability.

Based on the findings from the previous section, model number 4 and model number 1 were considered as appropriate approximations of GFRP bar long-term durability. Both models are based on the same mechanical principles where the bar strength deterioration is defined by the ratio of the damaged area (specified by the depth of penetration "x") to the undamaged area (calculated for the bar based on bar diameter reduction "$r_0 - x$"). A basic difference between both models appears in the definition of parameter "x", where model number 4 determines the depth of the penetration as an integration over a function of time (eq. 6.42) and the speed of penetration ("β"), while model number 1 defines "x" as a function of the diffusion coefficient (D), time and solution concentration. Thus, before model number 1 can be used, the additional task of conducting moisture absorption tests needs to be performed. To simplify the procedure, Model #4 was chosen for further investigation of GFRP bar property durability. All results presented in this section are based on strength predictions using model 4.

Deterioration of three (Company II: tensile, shear and flexure) and two (Company I: shear and flexure) different properties of GFRP bars were investigated, and results are presented herein. Full durability prediction procedure for shear and flexure strength is described in Appendix 9.

7.4.1 Tensile strength durability

As mentioned previously, the tensile strength durability was studied only for one type of the GFRP bars (SB) from one company (Company II). The procedure for the long-term strength retention prediction was presented in section 7.3.1. Results for two bar diameters M12 and M16, respectively, after 100 years of normal use (simulated conditions in temperature of 20˚C) are reported in Table 7.23 and Fig. 7.18.

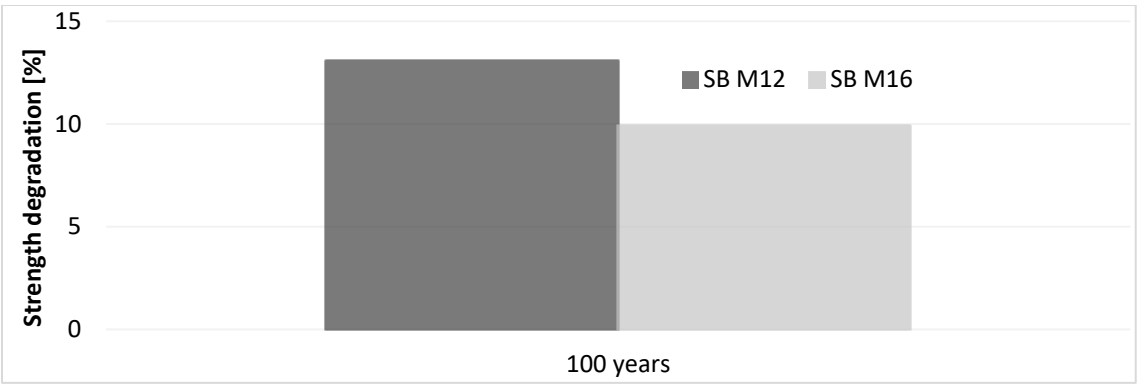

Fig. 7.18 – Tensile strength degradation after 100 years of use

Table 7.23 – Tensile strength deterioration after 100 years of normal use

Tensile strength deterioration [%]		
Bar type & size	SB M12	SB M16
100 years	13.06	9.88

Based on these results, it can be stated that the tendency of quicker degradation of the bars with smaller diameter observed during the alkaline immersion test (section 7.2) can also be noticed in the bar long-term behavior. This phenomenon is caused by the difference in the ratios of damaged to the undamaged area between both bars, where the ratio for smaller bars is larger than for bars with a bigger diameter. Thus, it can be assumed that the ratio is directly proportional to the bar cross-section area. The 12mm bars degraded around 1/3 times quicker than the 16mm bars. Using the same analogy for different bar diameters, the bar size influence on the speed of degradation can be determined. The normalized speed of degradation based on a 35mm bar is shown in Fig. 7.19. Thus, the 8mm bar deteriorates 4.38 times quicker than the 35mm bar. Based on this assumption, tensile strength deterioration can be calculated for different bar diameters (Fig. 7.20). Due to limitations introduced to the tensile strength retention studies, no further investigation of the bar type or bar surface finishing on the material deterioration process can be undertaken.

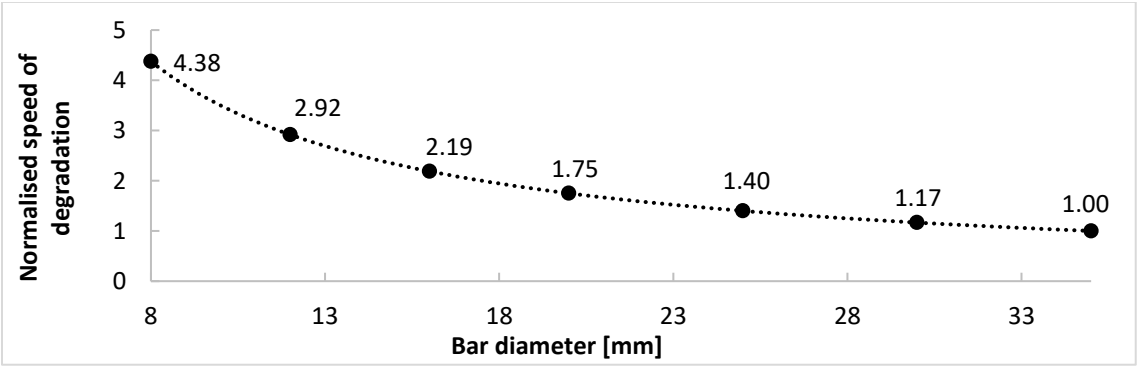

Fig. 7.19 – Normalized speed of degradation

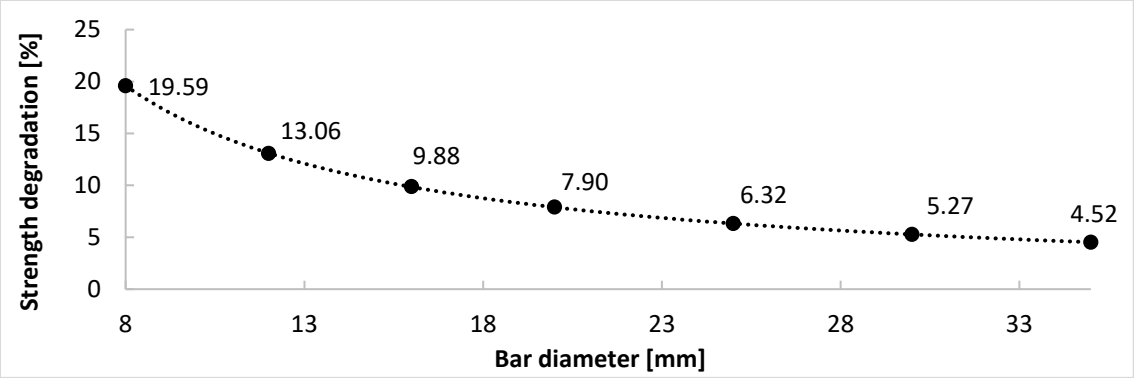

Fig. 7.20 – Tensile strength degradation for different bar diameters

7.4.2 Shear strength durability

Shear strength durability was investigated for both manufacturers, Company I and Company II, respectively, two different bar types (SB and BB bars), and two different diameters (Company I: #4 and #5; Company II M12 and M16). Results for shear strength degradation after 100 years of normal use are shown for Company I in Table 7.24 and Fig. 7.21, and for Company II in Table 7.22 and Fig. 7.24, respectively.

Even though all long-term durability models have been developed for GFRP bar tensile strength deterioration, no additional modification to the strength retention formula (eq. 7.2) was applied. Model #4 is valid for all bar properties where strength depends directly on the bar diameter (cross-section).

Table 7.24 – Shear strength deterioration after 100 years of normal use – Company I

Shear strength deterioration [%]				
Bar type & size	SB #4	SB #5	BB #4	BB #5
100 years	19.47	15.32	40.7	31.52

Fig. 7.21 – Shear strength degradation after 100 years of use – Company I

Based on the obtained results it can be noticed that the long-term shear strength retention is faster for bars with a smaller diameter. This phenomenon is common for tensile and shear properties because both directly depend on the bar cross-section area. Thus, as explained in the previous section, the ratio of damaged to the undamaged area is larger in the case of the smaller bar diameters. Following the same analogy as described for tensile strength deterioration, the shear degradation can also be predicted for different bar diameters (Fig. 7.22 – SB bars Fig. 7.23 – BB bars).

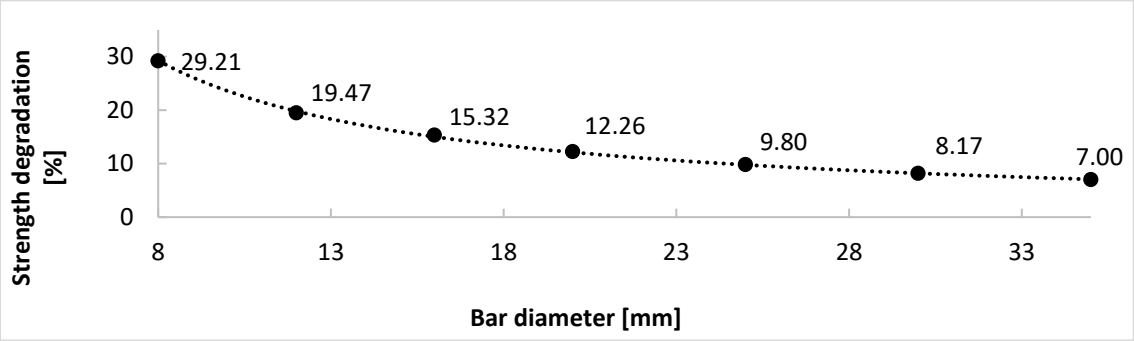

Fig. 7.22 – Shear strength deterioration for different bar diameters for Company I – SB

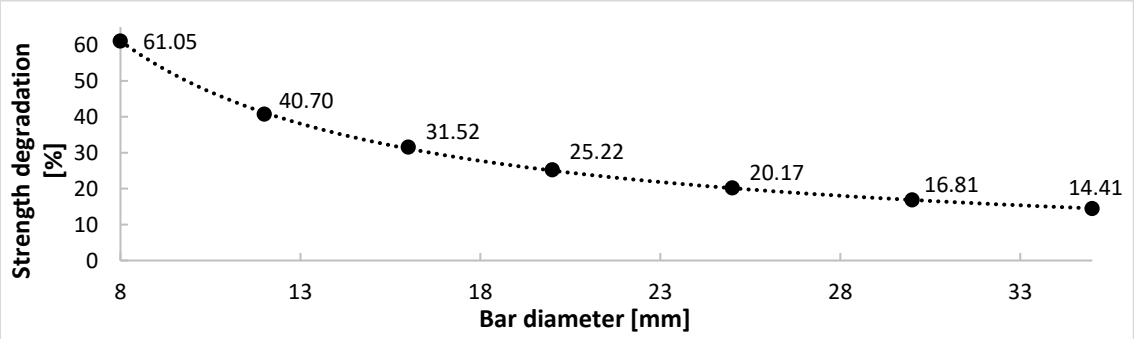

Fig. 7.23 – Shear strength deterioration for different bar diameters for Company I – BB

By different bar type comparison, it was observed that bent bar degradation occurs quicker than in the case of their straight equivalents. This phenomenon can be caused by different material parameters for bent and straight bars, where the BB bars are characterized by a lower fiber to matrix ratio, and by different resin properties. No different bar surface finishing influence can be analyzed based on obtained long-term durability data because the difference between the bent and the straight bar deterioration is mostly driven by material differences. However, using data obtained from the alkaline immersion test for 60˚C (section 7.2) it can be stated that the sand coating provides an additional protection against an aggressive environment. Similar to the results from Company I, shear strength deterioration from Company II has the same characteristics as the tensile strength deterioration. The results for Company II are shown in Table 7.25, and Fig. 7.24.

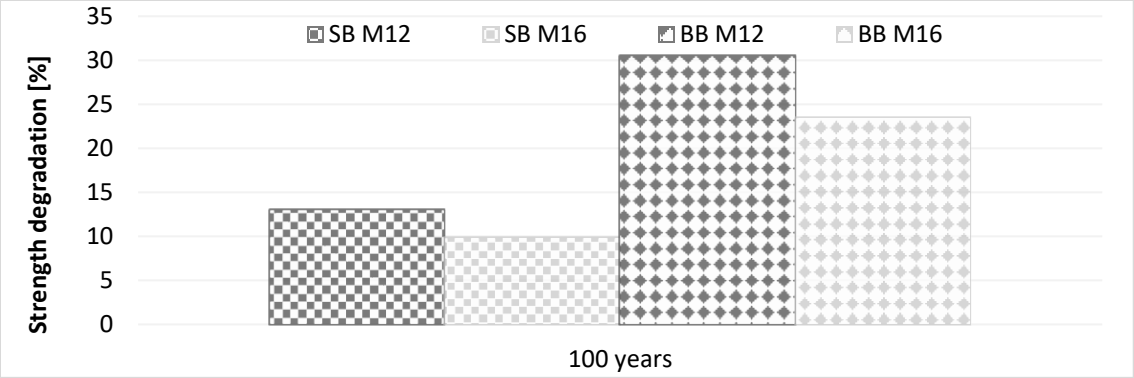

Fig. 7.24 – Shear degradation after 100 years of use – Company II

Table 7.25 – Shear strength deterioration after 100 years of normal use – Company II

shear strength deterioration [%]				
Bar type & size	SB M12	SB M16	SB M12	SB M16
100 years	13	9.84	30.54	23.43

The same analogy, as for the tensile strength retention for Company II and shear strength retention for Company I, was used to predict bars shear strength deterioration for different bar diameters for Company II (Fig.7.25 – SB bars; Fig.7.26 – BB bars).

By comparing the obtained results, it can be noticed that bent bars from Company II (same as bent bars for Company I) exhibit faster deterioration than straight bars. A cause of this phenomenon can be found in different material properties of BB and SB bars, where the BB bars are characterized by a smaller fiber to matrix ratio and different resin properties. Based on this fact, no further analysis can be performed to determine the influence of different bars finishing on shear strength deterioration. However, it is expected that the polyethylene sleeve on the BB bars provides an additional protection against an aggressive environment.

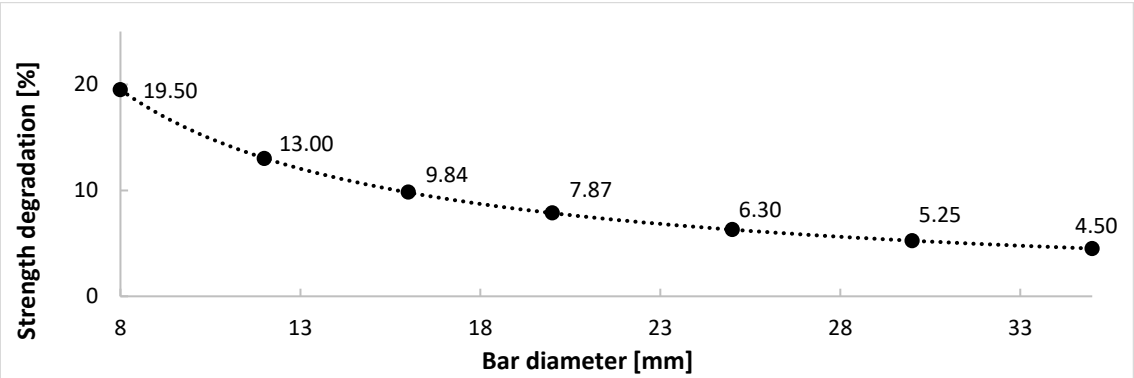

Fig. 7.25 – Shear strength deterioration for different bar diameters for Company II – SB

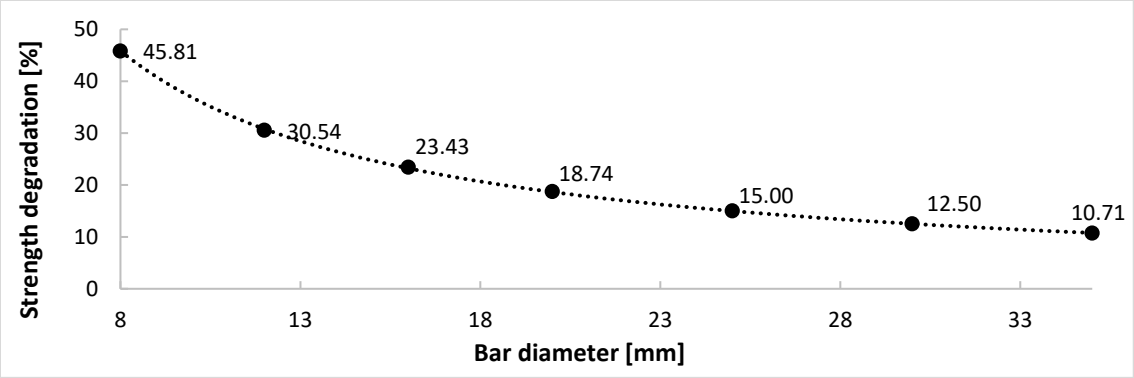

Fig. 7.26 – Shear strength deterioration for different bar diameters for Company II – BB

Direct comparison of the shear strength degradation data between both companies is shown in Fig. 7.27.

Fig. 7.27 – Results comparison for shear strength degradation after 100 years of use

It can be noticed that for both bar diameters and types, bars from Company I are characterized by a quicker deterioration than the bars from Company II. For the SB bars, bars from Company I degrade approximately ½ times quicker than the SB bars from Company II. For the BB bars, bars from Company I degrade approximately $^1/_3$ times quicker than the bars from Company II.

7.4.3 Flexure strength durability

Long-term flexure strength deterioration was investigated on bars from both manufacturers, two different bar types (SB and BB bars) and two different diameters (#4 and #5 for Company I; M12 and M16 for Company II). Results for the flexure strength deterioration after 100 years of normal use are presented: for Company I in Table 7.26 and Figure 7.28, for Company II in Table 7.27 and Figure 7.29.

An additional modification had to be applied to the strength retention formula described by Model #4 (eq. 7.2). The flexure strength of the GFRP bars does not depend on bar cross-section area, but rather indirectly on the bar diameter (moment of inertia and distance of the neutral axis to the outer fibers). In effect, the previously used durability strength prediction model can no longer be used. A new formula, developed based on the same as principles model of #4, has been obtained:

$$Y = 100 * \frac{I_1}{I_0} * \frac{c_0}{c_1} \tag{7.6}$$

$$\frac{I_1}{I_0} = A\left(1 - \frac{x}{r_0}\right)^4 ; \frac{c_0}{c_1} = B\left(\frac{1}{1 - \frac{x}{r_0}}\right)$$

$$Y = 100 * A\left(1 - \frac{x}{r_0}\right)^4 * B\left(\frac{1}{1 - \frac{x}{r_0}}\right) \tag{7.7}$$

$$x = 2\beta t^{0.5}$$

Where: Y – strength retention; x – depth of penetration (damaged zone); r_0 – bar radius; A – parameter accounting for moment of inertia; B – parameter accounting for distance to neutral axis; I_0, I_1- moment of inertia for sample before conditioning and sample after conditioning; c_0, c_1 – distance to N.A. for sample before conditioning and sample after conditioning

Presented model has been developed based on three primary assumptions:

- Diffusion is the main degradation mechanism
- Matrix and fibers in the depth of the damage zone "x" are ineffective in transferring a bending force
- Flexure strength of an undamaged zone is the same as that of a bar before exposure to the aggressive environment

Detailed derivation process for formula 7.6 is described in Appendix 10.

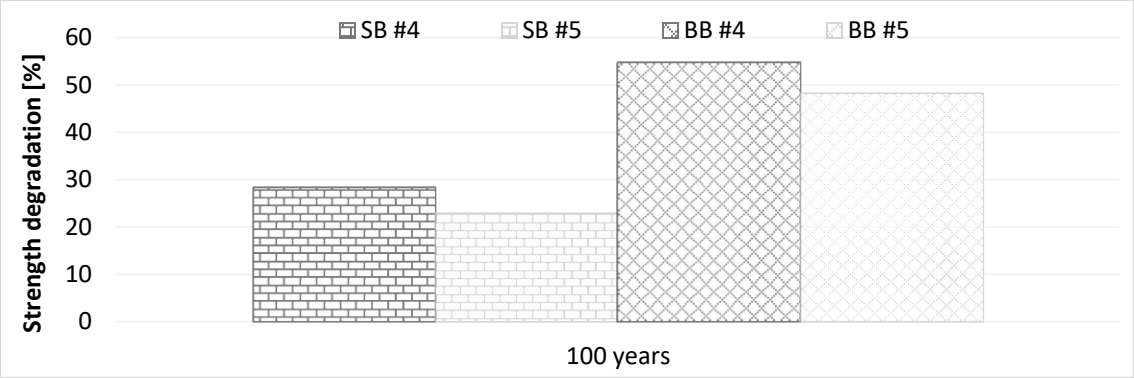

Fig. 7.28 – Flexure strength degradation after 100 years of use – Company I

Table 7.26 – Flexure strength deterioration after 100 years of normal use – Company I

Flexure strength deterioration [%]				
Bar type & size	SB #4	SB #5	BB #4	BB #5
100 years	28.3	22.67	54.74	48.18

Same as for the two previously investigated property deteriorations (tensile and shear), flexural strength degradation is quicker for a smaller bar diameter. However, a correlation between the bar size and the speed of degradation for long-term flexure strength retention is more complicated and the strength degradation for different bar diameters cannot be easily obtained. Moreover, based on the obtained results, it can be stated that discrepancies between the speed of degradation for bars with different diameters depend on the bar type. For SB bars, #4 bar degrades ¼ times faster than the #5 bar, while for BB bars, bar #4 degrades $^{1}/_{75}$ times faster than the #5 bar. Thus, it can be assumed that the speed of the flexure strength rotation depends on the material properties, what has not been observed either for the tensile or shear strength degradation.

Based on the direct comparison between the different bar types, it can be noticed that the bent bars exhibit a faster flexural strength deterioration than the straight bars. As explained previously, a cause for this phenomenon can be found in different SB and BB bar material properties, where the BB bars are characterized by a smaller fiber to matrix ratio and different resin properties.

No further analysis can be performed to investigate a different bar finishing influence on the degradation of flexural properties. However, based on the alkaline immersion test (section 7.2) it can be stated that that sand coating does not have an influence on the flexure strength deterioration.

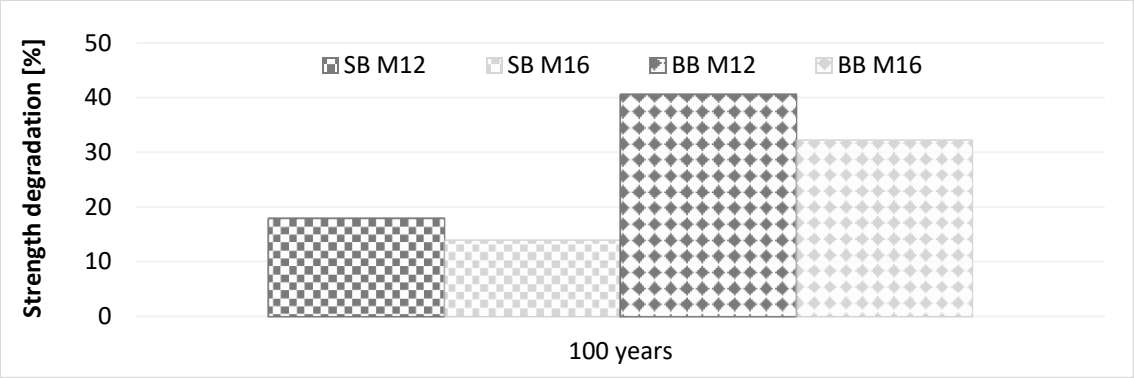

Fig. 7.29 – Flexure strength degradation after 100 years of use – Company II

Table 7.27 – Flexure strength deterioration after 100 years of normal use – Company II

Flexure strength deterioration [%]				
Bar type & size	SB M12	SB M16	SB M12	SB M16
100 years	17.87	13.85	40.4	32.13

Similar results were observed for the flexural strength retention of the bars from Company II where for SB M12 bars degrades $^{1}/_{35}$ times faster than the M16 bar, while for BB bars, the bar M12 degrades ¼ times faster than an M16 bar.

By comparing results for different bar types, it can be observed that the BB bars are characterized by a faster deterioration than the SB bars. This can be explained by SB – BB bar differences in material properties.

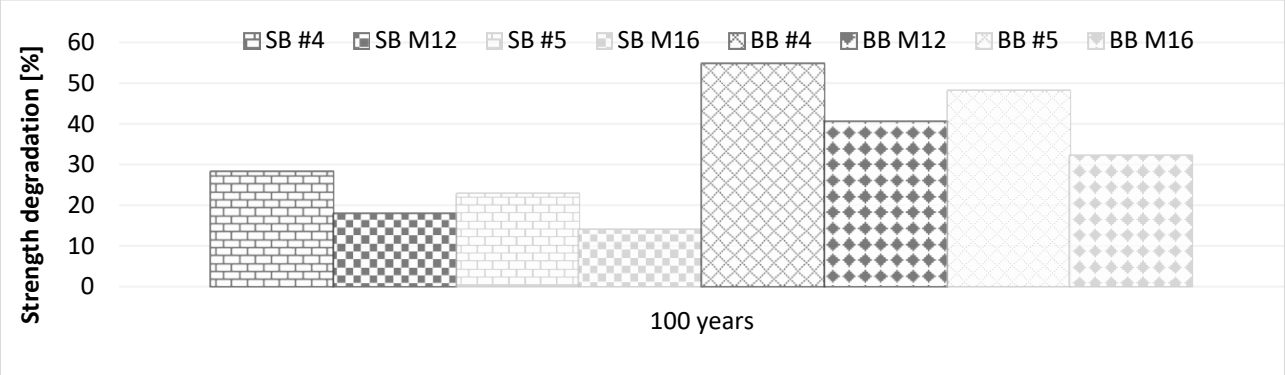

Fig. 7.30 – Results comparison for flexure strength degradation after 100 years of use

A direct comparison between the results obtained for bars from Company I and bars from Company II (Fig. 7.30) shows a faster deterioration of flexural strength for bars from Company I. It is noticeable for both bar types and diameters, respectively.

7.4.4 Different property degradation – overall results in comparison.

Direct comparison results between two different properties (shear and flexure Fig. 7.31) for Company I and three different properties (tensile, shear and flexure 7.32) for Company II are presented herein.

For both companies, it is noticeable that the flexure strength deterioration occurs faster than the shear and tensile (Company II) capacity degradation. Based on analysis of the failure mode of bars tested in flexure, where the bar capacity depends on the strength of the outer fiber, this observation is logical. External fibers of the bar are in a constant contact with an aggressive environment and the damage that occurs is larger than in the other bar sections.

In contrast, the tensile and shear strengths depend on overall cross-section area, thus the degradation of the outer fibers does not have as large an influence on the overall bar capacity as in the case of the flexure strength.

Fig. 7.31 – Results comparison for different property degradation after 100 years of use – Company I

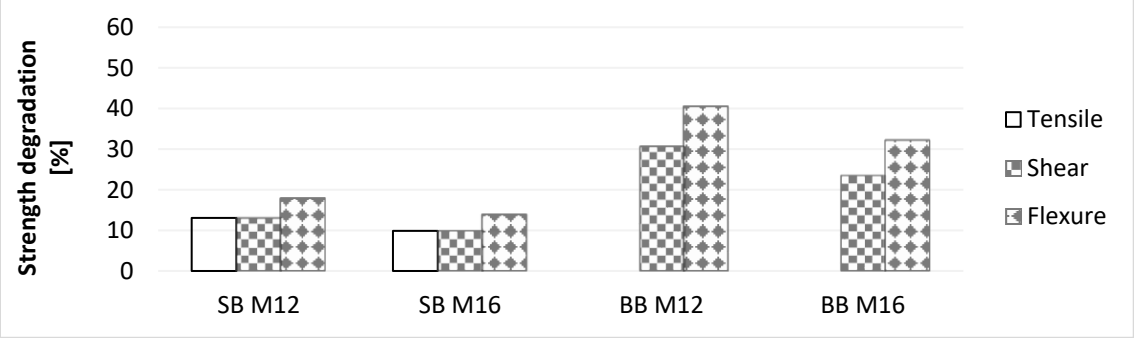

Fig. 7.32 – Results comparison for different property degradation after 100 years of use – Company II

Chapter 8

CONCLUSIONS AND RECOMMENDATIONS

8.1 Overview

The first of two main objectives of this study was to develop a better understanding of the mechanisms controlling tensile and flexural capacity of glass fiber reinforced polymer bars, and hence, investigate a possible correlation between the tensile strength of the composite in direct tension and tensile strength of outer fibers in three-point bending test (modulus of rupture). To evaluate the main properties of GFRP bars five tests were performed: tensile, shear, flexure, compression, and cure ratio test. In total 250, tests were conducted. A relatively wide range of physical, geometrical and material factors of specimens allowed to assess the performance of the test. The outcome of this evaluation is summarized in section 8.2 of this chapter. Subsequently, the influence of the material bimodularity (disregarded by standard procedures) on the modulus of rupture was studied. By the inclusion of two different moduli of elasticity into flexural strength analysis, an increase of modulus of rupture was observed. In effect, a difference between the standard and modified methodology was established to be within 10% of the bar original strength. Results from both analyses were included in further investigations. A better understanding of the tensile failure mechanisms occurring under the application of a direct tensile stress and tensile stress due to bending appeared to be key to the proper correlation between both tests. The stress and the flaw distributions were identified as the two main factors that control the tensile strength of GFRP bars. The Weibull "weakest link" model recognizes both distributions as indicators of sample failure; thus, it was incorporated in the further analysis. Finally, the correlation between the results obtained from direct tension and flexure test was established.

The second main objective of this research was focused on GFRP bar long-term performance. Since it would take too long to observe any degradation under typical service environment, an accelerated test methodology was used to speed up the degradation process (alkaline immersion test). Results obtained from short-term testing were used as a starting point for material durability investigation. Three elevated temperatures (50˚C, 60˚C, and 70˚C) were applied as accelerating

factors and subsequently, an Arrhenius law model was used to predict damage behavior at lower temperatures. The performance of four different strength retention models was investigated in terms of feasibility to describe deterioration of all basic properties of GFRP reinforcements. One model has been identified as a proper approximation of the two main properties: tensile and shear strength retention, and its modified version was used to assess the flexure strength deterioration. Subsequently, different strength degradations were evaluated in terms of physical, mechanical and material variability. Similarities between each of them were investigated.

The following sections summarize the obtained results, review the key findings of this study and make recommendations for further research.

8.2 Quality control tests assessment

Four different tests qualified as the standard quality control procedures (tensile, shear, flexure, and cure ratio tests) and compression strength investigation were performed in this research to determine the basic properties of GFRP bars. Three types of bars (smooth surface bars, straight bars, and bent bars) with two different diameters (#4 and #5 for Company I; and 12mm and 16mm – for company II) from two companies were tested. A relatively wide range of factors such as specimen shape, surface finishing, and mechanical characteristics (smooth surfaced bars, sand coating, polyethylene sleeve, different types of resin and different fiber content in bent bars, respectively) allowed to identify possible problems with testing protocols resulting from sample to sample variations.

8.2.1 Main findings

- A standardized procedure for tensile strength determination is considered to be impractical and costly for routine testing. The testing methodology requires large specimen size and machines with high capacity, which effectively limits facilities capable of performing the test. Specimen preparation is time-consuming and requires extensive knowledge according to the sample bond strength, ultimate tensile strength etc. (anchorage length recommendations provided by standard protocols are not universal, and specimens need to be pretested). However, if the test is properly done, it delivers consistent and reliable results.

- The shear strength determination test can potentially be used to determine the quality of resin, resin-fiber interface, and fiber content. The test itself is designed to assess the bar shear capacity. The testing procedure is relatively easy and quick. Regardless of the small size of the specimen (approximately 300mm), due to the double-shearing mechanism, a moderate capacity testing machine is required (more than 100kN capacity). Rigorous restriction according to the testing device makes the test impractical when bars with a large variety of sizes need to be tested.
- The flexure strength determination test is considered to be one of the easiest tests performed in this research. The testing procedure is relatively quick and does not require a machine with large capacity. Samples are small, however, it is worth mentioning that the force at failure is sample size sensitive and depends on bar diameter. A considerable test disadvantage is a specimen semi-circular shape that is challenging to achieve without a special equipment as for example a water jet cutter. The test provides information on the tensile strength of the outer fibers and modulus of elasticity in bending. After developing a proper correlation between the tensile failure of the outer fibers due to bending and tensile failure under direct tension, this test has a substantial potential to be used for tensile capacity determination.
- Two different procedures for compressive strength determination were included in the scope of this research. Both procedures are designed to provide an ultimate compression strength of the composite bar and modulus of elasticity in compression. The first method appears to be inconsistent in terms of modulus of elasticity determination, caused by surface finishing imperfections. Compression strength seems to be properly obtained. The second method provides a good estimate for both compression strength and modulus of elasticity, but it is more demanding in terms of time required for sample preparation and equipment use. If only compression strength results need to be obtained, the first procedure, which is much simpler, can be used.
- Cure ratio test is inconvenient to perform outside manufacturer testing facilities, due to patent restrictions and problems with obtaining a liquid resin from bar producers. The test provides adequate information about the resin properties, however, the value of the cure ratio strongly depends on sample localization within the bar cross-section.

8.2.2 Future study – comments and recommendations

Under frequently occurring changes in properties of products currently available on the market, all quality control tests need to be properly evaluated. The large variability of product property measurements, especially in terms of sample shape or physical appearance (like sand coating, additional sleeves or ribs), can have an influence on the outcome of the test or may involve additional procedures associated with sample preparation that needs to be considered. Some updates and protocol modifications/improvements need to be considered. Based on the results obtained from short-term testing some suggestions for test modification can be formulated. However, to perform a comprehensive evaluation of the test performance, more samples should be tested to develop an extensive data set for further statistical analysis.

8.3 Tensile strength vs modulus of rupture

The tensile strength of the composite reinforcement is one of the most important material properties that needs to be obtained. The bar tensile strength needs to be determined not only for the new product but also for each batch supplied to the construction site to assure its quality. Problems associated with the determination of the bar tensile strength capacity described in this research (section 4.2.1) can effectively limit the wider utilization of the material. A simple and efficient method that can be used to obtain the tensile strength of GFRP bars would be a major improvement for a quality control testing. Based on the results from short-term testing, a hypothesis was formulated that the tensile strength capacity can be approximately evaluated using a flexure (three-point bending) test.

8.3.1 Main findings

- To establish a correct correlation between tensile and flexure capacity of GFRP bars influence of material dual moduli on the modulus of rupture has to be investigated. Based on obtained results it can be stated that the material dual modulus does not have a significant influence on the modulus of rupture. However, the negligence of bi-modularity of GFRP bars needs to be carefully considered since the error depends on discrepancies between both moduli. A larger difference between tensile and compression modulus of elasticity will lead to a bigger error.

- The Weibull "weakest link" model can be considered as a proper methodology to determine a correlation between tensile and flexure tests. It allows establishing the distribution of the flaws along the sample volume, based on the flexure test only. The model identifies the flaw and the stress distribution as failure indicators, which allows comparison of strength values and ranges for different stress configurations.
- The presented analysis indicates that the correlation between tensile and flexure capacity can be assessed and established using information provided by the manufacturer (moduli of elasticity) and three-point bending tests only.

8.3.2 Future study – comments and recommendations

More research is required to validate the described correlation methodology. To assure a correctness of the distribution of the material flaws along the sample volume more specimens should be tested. The investigation should be extended to include different sample sizes and other (then included in this study) manufacturers. More testing is required to identify the correlation between different bar types as for example bent bars, which are characterized by different material properties (different resin and smaller fiber content). In addition, application of a different test setup should be considered as for e.g., four-point bending. This modification introduces a larger area of uniform tensile stresses. This will result in an increase of the effective volume of the sample (volume under maximum tensile stress), which in effect will leads to decrees of the modulus of rupture. Thus, it is worth mentioning that the flexure-tensile strength correlation directly depends on the way of load application.

8.4 GFRP bar durability

To assess GFRP bar durability and to identify how degradation mechanisms described by the available deterioration models can affect the main properties of composite reinforcement the research program was divided into three phases. Investigation of bars short-term degradation (alkaline immersion bath with a maximum duration of 150 days) in elevated temperatures was assessed in Phase 1. Results of this test were used to validate the existing strength-deterioration models available in the literature. The detailed long-term strength prediction procedure was described in Phase 2. Finally, GFRP bar properties durability was assessed. The speed of

degradation for different properties of composite reinforcements was evaluated according to bar size, bar type, and surface finishing.

8.4.1 Main findings

- The highly alkaline solution with pH up to 13 – 14 was used in this research to simulate the concrete environment and had an adverse effect on GFRP bar durability. Bars, kept in the solution for up to 150 days, exhibited substantial deficiencies in strength. An elevated temperature speeds up the degradation process. Thus, both alkaline solution and temperature can be used effectively as accelerating agents.
- The most commonly used strength prediction model presented in this study (Model #2) does not describe properly the complexity of the deterioration process. Not parallel regression lines in the Arrhenius relationship indicate changes in the degradation mechanism that occur during the exposure time. Thus, this procedure even, if frequently used does not assess correctly the durability of GFRP bars.
- Model #4 and Model #1 were identified as appropriate approximations for long-term durability prediction of GFRP reinforcement. Both methodologies were successfully applied to the short-term degradation data from the alkaline immersion test. Even if both models were found accurate, discrepancies within 12% were observed between the results, where model #4 was found more conservative than model # 1.
- Before Model #1 can be used, a time-consuming task of moisture absorption test needs to be undertaken to determine a diffusion coefficient. This procedure effectively increases the duration of the long-term durability prediction process. Model #1 cannot be used in neutral solutions (as, for example, water) since the concentration of the solution is required in the prediction process.
- Model #4 was found to be suitable for modification to represent a deterioration of the flexural strength.
- Based on the obtained results from both short and long-term degradation analysis of GFRP bars it was observed that the smaller bar diameters are characterized by larger speeds of degradation. This phenomenon is caused by the difference between the ratios of “damaged” to “undamaged” areas, where the ratio for smaller bars is larger than for bars with a larger diameter.

- Based on the obtained results for two bar sizes an approximation analysis to obtain the strength retention for another diameter can be performed
- Bent bars from both companies that are characterized by different resin properties and smaller fiber content, exhibit a more significant degradation than the straight bars.
- An additional surface finishing (sand coating, polyethylene sleeve) has small (shear test) or no (flexure test) influence on the GFRP bar deterioration.
- Tensile and shear properties of GFRP bars deteriorate in a similar way, while the flexure strength deterioration is quicker.

8.4.2 Future study – comments and recommendations

More research is required to understand the complexity of GFRP bar degradation mechanisms. Increasing the number of exposure temperatures and using the longer duration of the bar exposure to the aggressive environment can lead to the more precise prediction of the GFRP bar long-term durability. An additional investigation according to the protective influence of the polyethylene sleeve should be undertaken. It is recognized that any additional barrier between the composite material and aggressive environment should decrease the degradation speed. However, to make such a prediction valid, bars with the same material properties with and without the sleeve should be tested. It should be noted that strength retention models built on different principles can lead to a different outcome. All models presented in this research have limitations and they are just approximations of material deterioration, hence further investigation in this field should be undertaken.

References

ACI 440.3R – 04 “Guide Test Methodology for Fiber – Reinforced Polymer (FRPs) for Reinforcing or Strengthening Concrete Structures”

ACI 440.3R-04 “Guide Test Methods for Fiber – Reinforced Polymer (FRPs) for Reinforcing or Strengthening Concrete Structure”

Adimi, M.R. Rahman, A.H. Benmokrane, B. “New method for testing fiber-reinforced polymer rods under fatigue” Journal of composites for construction [1090-0268] Adimi, M R yr:2000 vol:4 iss:4 pg:206 -213

Aindow A.J., Oakley D.R., and Proctor B.A., “Comparison of the Weathering Behaviour of GRC with Predictions Made from Accelerated Aging Tests,” Cement and Concrete Research, 14(2), 1984, pp. 271-274

Alsayed S.H. and Al-Salloum Y.A. 1995 “Flexural Behaviour of Concrete Elements Reinforced by GFRP Bars” Taerve L. (Ed.) Non-metallic (FRP) reinforcement for concrete structure E & F Spon, London pp219-26

Ambartsumyan S. A. “Elasticity Theory of Different Modulus”. WU Rui-feng,ZHANG Yunzhen

ASTM D3410/D3410M - 03 “Standard Test Method for Compressive Properties of Polymer Matrix Composite Materials with Unsupported Gage Section by Shear Loading”

ASTM D4476/D4476M – 14 “Standard Test Method for Flexural Properties of Fiber Reinforced Pulltruded Plastic Rods”

ASTM D495 – 10 “Standard Test Method for Compression Properties of Rigid Plastics”

ASTM D7205/D7205M “Standard Test Method for Tensile Properties of Fiber Reinforced Polymer Matrix Composite Bars”

ASTM D4476-09 “Standard Test Method for Flexural Properties of Fiber Reinforced Pultruded Plastic Rods”

ASTM D695-10 Standard Test Method for Compressive Properties of Rigid Plastics

ASTM D7205/D7205M-06(2011) "Standard Test Method for Tensile Properties of Fiber Reinforced Polymer Matrix Composite Bars"

ASTM D7617/D7617M-11 "Standard Test Method for Transverse Shear Strength of Fiber-reinforced Polymer Matrix Composite Bars"

ASTM D7705/D7705M-12 "Standard Test Method for Alkali Resistance of Fiber Reinforced Polymer (FRP) Matrix Composite Bars used in Concrete Construction"

Bakis C.E., Nanni A., and Terosky J.A., "Smart Pseudo-Ductile, Reinforcing Rods for Concrete: Manufacture and Test", Proc. 1st Int. Conference On Composites in Infrastructures, ICCI 96, Tucson, Arizona, pp. 95-108.

Bakis C.E., Nanni A., and Terosky J.A., "Smart Pseudo-Ductile, Reinforcing Rods for Concrete: Manufacture and Test", Proc. 1st Int. Conference On Composites in Infrastructures, ICCI 96, Tucson, Arizona, pp. 95-108.

Bakis, E. C., Al-Dulaijan, S. U., Antonio Nanni, Boothby, T. E., and Al-Zahrani, M. M. (1998). "Effect of Cyclic Loading on Bond Behavior of GFRP Rods Embedded in Concrete Beams", Journal of Composites Technology & Research, JCTRER, Vol. 20(1), p.29-37

Bakis, E. C., Uppuluri, V. S., Nanni, A., and Boothby, T. E. (1998) "Analysis of bonding Mechanisms of Smooth and Lugged FRP Rods Embedded in Concrete", Composites Science and Technology, Vol. 58, p.1307-1319

Baleandran R., Ranat., Maqaood T., Tang W.C. "Application of FRP Bars as Reinforcement in Civil Engineering Structures" Structural Survey, Vol. 20 Iss:2, 2002, pp 62-97

Balendar R.V., Rana T.M., Maqsood T., Tang W.C. "Application of FRP Bars as Reinforcement in Civil Engineering Structures" Structural Survey,2002, Vol. 20 Iss: 2pp 62-97

Bank, L. C., and Puterman, M. (1997) " Microscopic Study of Surface Degradation of Glass Fiber-Reinforced Polymer Rods Embedded in Concrete Castings Subjected to Environmental Conditioning", High Temperature and Environmental Effects on Polymeric Composites: 2nd

Volume, ASTM STP 1302, Thomas S. Gates and Abdul-Hamid Zuerick, Eds, American Society for Testing and Materials, p.191-205.

Bank, L.C., Gentry, T.R. and Barkatt, A. (1995) "Accelerated Test Methods to Determine the Long-term Behavior of FRP Composite Structures: Environmental Effects", Journal of Reinforced Plastics and Composites, Volume 14(6), p.559- 587.

Bank, LC, Gentry, T.R., Thompson, B.P., and Russell, S.J., "A Model Specification for FRP Composites for Civil Engineering Structures," Construction and Building Materials, 17, 2003, pp. 405-437.

Beddow J, Purnell P. and Mottram T. "Application of GRC Accelerated Ageing Rationales to Pultruded Structural GRP" 9th International Conference on Fiber Reinforced Composites, University of Newcastle upon Tyne, UK, 2002, pp. 215–221.

Benmokrane B., Ali A.H., "Laboratory assessment and durability performance of vinyl-ester, polyester, and epoxy glass-FRP bars for concrete structures" Composites. Part B, Engineering [1359-8368] Benmokrane, B yr:2017 vol:114 pg:163 -174

Benmokrane, B., Rahman, A.H., Ton-That, M.-T and Robert, J.-F(1998) "Improvement of the Durability Performance of FRP Reinforcement for Concrete Structures", Proceedings of the First International Conference (CDCC 98), Sherbrooke (Québec) Canada, July 18, p. 571-598.

Benmokrane, B., Rahman, A.H., Ton-That, M.-T and Robert, J.-F(1998) "Improvement of the DurabilityPerformance of FRP Reinforcement for Concrete Structures", Proceedings of the First InternationalConference (CDCC 98), Sherbrooke (Québec) Canada, July 18, p. 571-598.

Benmokrane, B., Wang, P., Ton-That T.M., Rahman, H., Robert J.F. "Durability of Glass Fiber-reinforced Polymer Reinforcing Bars in Concrete Environment" Journal of Composites for Construction, 6(3), 2002, pp. 143-153.

Benmokrane, B., Wang, P., Ton-That, M. T., and Laoubi, K. "Durability of GFRP Composites Reinforcing Rods in Concrete Environment", FRPRCS-5: Durability of Fiber Reinforced Plastics, 2001, p.469-478.

Bradshaw, R. D., and Brinson, L. C. (1997) “Physical Aging in Polymer Composites: An Analysis and Method for Time Aging Time Superposition”, Polymer Engineering and Science, Vol.31, No.1, p.31-34

Bunsell A. R., Renard J. “Fundamentals of Fiber Reinforced Composite Materials” Taylor and Francis 2005

Castro, P.F., and Carino, N.J., (1998), “Tensile and Non-Destructive Testing of FRP bars”, J. Comp. Constr., Vol. 2, No. 1, February 1998, pp. 17-27

CEB – FIB Bulletin 40 “FRP reinforcement in RC structures” 2007

Charles, R. J. (1959). “Chapter 12: The Strength of Silicate Glasses and Some Crystalline Oxides,” in Fracture: Proceedings of an International Conference on the Atomic Mechanisms of Fracture Held in Swampscott, Massachusetts, April 12-16., p.225-249

Chen, Y., Davalos, J.F., Ray, I. and Kim, H.Y., “Accelerated Aging Tests for Evaluations of Durability Performance of FRP Reinforcing Bars for Concrete Structures,” Composite Structures, 78(1), 2007, pp. 101-111

Cowley, T. W., and Robertson, M.A., “Effect of pH and Temperature on Fiberglass Reinforced Composites in Sodium Hypochlorite Solutions,” Materials Performance, 30(7), 1991, pp. 46-49

Crank J., “The Mathematics of Diffusion,” Oxford University Press 1975.

CSA S806 – 12 “Design and construction of building structures with fiber – reinforced polymer”

CSA S806-12 “Design and construction of building structures with fiber – reinforced polymers”, 2012.

CSA S807 – 10 “Specification for fiber – reinforced polymers”

CSA S807-10 “Specification for fiber – reinforced polymers”, 2010.

Davalos J.F, Chen Y., and RayI. “Long-term Durability Prediction Models for GFRP Bars in Concrete Environment” Journal of Composites Article Materials 2012 46: 1899 originally published online 10 November 2011

Dejke, V., and Teppers, R. (2001) “Durability and Service Life Time Prediction of GFRP for Concrete Reinforcement”, FRPRCS-5: Durability of Fiber Reinforced Plastics, ed. Thomas Telford, Vol. 2, p.505-513.

Delre, L. C., and Miller, R. W. (1988) “Characterization and Weather Aging and Radiation Susceptibility”, Engineered Materials Handbook: Vol.2-Engineering Plastics. Metals Park, OH: ASM International, p.576-580

Devalapura, R.K., Gauchel, J.V., Greenwood, M.E., Hankin, A., and Humphrey, T., “Long-term Durability of Glass-Fiber Reinforced Polymer Composites in Alkaline Environments,” Proceeding of the 3rd International Symposium, Non-metallic (FRP) Reinforcement for Concrete Structures, Sapporo, Japan, 1997, pp. 83-90.

Duranovic N., Pilakoutas K., and Waldron P. "Tests on Concrete Beams Reinforced with Glas Fiber Reinforced Plastic Bars" Proceeding of the Third International Symposium on Non-Metallic (FRP) Reinforcement for Concrete Structures, Sapporo, Japan. Oct. 1997. Vo1.2, pp. 479-486.

Eddie D., Shallaby A, Rizkalla S. “Glass Fiber – Reinforcement Polymer Dowels for Concrete pavements” ACI structural Journal Title no. 98 – S20 March – April 2001

Ehrenstein, G.W. (2007), “Expert Report – GFRP – Reinforcing Bars ComBAR” Report No: STN Report Erlangen 2007 01 EN, 2007.

Ehsani M. R., 1993, “Glass-Fiber Reinforcing Bars,” Alternative Materials for the Reinforcement and Prestressing of Concrete, J. L. Clarke, Blackie Academic & Professional, London, pp. 35-54.

El-Sayed, A. K., El-Salakawy, E., and Benmokrane, B. “Mechanical and structural characterization of new carbon FRP stirrups for concrete members.” J. Compos. Constr., 2007, 11_4_, 352–362

Erik, M.A., and Rizkalla, S.H., (1993), “Anchorages for FRP Reinforcement”, Concrete Int., Vol. 15, No. 6, pp. 54-59.

Erki, M.A., and Rizkalla, S.H., (1993), “Anchorages for FRP Reinforcement”, Concrete Int., Vol. 15, No. 6, pp. 54-59.

Gaona FA. “Characterization of Design Parameters for Composite Reinforced Concrete Systems” Texas A&M University, 2003, 251p

Gentry T.R. “Transvers shear of GFRP rods: test method development and potential durability assessment” Durability and sustainability of fiber reinforced polymer (FRP) composites for construction and rehabilitation CDCC – 2011 pp. 221 – 228.

Gentry T.R. “Transvers shear of GFRP rods: test method development and potential durability assessment” Durability and sustainability of fiber reinforced polymer (FRP) composites for construction and rehabilitation CDCC – 2011 pp. 221 – 228.

Gentry, T. R., Bank, L. C, Barkatt, A. and Prian, L. (1998) “Accelerated Test Methods to Determine the Long-Term Behavior of Composite Highway Structures Subject to Environmental Loading”, Journal of Composites Technology and Research, JCTRER, Vol. 20, No.1, January 1998, p.38-50

German J. “Podstawy Mechaniki Kompozytow Wluknistych” Warszawa 2001.

Gonenc O. “Durability and Service-life Prediction of Concrete Reinforcing Materials” University of Wisconsin-Madison 2003

Gooranorimi O., Nanni A., “GFRP Reinforcement in Concrete after 15 Years of Service”. Journal of composites for construction [1090-0268] Gooranorimi, Omid yr:2017 pg:04017024

Gustafson D. P. “Epoxy Update” Civil Engineering ASCE V. 58 No 10, Oct 1988, pp38-41

Hamad B. S., Jirsa J. O. and D’Abreu de Palo N. “Anchorage Strength of Epoxy Coated Hooked Bars” ACI structural journal V.20 No 2 Mar-Ap. 1993 pp210-217

Hollaway L.C. “The Evolution of and the way Forward for Advanced Polymer Composites in The Civil Infrastructure” Construction and Building Materials Volume 17, Issues 6–7, September–October 2003, Pages 365–378 Fiber-reinforced polymer composites in construction

Holte L.E., Dolam C.W., and Schmidt R.J., “Glass FRP Reinforcing Bars for Concrete”, Fiber-Reinforced Plastics (FRP) Reinforcement for Concrete Structures – Properties and Applications Nanni Ed., Elsevier Pub. Co. Inc., NY, 1993, pp. 167-188.

Hull D. "An introduction to composite materials" Cambridge University Press New York, NY. 1981

Ishida, H. (1983). “Adhesion Aspects of Polymeric Coatings’’ (Ed. K. L. Mittal) Plenum Press, New York, 1983, p.20-43

ISIS Educational Module 2: “An Introduction to FRP Composites for Construction” Prepared by ISIS Canada and Canadian Network of Centres of Excellence Principal Contributor: L.A. Bisby, Ph.D., P.Eng. Department of Civil Engineering, Queen’s University Contributor: J. Fitzwilliam March 2006

Iskander M., Mohamed A., and Hassan M., “Durability of Recycled Fiber-reinforced Polymer Piling in Aggressive Environments,” Transportation Research Record, 1808(02-2310), 2002, pp. 153-161.

Jayaraman, K., and Reifsnider, K. L. (1993) “Elastic and Thermal Effects in the Interphase: Part 1 Comments on Characterization Methods, Journal of Composites Technology and Research, Vol. 15(1), p.3-13

Jones R. M. “Stress – Strain Relations for Materials with Different Moduli in Tension and Compression” AIAA Journal 1977, Vol 15 (1) pp. 16-23

Jones R.M. “Mechanics of Composite Materials with Different Moduli in Tension and Compression” Final Scientific Report Research Sponsored Under AFOSR Grant Number 73-7532 Air Force Office of Scientific Research Directorate of Aerospace Sciences Bolling Air Force Base D.C 20332. Approved for public release 1978

Karbhari V.M. “Durability Gap Analysis for Fiber-Reinforced Polymer Composites in Civil Infrastructure” Journal of Composites for Construction 2003 **7**(3): p. 238 – 247.

Kato, Y., Nishimura, T. and Uomoto, T., Yamaguchi, T. (1998) ”The Effect of Ultraviolet Rays to FRP Rods”, Durability of Fiber Reinforced Polymer (FRP) Composites for Construction, ed. Benmokrane, B., and Rahman, H., p.487-497

Katsuki F., and Uomoto T., “Prediction of Deterioration of FRP Rods Due to Alkali Attack,” Non-metallic (FRP) Reinforcement for Concrete Structures, RILEM, London,UK, 1995, pp. 82-89.

Laws V. “The Relationship between Tensile and Bending Properties of Non-linear Composite Materials” Journal of Material Science V17 1982, pp. 2919-2924

Litherland K.L., Oakley D.R., and Proctor B.A., “The Use of Accelerated Aging Procedures to Predict the Long-Term Strength of GRC Composites,” Cement and Concrete Research, 1(11), 1981, pp 455-466.

Loewenstein K.L. “The Manufacturing of Continues Glass Fibers” 3rd revised ed. Elsevier 1993.

Mallick P. K. “Fiber-Reinforced Composites Materials, Manufacturing, and Design” Third Edition CRC Press 2007

Malvar, L.J., Jamond, R.M., Hoffard, T.A., and Novinson, T., “GFRP Composites in Simulated Marine Environments,” Proceeding of 2nd International Conference on Durability of Fiber Reinforced Polymer (FRP) Composites for Construction, Montreal, Canada, 2002, pp. 153-164.

Mao, J., Zhang, H., “Mechanical properties and corrosion mechanism of GFRP rebar in alkaline solution”. Advances in Fracture and Damage Mechanics XIV. Mao, J. 2016 pg:217 -220

Maruyama T., Honma M., and Okamura H. "Experimental Study on Tensile Strength of Bent Portion of FRP Rods" American Concrete Institute, ACI SP-138, edited by A. Nanni and C.W. Dolan, pp. 163-176 1993.

Mechanics of Dissolution and Surface Cracking”, Physics and Chemistry of Glasses, Vol. 40(3), p.157-170

Medri G. “A Nonlinear Elastic Model for Isotropic Materials with Different Behavior in Tension and Compression”. Transactions of the ASME, 1982,26(104) :26 - 28.

Metcalfe, A.G., and Schmitz, G. K., “Mechanism of Stress Corrosion in E-glass Filaments,” Glass Technology, 13(1), 1972, pp. 5-16.

Micelli, F., Nanni, A., and Tegola, A.L., “Effects of Conditioning Environment on GFRP Bars,” Proceeding of 22nd SAMPE Europe International Conference, CNIT Paris, 2001

Michaluk C.R., Rizcalla S.H., Tadros G., and Benmokrane B., “Flexural Behavior of One-Way Concrete Slabs Reinforced by Fiber Reinforced Plastic 244 Reinforcements,” ACI Structural Journal, V. 95, No. 3, May-June 1998, pp. 353-365.

Miyata S., Tottori S., Terada T., and Sekijima K.,"Experimental Study on Tensile Strength of FRP Bent Bar" Transaction of the Japan Concrete Institute, vol. 11, pp.185-192 1989.

Morphy R.D “Behaviour of Fiber Reinforced Polymer (FRP) Stirrups as Shear Reinforcement for Concrete Structures” University of Manitoba 1999.

Nanni, A., Bakis, C.E., O’Neil, E.F., and Dixton, T.O., (1996), “Short-Term Sustained Loading of FRP Tendon-Anchor Systems”, Technical Report, The Pennsylvania State University.

Nelson W. “Accelerated Testing. Statistic models, test plans and data analyses” Wiley series in probability and mathematic statistic, 1990

Nkurunziza, G, Benmokrane, B, Debaiky, A.S. Masmoudi, R. “Effect of sustained load and environment on long-term tensile properties of glass fiber-reinforced polymer reinforcing bars” ACI structural journal [0889-3241] Nkurunziza, G yr:2005 vol:102 iss:4 pg:615 -621

Nkurunziza, G., Debaiky, A., Cousin, P., and Benmokrane, B. (2005) "Durability of GFRP bars: a critical review of the literature." Progress in Structural Engineering and Materials, 7(4), 194-209

Parera, G., Doremus, R. H., and Landford, W. A. (1991) ‘Dissolution Rates of Silicate Glasses in Water at pH 7’, Journal of the American Ceramic Society, Vol. 74(6), p.1269-1274.

Porter M.L final report “Investigation of Glass Fiber Composite Dowel Bars for Highway Pavements Slabs” June 2001

Porter M.L, Barnes B.A. “Accelerated Durability of FRP Reinforcement for Concrete Structures” 1st International Conference on Durability of Fiber Reinforced Polymer for Construction (CDCC’98), Sherbrooke, Canada, 1998: 191–202.

Porter M.L., “Durability Issues for FRP Reinforcement to Concrete Structures,” Proceeding of 44th International SAMPE Symposium, 1999, pp. 2246-2254.

Porter, M. L., and Barnes, B. A. (1998) “Accelerated Aging Degradation of Glass Fiber Composites”, Second International Conference on Composites in Infrastructure, ed. H. Saadatmanesh, M.R. Ehsani, 1998, p.446-459

Prian L. and Barkatt A. “Degradation Mechanism of Fiber Reinforced Plastic and its Implications to Prediction of Long-term Behaviour” Mater Sci 1999; 34(16): 3977–3989.

Quinn J. B, Quinn G.D “A Practical and Systematic Review of Weibull Statistics for Reporting Strength of Dental Materials” Dental Materials V26 2010, pp. 135-147

Rahman, A.H., Lauzier, C., Kingsley, C., Richard, J., and Crimi, J., “Experimental Investigation of the Mechanism of Deterioration of FRP Reinforcement for Concrete. Proceedings of 2nd International Conference on Composite in Infrastructure, Tucson, Arizona, 1998, pp. 501-511

Robert M., Cousion P., Benmokrane B. “Study of the Performance of FRP Reinforcing Bars Subjected to Extreme Conditions of Application”, 2011

Robert M., Benmokrane B., ”Combined effects of saline solution and moist concrete on long-term durability of GFRP reinforcing bars” Construction & building materials [0950-0618] Robert, M yr:2013 vol:38 pg:274 -284

Schutte, C. L. (1994) “Environmental Durability of Glass-Fiber Composites”, Journal of Material Science and Engineering, Vol. 13, p.265-323

Sen R, Mullins G, and Salem T. “Durability of E-glass/vinyl ester Reinforcement in Alkaline Solution” ACI Structural Journal 2002: 99(3): 369–375

Shehata E., Abdelrahman A., Tadros G., and Rizkalla S. "FRP for Large Span Highway Bridge in Canada" Recent Advances in Bridge Engineering Edited by Urs Meier and R. Betti, Zurich, Switzerland, pp. 251-258 1997.

Shehata E., Morphy R., Rizkalla S. “ Fiber reinforced polymer shear reinforcement for concrete members: behaviour and design guidelines” Canadian Journal of Civil Engineering (Impact Factor: 0.33). 02/2011; 27(5):859-872. DOI:10.1139/cjce-27-5-859

Shehata E.F.G. “Fiber – Reinforced Polymer (FRP) For Shear Reinforcement in Concrete Structure “University of Manitoba 1999

Stone, D., Koenigsfeld, D., Myers, J., Nanni, A., “Durability of GFRP Rods, Laminates and Sandwich Panels subjected to Various Environmental Conditionings,” Proceeding of 2nd International Conference on Durability of Fiber Reinforced Polymer (FRP) Composites for Construction, Montreal, Canada, 2002, pp. 213-224

Tannous F. and Saadatmanesh H. “Environmental Effects on the Mechanical Properties E-Glass FRP Rebars” ACI Materials Journal Vol. 95(2), p.87-100 1998.

Tannous, F.E., and Saadatmanesh, H., “Durability of AR Glass Fiber Reinforced Plastic Bars,” Journal of Composites for Construction, 3(1), 1999, pp. 12-19.

Tuttle, M. E. (1996). “A framework for long-term durability predictions of polymeric composites”, Progress in Durability Analysis of Composite Systems 1996, ed. A.H., Cardon, H., Fukuda, K. Reifsnider, p.169-176.

Uomoto T. “Development of New GFRP with High Alkali Resistivity” 4th International Conference on Advanced Composite Materials in Bridges and Structures ACMBS-IV, Calgary, Alberta, 2004

Uomoto, T., and Ohga, H. (2001) “Performance of Fiber Reinforced Plastics for Concrete Reinforcement”, Advanced Composite Materials in Bridges and Structures, 1996, p.125-132

Vijay K. “Standardization of Test Methods for Property Evaluation of FRP Bars” West Virginia University 2003

Vijay P. V. Gengarao H.V.S. et Kaalluri R “Hygrothermal Response of GFRP bars under different Conditioning Schemes” proceeding of the 1st International Conference on Durability of Fiber Reinforced Polymer for Construction (CDCC’98) Sherbrook, Canada p.243-252 1998

Weber A., Witt C. “Short Term and Long Term Properties of Newly Developed Bent GFRP Reinforcing Bars” International Conference (CDCC – 11) p.47 – 54

Weber A., Witt C. “Short Term and Long Term Properties of Newly Developed Bent GFRP Reinforcing Bars” International Conference (CDCC – 11) p.47 – 54

Weil N. A., Daniel I. M. “Analysis of Fracture Probability in Nonuniformly Stressed Brittle Materials” Journal of American Ceramic Society V47 1964. pp. 268-274

Wenzlick J.D. “Evaluation of Stainless Steel Reinforcement in Bridge Decks” Report prepared for the Missouri Department of Transportation Organizational Results, 2007

Wickert, C. L., Vieira, J. A., Dehne, J. A., Wang, X., Wilder, D. M., and Barkatt, A. (1999) “Effects of Salts on Silicate Glass Dissolution in Water: Kinetics and Mechanics of Dissolution and Surface Cracking”, Physics and Chemistry of Glasses, Vol. 40(3), p.157-170

Yamaguchi, T. (1998) “Study on deterioration of FRP Rods for Concrete Reinforcement on Ultra-Violet Rays and Creep-Rupture, Doctoral Thesis, University of Tokyo.

Yang W., He X., “Combined Effects of Curing Temperatures and Alkaline Concrete on Tensile Properties of GFRP Bars” Hindawi, International Journal of Polymer Science Volume 2017, Article ID 4262703

Yilmaz V.T, Glasser F.P. “Reaction of Alkali-resistant Glass Fibers with Cement Part I: Review, Assessment, and Microscopy” *Glass Technology* 1991: 32(3): 91–98.

Yilmaz, V. T., Lachowski, E. E., and Glasser, F. P. (1991) “Chemical and Microstructural Changes at Alkali-Resistant Glass Fiber-Cement Interfaces”, Journal of the American Ceramic Society, Vol. 74(12), p.5054-5060

Zoghi M. “The International Handbook of FRP Composites in Civil Engineering” ISBN 9780849320132-CA#2013, 2013

Appendix 1

TENSILE TEST RESULTS

A1.1 M12 bars

a)

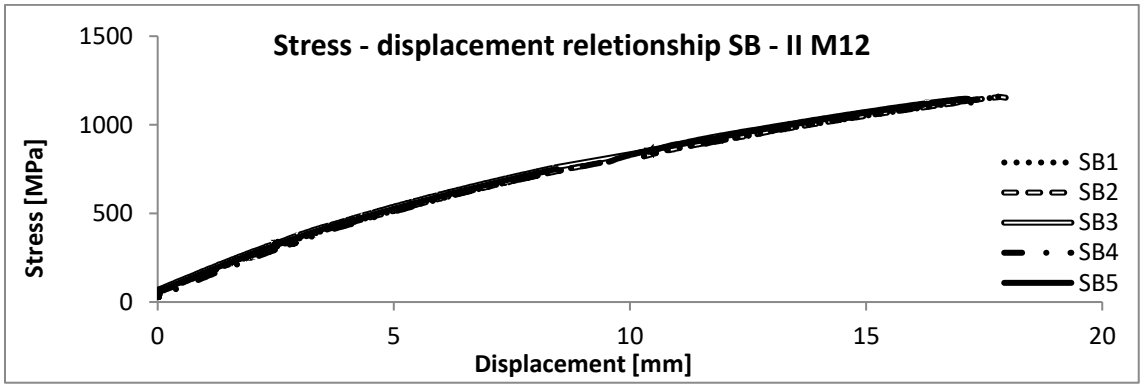

b)

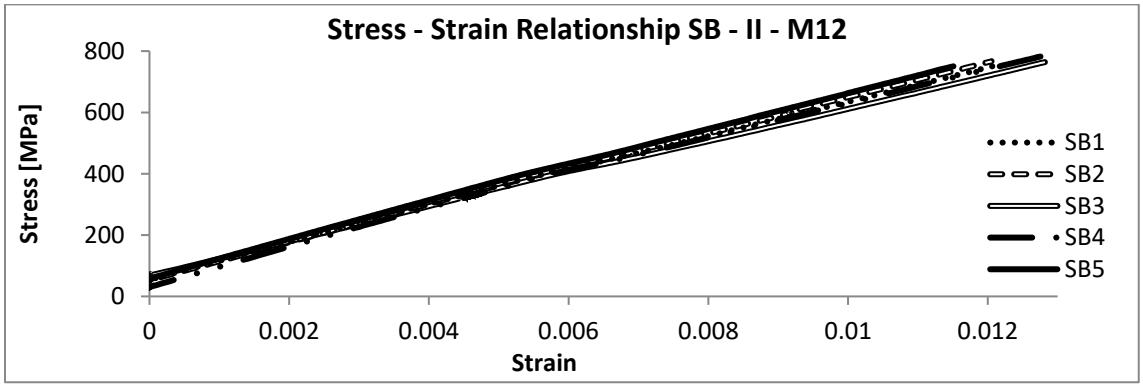

Fig. A1.1 – a) Stress-displacement and b) stress-strain relationship

a)

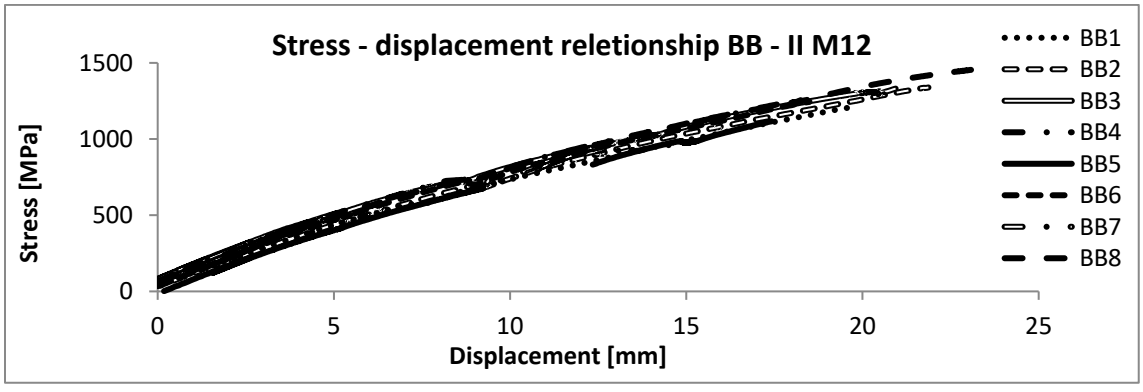

b)

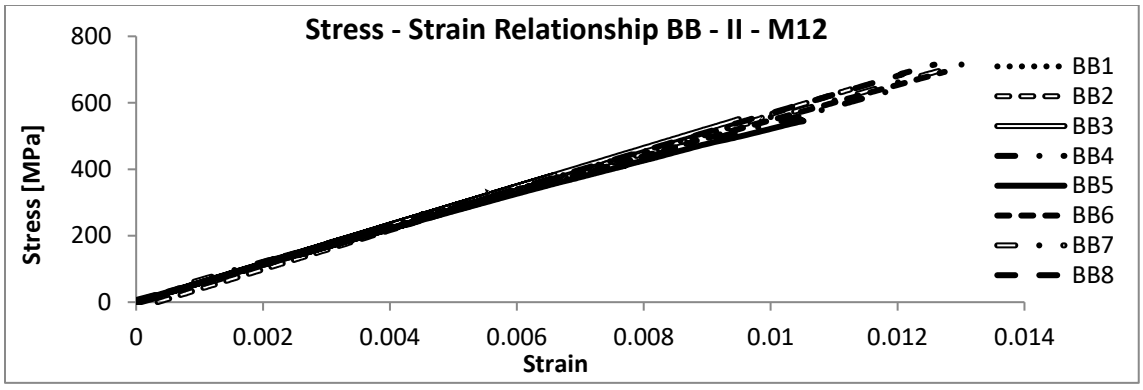

Fig. A1.2 – a) Stress-displacement and b) stress-strain relationship

A1.2 M16 bars

a)

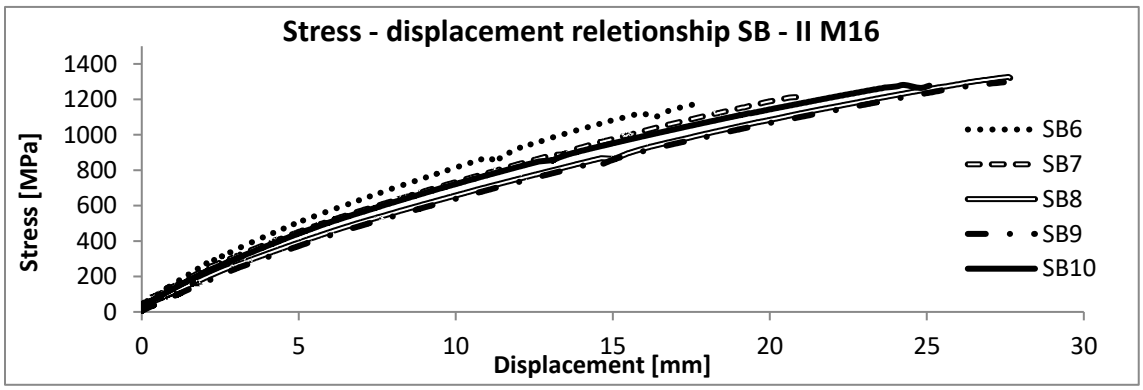

b)

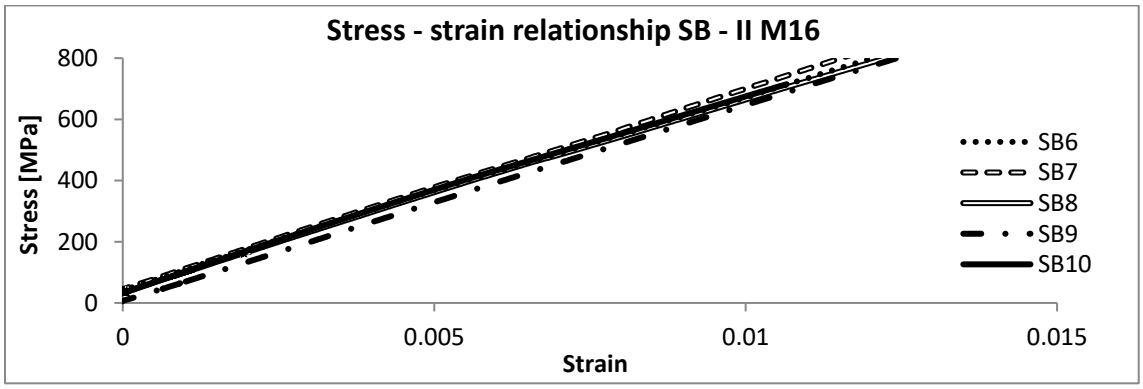

Fig. A1.3 – a) Stress-displacement and b) stress-strain relationship

a)

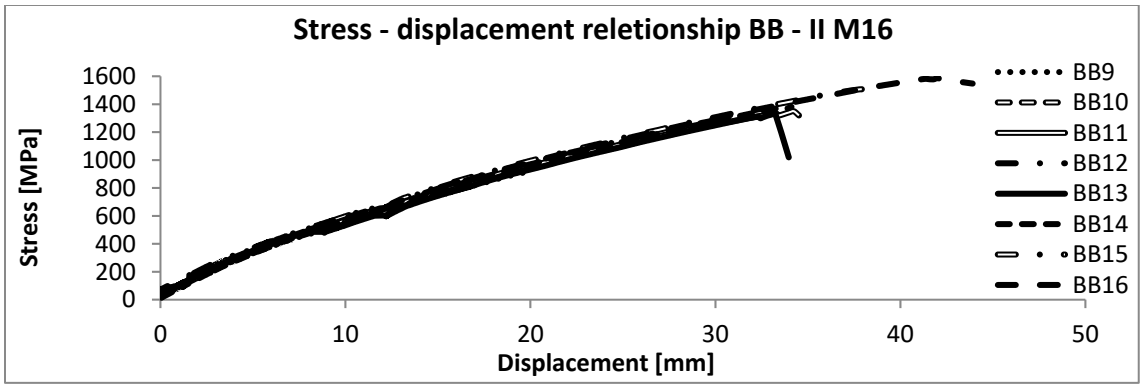

b)

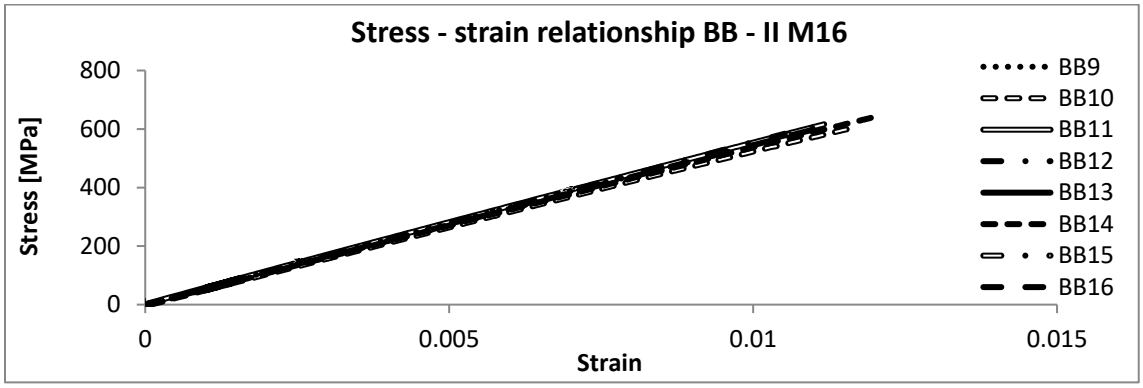

Fig. A1.4 – a) Stress-displacement and b) stress-strain relationship

Appendix 2

SHEAR TEST RESULTS

A2.1 #4 and M12 bars

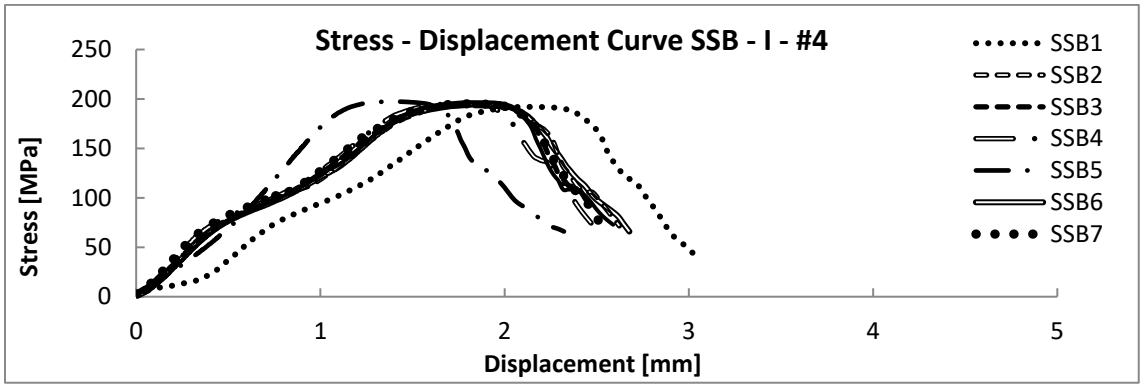

a)

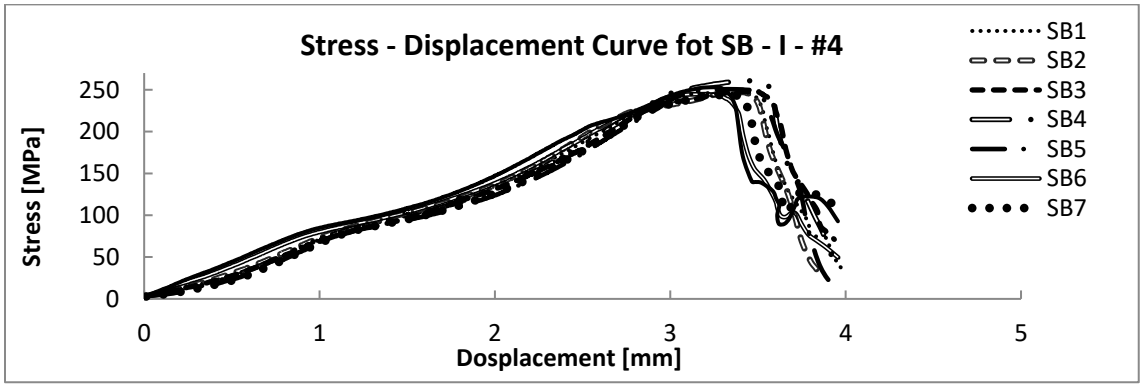

b)

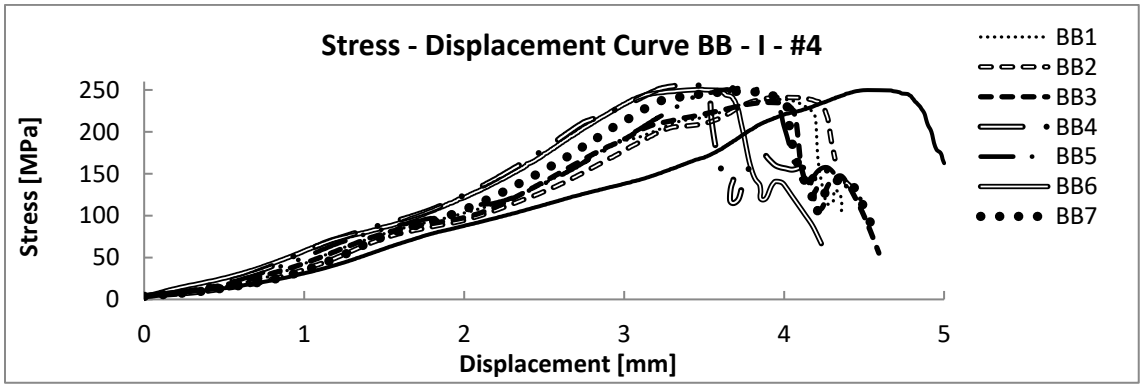

c)

Fig. A2.1 – Stress-displacement relationship for a) SSB b) SB c) BB #4 bars Company I

a)

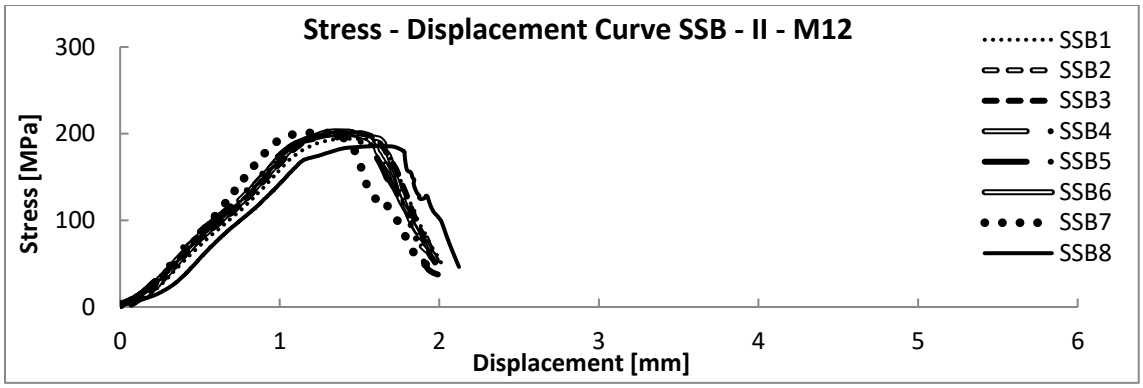

b)

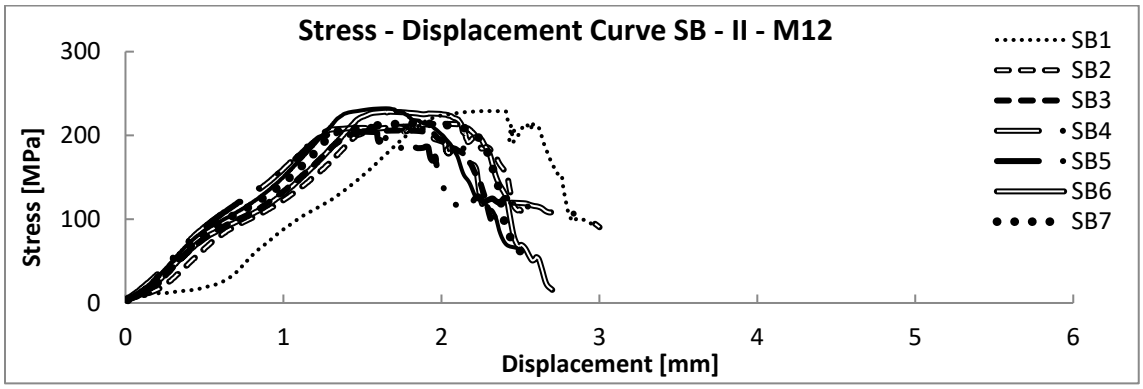

c)

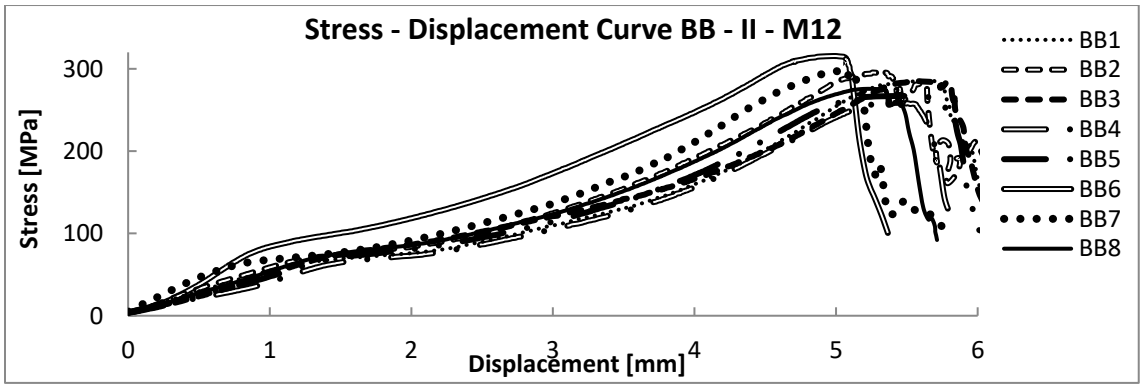

Fig. A2.2 – Stress-displacement relationship for a) SSB b) SB c) BB M12 bars Company II

A2.2 #5 and M16 bars

a)

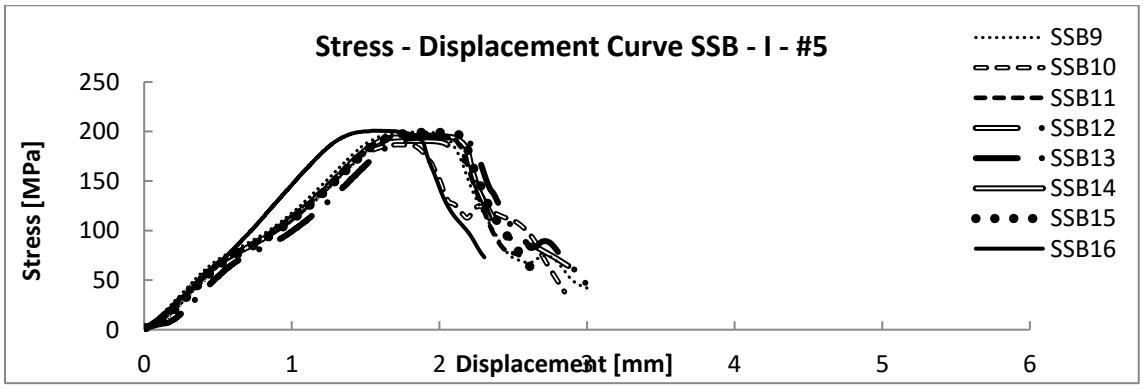

b)

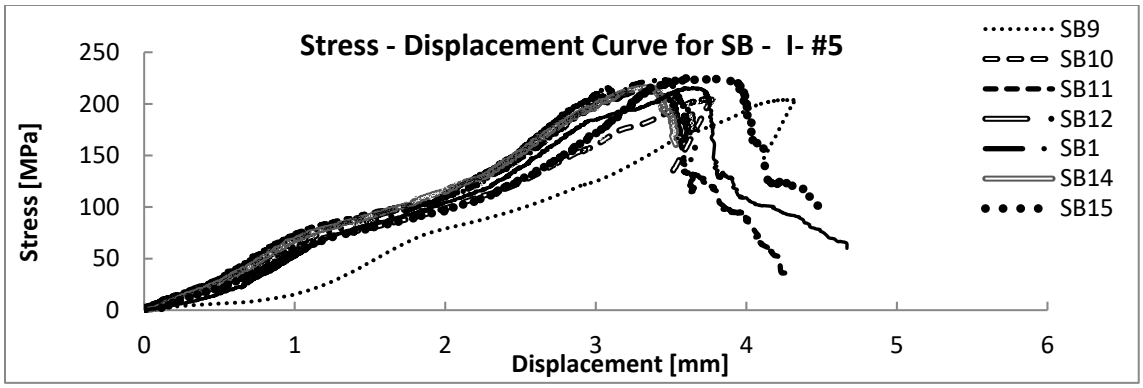

c)

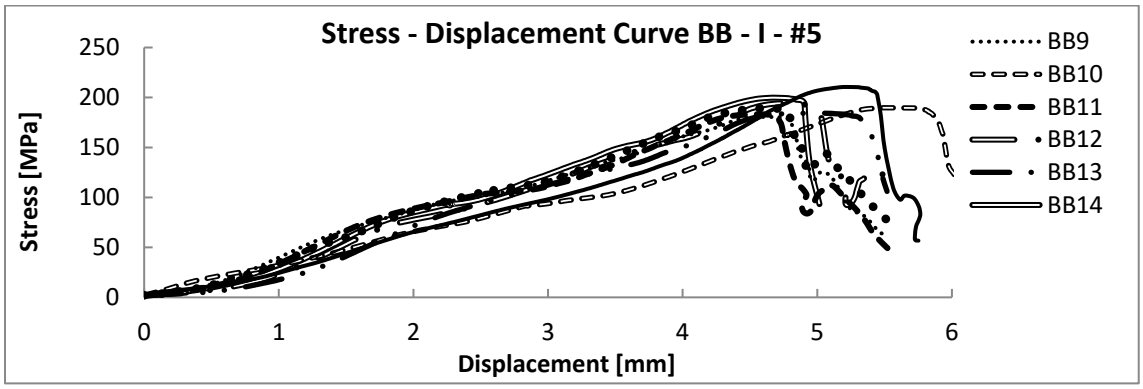

Fig. A2.3 – Stress-displacement relationship for a) SSB b) SB c) BB #5 bars Company I

a)

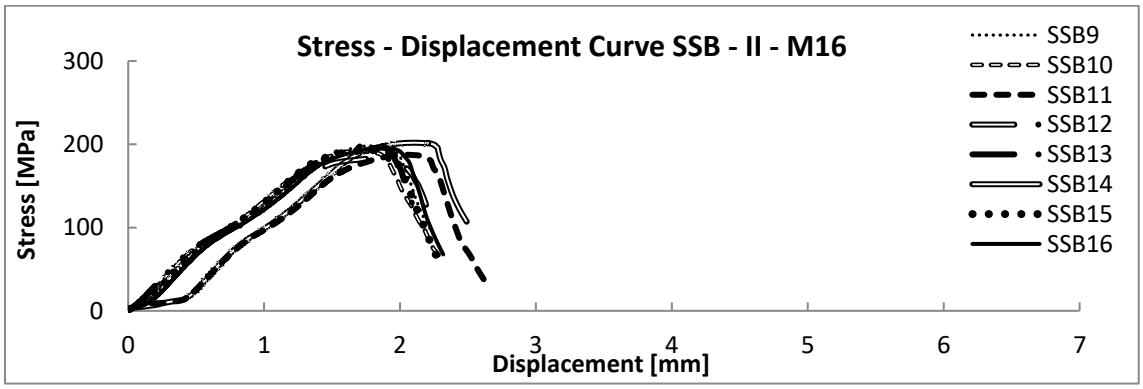

b)

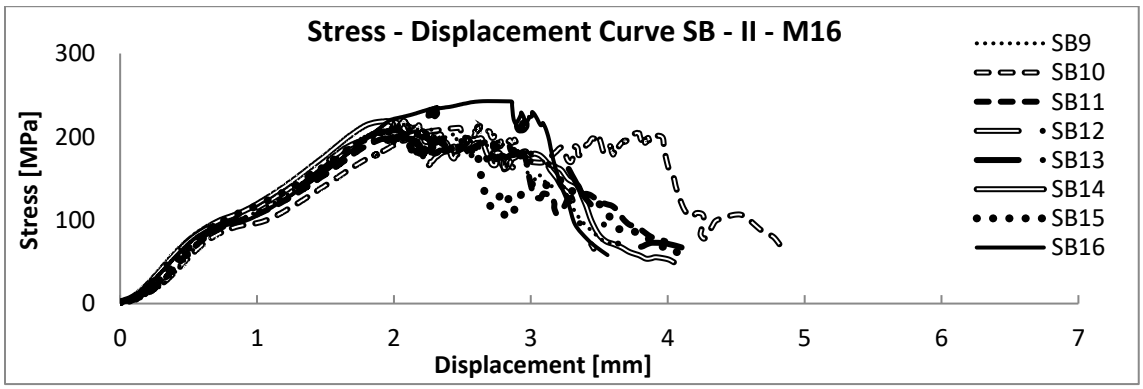

c)

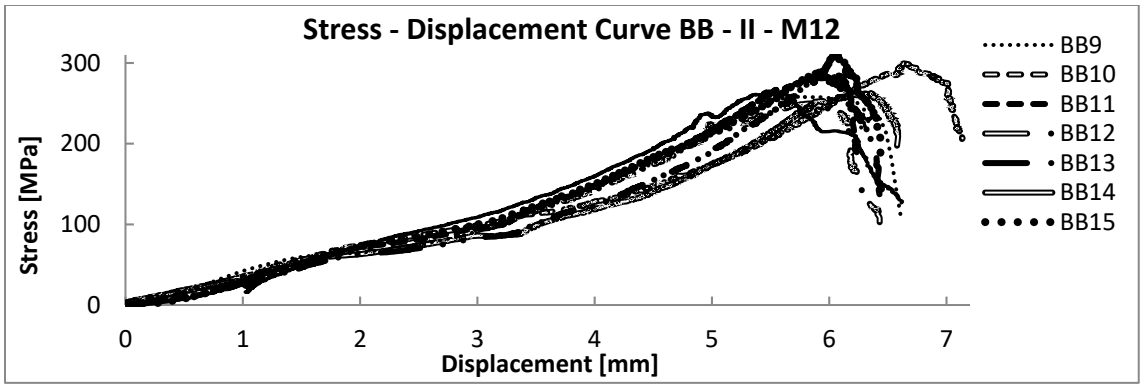

Fig. A2.4 – Stress-displacement relationship for a) SSB b) SB c) BB #5 bars Company II

Appendix 3

FLEXURE TEST RESULTS

A3.1 #4 and M12 bars

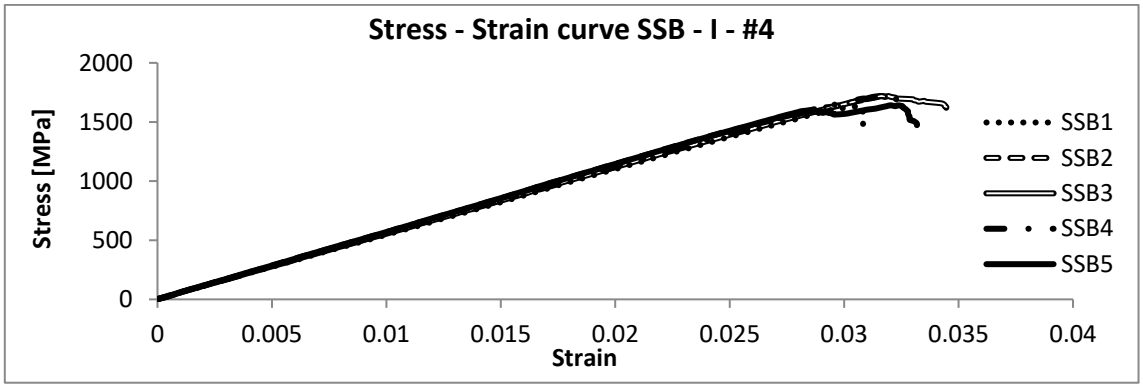

a)

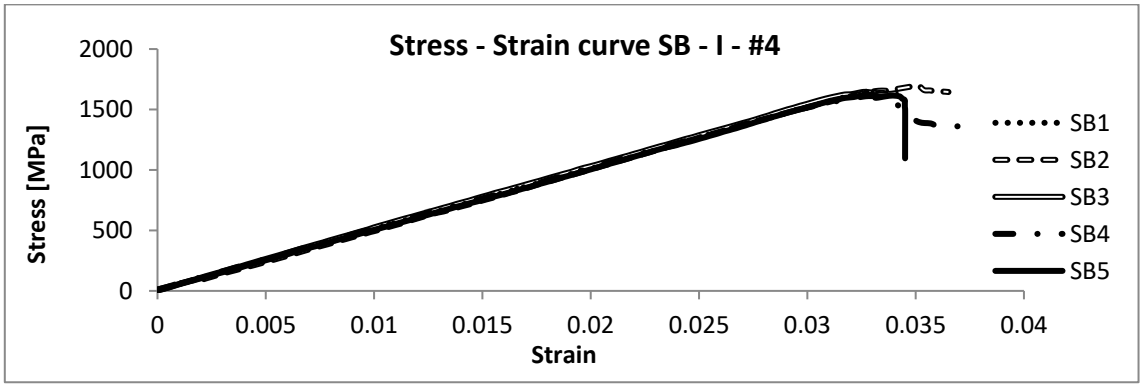

b)

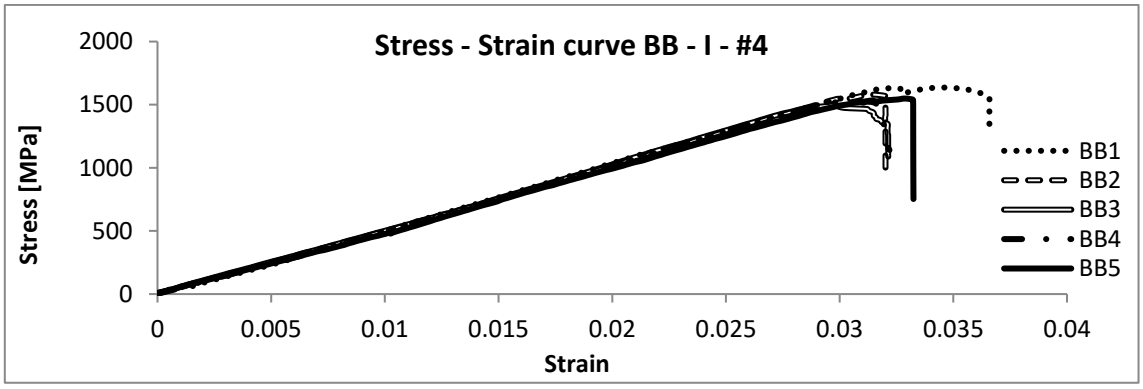

c)

Fig. A3.1 – Stress-strain relationship for a) SSB b) SB c) BB #4 bars Company I

a)

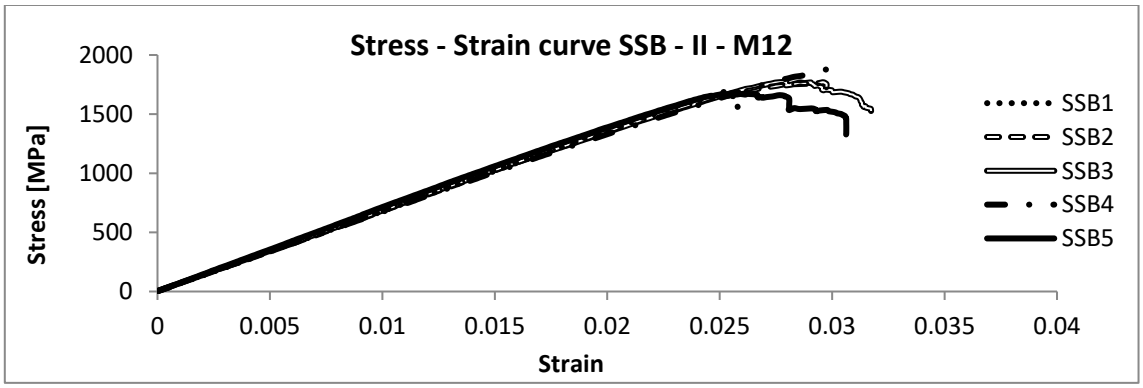

b)

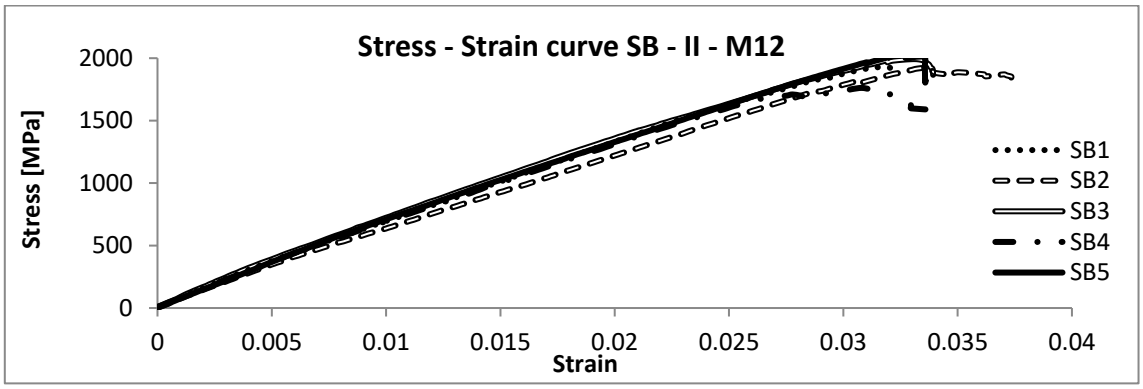

c)

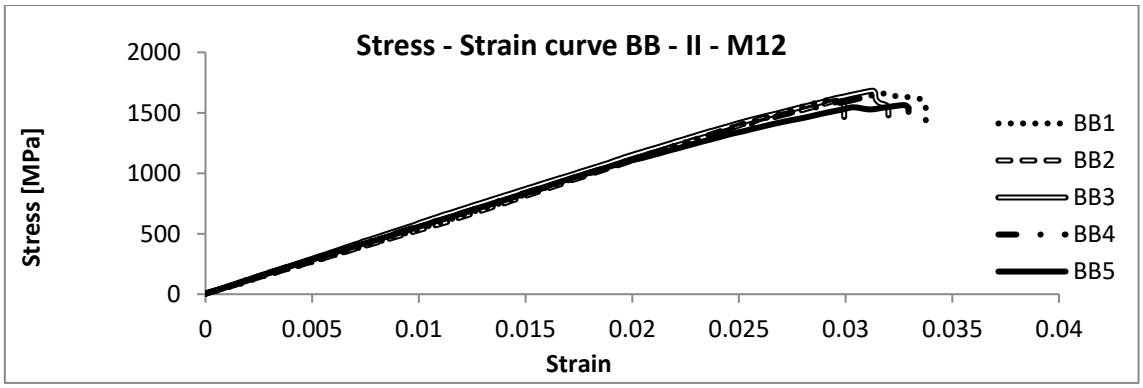

Fig. A3.2 – Stress-strain relationship for a) SSB b) SB c) BB M12 bars Company II

A3.2 #5 and M16 bars

a)

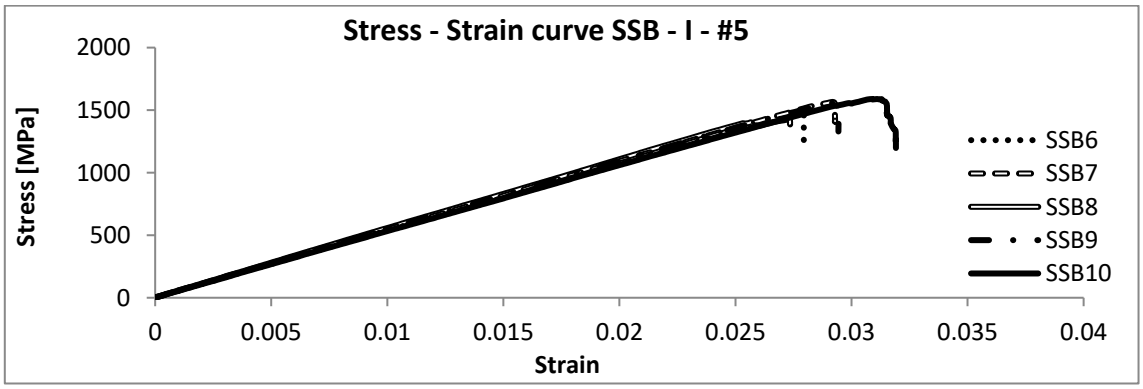

b)

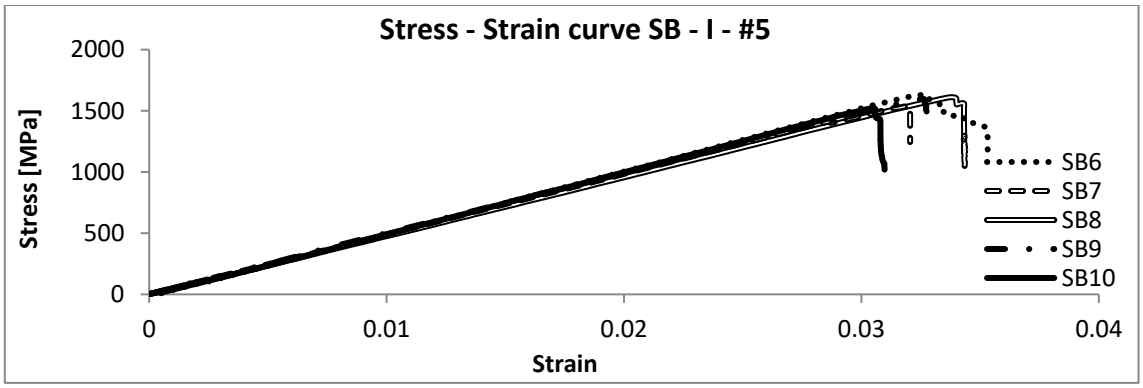

c)

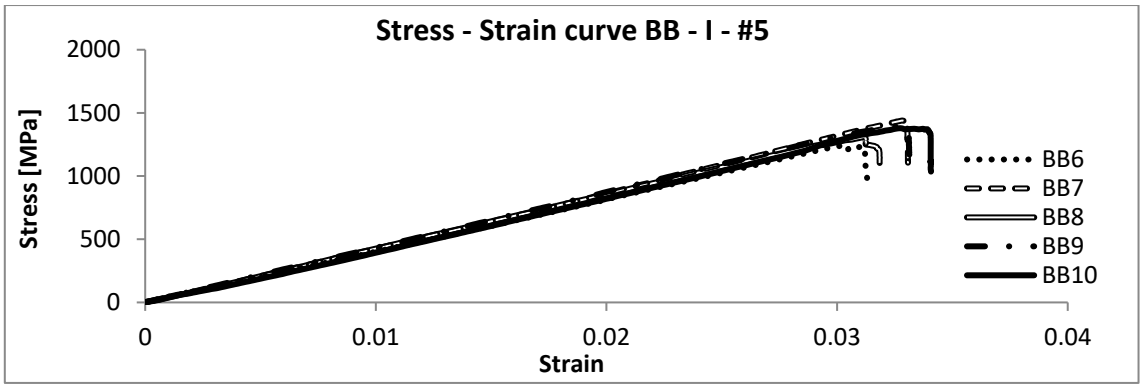

Fig. A3.3 – Stress-strain relationship for a) SSB b) SB c) BB #5 bars Company I

a)

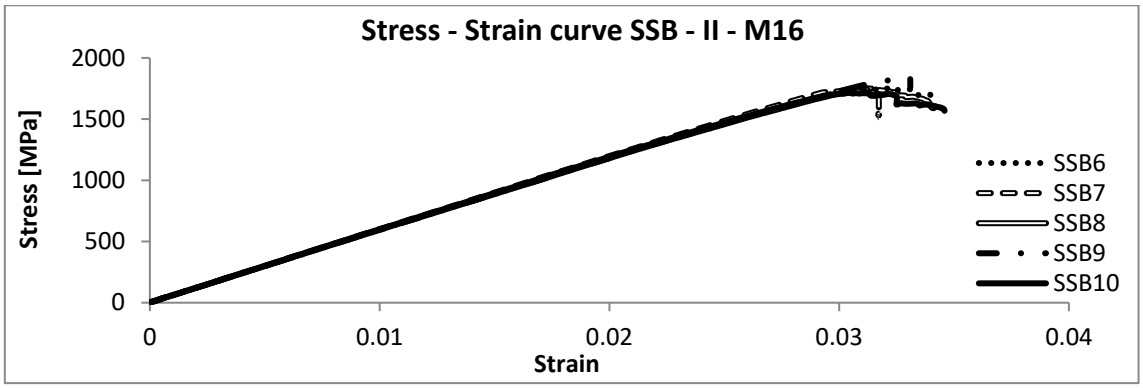

b)

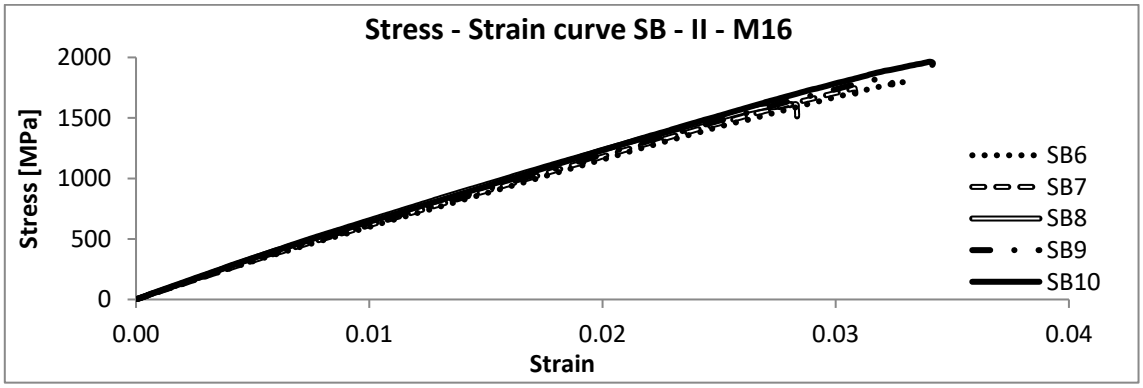

c)

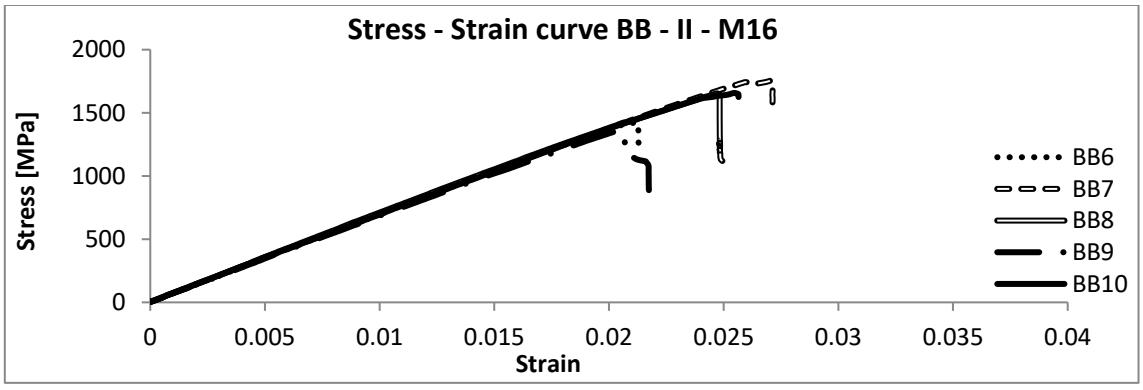

Fig. A3.4 – Stress-strain relationship for a) SSB b) SB c) BB M16 bars Company II

Appendix 4

EFFECTIVE VOLUME FOR RECTENGULAR ROD

Effective volume calculation for rectangular cross-sectioned sample – integration approach.

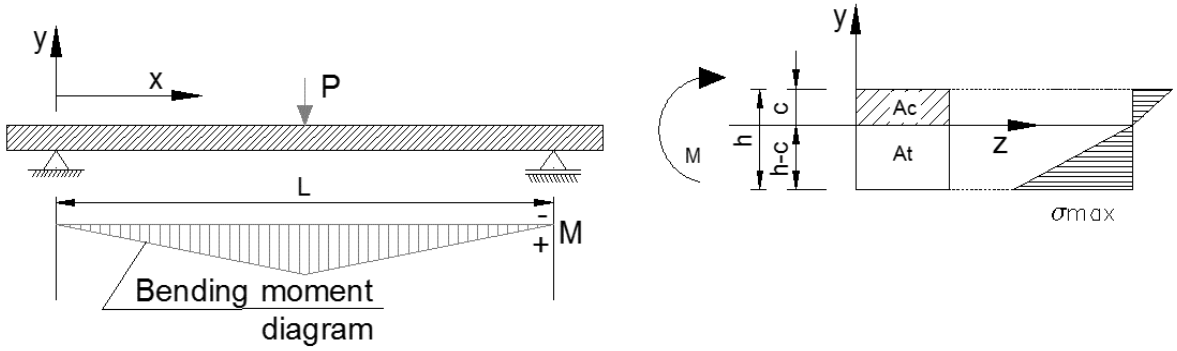

Fig.A4.1 – Bending moment diagram and stress distribution in sample due to bending.

In a case of three-point bending tensile stresses varies not only along the sample night with respect to the neutral axis but also along sample length with respect to the shape of bending moment diagram. So a Weibull effective volume according to Quinn (2010) can be expressed:

$$V_E = \int_{Vb} \left(\frac{\sigma b}{\sigma max}\right)^m dVb \qquad (A4.1)$$

Where: V – is the total volume of specimen σb – uniaxial tensile stress σmax – maximum tensile stress

The integration is performed over a sample volume that is stressed in tension. The effective volume for rectangular rod of height h and length L for the three-point bending is:

$$V_E = 2\int_0^{L/2} \int_{At} \left(\frac{\sigma b}{\sigma max}\right)^m dAt \qquad (A4.2)$$

Referring to the Fig A4.1:

- stress varies linearly with distance from neutral axis (h-c):

$$\sigma b = -\left(\frac{y}{(h-c)}\right)\sigma max \qquad (A4.3)$$

- also, stress varies linearly with distance from the sample support L (due to symmetry L/2)

$$\sigma b = \left(\frac{x}{l/2}\right)\sigma max = \left(\frac{2x}{l}\right)\sigma max \qquad (A4.4)$$

Combining equation A4.3 and A4.4:

$$\sigma b = \left(\frac{y}{(h-c)}\right)\left(\frac{2x}{l}\right)\sigma max \qquad (A4.5)$$

So the effective volume can be expressed as:

$$V_E = 2\int_0^{L/2}\int_{At}\left(\frac{-\left(\frac{y}{(h-c)}\right)\left(\frac{2x}{l}\right)\sigma max}{\sigma max}\right)^m dAt \qquad (A4.6)$$

Due to fact that it is a rectangular rod equation A4.6 can be written:

$$V_E = -2\int_0^{L/2}\int_0^{-(h-c)}\int_0^{a}\left(\frac{\left(\frac{y}{(h-c)}\right)\left(\frac{2x}{l}\right)\sigma max}{\sigma max}\right)^m dzdydx \qquad (A4.7)$$

Solving equation A4.7:

$$V_E = \frac{-2^{m+1}}{(h-c)^m L^m}\int_0^{\frac{L}{2}}\int_0^{-(h-c)}\int_0^{a} y^m x^m dzdydx =$$

$$= \frac{-2^{m+1}a}{(h-c)^m L^m}\int_0^{\frac{L}{2}}\int_0^{-(h-c)} y^m x^m\, dydx = \frac{-2^{m+1}a}{(h-c)^m L^m}\int_0^{\frac{L}{2}}\int_0^{-(h-c)} y^m x^m\, dydx =$$

$$= \frac{-2^{m+1}a}{(h-c)^m L^m} * \frac{-(h-c)^{m+1}}{(m+1)}\int_0^{\frac{L}{2}} x^m\, dx = \frac{-2^{m+1}a}{(h-c)^m L^m} * \frac{-(h-c)^{m+1}}{(m+1)} * \frac{\left(\frac{L}{2}\right)^{m+1}}{(m+1)} =$$

$$= \frac{a\left(2(h-c)\left(\frac{l}{2}\right)\right)^{m+1}}{(h-c)^m L^m (m+1)^2} = \frac{a(h-c)L*2}{(m+1)^2*2} = \frac{V}{2(m+1)^2}$$

Appendix 5

WEIBULL MODULUS

Table A5.1 – Data set for unmodified results for #4 bar for Company I

Unmodified results for #4				
i	Strength [Mpa]	x=ln(strength)	Pf=(i-0.5)/n	Y = ln{ln[1/(1-Pf)])
1	1569.6	7.358576089	0.1	-2.250367327
2	1623.13	7.392111663	0.3	-1.030930433
3	1645.98	7.40609123	0.5	-0.366512921
4	1651.23	7.409275744	0.7	0.185626759
5	1700.37	7.438601153	0.9	0.834032445

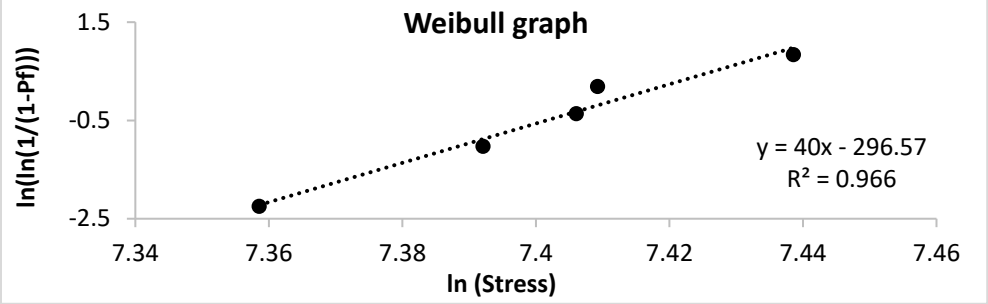

Fig.A5.1 – Weibull graph for unmodified results for #4 bar from Company I.

Table A5.2 – Data set for modified results for #4 bar for Company I

modified results for #4				
i	Strength [Mpa]	x=ln(strength)	Pf=(i-0.5)/n	Y = ln(ln[1/(1-Pf)])
1	1741.6	7.46255951	0.1	-2.250367327
2	1800.84	7.496008502	0.3	-1.030930433
3	1826.62	7.510222544	0.5	-0.366512921
4	1832.4	7.513381862	0.7	0.185626759
5	1886.61	7.542536847	0.9	0.834032445

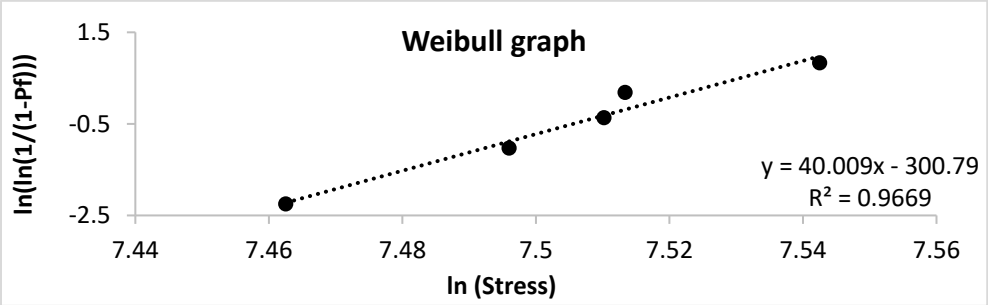

Fig.A5.2 – Weibull graph for modified results for #4 bar from Company I.

Table A5.3 – Data set for unmodified results for #5 bar for Company I

Unmodified results for #5				
i	Strength [Mpa]	x=ln(strength)	Pf=(i-0.5)/n	Y = ln{ln[1/(1-Pf)]}
1	1450.51	7.279670498	0.1	-2.250367327
2	1468.68	7.292119317	0.3	-1.030930433
3	1531.6	7.33406822	0.5	-0.366512921
4	1544.73	7.342604417	0.7	0.185626759
5	1554.65	7.349005719	0.9	0.834032445

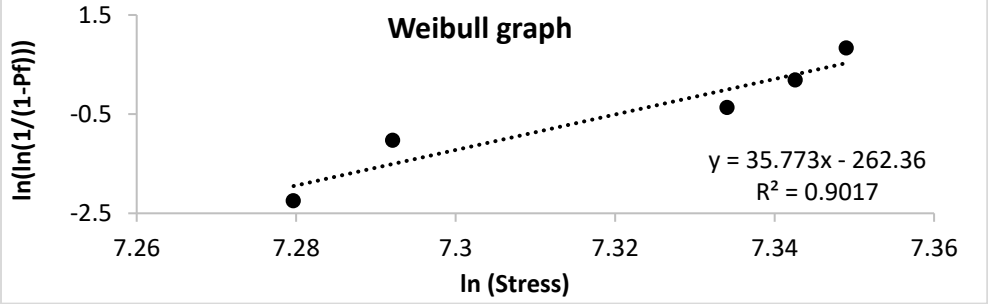

Fig.A5.3 – Weibull graph for unmodified results for #4 bar from Company I.

Table A5.4 – Data set for modified results for #5 bar for Company I

modified results for #5				
i	Strength [Mpa]	x=ln(strength)	Pf=(i-0.5)/n	Y = ln{ln[1/(1-Pf)]}
1	1587.67	7.370022812	0.1	-2.250367327
2	1607.8	7.382622064	0.3	-1.030930433
3	1676.9	7.42470213	0.5	-0.366512921
4	1691.24	7.433217267	0.7	0.185626759
5	1701.57	7.439306633	0.9	0.834032445

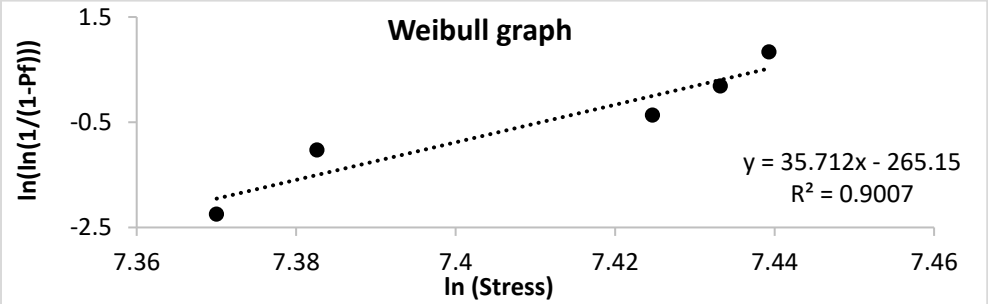

Fig.A5.4 – Weibull graph for modified results for #4 bar from Company I.

Table A5.5 – Data set for unmodified results for M12 bar for Company II

Unmodified results for M12				
i	Strength [Mpa]	x=ln(strength)	Pf=(i-0.5)/n	Y = ln{ln[1/(1-Pf)]}
1	1762.07	7.474244533	0.1	-2.250367327
2	1923.26315	7.56177858	0.3	-1.030930433
3	1928.64495	7.564572937	0.5	-0.366512921
4	1992.829223	7.597310628	0.7	0.185626759
5	2028.24	7.614923701	0.9	0.834032445

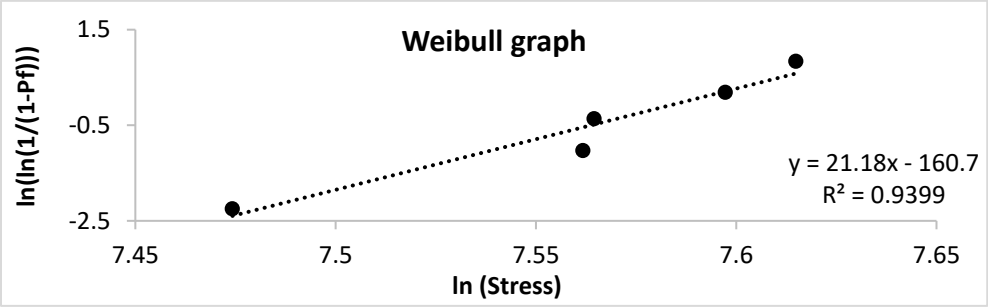

Fig.A5.5 – Weibull graph for unmodified results for M12 bar from Company II.

Table A5.6 – Data set for modified results for M12 bar for Company II

modified results for #4				
i	Strength [Mpa]	x=ln(strength)	Pf=(i-0.5)/n	Y = ln{ln[1/(1-Pf)]}
1	1837.5	7.516161231	0.1	-2.250367327
2	2005.89	7.603843132	0.3	-1.030930433
3	2011.13	7.606452032	0.5	-0.366512921
4	2077.91	7.63911786	0.7	0.185626759
5	2115.62	7.657103193	0.9	0.834032445

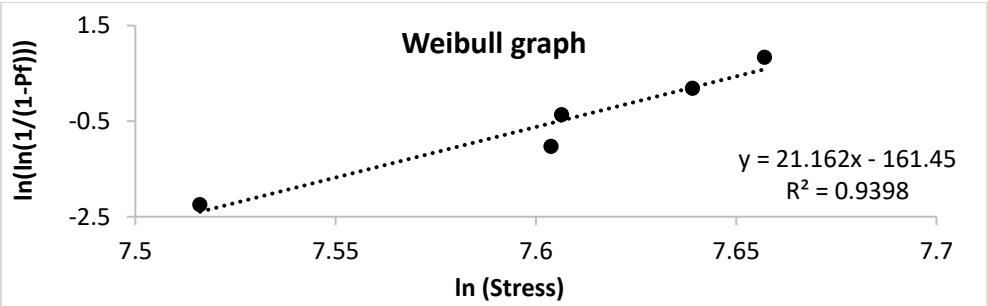

Fig.A5.6 – Weibull graph for modified results for M12 bar from Company II.

Table A5.7 – Data set for unmodified results for M16 bar for Company II

Unmodified results for M16				
i	Strength [Mpa]	x=ln(strength)	Pf=(i-0.5)/n	Y = ln{ln[1/(1-Pf)]}
1	1672.2	7.421895404	0.1	-2.250367327
2	1781.86	7.485413042	0.3	-1.030930433
3	1806.31	7.499041369	0.5	-0.366512921
4	1859.81	7.528229611	0.7	0.185626759
5	1894.28	7.546594098	0.9	0.834032445

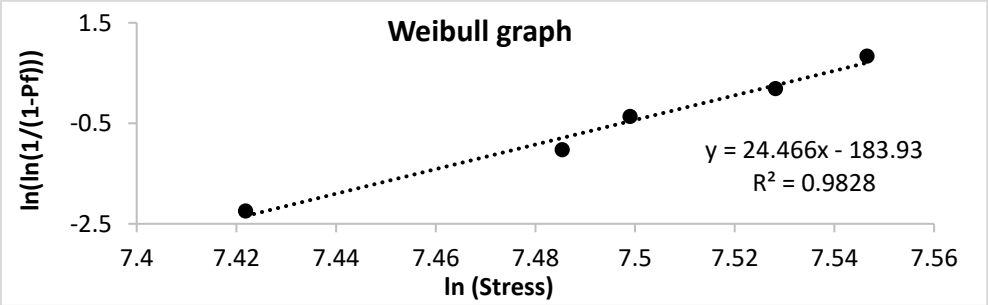

Fig.A5.7 – Weibull graph for unmodified results for M16 bar from Company II.

Table A5.8 – Data set for modified results for M16 bar for Company II

modified results for M16				
i	Strength [Mpa]	x=ln(strength)	Pf=(i-0.5)/n	Y = lnln[1/(1-Pf)]
1	1751.53	7.468244971	0.1	-2.250367327
2	1866.4	7.531766721	0.3	-1.030930433
3	1892.15	7.545469028	0.5	-0.366512921
4	1948.01	7.574563618	0.7	0.185626759
5	1984.1	7.59292069	0.9	0.834032445

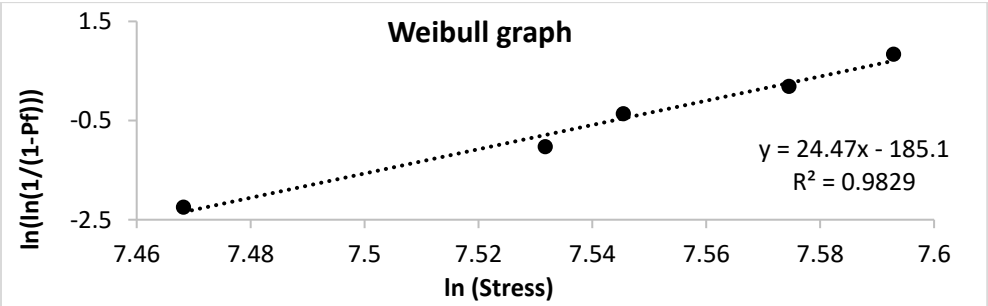

Fig.A5.8 – Weibull graph for modified results for M16 bar from Company II.

Appendix 6

ALKALINE IMMERSION TEST
TENSILE STRENGTH DEGRADATION

Table A6.1 – Tensile strength degradation SB bars Company II in 50˚C solution

Straight bars (SB) properties after 0 days in alkaline solution							
Sample	M12			Sample	M16		
	Ultimate capacity [kN]	Tensile strength [MPa]	Modulus of elasticity [GPa]		Ultimate capacity [kN]	Tensile strength [MPa]	Modulus of elasticity [GPa]
mean	139	1223	62	mean	255	1270	63
s.d	4	32	3.4	s.d	4	56	1
cov	0.03		0.05	cov	0.04		0.02
Straight bars (SB) properties after 30 days in alkaline solution							
Sample	M12			Sample	M16		
	Ultimate capacity [kN]	Tensile strength [MPa]	Modulus of elasticity [GPa]		Ultimate capacity [kN]	Tensile strength [MPa]	Modulus of elasticity [GPa]
mean	134	1186	62	mean	252	1253	62
s.d	0.8	7	1.6	s.d	7.5	34.4	1.7
cov	0.006		0.03	cov	0.03		0.03
Straight bars (SB) properties after 90 days in alkaline solution							
Sample	M12			Sample	M16		
	Ultimate capacity [kN]	Tensile strength [MPa]	Modulus of elasticity [GPa]		Ultimate capacity [kN]	Tensile strength [MPa]	Modulus of elasticity [GPa]
mean	131	1167	61.3	mean	249	1240	61
s.d	1.3	14.8	1.3	s.d	10	54.2	1
cov	0.01		0.02	cov	0.04		0.02
Straight bars (SB) properties after 150 days in alkaline solution							
Sample	M12			Sample	M16		
	Ultimate capacity [kN]	Tensile strength [MPa]	Modulus of elasticity [GPa]		Ultimate capacity [kN]	Tensile strength [MPa]	Modulus of elasticity [GPa]
mean	130	1157	61	mean	248	1235	62
s.d	3.9	30	1.8	s.d	17.3	85	1.4
cov	0.03		0.03	cov	0.07		0.02

Table A6.2 – Tensile strength degradation SB bars Company II in 60˚C solution

Straight bars (SB) properties after 0 days in alkaline solution							
Sample	M12			Sample	M16		
	Ultimate capacity [kN]	Tensile strength [MPa]	Modulus of elasticity [GPa]		Ultimate capacity [kN]	Tensile strength [MPa]	Modulus of elasticity [GPa]
mean	139	1223	62	mean	255	1270	63
s.d	4	32	3.4	s.d	4	56	1
cov	0.03		0.05	cov	0.04		0.02
Straight bars (SB) properties after 30 days in alkaline solution							
Sample	M12			Sample	M16		
	Ultimate capacity [kN]	Tensile strength [MPa]	Modulus of elasticity [GPa]		Ultimate capacity [kN]	Tensile strength [MPa]	Modulus of elasticity [GPa]
mean	131	1158	62	mean	247	1229	61
s.d	1.3	11.7	0.7	s.d	3.5	17.5	0.8
cov	0.01		0.01	cov	0.01		0.01
Straight bars (SB) properties after 90 days in alkaline solution							
Sample	M12			Sample	M16		
	Ultimate capacity [kN]	Tensile strength [MPa]	Modulus of elasticity [GPa]		Ultimate capacity [kN]	Tensile strength [MPa]	Modulus of elasticity [GPa]
mean	124	1122	62	mean	241	1199	62
s.d	5.5	50	0.5	s.d	3.8	19	0.3
cov	0.05		0.01	cov	0.02		0.01
Straight bars (SB) properties after 150 days in alkaline solution							
Sample	M12			Sample	M16		
	Ultimate capacity [kN]	Tensile strength [MPa]	Modulus of elasticity [GPa]		Ultimate capacity [kN]	Tensile strength [MPa]	Modulus of elasticity [GPa]
mean	124	1097	62	mean	237	1181	61
s.d	2.1	18.6	0.5	s.d	2.5	12.5	1
cov	0.02		0.01	cov	0.01		0.02

Table A6.2 – Tensile strength degradation SB bars Company II in 70˚C solution

Straight bars (SB) properties after 0 days in alkaline solution							
Sample	M12			Sample	M16		
	Ultimate capacity [kN]	Tensile strength [MPa]	Modulus of elasticity [GPa]		Ultimate capacity [kN]	Tensile strength [MPa]	Modulus of elasticity [GPa]
mean	139	1223	62	mean	255	1270	63
s.d	4	32	3.4	s.d	4	56	1
cov	0.03		0.05	cov	0.04		0.02

Straight bars (SB) properties after 30 days in alkaline solution							
Sample	M12			Sample	M16		
	Ultimate capacity [kN]	Tensile strength [MPa]	Modulus of elasticity [GPa]		Ultimate capacity [kN]	Tensile strength [MPa]	Modulus of elasticity [GPa]
mean	130	1148	60	mean	243	1209	61
s.d	8	70	0.4	s.d	9.8	49	1.5
cov	0.06		0.01	cov	0.04		0.03
Straight bars (SB) properties after 90 days in alkaline solution							
Sample	M12			Sample	M16		
	Ultimate capacity [kN]	Tensile strength [MPa]	Modulus of elasticity [GPa]		Ultimate capacity [kN]	Tensile strength [MPa]	Modulus of elasticity [GPa]
mean	120	1059	61	mean	228	1136	62
s.d	10.7	95	0.5	s.d	3.5	17.5	0.8
cov	0.09		0.01	cov	0.02		0.01
Straight bars (SB) properties after 150 days in alkaline solution							
Sample	M12			Sample	M16		
	Ultimate capacity [kN]	Tensile strength [MPa]	Modulus of elasticity [GPa]		Ultimate capacity [kN]	Tensile strength [MPa]	Modulus of elasticity [GPa]
mean	113	1004	62	mean	220	1098	62
s.d	10.3	92	0.7	s.d	15.2	76	1.1
cov	0.09		0.01	cov	0.07		0.02

Appendix 7

ALKALINE IMMERSION TEST
SHEAR STRENGTH DEGRADATION

The Appendix contain all results from shear alkaline immersion test. Due to high similarity, graphs just from one temperature 60˚C are presented herein.

A7.1. Company I

Table A7.1 – Shear strength degradation SSB bars Company I in 60˚C solution

Smooth bars (SSB) properties after 0 days in alkaline solution				
Sample	#4		#5	
	Shear Strength [MPa]	Ultimate capacity [kN]	Shear Strength [MPa]	Ultimate capacity [kN]
mean	195	60	192	98
s.d.	1.7	6	12	5.8
cov	0.01		0.06	
Smooth bars (SSB) properties after 30 days in alkaline solution				
Sample	#4		#5	
	Shear Strength [MPa]	Ultimate capacity [kN]	Shear Strength [MPa]	Ultimate capacity [kN]
mean	180	55	182	92
s.d.	2.5	0.8	4.6	2.3
cov	0.01		0.03	
Smooth bars (SSB) properties after 90 days in alkaline solution				
Sample	#4		#5	
	Shear Strength [MPa]	Ultimate capacity [kN]	Shear Strength [MPa]	Ultimate capacity [kN]
mean	171	53	174	89
s.d.	2.7	0.8	5.12	2.6
cov	0.02		0.03	
Smooth bars (SSB) properties after 90 days in alkaline solution				
Sample	#4		#5	
	Shear Strength [MPa]	Ultimate capacity [kN]	Shear Strength [MPa]	Ultimate capacity [kN]
mean	168	52	170	87
s.d.	3.2	1	2	1
cov	0.02		0.01	

Table A7.2 – Shear strength degradation SB bars Company I in 50˚C solution

Straight bars (SB) properties after 0 days in alkaline solution				
Sample	#4		#5	
	Shear Strength [MPa]	Ultimate capacity [kN]	Shear Strength [MPa]	Ultimate capacity [kN]
mean	242	74	214	109
s.d.	24	7.4	5	3.3
cov	0.1		0.03	
Straight bars (SB) properties after 30 days in alkaline solution				
Sample	#4		#5	
	Shear Strength [MPa]	Ultimate capacity [kN]	Shear Strength [MPa]	Ultimate capacity [kN]
mean	232	71	208	106
s.d.	11	3.4	4	2
cov	0.05		0.02	
Straight bars (SB) properties after 90 days in alkaline solution				
Sample	#4		#5	
	Shear Strength [MPa]	Ultimate capacity [kN]	Shear Strength [MPa]	Ultimate capacity [kN]
mean	227	70	205	104
s.d.	13	4	3.2	1.6
cov	0.06		0.02	
Straight bars (SB) properties after 90 days in alkaline solution				
Sample	#4		#5	
	Shear Strength [MPa]	Ultimate capacity [kN]	Shear Strength [MPa]	Ultimate capacity [kN]
mean	225	69	202	102
s.d.	5	1.5	7	3.5
cov	0.02		0.03	

Table A7.3 – Shear strength degradation SB bars Company I in 60˚C solution

Straight bars (SB) properties after 0 days in alkaline solution				
Sample	#4		#5	
	Shear Strength [MPa]	Ultimate capacity [kN]	Shear Strength [MPa]	Ultimate capacity [kN]
mean	242	74	214	109
s.d.	24	7.4	5	3.3
cov	0.1		0.03	
Straight bars (SB) properties after 30 days in alkaline solution				
Sample	#4		#5	
	Shear Strength [MPa]	Ultimate capacity [kN]	Shear Strength [MPa]	Ultimate capacity [kN]
mean	225	69	202	103
s.d.	17	5.2	3	1.5
cov	0.08		0.02	
Straight bars (SB) properties after 90 days in alkaline solution				
Sample	#4		#5	

	Shear Strength [MPa]	Ultimate capacity [kN]	Shear Strength [MPa]	Ultimate capacity [kN]
mean	218	67	197	100
s.d.	4	1.2	11	5.6
cov	0.02		0.06	
Straight bars (SB) properties after 90 days in alkaline solution				
Sample	#4		#5	
	Shear Strength [MPa]	Ultimate capacity [kN]	Shear Strength [MPa]	Ultimate capacity [kN]
mean	212	65	193	98
s.d.	2	0.6	8	4
cov	0.01		0.04	

Table A7.4 – Shear strength degradation SB bars Company I in 70˚C solution

Straight bars (SB) properties after 0 days in alkaline solution				
Sample	#4		#5	
	Shear Strength [MPa]	Ultimate capacity [kN]	Shear Strength [MPa]	Ultimate capacity [kN]
mean	242	74	214	109
s.d.	24	7.4	5	3.3
cov	0.1		0.03	
Straight bars (SB) properties after 30 days in alkaline solution				
Sample	#4		#5	
	Shear Strength [MPa]	Ultimate capacity [kN]	Shear Strength [MPa]	Ultimate capacity [kN]
mean	219	67	198	101
s.d.	1	0.3	11	5.6
cov	0.005		0.06	
Straight bars (SB) properties after 90 days in alkaline solution				
Sample	#4		#5	
	Shear Strength [MPa]	Ultimate capacity [kN]	Shear Strength [MPa]	Ultimate capacity [kN]
mean	209	64	192	97
s.d.	3.5	107	7	3.5
cov	0.02		0.03	
Straight bars (SB) properties after 90 days in alkaline solution				
Sample	#4		#5	
	Shear Strength [MPa]	Ultimate capacity [kN]	Shear Strength [MPa]	Ultimate capacity [kN]
mean	203	62	186	95
s.d.	2.4	0.7	7.4	3.8
cov	0.01		0.04	

Table A7.5 – Shear strength degradation BB bars Company I in 50˚C solution

Bent bars (BB) properties after 0 days in alkaline solution				
Sample	#4		#5	
	Shear Strength [MPa]	Ultimate capacity [kN]	Shear Strength [MPa]	Ultimate capacity [kN]
mean	247	56	191	77
s.d.	7	1.7	10	4
cov	0.03		0.05	
Bent bars (BB) properties after 30 days in alkaline solution				
Sample	#4		#5	
	Shear Strength [MPa]	Ultimate capacity [kN]	Shear Strength [MPa]	Ultimate capacity [kN]
mean	235	53	184	74
s.d.	2.4	0.5	14	5.6
cov	0.01		0.08	
Bent bars (BB) properties after 90 days in alkaline solution				
Sample	#4		#5	
	Shear Strength [MPa]	Ultimate capacity [kN]	Shear Strength [MPa]	Ultimate capacity [kN]
mean	228	52	181	73
s.d.	6	1.4	18	7.3
cov	0.03		0.1	
Bent bars (BB) properties after 90 days in alkaline solution				
Sample	#4		#5	
	Shear Strength [MPa]	Ultimate capacity [kN]	Shear Strength [MPa]	Ultimate capacity [kN]
mean	226	51	179	72
s.d.	8	1.8	4	1.6
cov	0.04		0.02	

Table A7.6 – Shear strength degradation BB bars Company I in 60˚C solution

Bent bars (BB) properties after 0 days in alkaline solution				
Sample	#4		#5	
	Shear Strength [MPa]	Ultimate capacity [kN]	Shear Strength [MPa]	Ultimate capacity [kN]
mean	247	56	191	77
s.d.	7	1.7	10	4
cov	0.03		0.05	
Bent bars (BB) properties after 30 days in alkaline solution				
Sample	#4		#5	
	Shear Strength [MPa]	Ultimate capacity [kN]	Shear Strength [MPa]	Ultimate capacity [kN]
mean	229	52	180	72
s.d.	15.6	3.5	2	0.8
cov	0.07		0.01	
Bent bars (BB) properties after 90 days in alkaline solution				
Sample	#4		#5	

	Shear Strength [MPa]	Ultimate capacity [kN]	Shear Strength [MPa]	Ultimate capacity [kN]
mean	220	50	174	70
s.d.	21	4.8	7	2.8
cov	0.09		0.05	
Bent bars (BB) properties after 90 days in alkaline solution				
Sample	#4		#5	
	Shear Strength [MPa]	Ultimate capacity [kN]	Shear Strength [MPa]	Ultimate capacity [kN]
mean	217	49	172	69
s.d.	12	2.7	2.2	0.9
cov	0.06		0.01	

Table A7.7 – Shear strength degradation BB bars Company I in 70˚C solution

Bent bars (BB) properties after 0 days in alkaline solution				
Sample	#4		#5	
	Shear Strength [MPa]	Ultimate capacity [kN]	Shear Strength [MPa]	Ultimate capacity [kN]
mean	247	56	191	77
s.d.	7	1.7	10	4
cov	0.03		0.05	
Bent bars (BB) properties after 30 days in alkaline solution				
Sample	#4		#5	
	Shear Strength [MPa]	Ultimate capacity [kN]	Shear Strength [MPa]	Ultimate capacity [kN]
mean	226	51	178	71
s.d.	11	2.5	11	4.4
cov	0.05		0.06	
Bent bars (BB) properties after 90 days in alkaline solution				
Sample	#4		#5	
	Shear Strength [MPa]	Ultimate capacity [kN]	Shear Strength [MPa]	Ultimate capacity [kN]
mean	214	48	170	68
s.d.	2.2	0.05	5.3	2
cov	0.01		0.03	
Bent bars (BB) properties after 90 days in alkaline solution				
Sample	#4		#5	
	Shear Strength [MPa]	Ultimate capacity [kN]	Shear Strength [MPa]	Ultimate capacity [kN]
mean	210	47	167	67
s.d.	12	2.7	10	4
cov	0.06		0.06	

a)

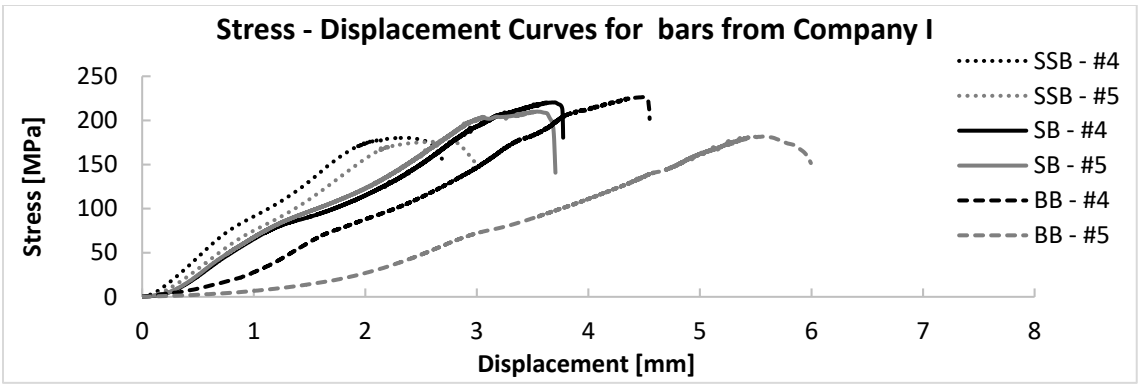

b)

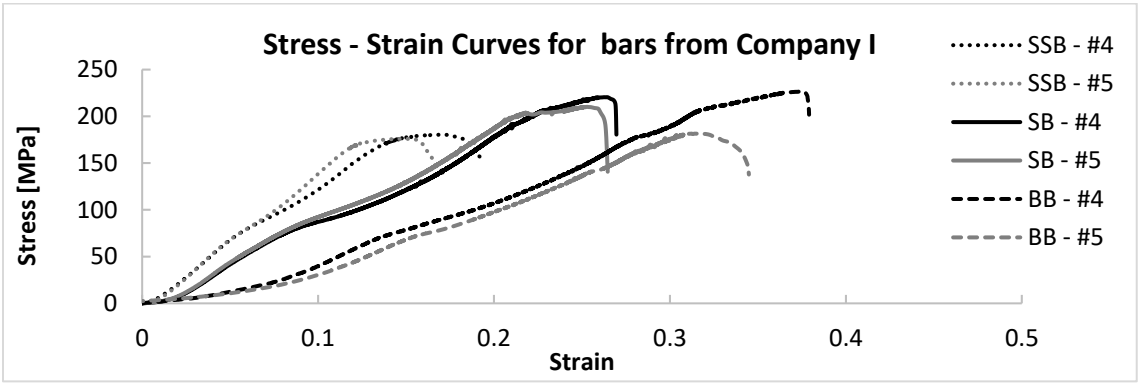

Fig. A7.1 – a) Stress-displacement b) stress-strain curves for bars from Company I after 30 days in alkaline solution heated to 60˚C

a)

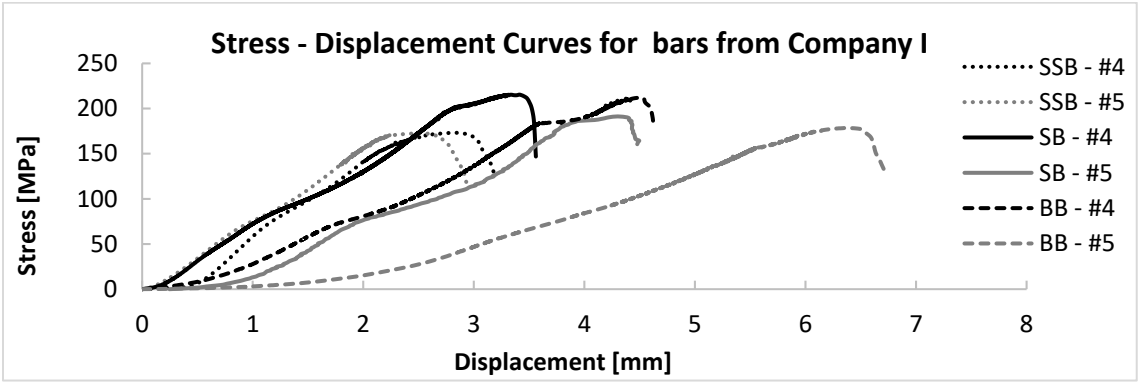

b)

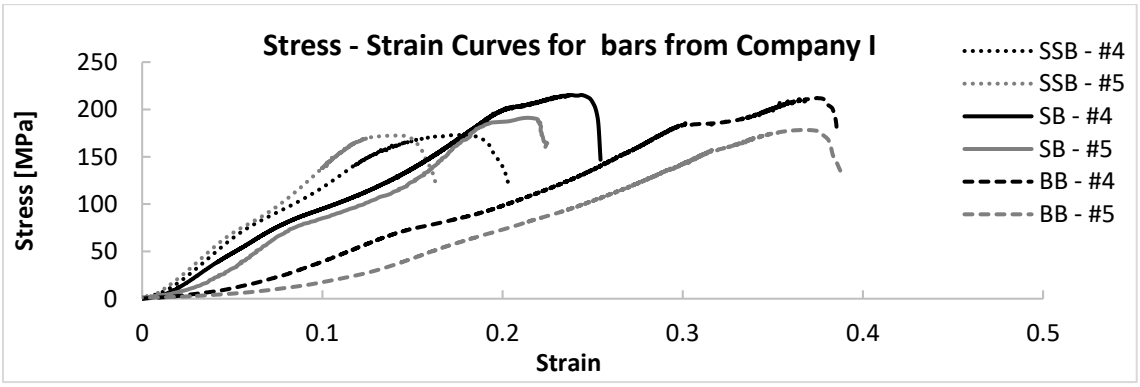

Fig. A7.2 – a) Stress-displacement b) stress-strain curves for bars from Company I after 90 days in alkaline solution heated to 60˚C

a)

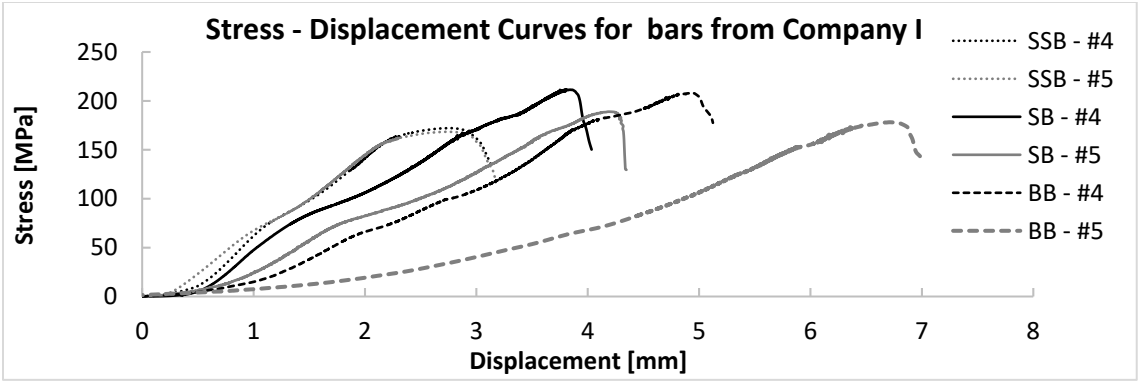

b)

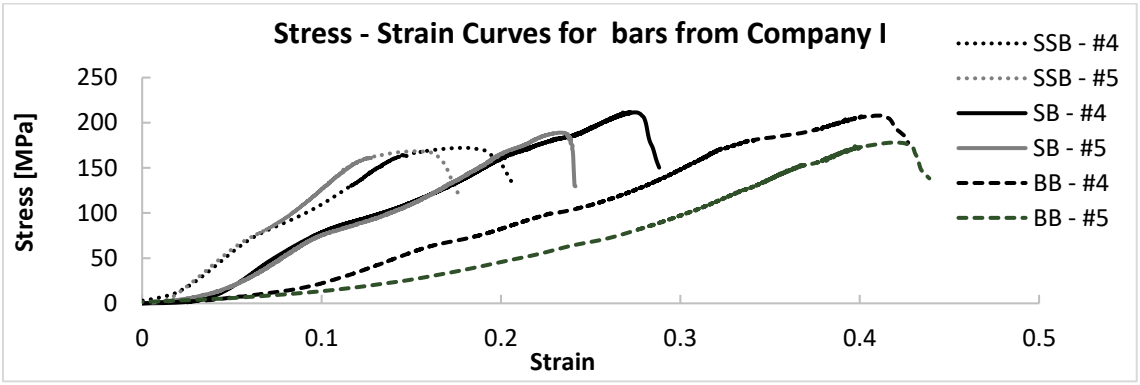

Fig. A7.3 – a) Stress-displacement b) stress-strain curves for bars from Company I after 150 days in alkaline solution heated to 60˚C

A7.2 Company II

Table A7.8 – Shear strength degradation SSB bars Company II in 60˚C solution

Smooth bars (SSB) properties after 0 days in alkaline solution				
Sample	M12		M16	
	Shear Strength [MPa]	Ultimate capacity [kN]	Shear Strength [MPa]	Ultimate capacity [kN]
mean	197	56	194	99
s.d.	5.7	1.7	5.7	3
cov	0.03		0.03	
Smooth bars (SSB) properties after 30 days in alkaline solution				
Sample	M12		M16	
	Shear Strength [MPa]	Ultimate capacity [kN]	Shear Strength [MPa]	Ultimate capacity [kN]
mean	187	49	185	94
s.d.	4	1	2.4	1.2
cov	0.02		0.01	
Smooth bars (SSB) properties after 90 days in alkaline solution				
Sample	M12		M16	
	Shear Strength [MPa]	Ultimate capacity [kN]	Shear Strength [MPa]	Ultimate capacity [kN]
mean	182	48.3	180	92
s.d.	1.4	0.37	5.6	2.9
cov	0.01		0.03	

Smooth bars (SSB) properties after 90 days in alkaline solution				
Sample	M12		M16	
	Shear Strength [MPa]	Ultimate capacity [kN]	Shear Strength [MPa]	Ultimate capacity [kN]
mean	180	48	179	91
s.d.	8	2	3.2	1.6
cov	0.04		0.02	

Table A7.9 – Shear strength degradation SB bars Company II in 50˚C solution

Straight bars (SB) properties after 0 days in alkaline solution				
Sample	M12		M16	
	Shear Strength [MPa]	Ultimate capacity [kN]	Shear Strength [MPa]	Ultimate capacity [kN]
mean	221	50	210	84
s.d.	10.7	2.5	17	6.7
cov	0.05		0.08	
Straight bars (SB) properties after 30 days in alkaline solution				
Sample	M12		M16	
	Shear Strength [MPa]	Ultimate capacity [kN]	Shear Strength [MPa]	Ultimate capacity [kN]
mean	214	48.5	206	83
s.d.	8	1.8	19	7.6
cov	0.04		0.09	
Straight bars (SB) properties after 90 days in alkaline solution				
Sample	M12		M16	
	Shear Strength [MPa]	Ultimate capacity [kN]	Shear Strength [MPa]	Ultimate capacity [kN]
mean	210	47.5	203	81.5
s.d.	14	3.2	11	4.4
cov	0.07		0.05	
Straight bars (SB) properties after 90 days in alkaline solution				
Sample	M12		M16	
	Shear Strength [MPa]	Ultimate capacity [kN]	Shear Strength [MPa]	Ultimate capacity [kN]
mean	208	47	201	81
s.d.	2.2	0.5	14	5.6
cov	0.01		0.07	

Table A7.10 – Shear strength degradation SB bars Company II in 60˚C solution

Straight bars (SB) properties after 0 days in alkaline solution				
Sample	M12		M16	
	Shear Strength [MPa]	Ultimate capacity [kN]	Shear Strength [MPa]	Ultimate capacity [kN]
mean	221	50	210	84
s.d.	10.7	2.5	17	6.7
cov	0.05		0.08	
Straight bars (SB) properties after 30 days in alkaline solution				
Sample	M12		M16	

	Shear Strength [MPa]	Ultimate capacity [kN]	Shear Strength [MPa]	Ultimate capacity [kN]
mean	208	47	201	81
s.d.	1.5	0.3	14	5.6
cov	0.01		0.07	
Straight bars (SB) properties after 90 days in alkaline solution				
Sample	M12		M16	
	Shear Strength [MPa]	Ultimate capacity [kN]	Shear Strength [MPa]	Ultimate capacity [kN]
mean	202	46	196	79
s.d.	8		8	3.2
cov	0.04		0.04	
Straight bars (SB) properties after 90 days in alkaline solution				
Sample	M12		M16	
	Shear Strength [MPa]	Ultimate capacity [kN]	Shear Strength [MPa]	Ultimate capacity [kN]
mean	199	45	193	78
s.d.	6	1.3	12	4.8
cov	0.03		0.06	

Table A7.11 – Shear strength degradation SB bars Company II in 70˚C solution

Straight bars (SB) properties after 0 days in alkaline solution				
Sample	M12		M16	
	Shear Strength [MPa]	Ultimate capacity [kN]	Shear Strength [MPa]	Ultimate capacity [kN]
mean	221	50	210	84
s.d.	10.7	2.5	17	6.7
cov	0.05		0.08	
Straight bars (SB) properties after 30 days in alkaline solution				
Sample	M12		M16	
	Shear Strength [MPa]	Ultimate capacity [kN]	Shear Strength [MPa]	Ultimate capacity [kN]
mean	203	46	197	79
s.d.	20	4.6	2	0.8
cov	0.1		0.01	
Straight bars (SB) properties after 90 days in alkaline solution				
Sample	M12		M16	
	Shear Strength [MPa]	Ultimate capacity [kN]	Shear Strength [MPa]	Ultimate capacity [kN]
mean	188	43	189	76
s.d.	8	2	6.5	2.6
cov	0.04		0.03	
Straight bars (SB) properties after 90 days in alkaline solution				
Sample	M12		M16	
	Shear Strength [MPa]	Ultimate capacity [kN]	Shear Strength [MPa]	Ultimate capacity [kN]
mean	183	41	184	74
s.d.	12	2.7	18	7.4
cov	0.07		0.1	

Table A7.12 – Shear strength degradation BB bars Company II in 50˚C solution

Bent bars (BB) properties after 0 days in alkaline solution				
Sample	M12		M16	
	Shear Strength [MPa]	Ultimate capacity [kN]	Shear Strength [MPa]	Ultimate capacity [kN]
mean	289	65	280	112
s.d.	18	4	22	9
cov	0.06		0.08	
Bent bars (BB) properties after 30 days in alkaline solution				
Sample	M12		M16	
	Shear Strength [MPa]	Ultimate capacity [kN]	Shear Strength [MPa]	Ultimate capacity [kN]
mean	280	63	273	110
s.d.	6	1.35	8.5	3.4
cov	0.02		0.03	
Bent bars (BB) properties after 90 days in alkaline solution				
Sample	M12		M16	
	Shear Strength [MPa]	Ultimate capacity [kN]	Shear Strength [MPa]	Ultimate capacity [kN]
mean	274	62	267	108
s.d.	10	2.3	8.3	3.3
cov	0.04		0.03	
Bent bars (BB) properties after 90 days in alkaline solution				
Sample	M12		M16	
	Shear Strength [MPa]	Ultimate capacity [kN]	Shear Strength [MPa]	Ultimate capacity [kN]
mean	270	61	264	106
s.d.	10	2.3	10	4
cov	0.04		0.04	

Table A7.13 – Shear strength degradation BB bars Company II in 60˚C solution

Bent bars (BB) properties after 0 days in alkaline solution				
Sample	M12		M16	
	Shear Strength [MPa]	Ultimate capacity [kN]	Shear Strength [MPa]	Ultimate capacity [kN]
mean	289	65	280	112
s.d.	18	4	22	9
cov	0.06		0.08	
Bent bars (BB) properties after 30 days in alkaline solution				
Sample	M12		M16	
	Shear Strength [MPa]	Ultimate capacity [kN]	Shear Strength [MPa]	Ultimate capacity [kN]
mean	275	62	270	109
s.d.	7	1.6	19	7.7
cov	0.02		0.07	
Bent bars (BB) properties after 90 days in alkaline solution				
Sample	M12		M16	

	Shear Strength [MPa]	Ultimate capacity [kN]	Shear Strength [MPa]	Ultimate capacity [kN]
mean	268	61	264	106
s.d.	22	5	16	6.4
cov	0.08		0.06	
Bent bars (BB) properties after 90 days in alkaline solution				
Sample	M12		M16	
	Shear Strength [MPa]	Ultimate capacity [kN]	Shear Strength [MPa]	Ultimate capacity [kN]
mean	262	60	259	104
s.d.	17	4	5	2
cov	0.07		0.02	

Table A7.14 – Shear strength degradation BB bars Company II in 70˚C solution

Bent bars (BB) properties after 0 days in alkaline solution				
Sample	M12		M16	
	Shear Strength [MPa]	Ultimate capacity [kN]	Shear Strength [MPa]	Ultimate capacity [kN]
mean	289	65	280	112
s.d.	18	4	22	9
cov	0.06		0.08	
Bent bars (BB) properties after 30 days in alkaline solution				
Sample	M12		M16	
	Shear Strength [MPa]	Ultimate capacity [kN]	Shear Strength [MPa]	Ultimate capacity [kN]
mean	270	61	267	107
s.d.	8	1.8	30	12
cov	0.03		0.11	
Bent bars (BB) properties after 90 days in alkaline solution				
Sample	M12		M16	
	Shear Strength [MPa]	Ultimate capacity [kN]	Shear Strength [MPa]	Ultimate capacity [kN]
mean	257	58	255	102
s.d.	10	2.2	9	3.6
cov	0.04		0.03	
Bent bars (BB) properties after 90 days in alkaline solution				
Sample	M12		M16	
	Shear Strength [MPa]	Ultimate capacity [kN]	Shear Strength [MPa]	Ultimate capacity [kN]
mean	251	57	247	99
s.d.	33	7.5	24	9.6
cov	0.13		0.1	

a)

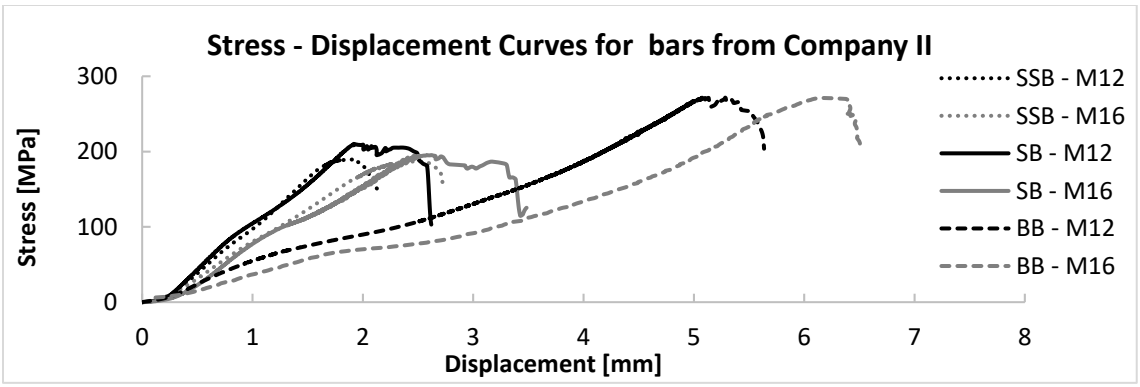

b)

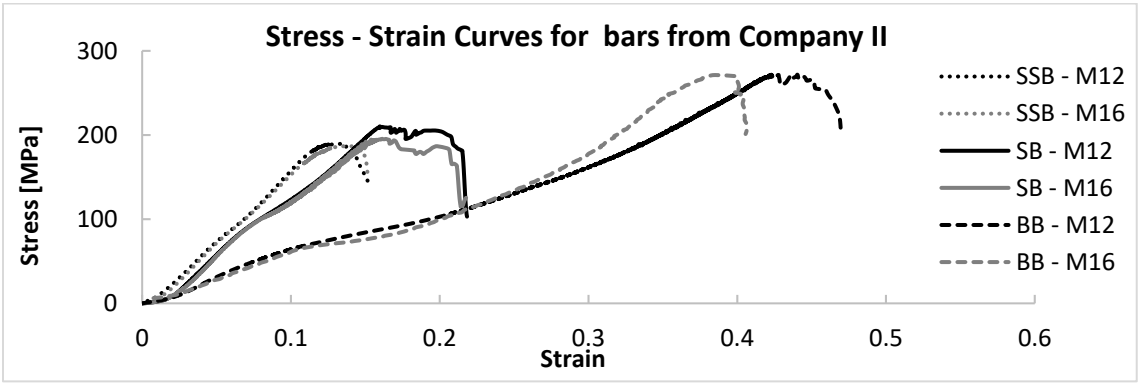

Fig. A7.4 – a) Stress-displacement b) stress-strain curves for bars from Company II after 30 days in alkaline solution heated to 60˚C

a)

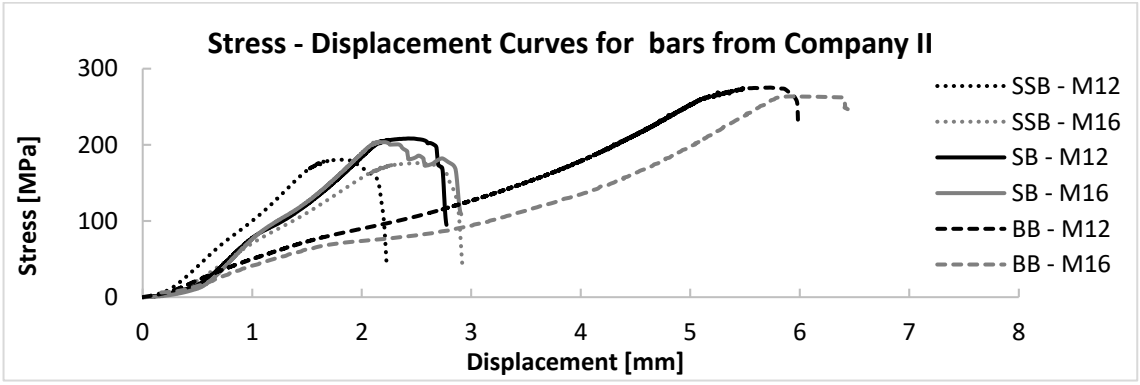

b)

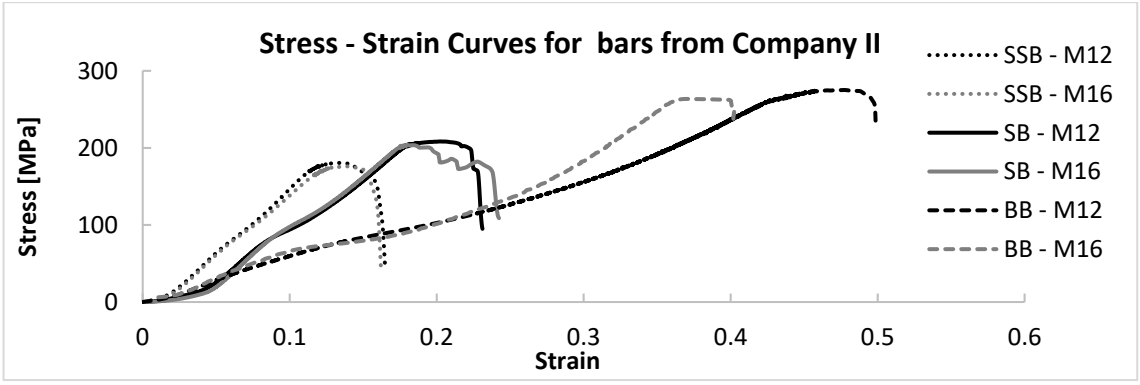

Fig. A7.5 – a) Stress-displacement b) stress-strain curves for bars from Company II after 90 days in alkaline solution heated to 60˚C

a)

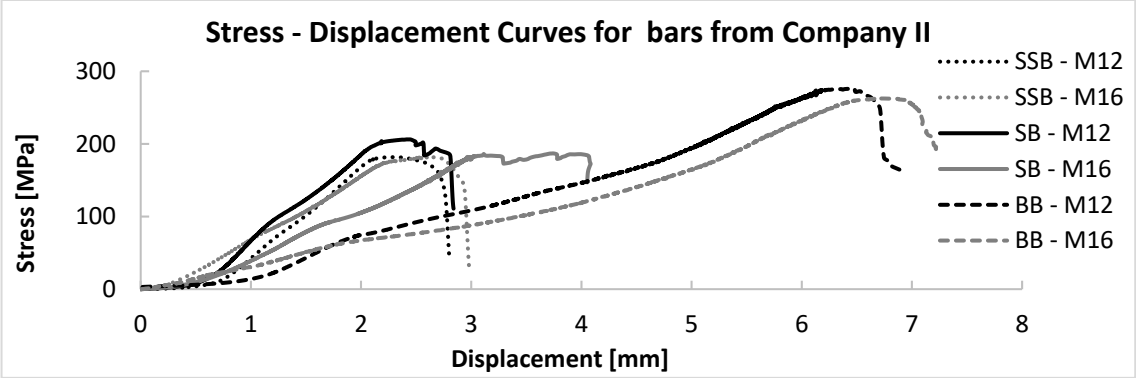

b)

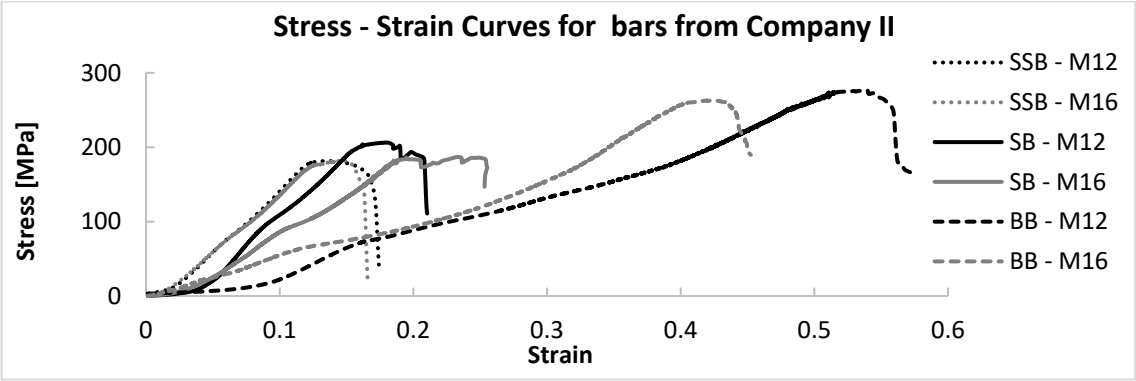

Fig. A7.6 – a) Stress-displacement b) stress-strain curves for bars from Company II after 150 days in alkaline solution heated to 60˚C

Appendix 8

ALKALINE IMMERSION TEST
FLEXURAL STRENGTH DEGRADATION

The Appendix contain all results from flexure alkaline immersion test. Due to high similarity, graphs just from one temperature 60˚C are presented herein.

A8.1 Company I

Table A8.1 – Flexural strength degradation SSB bars Company I in 60˚C solution

Smooth surface bar (SSB) properties after 0 days in alkaline solution					
Sample	#4		Sample	#5	
	Strength [MPa]	Modulus of elasticity [GPa]		Strength [MPa]	Modulus of elasticity [GPa]
mean	1687	56.8	mean	1544	54.3
s.d	46	1.5	s.d	56	1
cov	0.02	0.03	cov	0.03	0.02
Smooth surface bar (SSB) properties after 30 days in alkaline solution					
Sample	#4		Sample	#5	
	Strength [MPa]	Modulus of elasticity [GPa]		Strength [MPa]	Modulus of elasticity [GPa]
mean	1527	54	mean	1410	52
s.d	54	1.2	s.d	85	2.4
cov	0.03	0.02	cov	0.06	0.04
Smooth surface bar (SSB) properties after 90 days in alkaline solution					
Sample	#4		Sample	#5	
	Strength [MPa]	Modulus of elasticity [GPa]		Strength [MPa]	Modulus of elasticity [GPa]
mean	1463	53	mean	1356	47
s.d	70	1.5	s.d	40	0.5
cov	0.04	0.03	cov	0.03	0.12
Smooth surface bar (SSB) properties after 150 days in alkaline solution					
Sample	#4		Sample	#5	
	Strength [MPa]	Modulus of elasticity [GPa]		Strength [MPa]	Modulus of elasticity [GPa]
mean	1427	51	mean	1328	45
s.d	30	3	s.d	7.2	1.1
cov	0.02	0.06	cov	0.005	0.02

a)

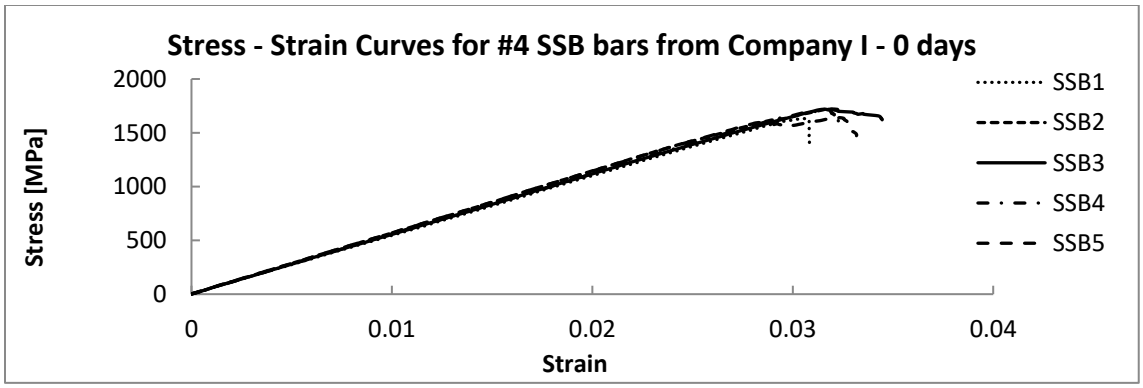

b)

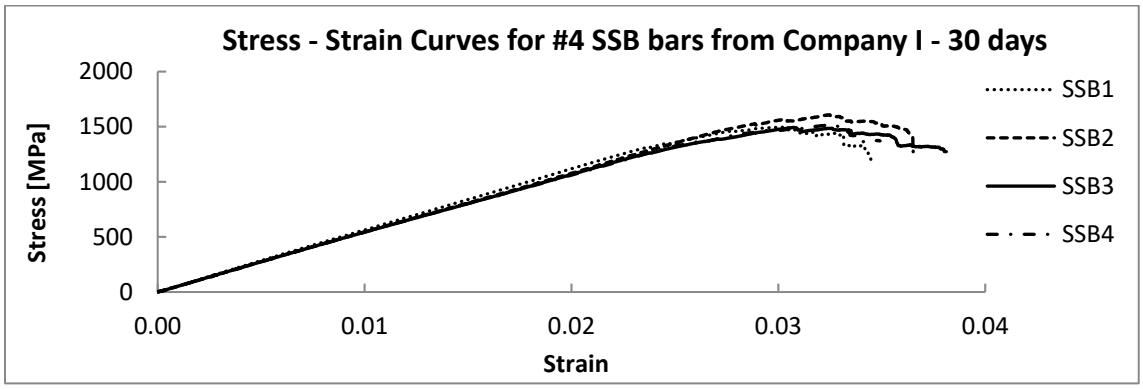

c)

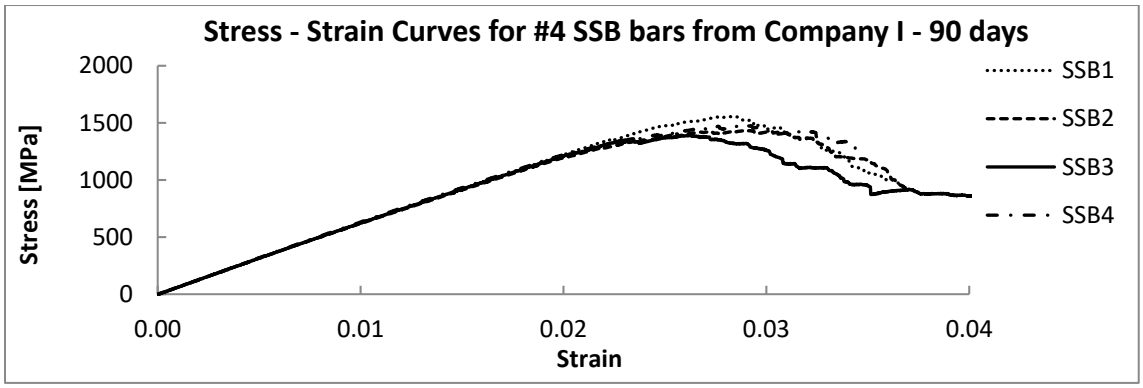

d)

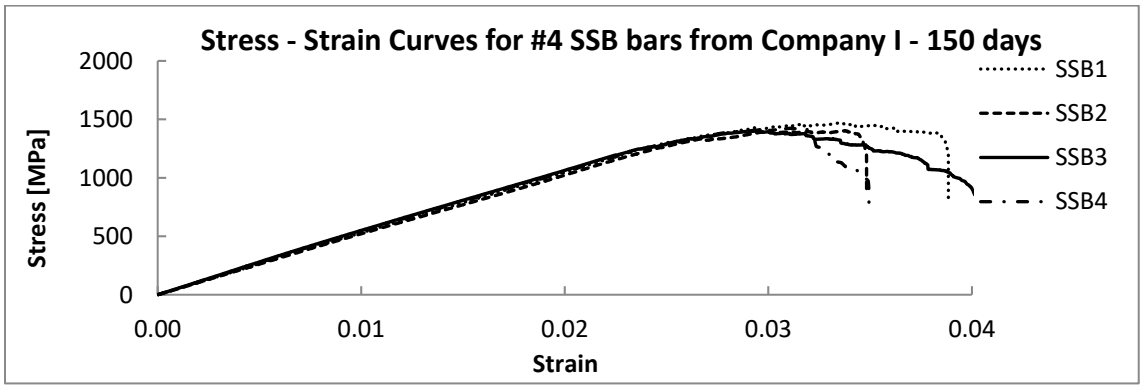

Fig. A8.1 – Stress-strain curves for #4 SSB bars from Company I after a) 0, b) 30 c) 90, d) 150 days in alkaline solution heated to 60˚C

a)

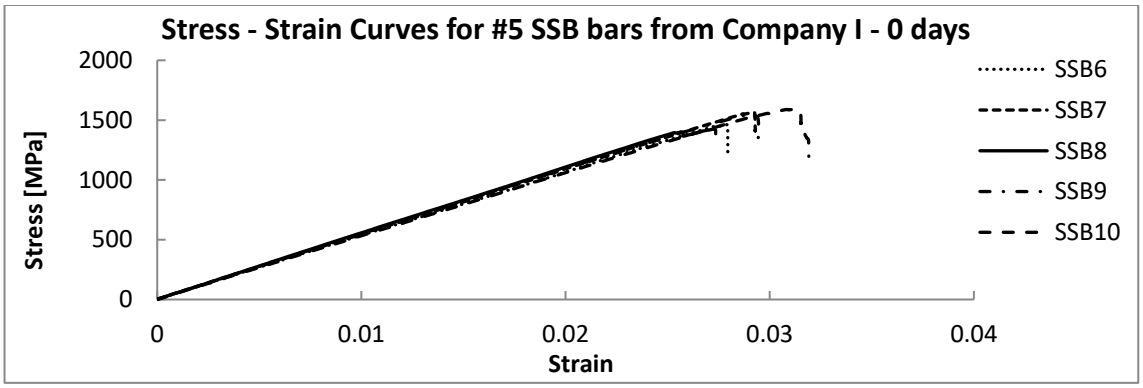

b)

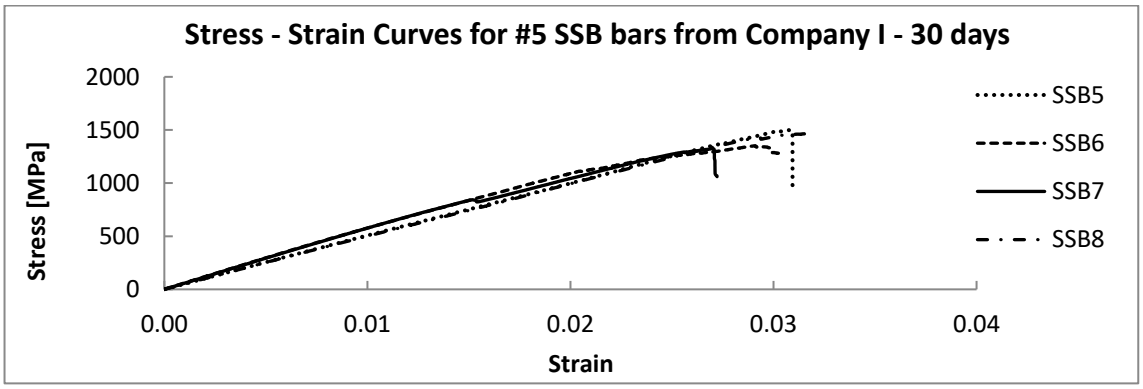

c)

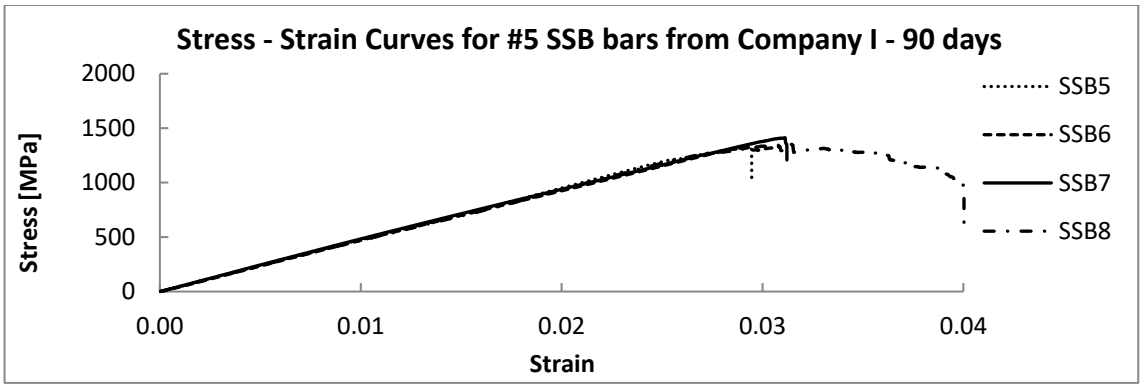

d)

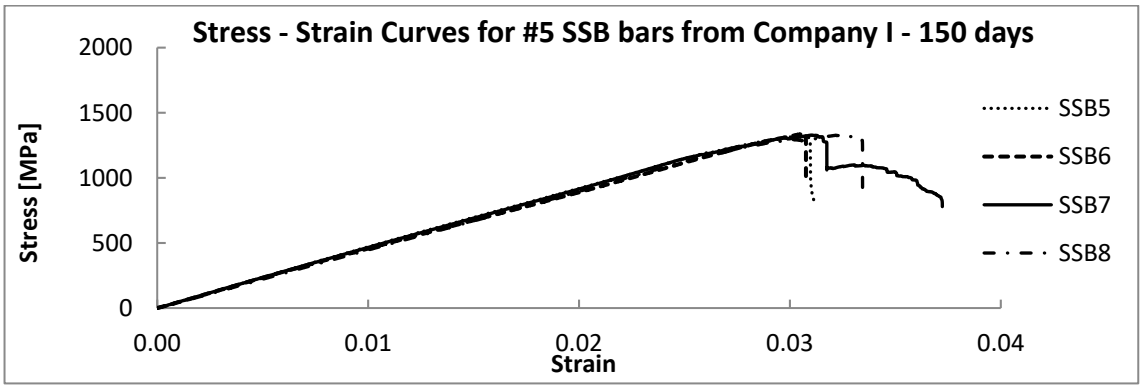

Fig. A8.2 – Stress-strain curves for #5 SSB bars from Company I after a) 0, b) 30 c) 90, d) 150 days in alkaline solution heated to 60˚C

Table A8.2 – Flexural strength degradation SB bars Company I in 50˚C solution

Straight bars (SB) properties after 0 days in alkaline solution					
Sample	#4		Sample	#5	
	Strength [MPa]	Modulus of elasticity [GPa]		Strength [MPa]	Modulus of elasticity [GPa]
mean	1646	51	mean	1510	47
s.d	42	0.7	s.d	46	2.2
cov	0.03	0.01	cov	0.03	0.04
Straight bars (SB) properties after 30 days in alkaline solution					
Sample	#4		Sample	#5	
	Strength [MPa]	Modulus of elasticity [GPa]		Strength [MPa]	Modulus of elasticity [GPa]
mean	1564	51	mean	1457	45
s.d	29	1.23	s.d	53	0.6
cov	0.02	0.02	cov	0.03	0.01
Straight bars (SB) properties after 90 days in alkaline solution					
Sample	#4		Sample	#5	
	Strength [MPa]	Modulus of elasticity [GPa]		Strength [MPa]	Modulus of elasticity [GPa]
mean	1482	51	mean	1410	43
s.d	34	0.3	s.d	37	1
cov	0.02	0.006	cov	0.03	0.02
Straight bars (SB) properties after 150 days in alkaline solution					
Sample	#4		Sample	#5	
	Strength [MPa]	Modulus of elasticity [GPa]		Strength [MPa]	Modulus of elasticity [GPa]
mean	1454	50	mean	1349	43
s.d	27	2	s.d	40	0.8
cov	0.02	0.03	cov	0.03	0.02

Table A8.3 – Flexural strength degradation SB bars Company I in 60˚C solution

Straight bars (SB) properties after 0 days in alkaline solution					
Sample	#4		Sample	#5	
	Strength [MPa]	Modulus of elasticity [GPa]		Strength [MPa]	Modulus of elasticity [GPa]
mean	1646	51	mean	1510	47
s.d	42	0.7	s.d	46	2.2
cov	0.03	0.01	cov	0.03	0.04
Straight bars (SB) properties after 30 days in alkaline solution					
Sample	#4		Sample	#5	
	Strength [MPa]	Modulus of elasticity [GPa]		Strength [MPa]	Modulus of elasticity [GPa]
mean	1478	54	mean	1396	44
s.d	34	3	s.d	52	2
cov	0.02	0.06	cov	0.03	0.05
Straight bars (SB) properties after 90 days in alkaline solution					
Sample	#4		Sample	#5	
	Strength [MPa]	Modulus of elasticity [GPa]		Strength [MPa]	Modulus of elasticity [GPa]

mean	1409	54	mean	1302	41
s.d	30	2	s.d	42	1.2
cov	0.02	0.04	cov	0.03	0.03
Straight bars (SB) properties after 150 days in alkaline solution					
Sample	#4		Sample	#5	
	Strength [MPa]	Modulus of elasticity [GPa]		Strength [MPa]	Modulus of elasticity [GPa]
mean	1352	41	mean	1257	40
s.d	31	1	s.d	49	0.3
cov	0.02	0.02	cov	0.04	0.01

a)

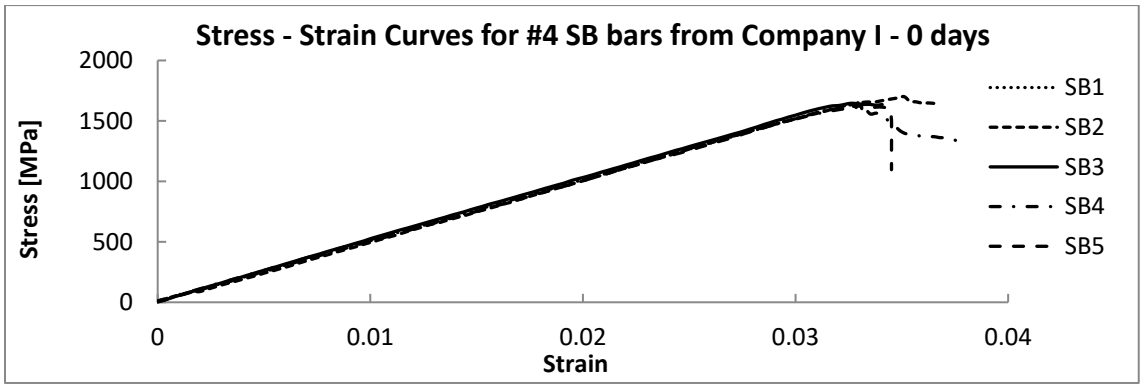

b)

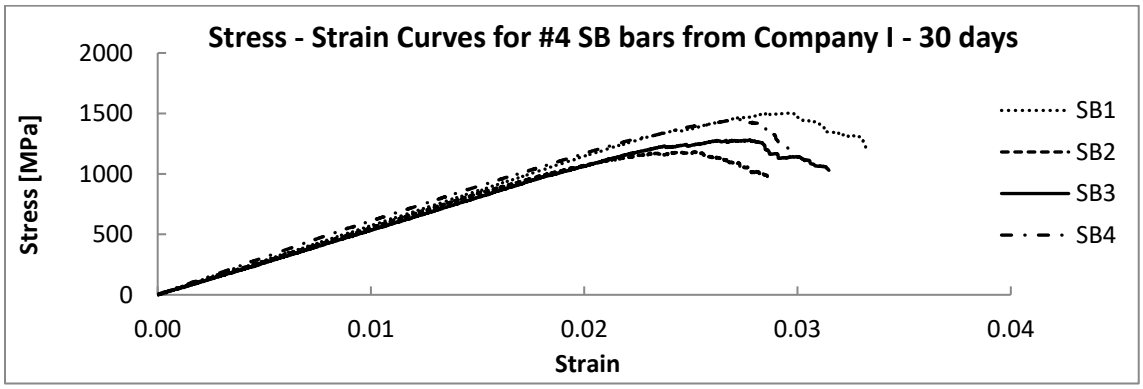

c)

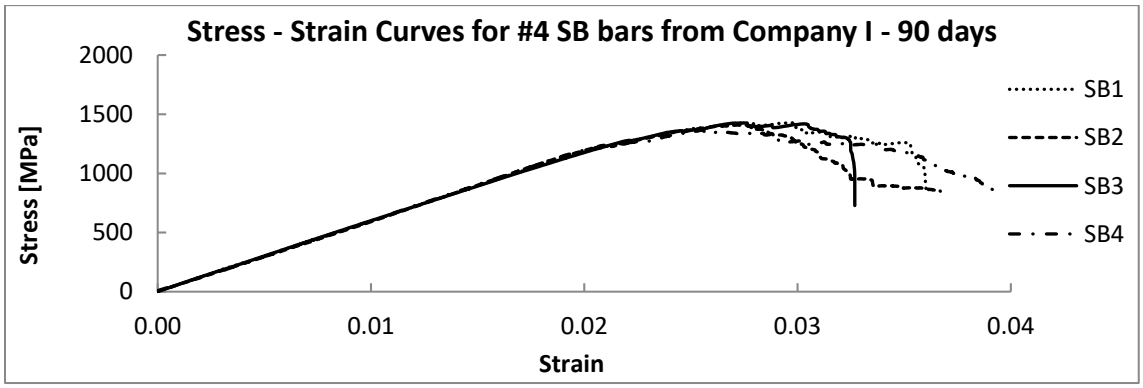

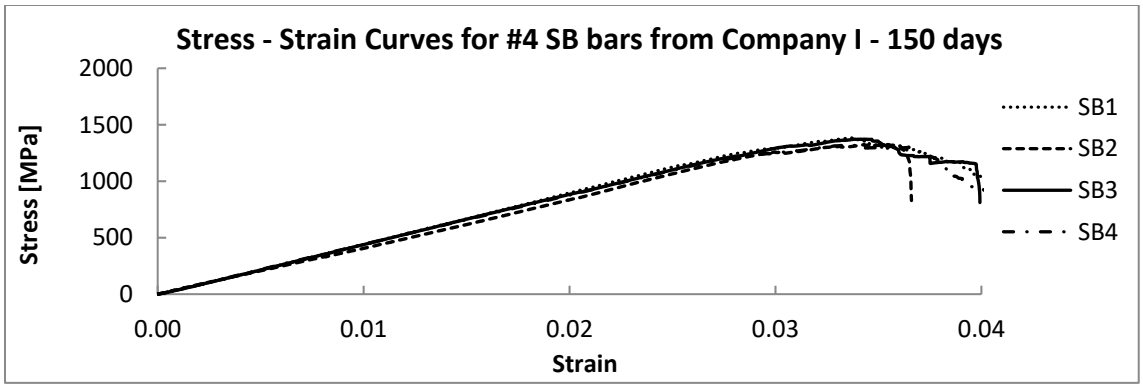

d)

Fig. A8.3 – Stress-strain curves for #4 SB bars from Company I after a) 0, b) 30 c) 90, d)150 days in alkaline solution heated to 60˚C

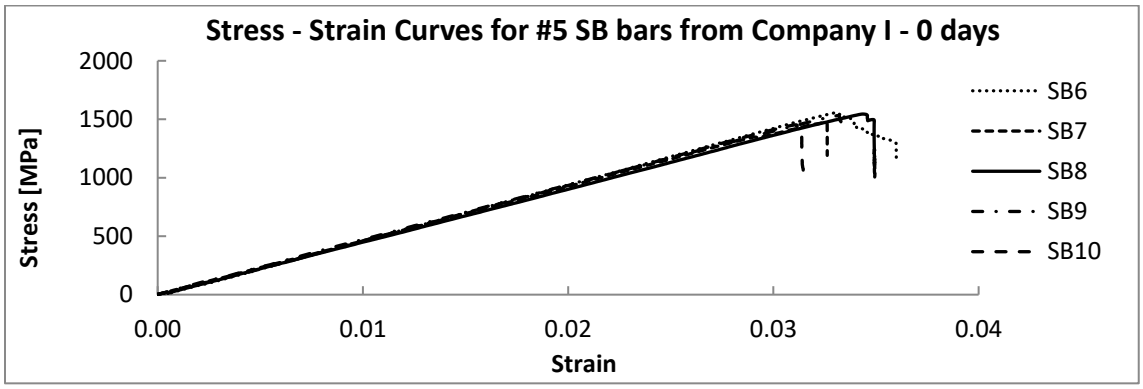

a)

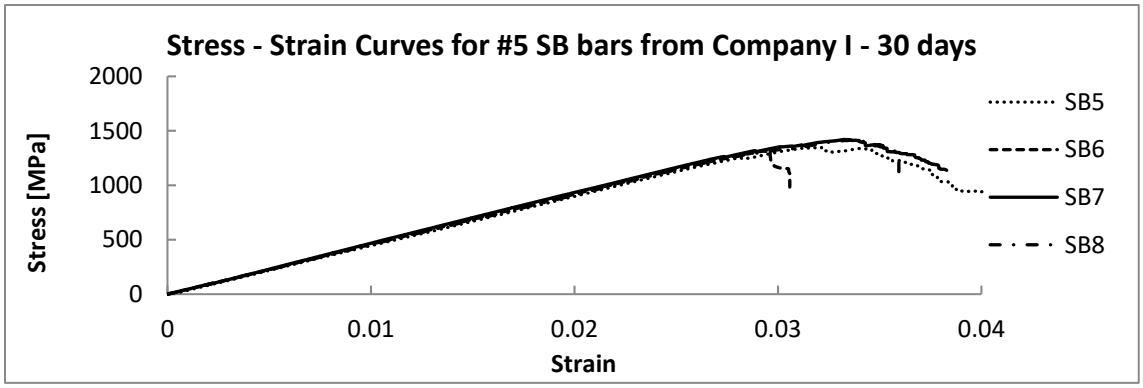

b)

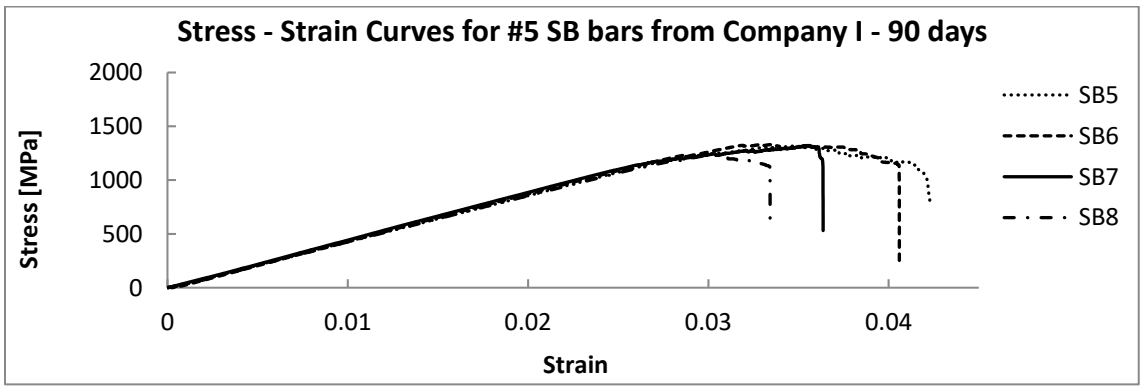

c)

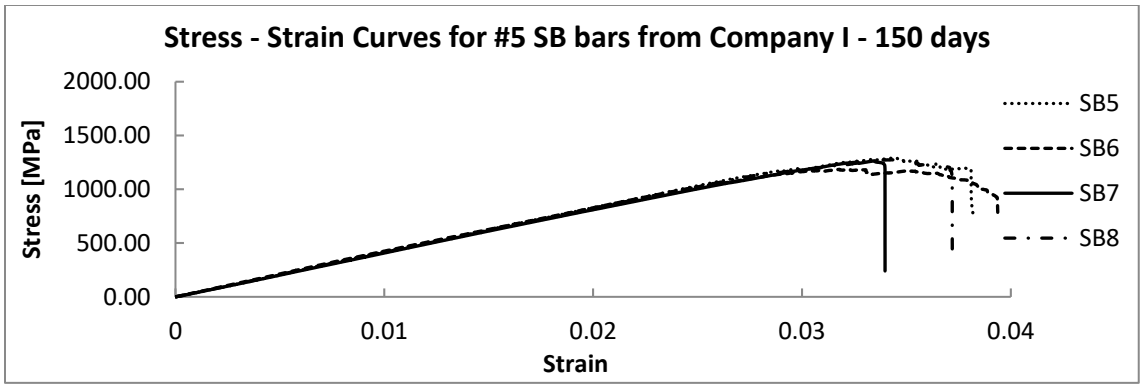

d)

Fig. A8.4 – Stress-strain curves for #5 SB bars from Company I after a) 0, b) 30 c) 90, d)150 days in alkaline solution heated to 60˚C

Table A8.4 – Flexural strength degradation SB bars Company I in 70˚C solution

Straight bars (SB) properties after 0 days in alkaline solution					
Sample	#4		Sample	#5	
	Strength [MPa]	Modulus of elasticity [GPa]		Strength [MPa]	Modulus of elasticity [GPa]
mean	1646	51	mean	1510	47
s.d	42	0.7	s.d	46	2.2
cov	0.03	0.01	cov	0.03	0.04
Straight bars (SB) properties after 30 days in alkaline solution					
Sample	#4		Sample	#5	
	Strength [MPa]	Modulus of elasticity [GPa]		Strength [MPa]	Modulus of elasticity [GPa]
mean	1396	43	mean	1329	41
s.d	16	1.3	s.d	25	1
cov	0.01	0.03	cov	0.02	0.03
Straight bars (SB) properties after 90 days in alkaline solution					
Sample	#4		Sample	#5	
	Strength [MPa]	Modulus of elasticity [GPa]		Strength [MPa]	Modulus of elasticity [GPa]
mean	1295	42	mean	1221	38
s.d	38	0.8	s.d	47	0.6
cov	0.03	0.02	cov	0.03	0.02
Straight bars (SB) properties after 150 days in alkaline solution					
Sample	#4		Sample	#5	
	Strength [MPa]	Modulus of elasticity [GPa]		Strength [MPa]	Modulus of elasticity [GPa]
mean	1222	40	mean	1166	36
s.d	28	0.9	s.d	59	0.5
cov	0.02	0.02	cov	0.05	0.01

Table A8.5 – Flexural strength degradation BB bars Company I in 50˚C solution

Straight portion of the bent bars (BB) properties after 0 days in alkaline solution					
Sample	#4		Sample	#5	
	Strength [MPa]	Modulus of elasticity [GPa]		Strength [MPa]	Modulus of elasticity [GPa]
mean	1557	50	mean	1403	44
s.d	54	0.8	s.d	49	3
cov	0.03	0.02	cov	0.03	0.06
Straight portion of the bent bars (BB) properties after 30 days in alkaline solution					
Sample	#4		Sample	#5	
	Strength [MPa]	Modulus of elasticity [GPa]		Strength [MPa]	Modulus of elasticity [GPa]
mean	1454	43	mean	1316	38
s.d	53	1	s.d	61	2
cov	0.03	0.02	cov	0.05	0.05
Straight portion of the bent bars (BB) properties after 90 days in alkaline solution					
Sample	#4		Sample	#5	
	Strength [MPa]	Modulus of elasticity [GPa]		Strength [MPa]	Modulus of elasticity [GPa]
mean	1398	42	mean	1264	40
s.d	18	0.9	s.d	140	1
cov	0.01	0.02	cov	0.11	0.03
Straight portion of the bent bars (BB) properties after 150 days in alkaline solution					
Sample	#4		Sample	#5	
	Strength [MPa]	Modulus of elasticity [GPa]		Strength [MPa]	Modulus of elasticity [GPa]
mean	1367	44	mean	1245	36
s.d	10	1	s.d	49	2
cov	0.01	0.03	cov	0.04	0.05

Table A8.6 – Flexural strength degradation BB bars Company I in 60˚C solution

Straight portion of the bent bars (BB) properties after 0 days in alkaline solution					
Sample	#4		Sample	#5	
	Strength [MPa]	Modulus of elasticity [GPa]		Strength [MPa]	Modulus of elasticity [GPa]
mean	1557	60	mean	1403	47
s.d	54	2	s.d	49	1
cov	0.03	0.03	cov	0.03	0.02
Straight portion of the bent bars (BB) properties after 30 days in alkaline solution					
Sample	#4		Sample	#5	
	Strength [MPa]	Modulus of elasticity [GPa]		Strength [MPa]	Modulus of elasticity [GPa]
mean	1423	52	mean	1286	44
s.d	125	2	s.d	31	3
cov	0.09	0.04	cov	0.02	0.06
Straight portion of the bent bars (BB) properties after 90 days in alkaline solution					
Sample	#4		Sample	#5	

	Strength [MPa]	Modulus of elasticity [GPa]		Strength [MPa]	Modulus of elasticity [GPa]
mean	1338	50	mean	1225	40
s.d	27	0.8	s.d	64	0.8
cov	0.02	0.01	cov	0.05	0.02
Straight portion of the bent bars (BB) properties after 150 days in alkaline solution					
Sample	#4		Sample	#5	
	Strength [MPa]	Modulus of elasticity [GPa]		Strength [MPa]	Modulus of elasticity [GPa]
mean	1287	38	mean	1194	38
s.d	58	0.6	s.d	21	2
cov	0.04	0.02	cov	0.02	0.06

a)

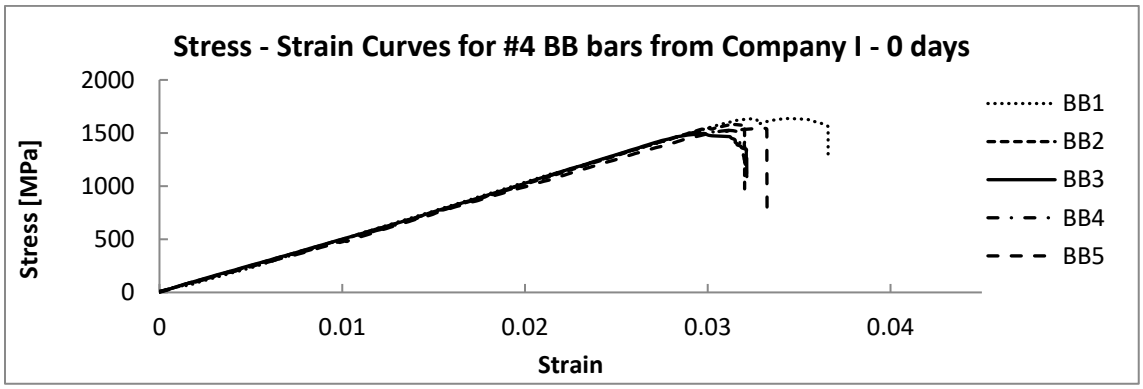

b)

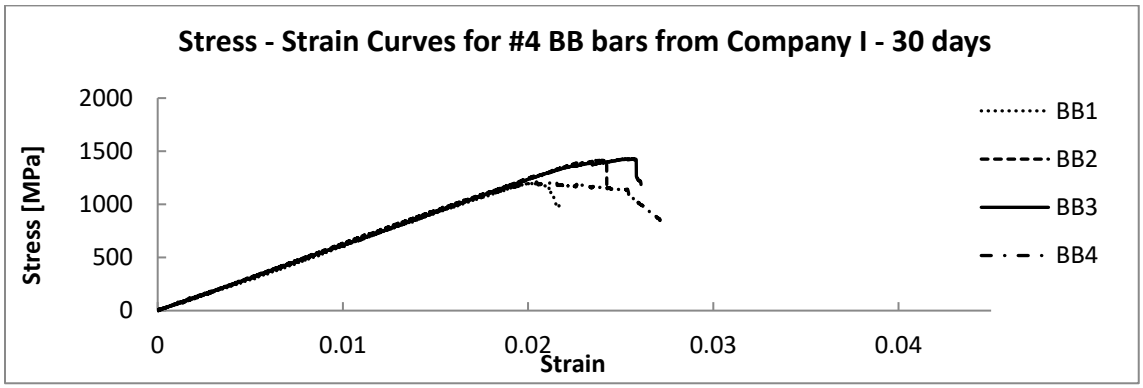

c)

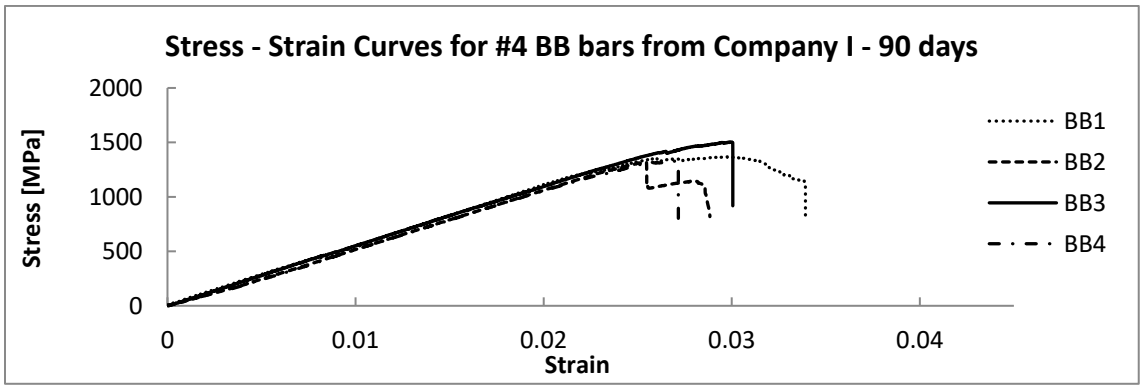

d)

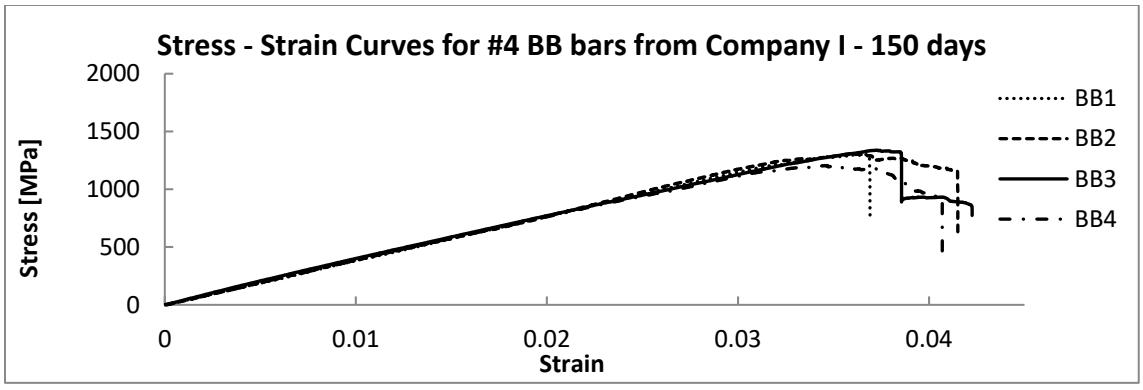

Fig. A8.5 – Stress-strain curves for #4 BB bars from Company I after a) 0, b) 30 c) 90, d)150 days in alkaline solution heated to 60˚C

a)

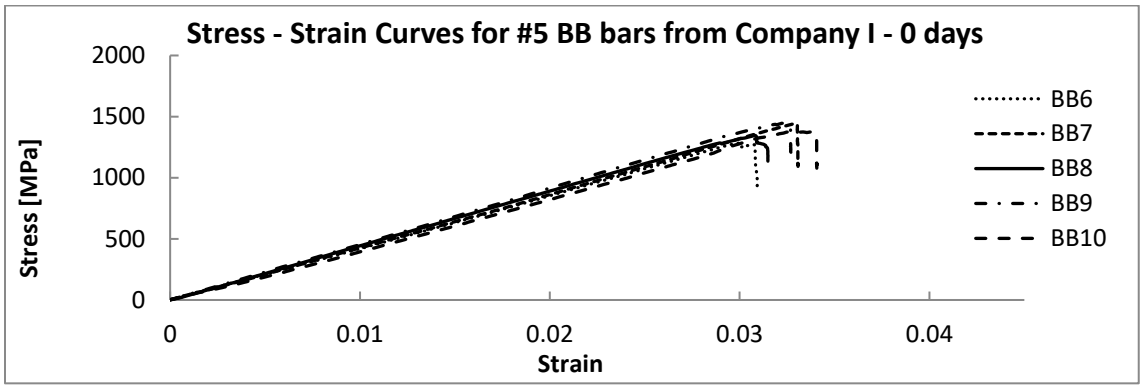

b)

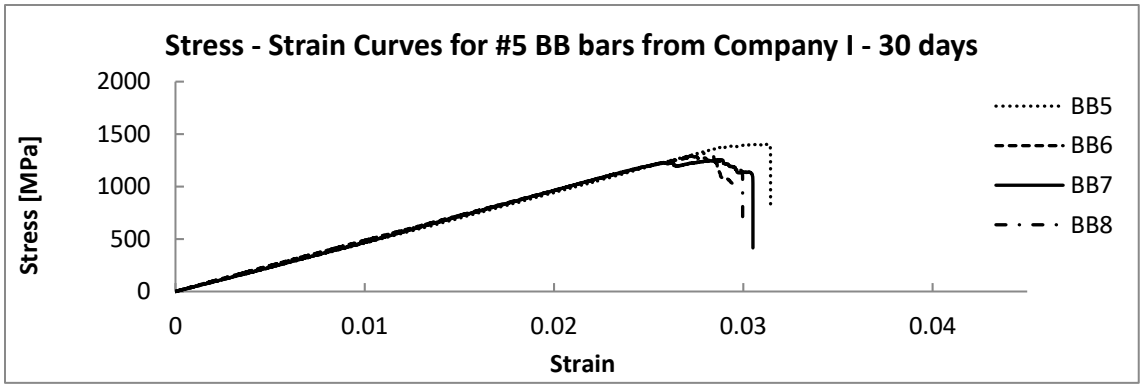

c)

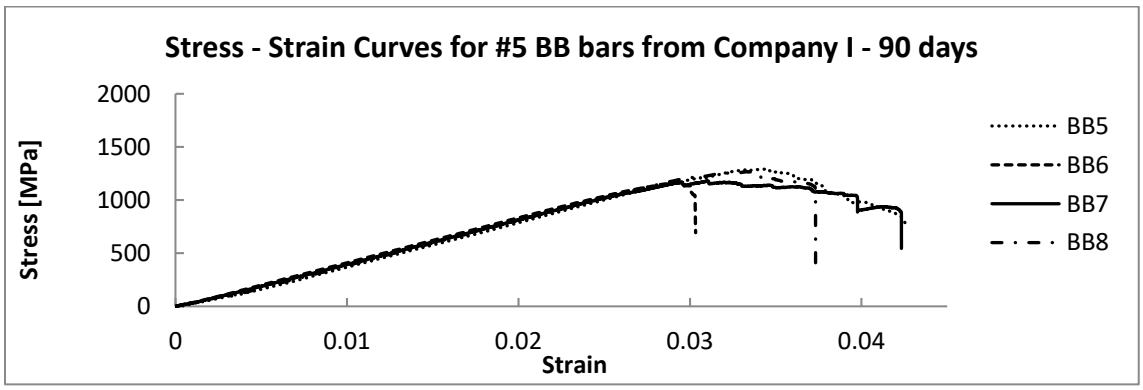

d)

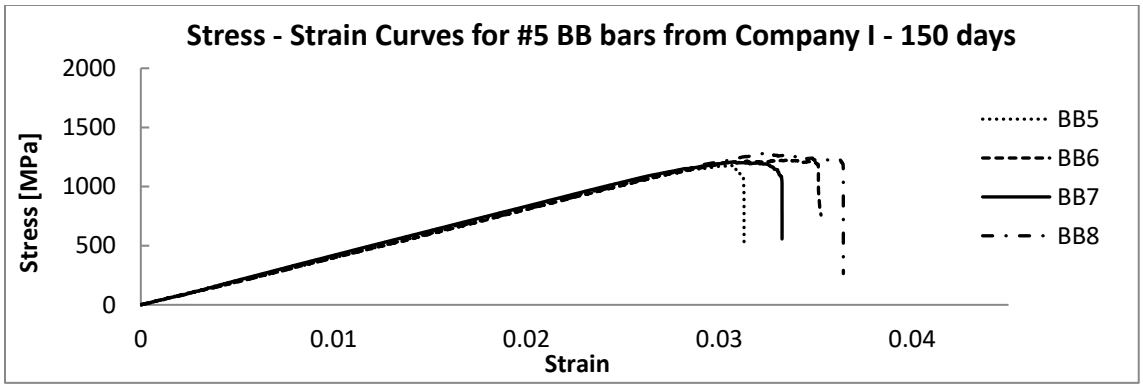

Fig. A8.6 – Stress-strain curves for #5 BB bars from Company I after a) 0, b) 30 c) 90, d)150 days in alkaline solution heated to 60˚C

Table A8.7– Flexural strength degradation BB bars Company I in 70˚C solution

Straight portion of the bent bars (BB) properties after 0 days in alkaline solution					
Sample	#4		Sample	#5	
	Strength [MPa]	Modulus of elasticity [GPa]		Strength [MPa]	Modulus of elasticity [GPa]
mean	1557	60	mean	1403	47
s.d	54	2	s.d	49	1
cov	0.03	0.03	cov	0.03	0.02
Straight portion of the bent bars (BB) properties after 30 days in alkaline solution					
Sample	#4		Sample	#5	
	Strength [MPa]	Modulus of elasticity [GPa]		Strength [MPa]	Modulus of elasticity [GPa]
mean	1356	46	mean	1234	39
s.d	20	3	s.d	22	1
cov	0.01	0.06	cov	0.02	0.02
Straight portion of the bent bars (BB) properties after 90 days in alkaline solution					
Sample	#4		Sample	#5	
	Strength [MPa]	Modulus of elasticity [GPa]		Strength [MPa]	Modulus of elasticity [GPa]
mean	1259	42	mean	1168	36
s.d	11	3	s.d	83	1
cov	0.01	0.07	cov	0.07	0.03
Straight portion of the bent bars (BB) properties after 150 days in alkaline solution					
Sample	#4		Sample	#5	
	Strength [MPa]	Modulus of elasticity [GPa]		Strength [MPa]	Modulus of elasticity [GPa]
mean	1204	40	mean	1125	37
s.d	114	3	s.d	116	0.22
cov	0.11	0.08	cov	0.1	0.01

A8.2 Company II

Table A8.8 – Flexural strength degradation SSB bars Company II in 60˚C solution

Smooth surface bar (SSB) properties after 0 days in alkaline solution					
Sample	M12		Sample	M16	
	Strength [MPa]	Modulus of elasticity [GPa]		Strength [MPa]	Modulus of elasticity [GPa]
mean	1757	66	mean	1763	60
s.d	80	0.9	s.d	46	0.1
cov	0.04	0.01	cov	0.02	0.002
Smooth surface bar (SSB) properties after 30 days in alkaline solution					
Sample	M12		Sample	M16	
	Strength [MPa]	Modulus of elasticity [GPa]		Strength [MPa]	Modulus of elasticity [GPa]
mean	1658	59	mean	1657	57
s.d	59	1.5	s.d	60	1.3
cov	0.03	0.02	cov	0.03	0.02
Smooth surface bar (SSB) properties after 90 days in alkaline solution					
Sample	M12		Sample	M16	
	Strength [MPa]	Modulus of elasticity [GPa]		Strength [MPa]	Modulus of elasticity [GPa]
mean	1604	55	mean	1593	55
s.d	35	2	s.d	85	1.6
cov	0.02	0.04	cov	0.05	0.03
Smooth surface bar (SSB) properties after 150 days in alkaline solution					
Sample	M12		Sample	M16	
	Strength [MPa]	Modulus of elasticity [GPa]		Strength [MPa]	Modulus of elasticity [GPa]
mean	1580	50	mean	1570	54
s.d	42	2	s.d	71	1.4
cov	0.03	0.04	cov	0.04	0.03

a)

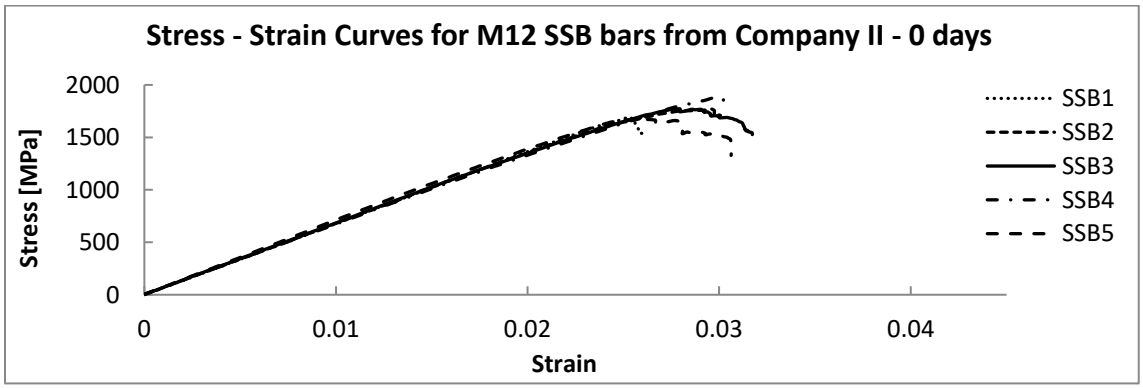

b)

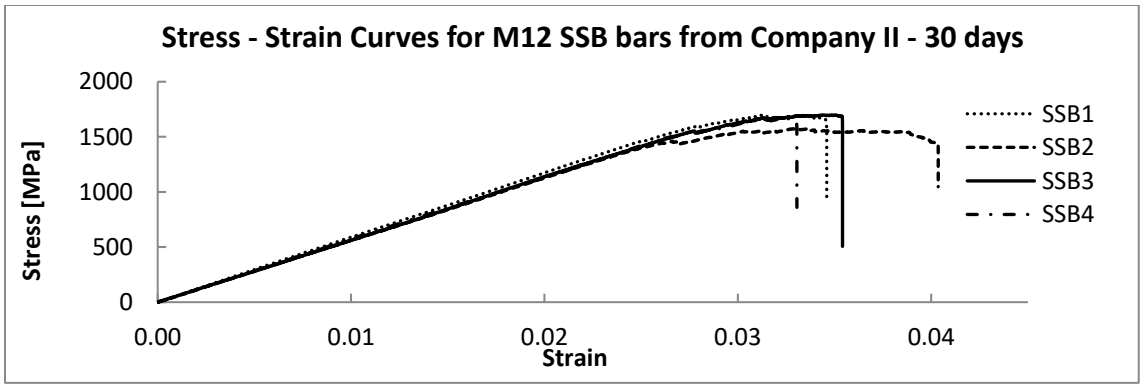

c)

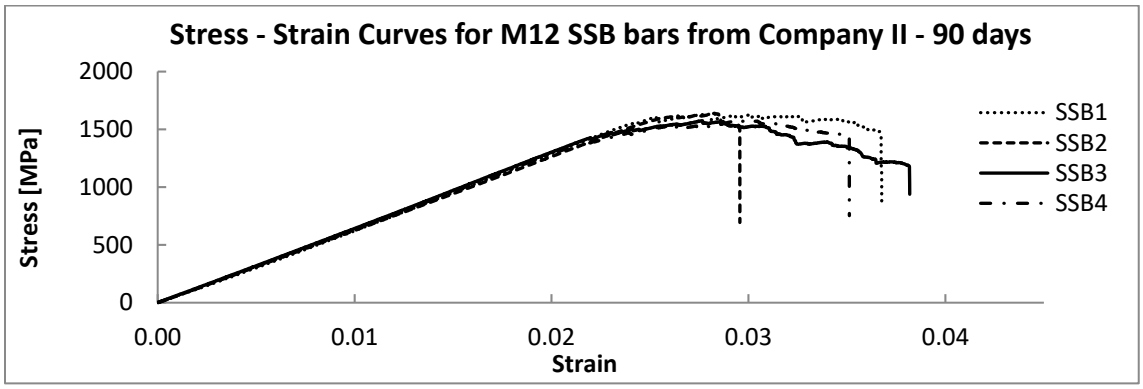

d)

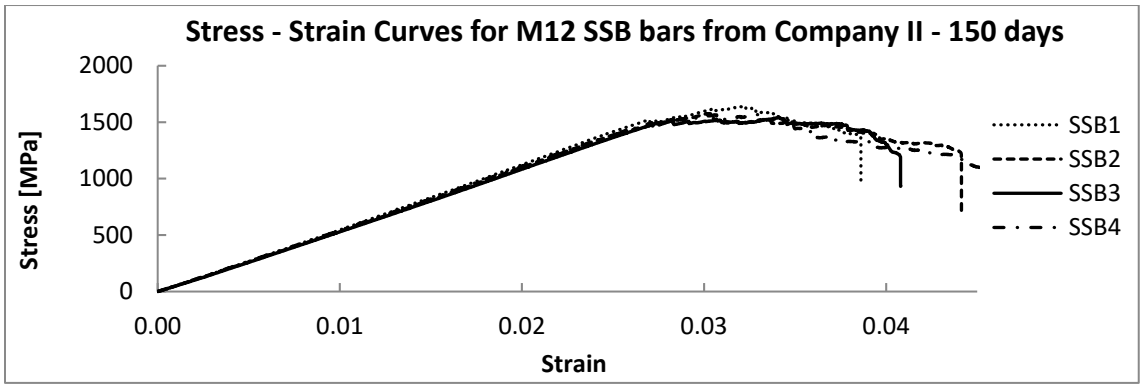

Fig. A8.7 – Stress-strain curves for M12 SSB bars from Company II after a) 0, b) 30 c) 90, d) 150 days in alkaline solution heated to 60˚C

a)

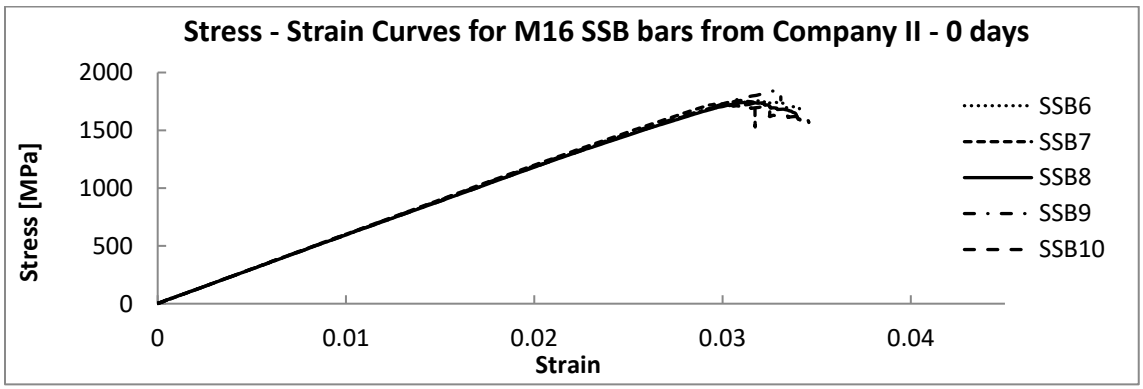

b)

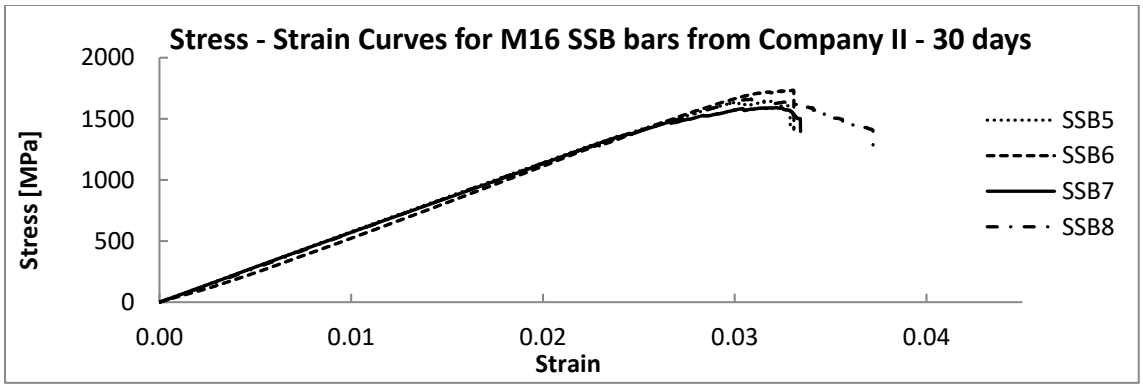

c)

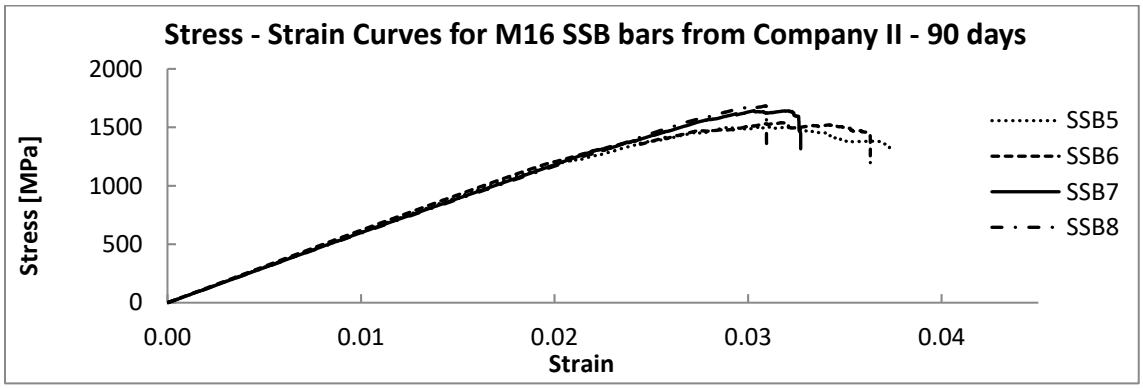

d)

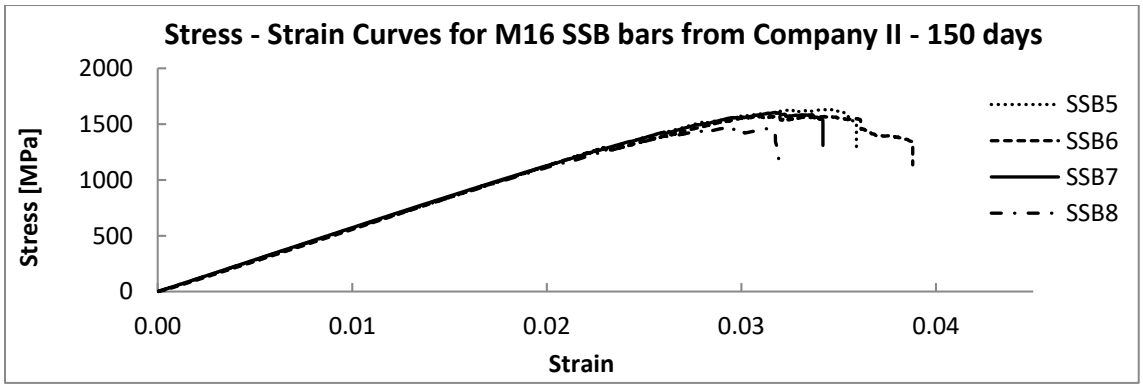

Fig. A8.8 – Stress-strain curves for M16 SSB bars from Company II after a) 0, b) 30 c) 90, d) 150 days in alkaline solution heated to 60˚C

Table A8.9 – Flexural strength degradation SB bars Company II in 50˚C solution

Straight bars (SB) properties after 0 days in alkaline solution					
Sample	M12		Sample	M16	
	Strength [MPa]	Modulus of elasticity [GPa]		Strength [MPa]	Modulus of elasticity [GPa]
mean	1920	67	mean	1835	64
s.d	105	3	s.d	85	2
cov	0.05	0.05	cov	0.04	0.03
Straight bars (SB) properties after 30 days in alkaline solution					
Sample	M12		Sample	M16	
	Strength [MPa]	Modulus of elasticity [GPa]		Strength [MPa]	Modulus of elasticity [GPa]
mean	1843	63	mean	1790	63

s.d	53	0.8	s.d	57	0.4
cov	0.03	0.02	cov	0.03	0.006
Straight bars (SB) properties after 90 days in alkaline solution					
Sample	M12		Sample	M16	
	Strength [MPa]	Modulus of elasticity [GPa]		Strength [MPa]	Modulus of elasticity [GPa]
mean	1810	58	mean	1756	62
s.d	21	1	s.d	73	0.2
cov	0.01	0.01	cov	0.04	0.003
Straight bars (SB) properties after 150 days in alkaline solution					
Sample	M12		Sample	M16	
	Strength [MPa]	Modulus of elasticity [GPa]		Strength [MPa]	Modulus of elasticity [GPa]
mean	1771	56	mean	1725	58
s.d	75	0.2	s.d	18	0.8
cov	0.04	0.005	cov	0.01	0.01

Table A8.10 – Flexural strength degradation SB bars Company II in 60˚C solution

Straight bars (SB) properties after 0 days in alkaline solution					
Sample	M12		Sample	M16	
	Strength [MPa]	Modulus of elasticity [GPa]		Strength [MPa]	Modulus of elasticity [GPa]
mean	1920	67	mean	1835	64
s.d	105	3	s.d	85	2
cov	0.05	0.05	cov	0.04	0.03
Straight bars (SB) properties after 30 days in alkaline solution					
Sample	M12		Sample	M16	
	Strength [MPa]	Modulus of elasticity [GPa]		Strength [MPa]	Modulus of elasticity [GPa]
mean	1796	60	mean	1737	60
s.d	112	0.7	s.d	99	3
cov	0.06	0.01	cov	0.05	0.04
Straight bars (SB) properties after 90 days in alkaline solution					
Sample	M12		Sample	M16	
	Strength [MPa]	Modulus of elasticity [GPa]		Strength [MPa]	Modulus of elasticity [GPa]
mean	1709	58	mean	1672	56
s.d	27	1	s.d	49	2.5
cov	0.01	0.02	cov	0.03	0.04
Straight bars (SB) properties after 150 days in alkaline solution					
Sample	M12		Sample	M16	
	Strength [MPa]	Modulus of elasticity [GPa]		Strength [MPa]	Modulus of elasticity [GPa]
mean	1665	52	mean	1648	52
s.d	50	2	s.d	18	1
cov	0.03	0.03	cov	0.01	0.02

a)

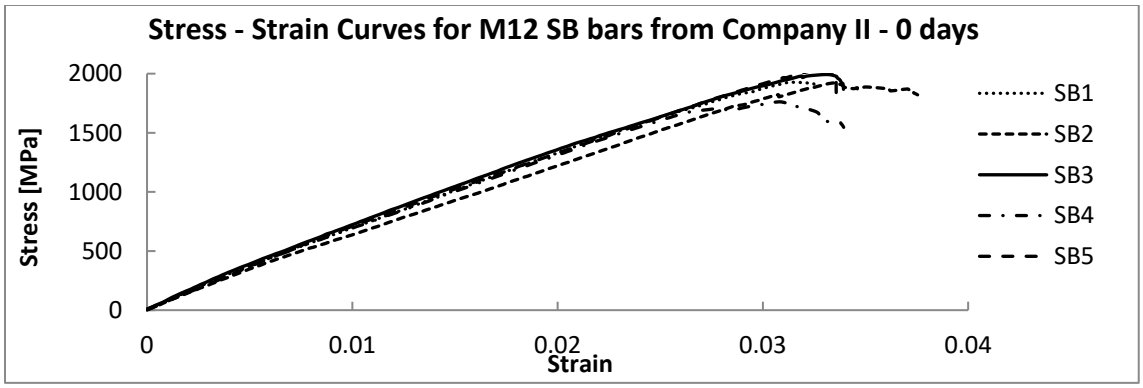

b)

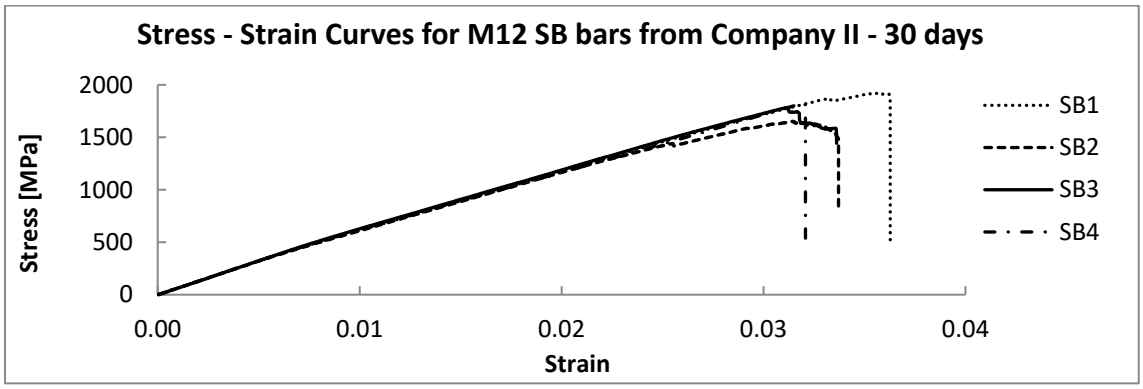

c)

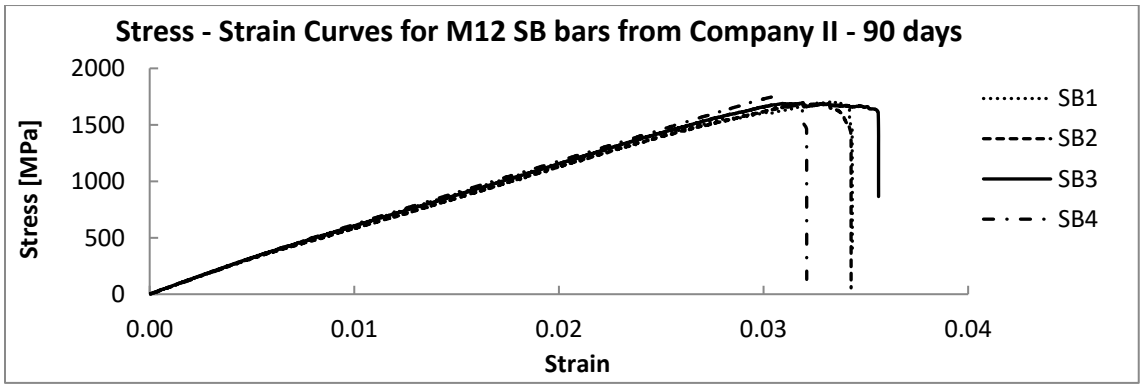

d)

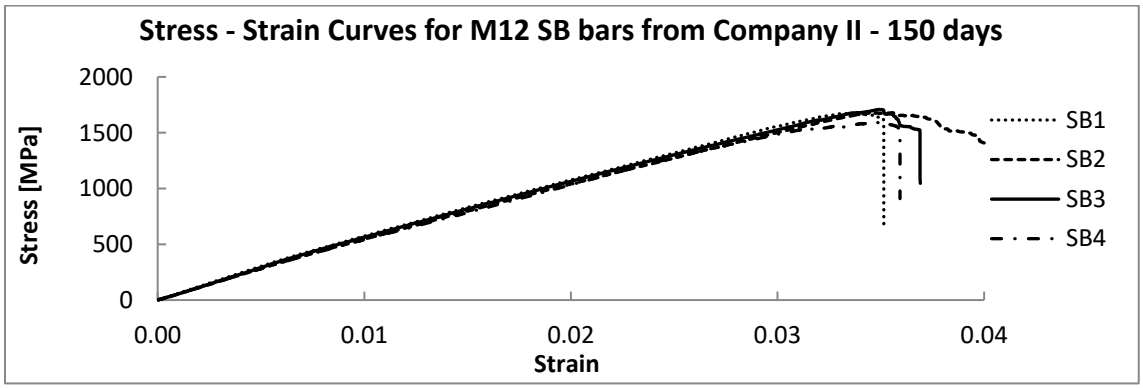

Fig. A8.9 – Stress-strain curves for M12 SB bars from Company II after a) 0, b) 30 c) 90, d) 150 days in alkaline solution heated to 60˚C

a)

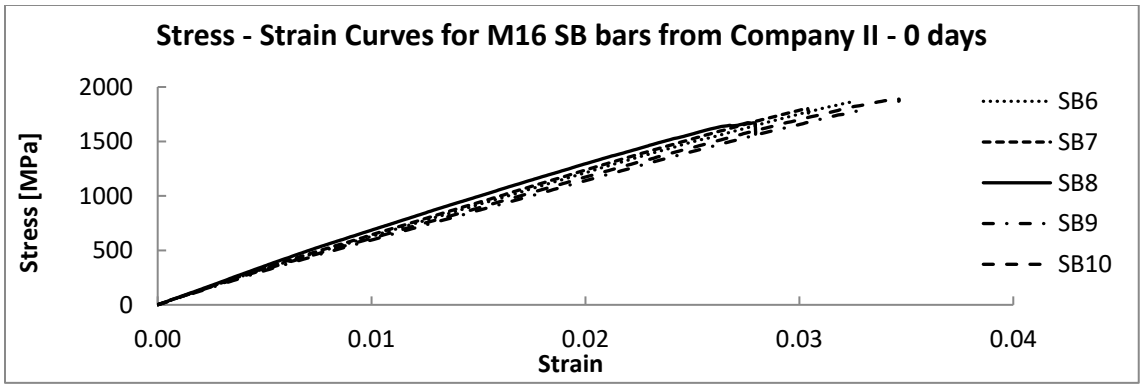

b)

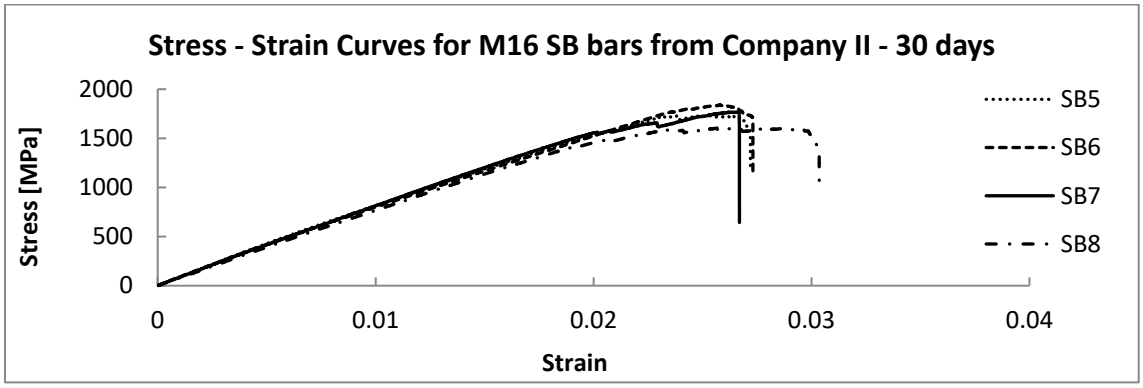

c)

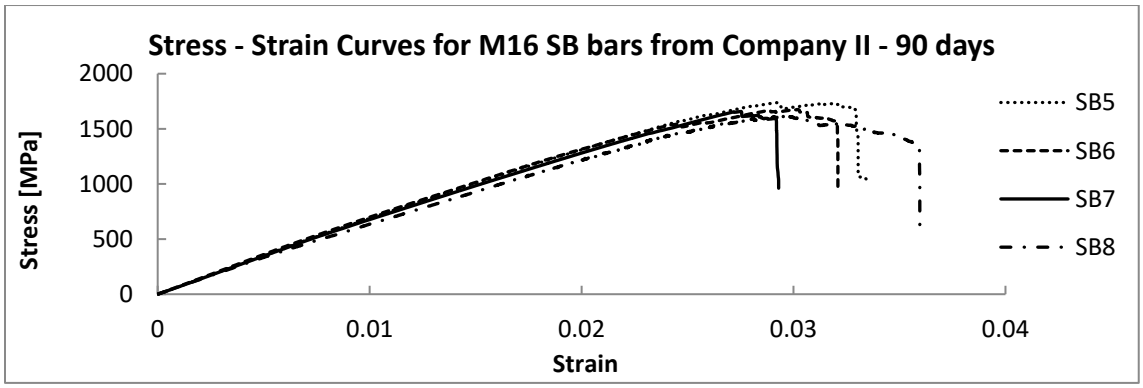

d)

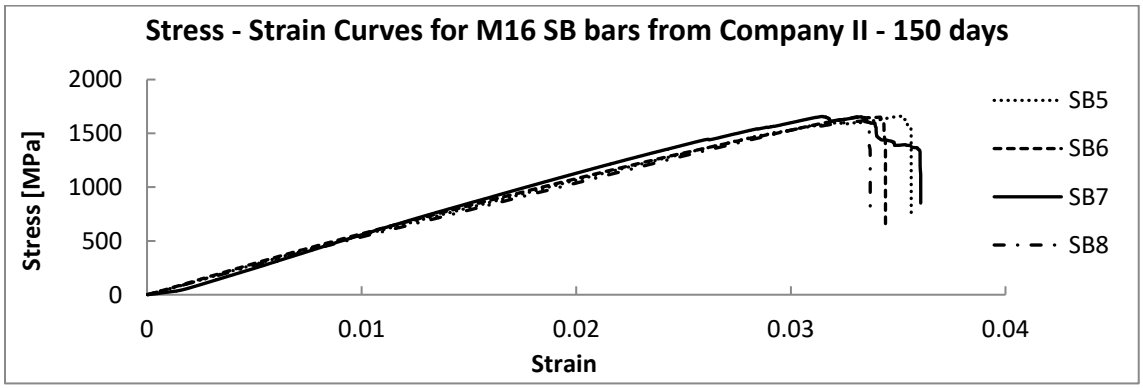

Fig. A8.10 – Stress-strain curves for M16 SB bars from Company II after a) 0, b) 30 c) 90, d) 150 days in alkaline solution heated to 60˚C

Table A8.11 – Flexural strength degradation SB bars Company II in 70˚C solution

Straight bars (SB) properties after 0 days in alkaline solution					
Sample	M12		Sample	M16	
	Strength [MPa]	Modulus of elasticity [GPa]		Strength [MPa]	Modulus of elasticity [GPa]
mean	1920	67	mean	1835	64
s.d	105	3	s.d	85	2
cov	0.05	0.05	cov	0.04	0.03
Straight bars (SB) properties after 30 days in alkaline solution					
Sample	M12		Sample	M16	
	Strength [MPa]	Modulus of elasticity [GPa]		Strength [MPa]	Modulus of elasticity [GPa]
mean	1712	56	mean	1666	58
s.d	107	1	s.d	66	1.5
cov	0.06	0.02	cov	0.04	0.02
Straight bars (SB) properties after 90 days in alkaline solution					
Sample	M12		Sample	M16	
	Strength [MPa]	Modulus of elasticity [GPa]		Strength [MPa]	Modulus of elasticity [GPa]
mean	1599	54	mean	1553	53
s.d	73	1.5	s.d	128	0.7
cov	0.04	0.03	cov	0.08	0.01
Straight bars (SB) properties after 150 days in alkaline solution					
Sample	M12		Sample	M16	
	Strength [MPa]	Modulus of elasticity [GPa]		Strength [MPa]	Modulus of elasticity [GPa]
mean	1511	52	mean	1490	48
s.d	137	4	s.d	207	7
cov	0.09	0.07	cov	0.14	0.13

Table A8.12 – Flexural strength degradation BB bars Company II in 50˚C solution

Straight portion of the bent bars (BB) properties after 0 days in alkaline solution					
Sample	M12		Sample	M16	
	Strength [MPa]	Modulus of elasticity [GPa]		Strength [MPa]	Modulus of elasticity [GPa]
mean	1684	66	mean	1572	65
s.d	82	4	s.d	165	5
cov	0.05	0.07	cov	0.1	0.08
Straight portion of the bent bars (BB) properties after 30 days in alkaline solution					
Sample	M12		Sample	M16	
	Strength [MPa]	Modulus of elasticity [GPa]		Strength [MPa]	Modulus of elasticity [GPa]
mean	1603	62	mean	1466	58
s.d	87	2	s.d	73	0.5
cov	0.05	0.04	cov	0.05	0.01
Straight portion of the bent bars (BB) properties after 90 days in alkaline solution					
Sample	M12		Sample	M16	

	Strength [MPa]	Modulus of elasticity [GPa]		Strength [MPa]	Modulus of elasticity [GPa]
mean	1564	61	mean	1421	54
s.d	202	2	s.d	69	3
cov	0.13	0.04	cov	0.05	0.06
Straight portion of the bent bars (BB) properties after 150 days in alkaline solution					
Sample	M12		Sample	M16	
	Strength [MPa]	Modulus of elasticity [GPa]		Strength [MPa]	Modulus of elasticity [GPa]
mean	1517	58	mean	1389	50
s.d	50	6	s.d	42	0.6
cov	0.03	0.1	cov	0.03	0.01

Table A8.13 – Flexural strength degradation BB bars Company II in 60˚C solution

Straight portion of the bent bars (BB) properties after 0 days in alkaline solution					
Sample	M12		Sample	M16	
	Strength [MPa]	Modulus of elasticity [GPa]		Strength [MPa]	Modulus of elasticity [GPa]
mean	1684	66	mean	1572	65
s.d	82	4	s.d	165	5
cov	0.05	0.07	cov	0.1	0.08
Straight portion of the bent bars (BB) properties after 30 days in alkaline solution					
Sample	M12		Sample	M16	
	Strength [MPa]	Modulus of elasticity [GPa]		Strength [MPa]	Modulus of elasticity [GPa]
mean	1573	56	mean	1485	52
s.d	159	3	s.d	57	2
cov	0.1	0.05	cov	0.04	0.04
Straight portion of the bent bars (BB) properties after 90 days in alkaline solution					
Sample	M12		Sample	M16	
	Strength [MPa]	Modulus of elasticity [GPa]		Strength [MPa]	Modulus of elasticity [GPa]
mean	1499	54	mean	1432	50
s.d	151	2.5	s.d	58	2
cov	0.1	0.04	cov	0.04	0.04
Straight portion of the bent bars (BB) properties after 150 days in alkaline solution					
Sample	M12		Sample	M16	
	Strength [MPa]	Modulus of elasticity [GPa]		Strength [MPa]	Modulus of elasticity [GPa]
mean	1430	52	mean	1395	47
s.d	107	1.5	s.d	45	2
cov	0.07	0.03	cov	0.03	0.04

a)

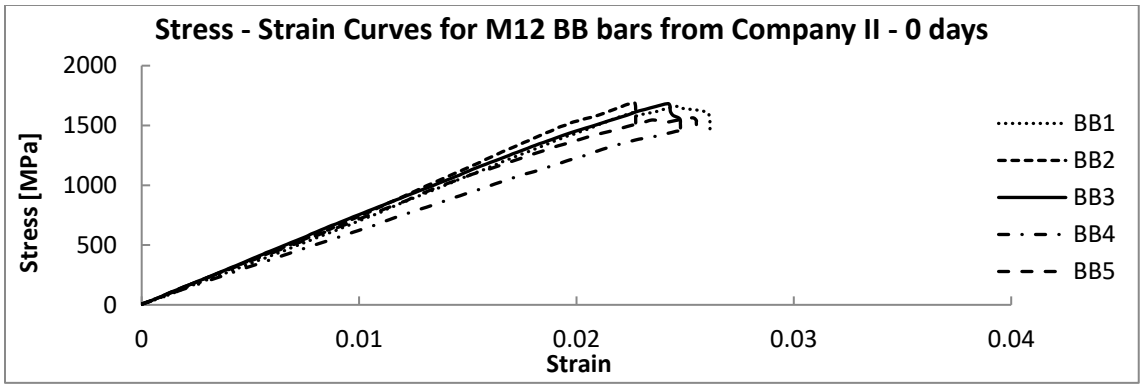

b)

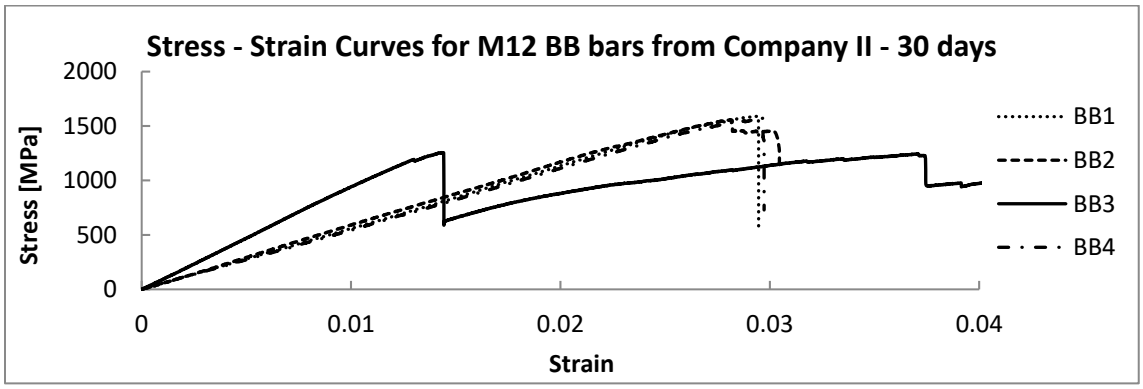

c)

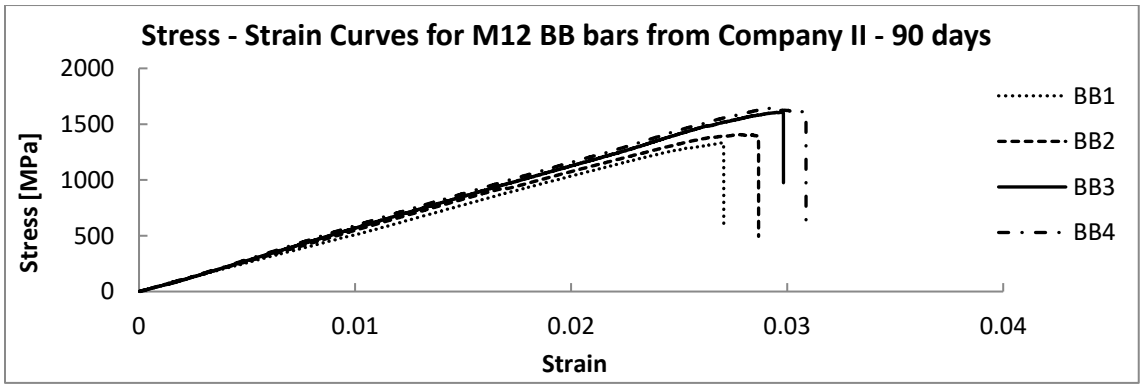

d)

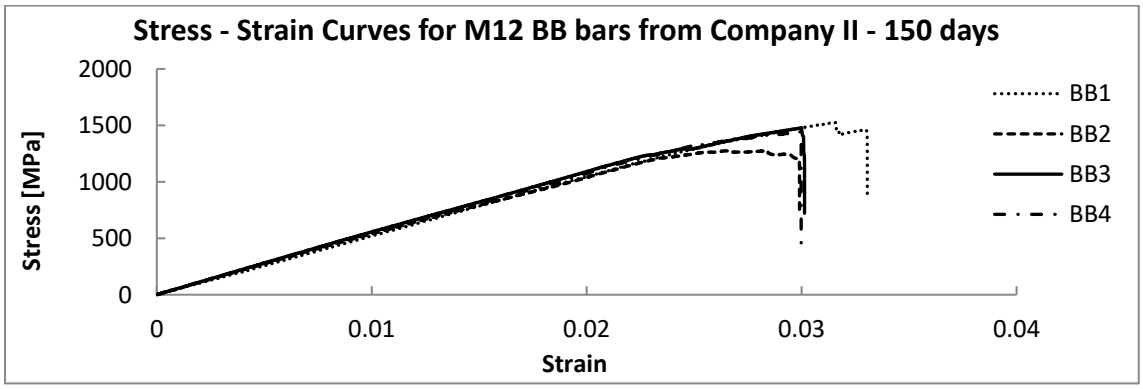

Fig. A8.11 – Stress-strain curves for M12 BB bars from Company II after a) 0, b) 30 c) 90, d) 150 days in alkaline solution heated to 60˚C

a)

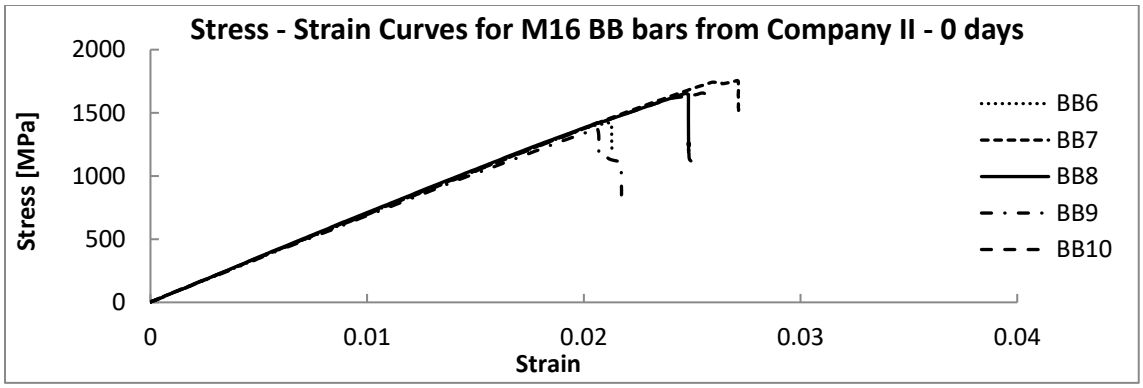

b)

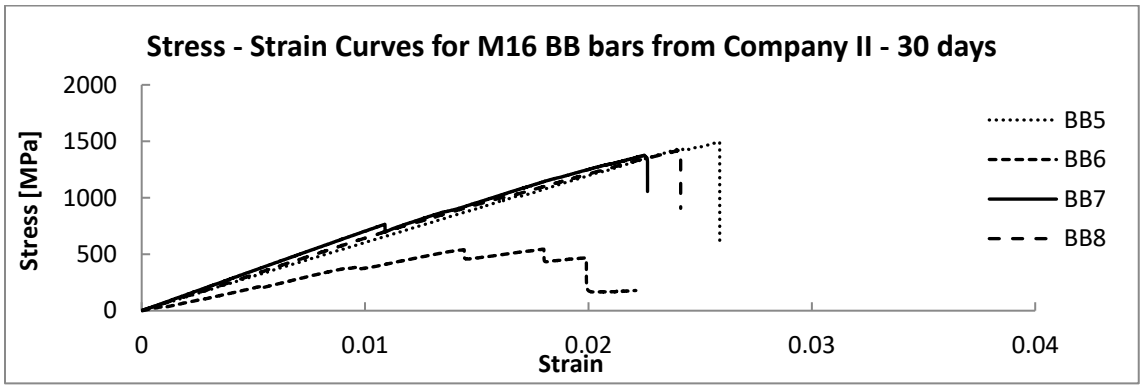

c)

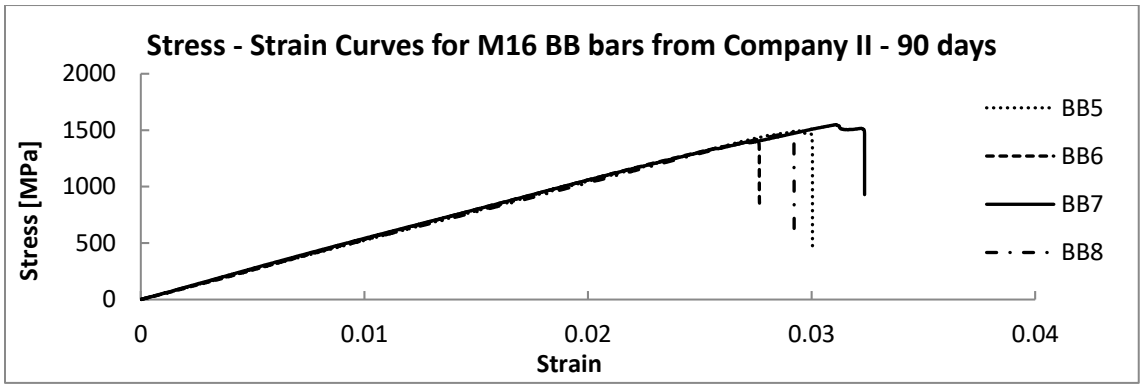

d)

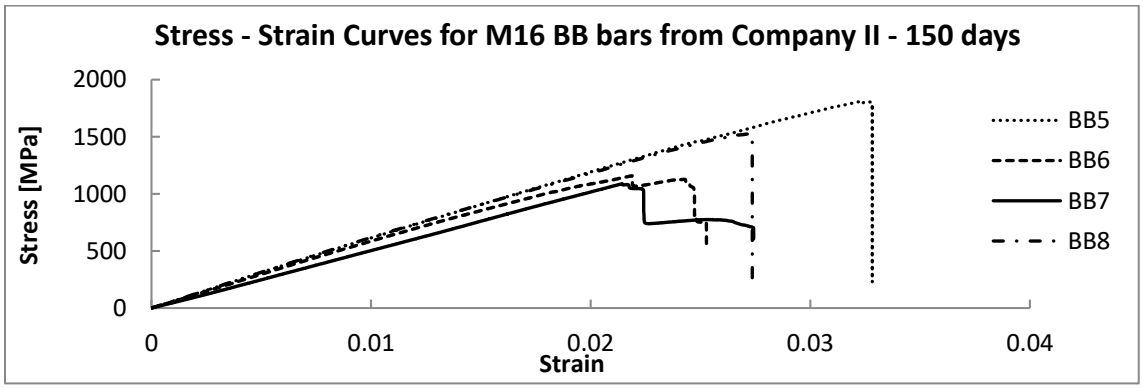

Fig. A8.12 – Stress-strain curves for M16 BB bars from Company II after a) 0, b) 30 c) 90, d) 150 days in alkaline solution heated to 60˚C

Table A8.14 – Flexural strength degradation BB bars Company II in 70˚C solution

Straight portion of the bent bars (BB) properties after 0 days in alkaline solution					
Sample	M12		Sample	M16	
	Strength [MPa]	Modulus of elasticity [GPa]		Strength [MPa]	Modulus of elasticity [GPa]
mean	1684	66	mean	1572	65
s.d	82	4	s.d	165	5
cov	0.05	0.07	cov	0.1	0.08
Straight portion of the bent bars (BB) properties after 30 days in alkaline solution					
Sample	M12		Sample	M16	
	Strength [MPa]	Modulus of elasticity [GPa]		Strength [MPa]	Modulus of elasticity [GPa]
mean	1497	57	mean	1375	50
s.d	98	4	s.d	96	4
cov	0.06	0.07	cov	0.07	0.09
Straight portion of the bent bars (BB) properties after 90 days in alkaline solution					
Sample	M12		Sample	M16	
	Strength [MPa]	Modulus of elasticity [GPa]		Strength [MPa]	Modulus of elasticity [GPa]
mean	1359	56	mean	1268	47
s.d	67	1	s.d	70	3
cov	0.05	0.02	cov	0.05	0.06
Straight portion of the bent bars (BB) properties after 150 days in alkaline solution					
Sample	M12		Sample	M16	
	Strength [MPa]	Modulus of elasticity [GPa]		Strength [MPa]	Modulus of elasticity [GPa]
mean	1316	54	mean	1224	45
s.d	153	5	s.d	165	2
cov	0.09	0.09	cov	0.13	0.04

Appendix 9

DETERIORATION OF GFRP BARS PROPERTIES

A9.1 Shear strength deterioration

A9.1.1 Company I

Table A9.1 – Rate constant "β" for SB Bars Company I

Temperature	β[mm/s]	R^2 for #4	R^2 for #5
50˚C	1.157 * (10^{-7})	0.81	0.92
60˚C	2.199 * (10^{-7})	0.81	0.82
70˚C	3.067 * (10^{-7})	0.80	0.86

Table A9.2 – Rate constant "β" for BB Bars Company I

Temperature	β[mm/s]	R^2 for #4	R^2 for #5
50˚C	1.273 * (10^{-7})	0.85	0.93
60˚C	1.909 * (10^{-7})	0.80	0.85
70˚C	2.430 * (10^{-7})	0.89	0.92

a)

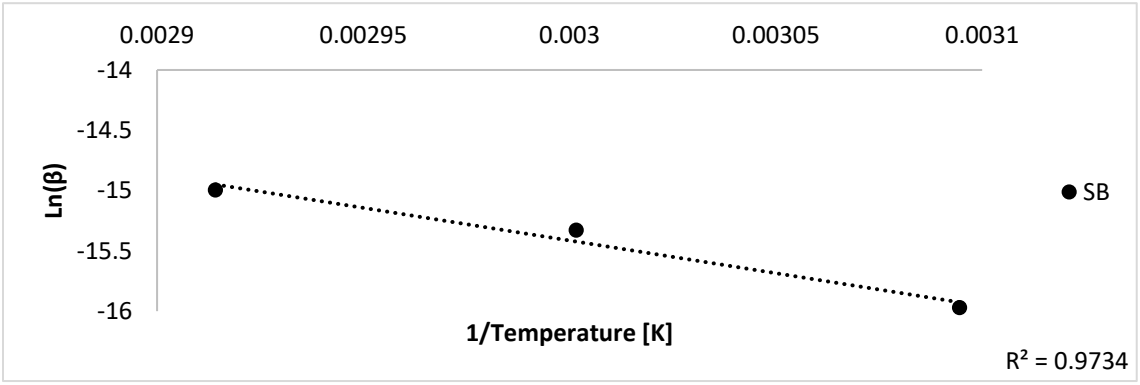

b)

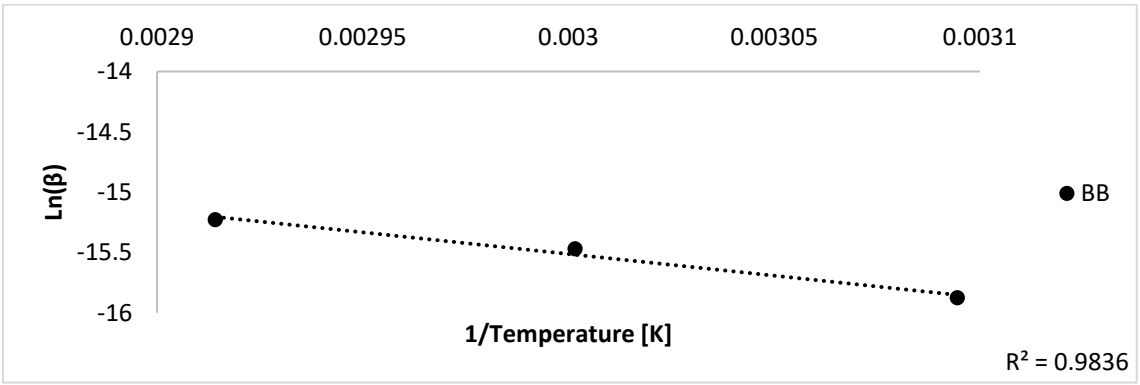

Fig. A9.1 – Arrhenius plot for rate parameter "β" for a) SB s and b) BB bars

- **Step 1**

a)

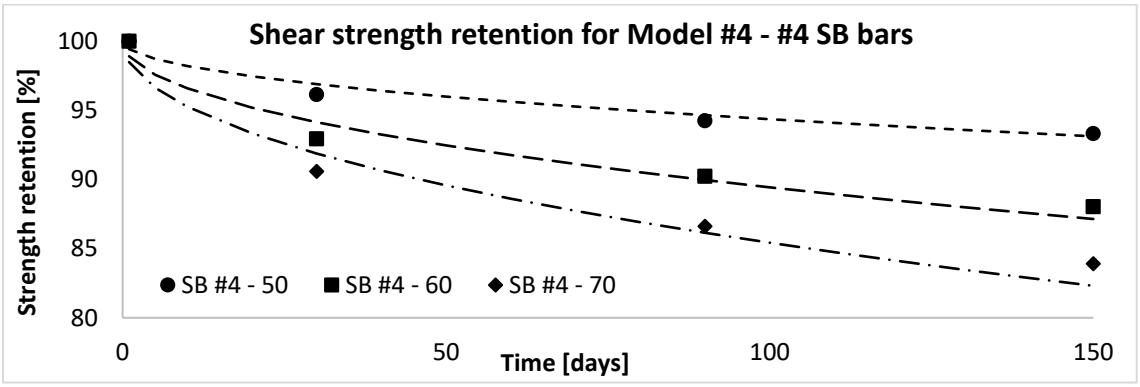

b)

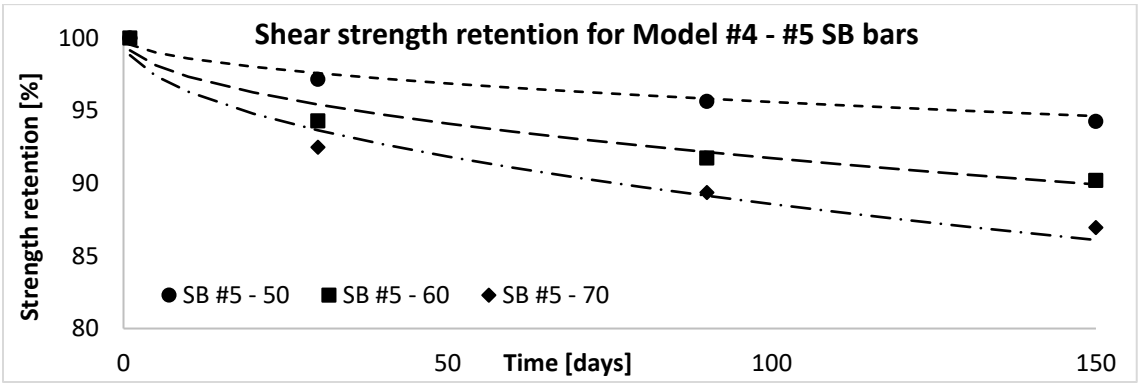

Fig. A9.2 – Shear strength retention a) SB #4, b) SB #5 bars

a)

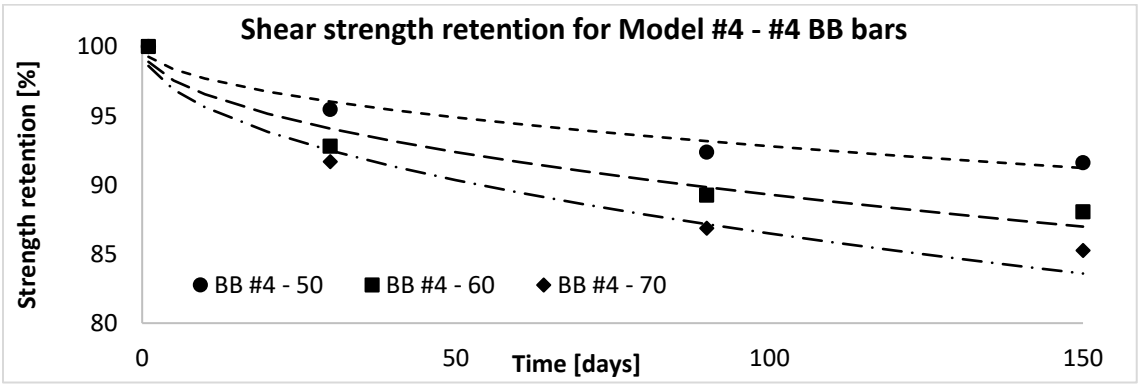

b)

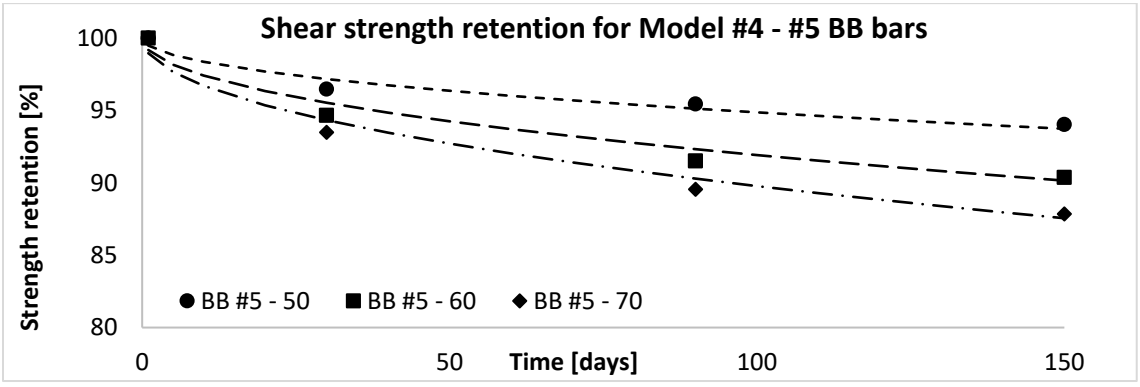

Fig. A9.3 – Shear strength retention a) BB #4, b) BB #5 bars

- **Step 2**

Table A9.3 – Required time in alkaline solution bath to reach specific shear strength retention for SB bars

Retention	SB #4 - 50	SB #4 - 60	SB #4 - 70	SB #5- 50	SB #5 - 60	SB #5 - 70
	Time to reach specific retention [days]					
95	78.54	21.76	11.18	129.83	35.96	18.49
85	746.16	206.69	106.25	1233.45	341.68	175.64
75	2198.78	609.08	313.10	3634.71	1006.85	517.58

Table A9.4 – Required time in alkaline solution bath to reach specific shear strength retention for BB bars

Retention	BB #4 - 50	BB #4 - 60	BB #4 - 70	BB #5- 50	BB #5 - 60	BB #5 - 70
	Time to reach specific retention [days]					
95	47.69	21.19	13.08	94.84	37.68	23.26
85	453.06	201.36	124.31	901.05	357.97	220.99
75	1335.06	593.36	366.31	2655.21	1054.87	651.22

- **Step 3**

a)

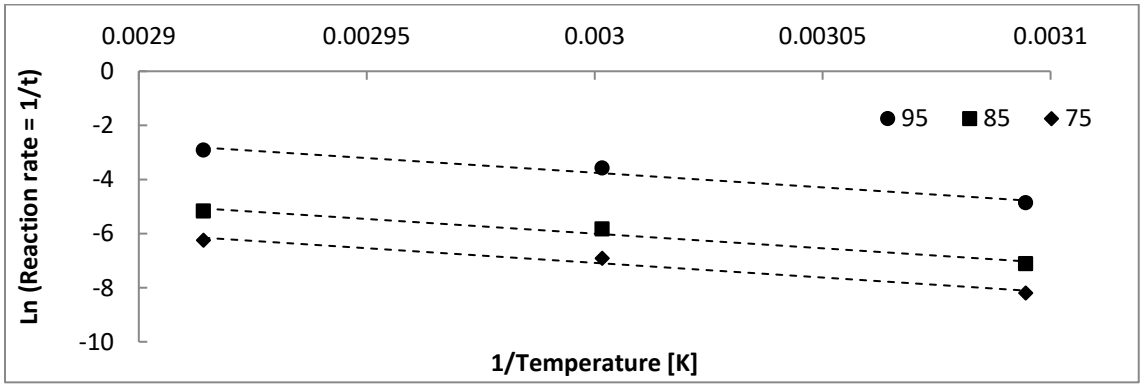

b)

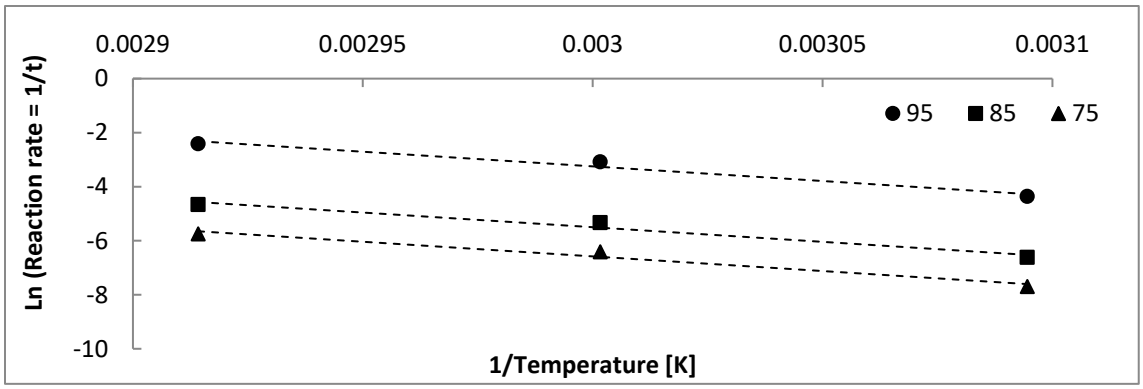

Fig. A9.4 – Arrhenius plot for a) #4 and b) #5 SB bars

a)

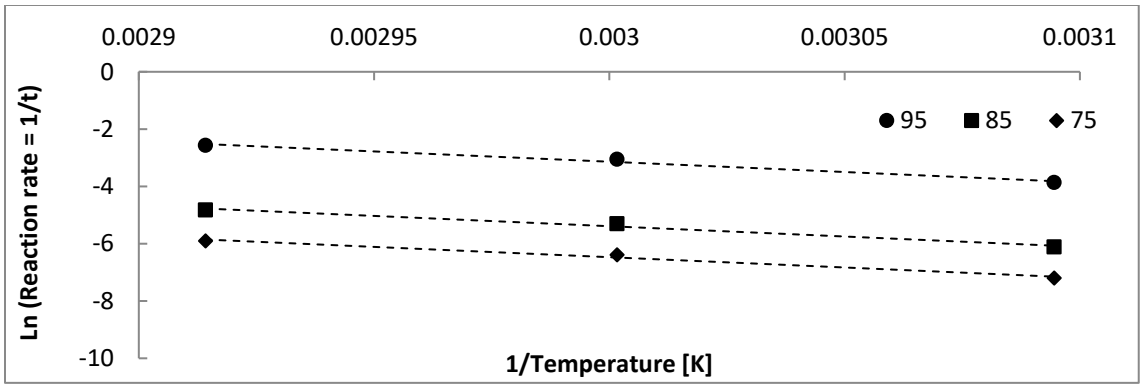

b)

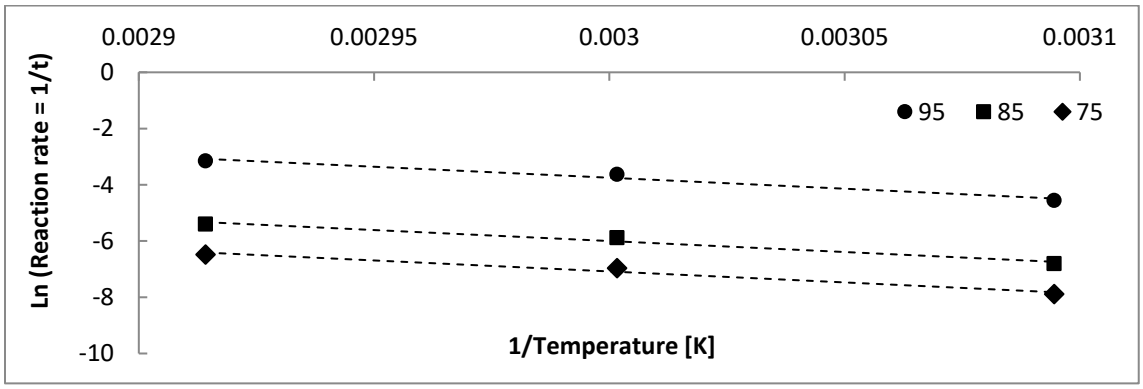

Fig. A9.5 – Arrhenius plot for a) #4 and b) #5 BB bars

Table A9.5 – Regression coefficient $\left(\frac{E_a}{R}\right)$ and correlation coefficient for SB bars

Temperature	$\left(\frac{E_a}{R}\right)$ for #4	R^2 for #4	$\left(\frac{E_a}{R}\right)$ for #5	R^2 for #5
50˚C	10806	0.99	10806	0.99
60˚C	10806	0.99	10806	0.99
70˚C	10806	0.99	10806	0.99

Table A9.6 – Regression coefficient $\left(\frac{E_a}{R}\right)$ and correlation coefficient for BB bars

Temperature	$\left(\frac{E_a}{R}\right)$ for #4	R^2 for #4	$\left(\frac{E_a}{R}\right)$ for #5	R^2 for #5
50˚C	7170	0.98	7792	0.97
60˚C	7171	0.98	7792	0.97
70˚C	7170	0.98	7792	0.97

For further analysis of the BB bars deterioration, the mean value of regression coefficient $\left(\frac{E_a}{R}\right)$ have been calculated as 7481.

- **Step 4**

Table A9.7 – Acceleration Factors for SB bars

Temperature	AF
50˚C	30.64
60˚C	83.61
70˚C	215.18

Table A9.8 – Acceleration Factors for BB bars

Temperature	AF
50˚C	10.69
60˚C	21.42
70˚C	41.21

- **Step 5**

a)

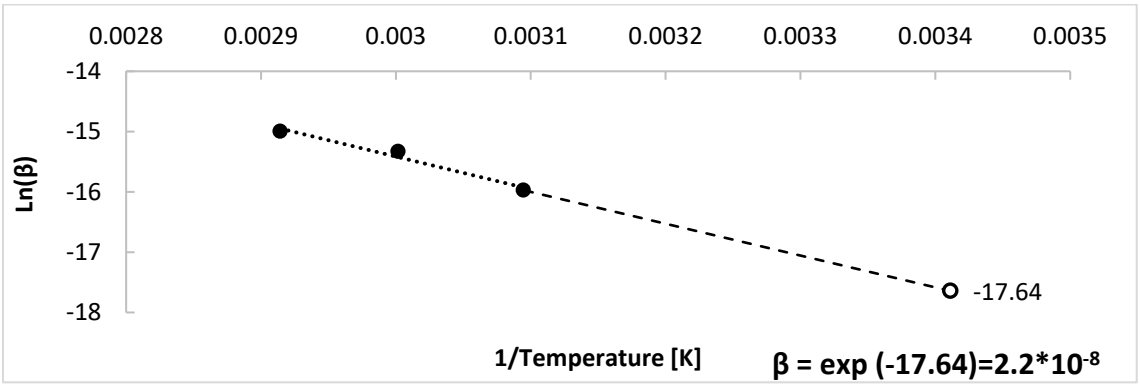

b)

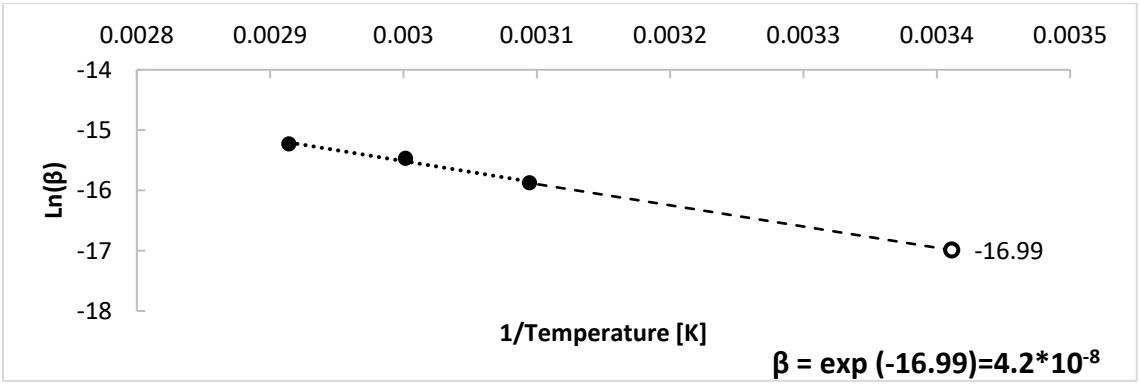

Fig. A9.6 – Arrhenius plot for rate parameter "β" including 20˚C for a) SB and b) BB bars

Table A9.9 – Rate constant "β" for SB and BB bars from Company I at 20˚C

Temperature	β[mm/s]	R^2 for #4	R^2 for #5
SB	$2.2 * (10^{-8})$	0.91	0.91
BB	$4.2 * (10^{-8})$	0.81	0.91

Table A9.10– Long term shear strength retention for SB bars

Shear strength retention			
Time in Bath	Time in Construction	SB #4 [%]	SB #5 [%]
[days]	[years]	50˚C	
30	2.5	96.16	97.16
90	7.6	94.24	95.63
150	12.6	93.32	94.26
[days]	[years]	60˚C	
30	6.9	92.93	94.30
90	20.6	90.22	91.74
150	34.4	88.02	90.19
[days]	[years]	70˚C	
30	17.7	90.58	92.49
90	53.1	86.62	89.37
150	88.4	83.91	86.96

Table A9.11 – Long term shear strength retention for BB bars

Shear strength retention			
Time in Bath	Time in Construction	BB #4 [%]	BB #5 [%]
[days]	[years]	50˚C	
30	0.9	95.44	96.47
90	2.6	92.36	95.45
150	4.4	91.59	94.26
[days]	[years]	60˚C	
30	1.8	92.78	94.66
90	5.3	89.24	91.51
150	8.8	88.04	90.37
[days]	[years]	70˚C	
30	3.4	91.67	93.49
90	10.2	86.87	89.55
150	16.9	85.25	87.85

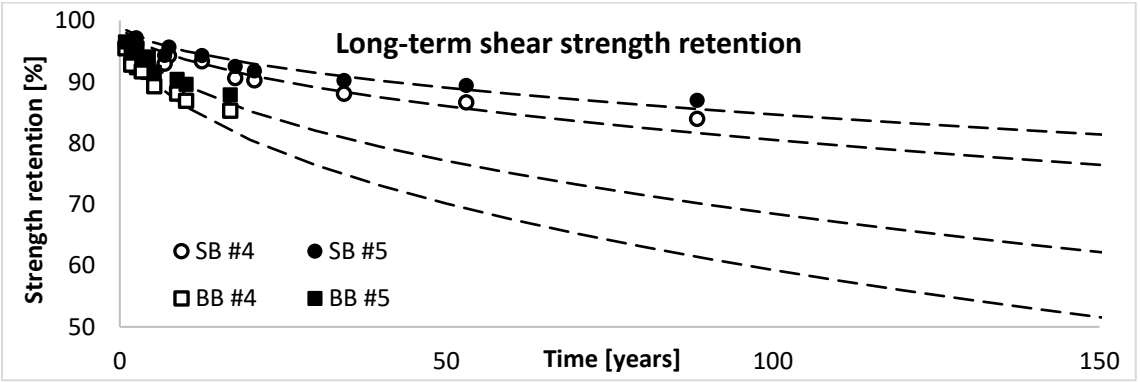

Fig. A9.7 – Long-term shear strength retention at 20˚C for Model #4 – Company I

A9.1.2 Company II

Table A9.12 – Rate constant "β" for SB Bars Company II

Temperature	β[mm/s]	R^2 for M12	R^2 for M16
50˚C	7.870 * (10^{-8})	0.89	0.87
60˚C	1.562 * (10^{-7})	0.81	0.86
70˚C	2.314 * (10^{-7})	0.81	0.89

Table A9.13 – Rate constant "β" for BB Bars Company II

Temperature	β[mm/s]	R^2 for M12	R^2 for M16
50˚C	1.041 * (10^{-7})	0.97	0.93
60˚C	1.338 * (10^{-7})	0.95	0.92
70˚C	2.083 * (10^{-7})	0.97	0.93

a)

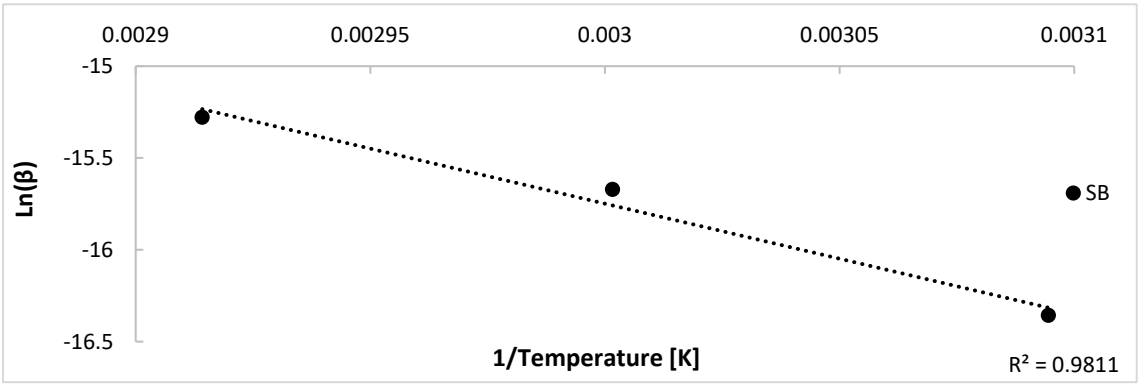

b)

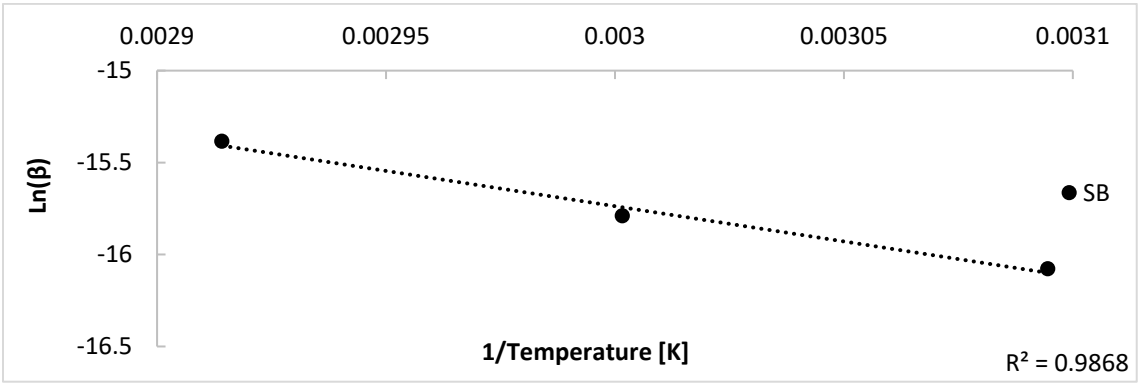

Fig. A9.8 – Arrhenius plot for rate parameter "β" for a) SB s and b) BB bars

- **Step 1**

a)

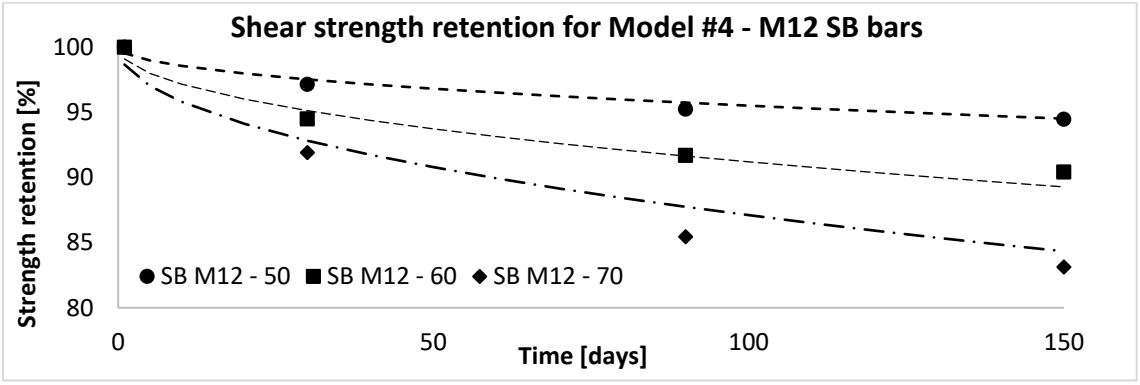

b)

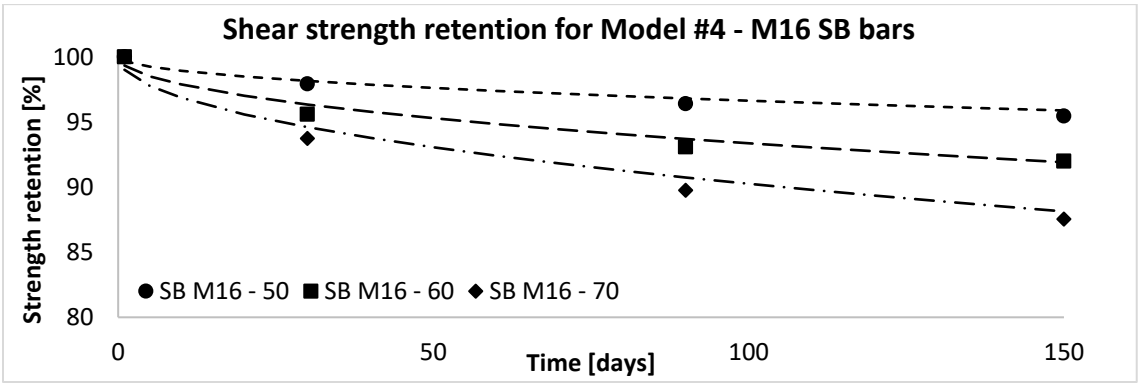

Fig. A9.9 – Shear strength retention a) SB M12, b) SB M16 bars

a)

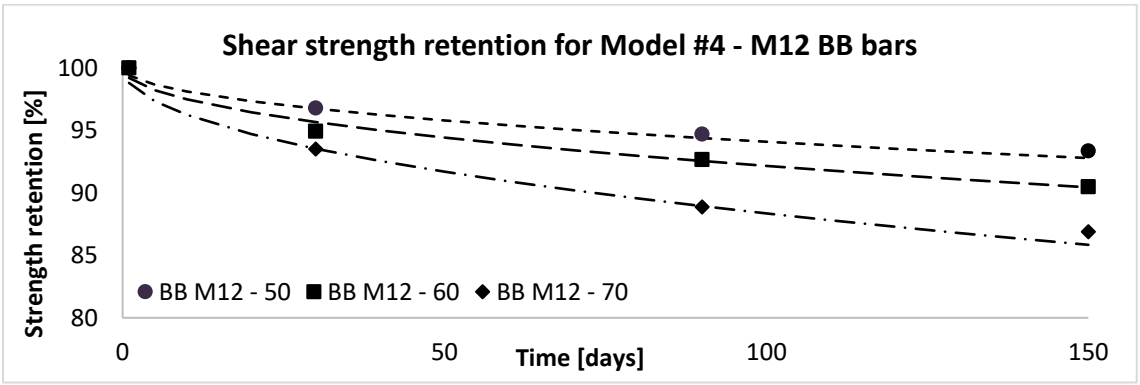

b)

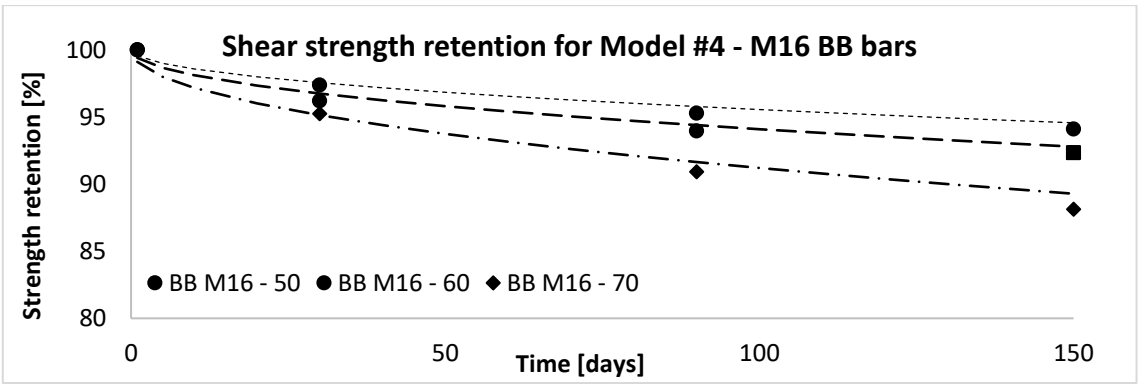

Fig. A9.10 – Shear strength retention a) BB M12, b) BB M16 bars

- **Step 2**

Table A9.14 – Required time in alkaline solution bath to reach specific shear strength retention for SB bars

Retention	SB M12 - 50	SB M12 - 60	SB M12- 70	SB M16- 50	SB M16 - 60	SB M16 - 70
	Time to reach specific retention [days]					
95	124.79	31.66	14.43	221.84	56.29	25.65
85	1185.55	300.80	137.05	2107.65	534.75	243.64
75	3493.57	886.38	403.86	6210.79	1575.79	717.97

Table A9.15 – Required time in alkaline solution bath to reach specific shear strength retention for BB bars

Retention	BB M12 - 50	BB M12 - 60	BB M12 - 70	BB M16- 50	BB M16 - 60	BB M16 - 70
	Time to reach specific retention [days]					
95	71.24	40.07	17.81	126.64	71.24	31.66
85	676.79	380.69	169.20	1203.18	676.79	300.80
75	1994.35	1121.82	498.59	3545.52	1994.35	886.38

- **Step 3**

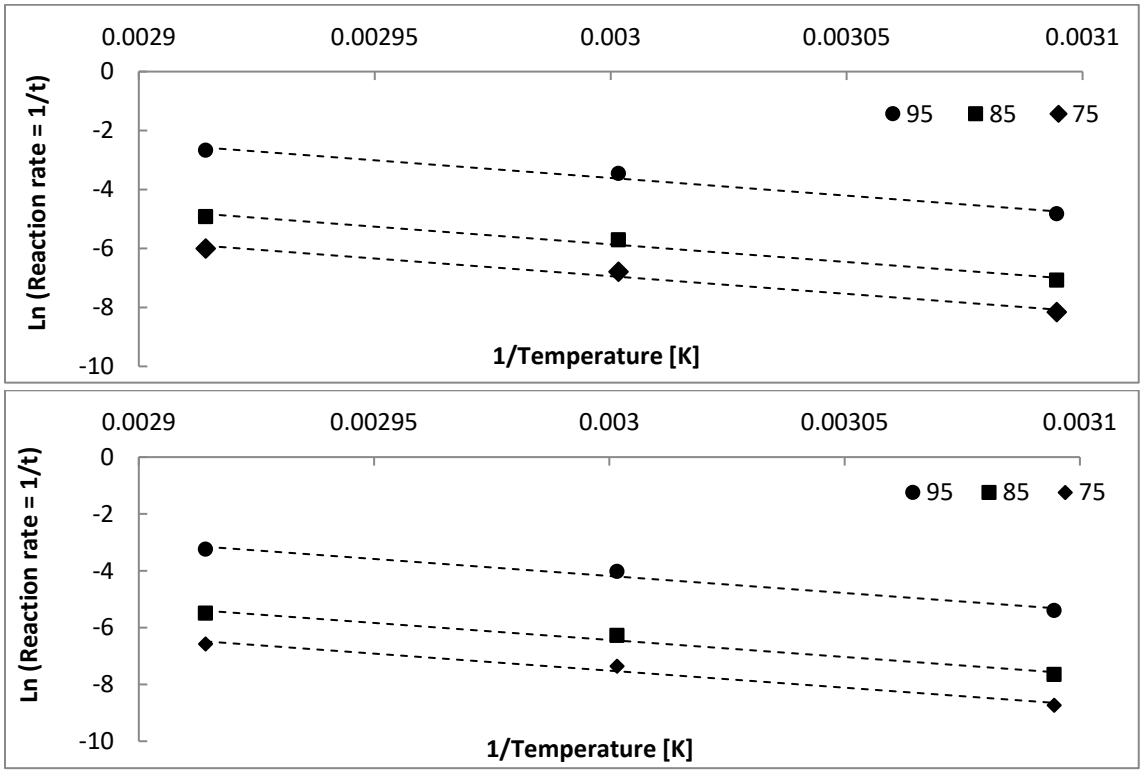

Fig. A9.11 – Arrhenius plot for a) M12 and b) M16 SB bars

a)

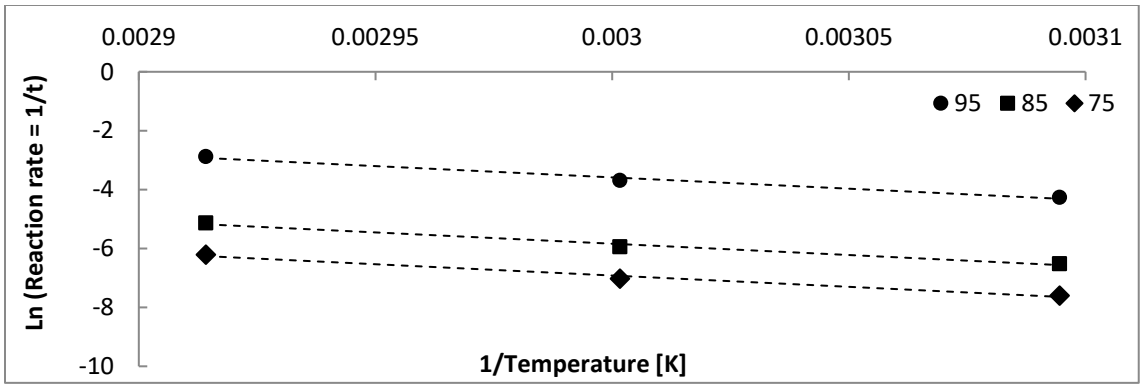

b)

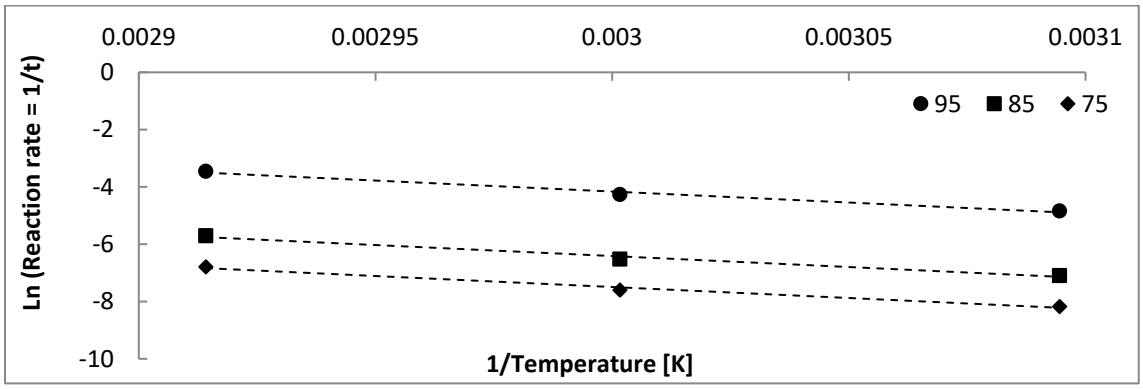

Fig. A9.12– Arrhenius plot for a) M12 and b) M16 BB bars

Table A9.16 – Regression coefficient $\left(\frac{E_a}{R}\right)$ and correlation coefficient for SB bars

Temperature	$\left(\frac{E_a}{R}\right)$ for M12	R^2 for M12	$\left(\frac{E_a}{R}\right)$ for M16	R^2 for M16
50˚C	11963	0.99	11963	0.99
60˚C	11963	0.99	11963	0.99
70˚C	11962	0.99	11963	0.99

Table A9.17 – Regression coefficient $\left(\frac{E_a}{R}\right)$ and correlation coefficient for BB bars

Temperature	$\left(\frac{E_a}{R}\right)$ for M12	R^2 for M12	$\left(\frac{E_a}{R}\right)$ for M16	R^2 for M16
50˚C	7686	0.98	7686	0.98
60˚C	7686	0.98	7686	0.98
70˚C	7686	0.98	7686	0.98

- **<u>Step 4</u>**

Table A9.18 – Acceleration Factors for SB bars

Temperature	AF
50˚C	44.19
60˚C	134.24
70˚C	382.24

Table A9.19 – Acceleration Factors for BB bars

Temperature	AF
50˚C	11.41
60˚C	23.29
70˚C	45.62

- **Step 5**

a)

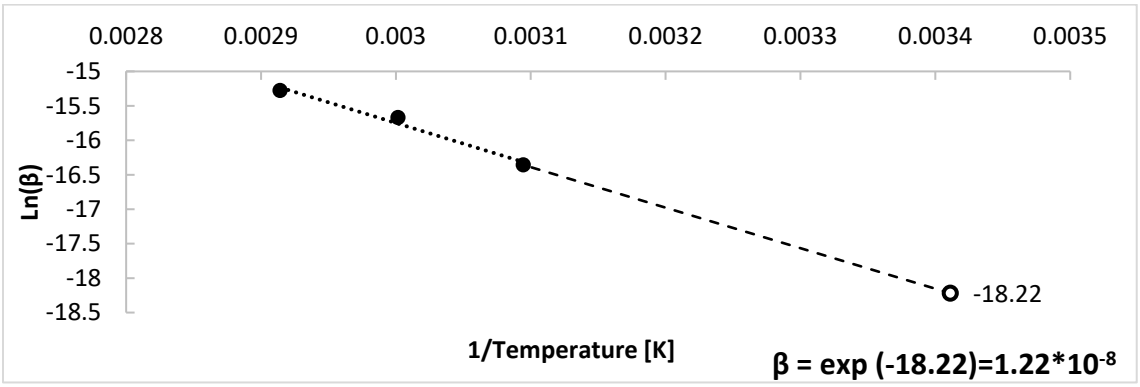

b)

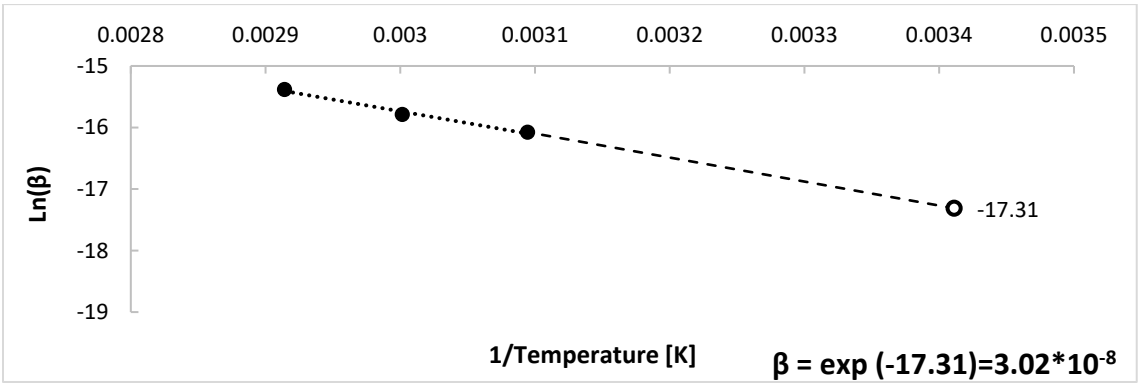

Fig. A9.13 – Arrhenius plot for rate parameter "β" including 20˚C for a) SB and b) BB bars

Table A9.20 – Rate constant "β" for SB and BB bars from Company I at 20˚C

Temperature	β[mm/s]	R^2 for M12	R^2 for M16
SB	1.22 * (10^{-8})	0.96	0.95
BB	3.02 * (10^{-8})	0.98	0.95

Table A9.21 – Long term shear strength retention for SB bars

Shear strength retention			
Time in Bath	Time in Construction	SB M12 [%]	SB M16 [%]
[days]	[years]	50˚C	
30	3.6	97.14	97.9
90	10.9	95.24	96.4
150	18.2	94.46	95.45
[days]	[years]	60˚C	
30	11	94.69	95.58
90	33.1	91.69	93.08

150	55.2	90.40	91.98
[days]	[years]	70˚C	
30	31.4	91.9	93.73
90	94.3	85.44	89.75
150	157.1	83.13	87.54

Table A9.22 – Long term shear strength retention for BB bars

Shear strength retention			
Time in Bath	Time in Construction	BB M12 [%]	BB M16 [%]
[days]	[years]	50˚C	
30	0.9	96.78	97.38
90	2.8	94.70	95.27
150	4.7	93.35	94.10
[days]	[years]	60˚C	
30	1.9	94.93	96.20
90	5.7	92.67	90.49
150	9.6	90.49	92.33
[days]	[years]	70˚C	
30	3.7	93.50	95.24
90	11.2	88.87	90.92
150	18.7	86.88	88.13

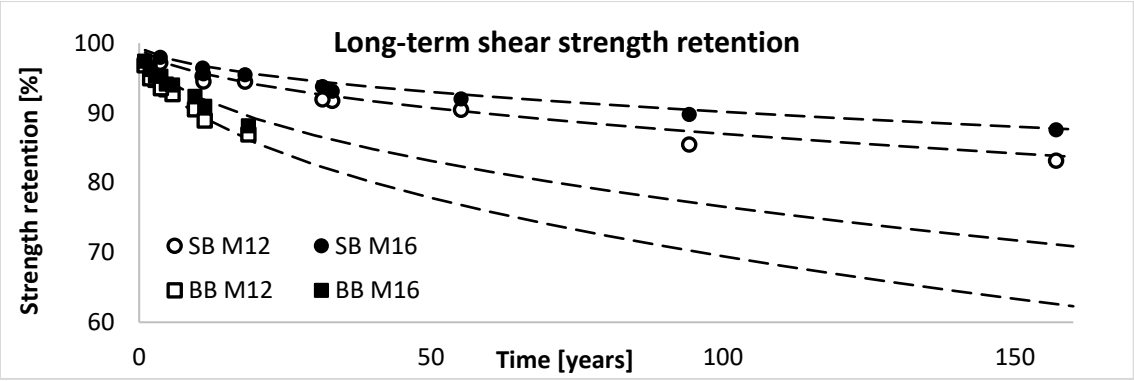

Fig. A9.14 – Long-term shear strength retention at 20˚C for Model #4 – Company II

A9.2 Flexure strength deterioration

A9.2.1 Company I

Table A9.23 – Rate constant "β" for SB Bars Company I

Temperature	β[mm/s]	R^2 for #4	R^2 for #5
50˚C	$1.157 * (10^{-7})$	0.85	0.80
60˚C	$2.199 * (10^{-7})$	0.81	0.91
70˚C	$3.125 * (10^{-7})$	0.86	0.85

Table A9.24 – Rate constant "β" for BB Bars Company I

Temperature	β[mm/s]	R^2 for #4	R^2 for #5
50˚C	1.273 * (10^{-7})	0.94	0.89
60˚C	1.909 * (10^{-7})	0.90	0.88
70˚C	2.430 * (10^{-7})	0.93	0.83

a)

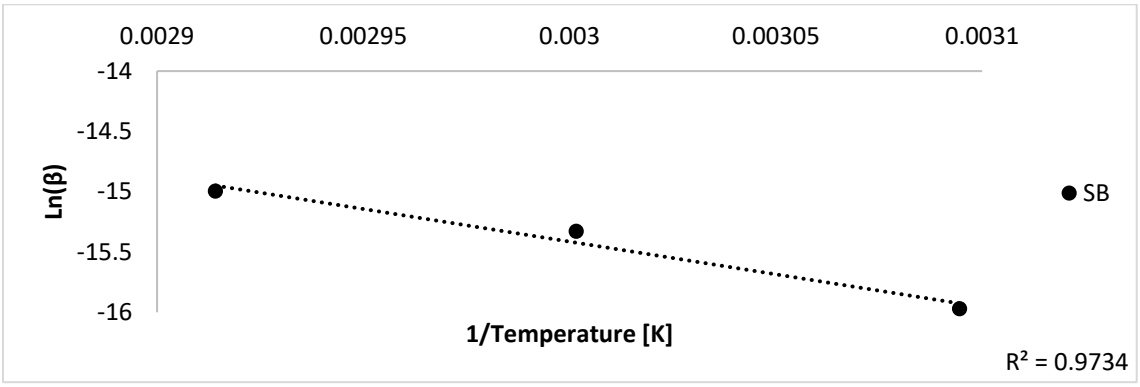

b)

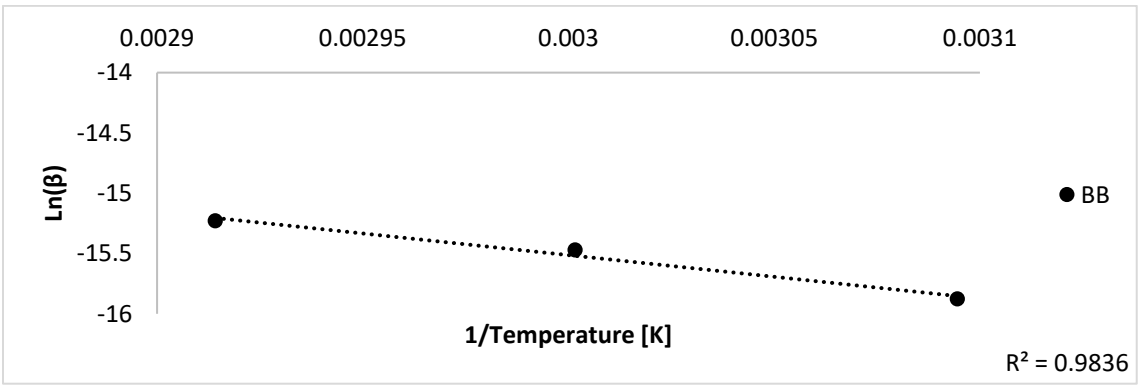

Fig. A9.15 – Arrhenius plot for rate parameter "β" for a) SB s and b) BB bars

- **<u>Step 1</u>**

a)

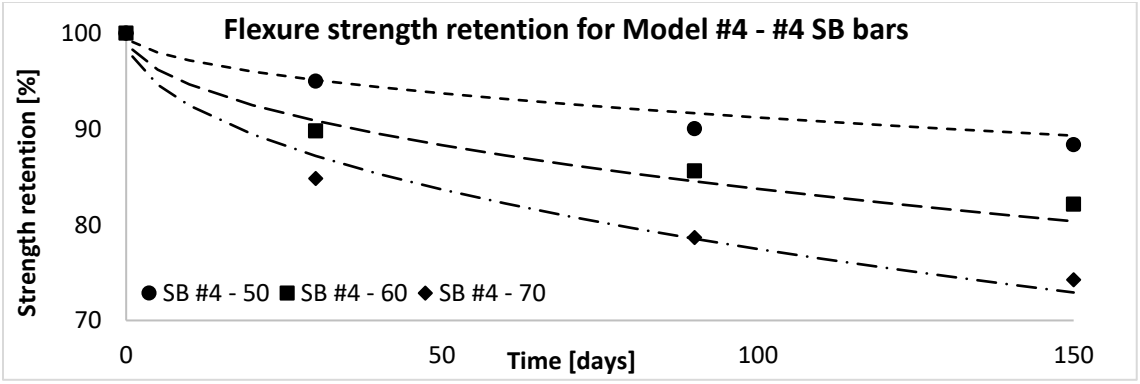

b)

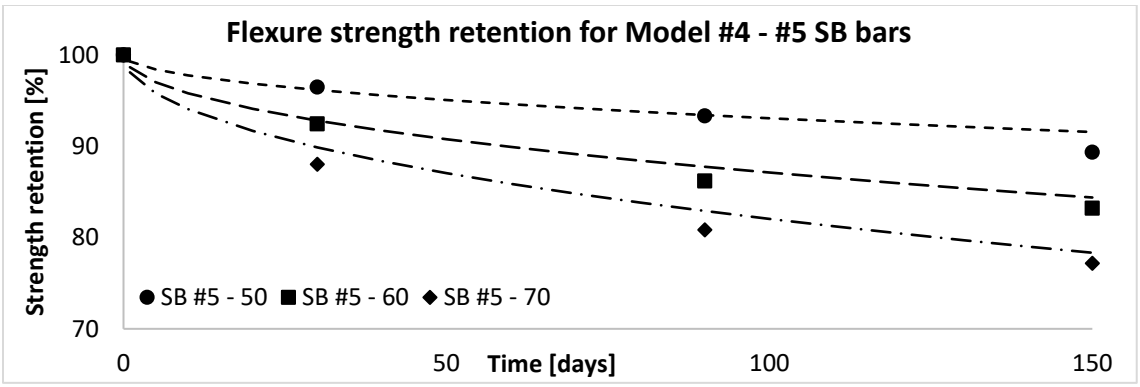

Fig. A9.16 – Flexure strength retention a) SB #4, b) SB #5 bars

a)

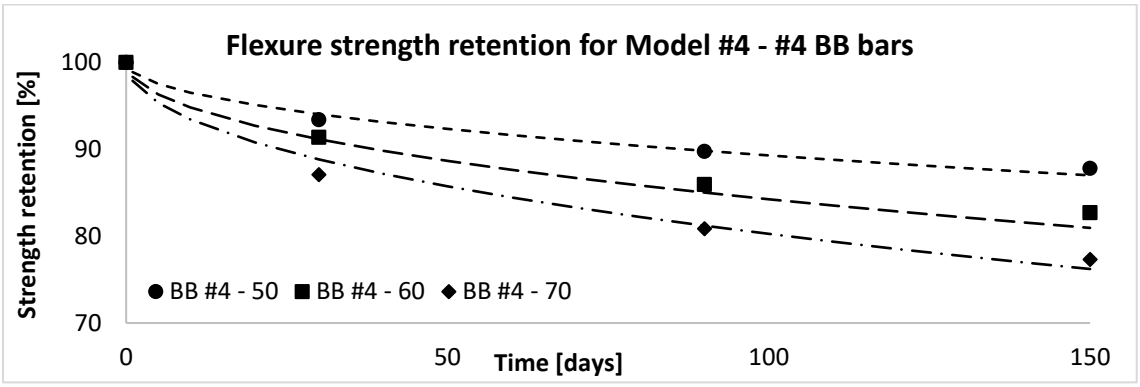

b)

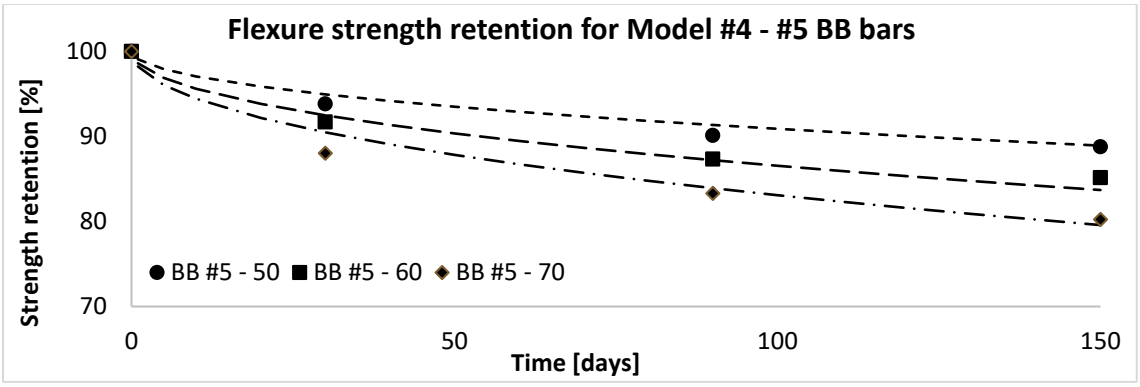

Fig. A9.17 – Flexure strength retention a) BB #4, b) BB #5 bars

- **<u>Step 2</u>**

Table A9.25 – Required time in alkaline solution bath to reach specific flexure strength retention for SB bars

Retention	SB #4 - 50	SB #4 - 60	SB #4 - 70	SB #5- 50	SB #5 - 60	SB #5 - 70
	Time to reach specific retention [days]					
95	31.48	8.72	4.32	51.43	14.25	7.06
85	304.59	84.37	41.78	497.63	137.85	68.26
75	915.85	253.70	125.63	1496.26	414.48	205.25

Table A9.26 – Required time in alkaline solution bath to reach specific flexure strength retention for BB bars

Retention	BB #4 - 50	BB #4 - 60	BB #4 - 70	BB #5- 50	BB #5 - 60	BB #5 - 70
	Time to reach specific retention [days]					
95	20.97	9.32	5.75	29.24	13.00	8.02
85	202.94	90.20	55.68	282.88	125.72	77.62
75	610.23	271.22	167.43	850.39	377.95	233.33

- **Step 3**

a)

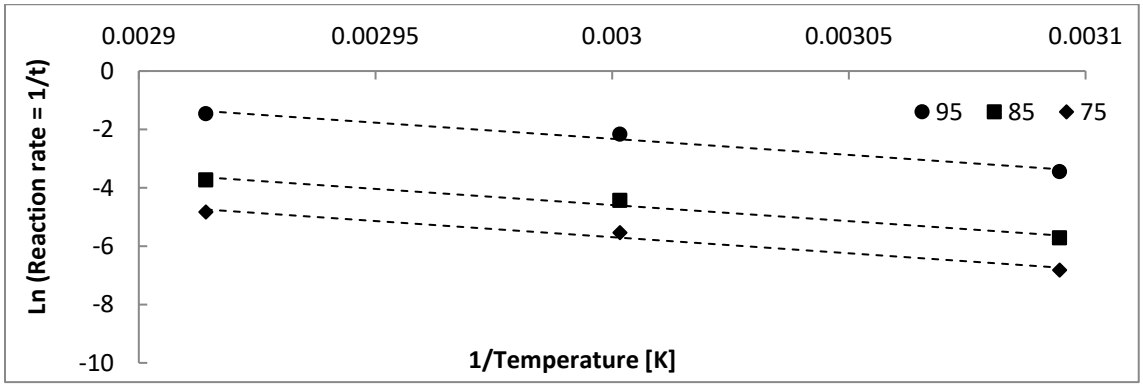

b)

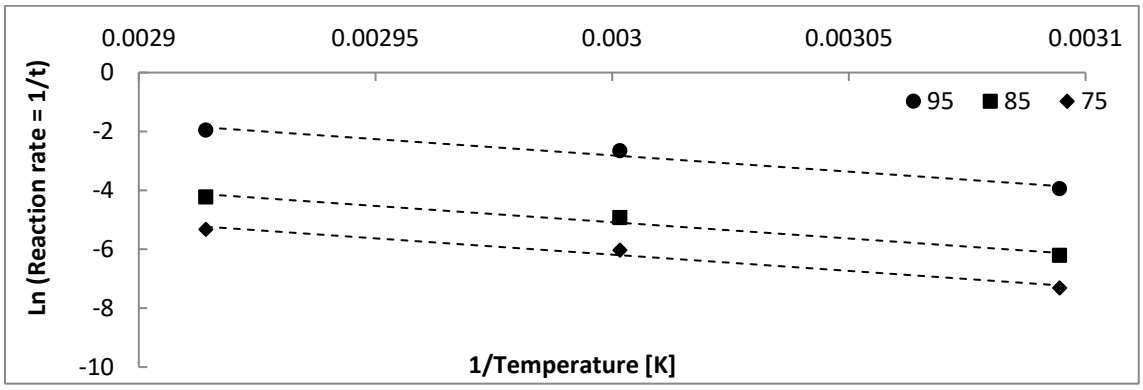

Fig. A9.18 – Arrhenius plot for a) #4 and b) #5 SB bars

a)

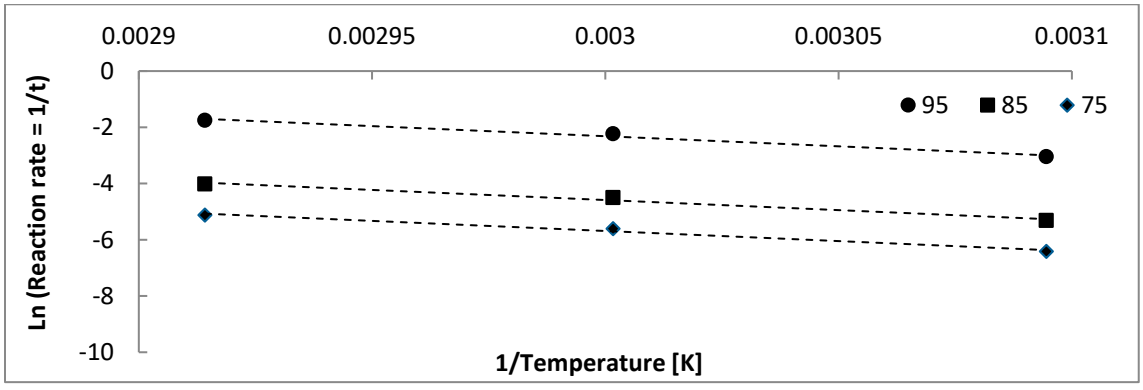

b) 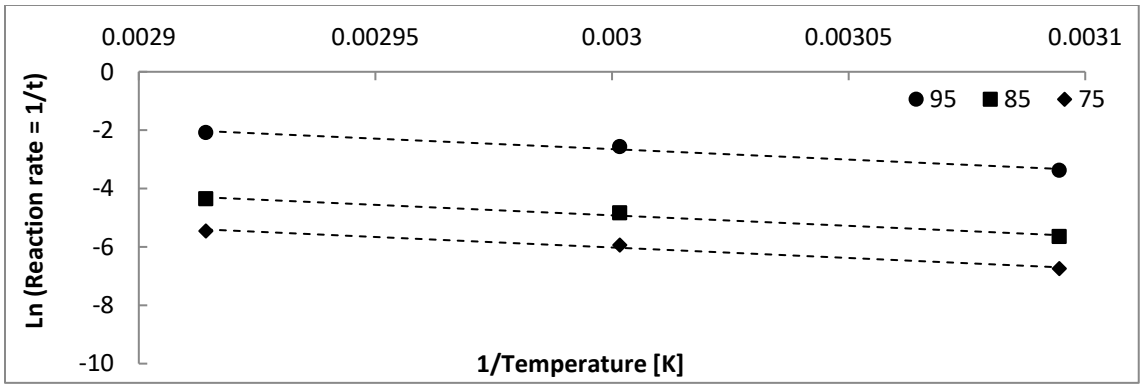

Fig. A9.19 – Arrhenius plot for a) #4 and b) #5 BB bars

Table A9.27 – Regression coefficient $\left(\frac{E_a}{R}\right)$ and correlation coefficient for SB bars

Temperature	$\left(\frac{E_a}{R}\right)$ for #4	R^2 for #4	$\left(\frac{E_a}{R}\right)$ for #5	R^2 for #5
50˚C	11014	0.99	11014	0.99
60˚C	11014	0.99	11014	0.99
70˚C	11014	0.99	11014	0.99

Table A9.28 – Regression coefficient $\left(\frac{E_a}{R}\right)$ and correlation coefficient for BB bars

Temperature	$\left(\frac{E_a}{R}\right)$ for #4	R^2 for #4	$\left(\frac{E_a}{R}\right)$ for #5	R^2 for #5
50˚C	7170	0.98	7170	0.97
60˚C	7171	0.98	7170	0.97
70˚C	7170	0.98	7170	0.97

- **<u>Step 4</u>**

Table A9.29 – Acceleration Factors for SB bars

Temperature	AF
50˚C	32.72
60˚C	91.02
70˚C	238.54

Table A9.30 – Acceleration Factors for BB bars

Temperature	AF
50˚C	9.69
60˚C	18.86
70˚C	35.30

- **Step 5**

a)

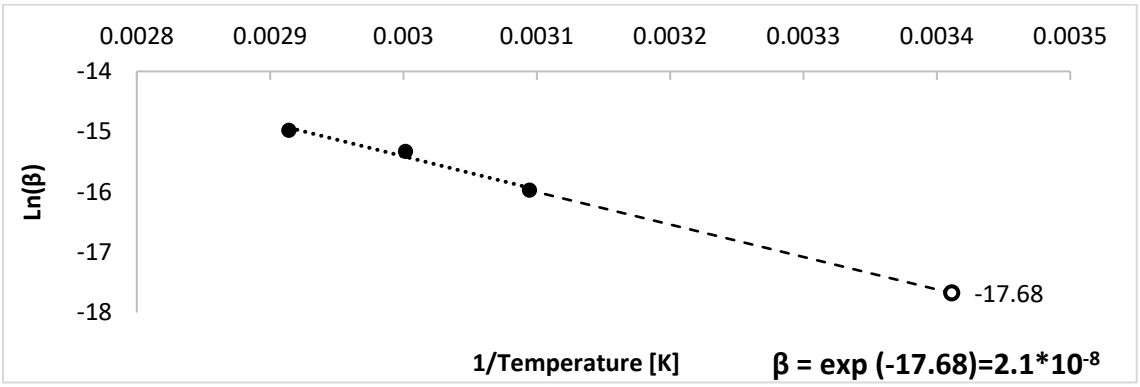

b)

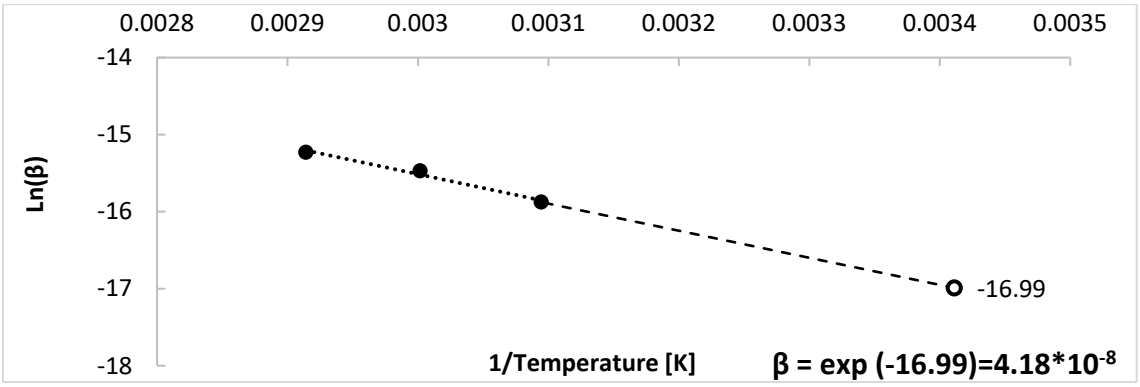

Fig. A9.20 – Arrhenius plot for rate parameter "β" including 20˚C for a) SB and b) BB bars

Table A9.31 – Rate constant "β" for SB and BB bars from Company I at 20˚C

Temperature	β[mm/s]	R^2 for #4	R^2 for #5
SB	2.1 * (10^{-8})	0.95	0.93
BB	4.18 * (10^{-8})	0.96	0.92

Table A9.32 – Long term flexure strength retention for SB bars

Flexure strength retention			
Time in Bath	Time in Construction	SB #4 [%]	SB #5 [%]
[days]	[years]	50˚C	
30	2.7	94.98	96.48
90	8.1	90.03	93.33
150	13.4	88.35	59.34
[days]	[years]	60˚C	
30	7.5	89.78	92.45
90	22.4	85.61	86.18
150	37.4	82.13	83.22
[days]	[years]	70˚C	
30	19.6	84.84	88.02
90	58.8	78.65	80.84
150	98	74.25	77.17

Table A9.33 – Long term Flexure strength retention for BB bars

Flexure strength retention			
Time in Bath	Time in Construction	BB #4 [%]	BB #5 [%]
[days]	[years]	50˚C	
30	0.8	93.39	93.82
90	2.4	89.75	90.12
150	4.0	87.8	88.77
[days]	[years]	60˚C	
30	1.5	91.37	91.7
90	4.6	85.93	87.33
150	7.7	82.69	85.14
[days]	[years]	70˚C	
30	2.9	87.08	88.03
90	8.7	80.84	83.31
150	14.5	77.31	80.23

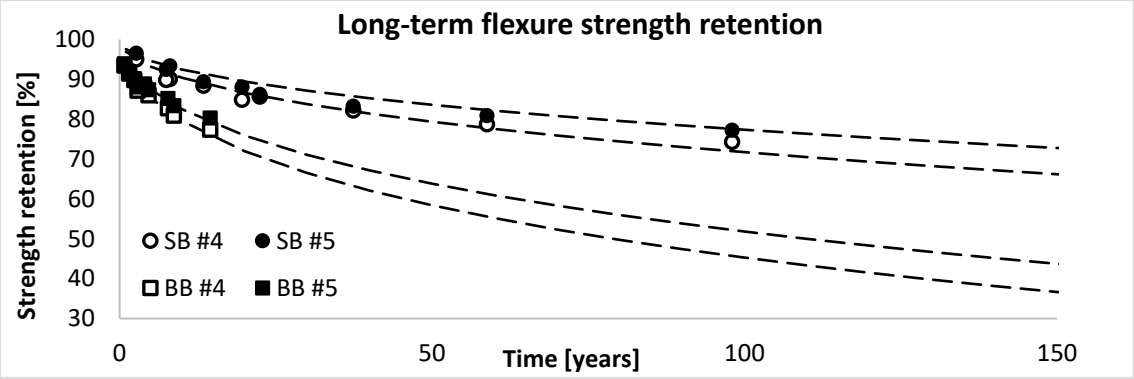

Fig. A9.21 – Long-term flexure strength retention at 20˚C for Model #4 – Company I

A9.2.2 Company II

Table A9.34 – Rate constant "β" for SB Bars Company II

Temperature	β[mm/s]	R^2 for M12	R^2 for M16
50˚C	$7.523 * (10^{-8})$	0.84	0.89
60˚C	$1.389 * (10^{-7})$	0.91	0.85
70˚C	$2.257 * (10^{-7})$	0.83	0.96

Table A9.35 – Rate constant "β" for BB Bars Company II

Temperature	β[mm/s]	R^2 for M12	R^2 for M16
50˚C	$9.838 * (10^{-8})$	0.82	0.95
60˚C	$1.338 * (10^{-7})$	0.96	0.96
70˚C	$2.083 * (10^{-7})$	0.95	0.81

a)

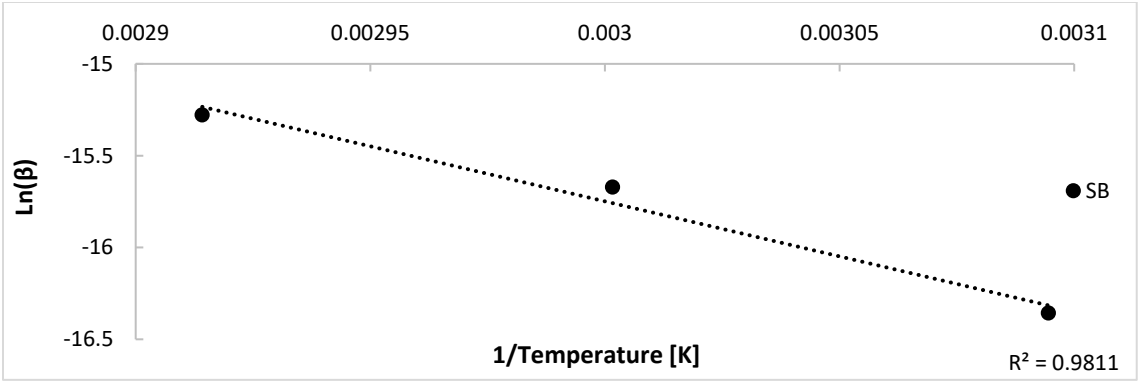

b)

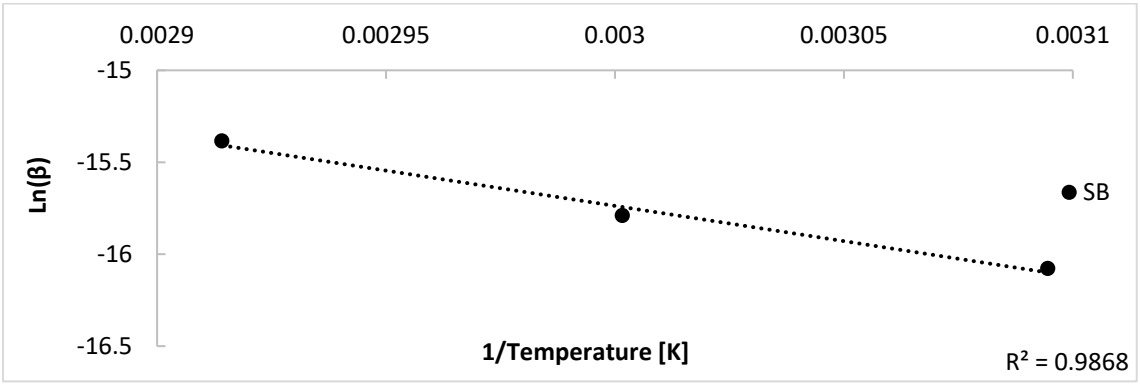

Fig. A9.22 – Arrhenius plot for rate parameter "β" for a) SB s and b) BB bars

- **Step 1**

a)

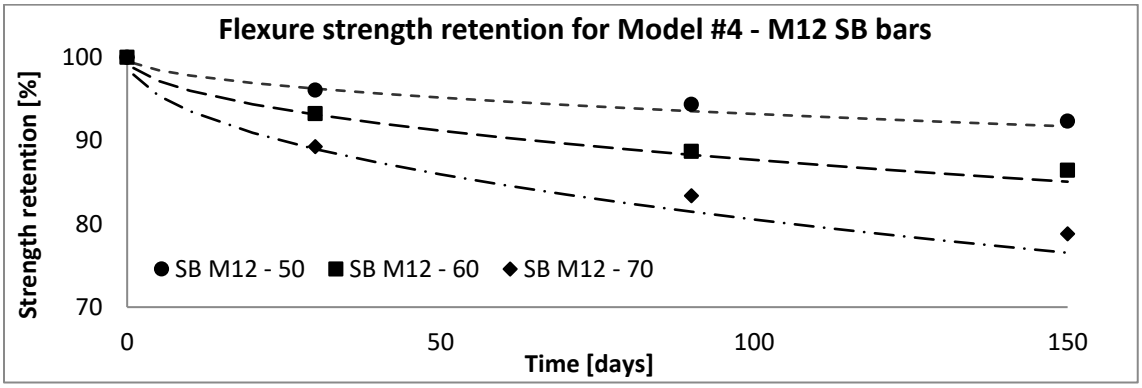

b)

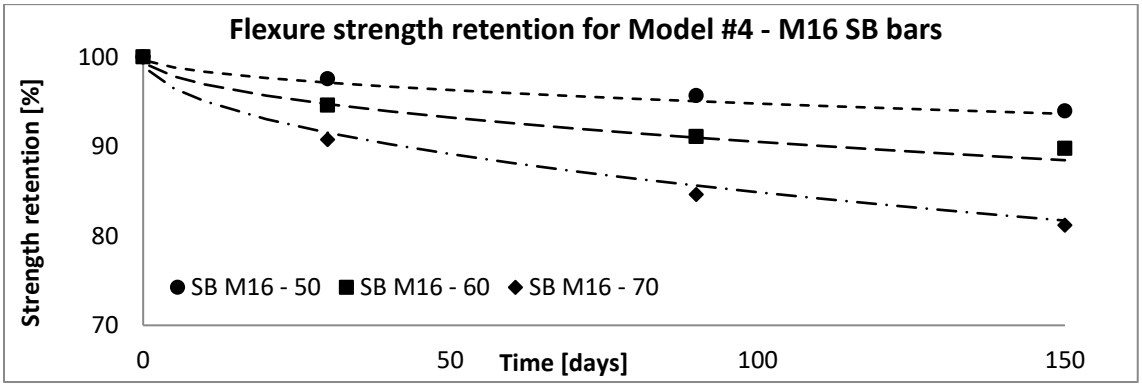

Fig. A9.23 – Flexure strength retention a) SB M12, b) SB M16 bars

a)

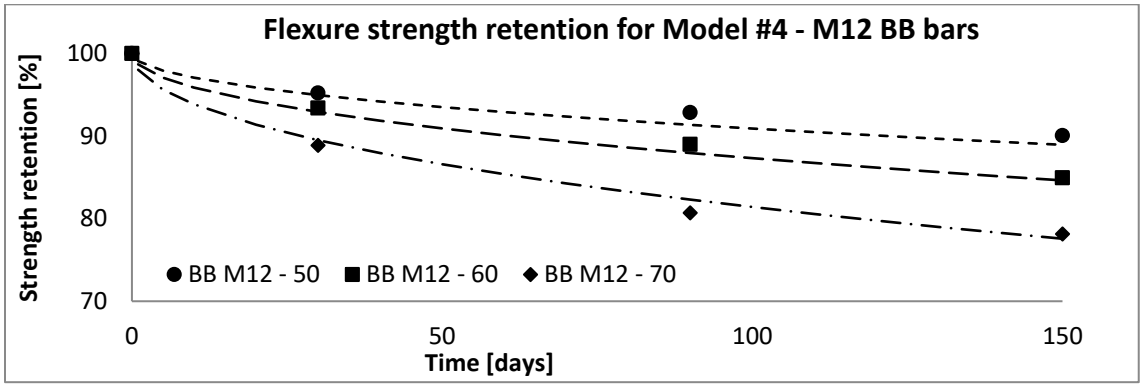

b)

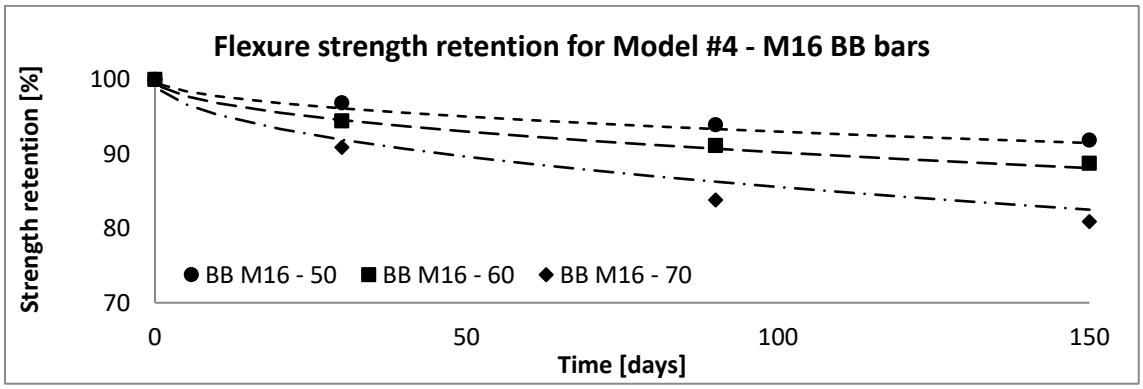

Fig. A9.24 – Flexure strength retention a) BB M12, b) BB M16 bars

- **<u>Step 2</u>**

Table A9.36 – Required time in alkaline solution bath to reach specific flexure strength retention for SB bars

Retention	SB M12 - 50	SB M12 - 60	SB M12- 70	SB M16- 50	SB M16 - 60	SB M16 - 70
	Time to reach specific retention [days]					
95	53.31	15.64	5.92	91.44	26.83	10.16
85	515.74	151.32	57.30	884.63	259.55	98.29
75	1550.67	454.97	172.30	2659.70	780.36	295.52

Table A9.37 – Required time in alkaline solution bath to reach specific flexure strength retention for BB bars

Retention	BB M12 - 50	BB M12 - 60	BB M12 - 70	BB M16- 50	BB M16 - 60	BB M16 - 70
	Time to reach specific retention [days]					
95	29.35	14.73	6.54	50.17	25.17	11.19
85	283.93	142.46	63.32	485.33	243.51	108.23
75	853.64	428.30	190.36	1459.06	732.06	325.36

- **Step 3**

a)

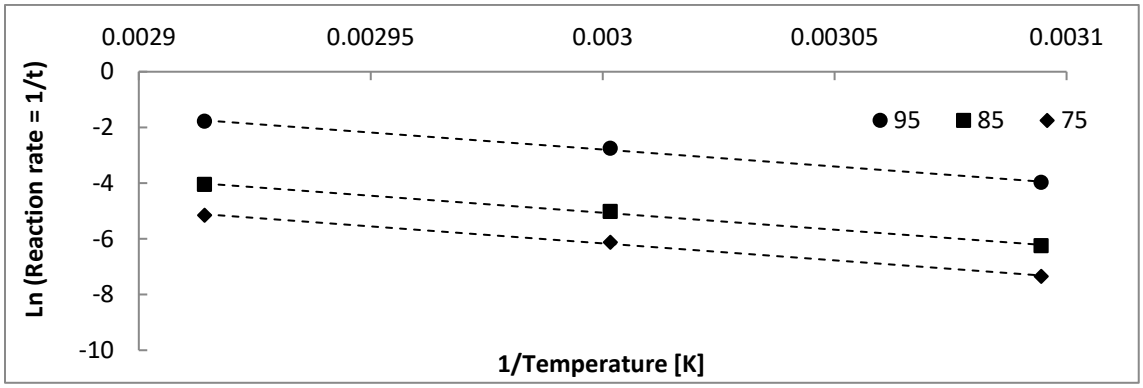

b)

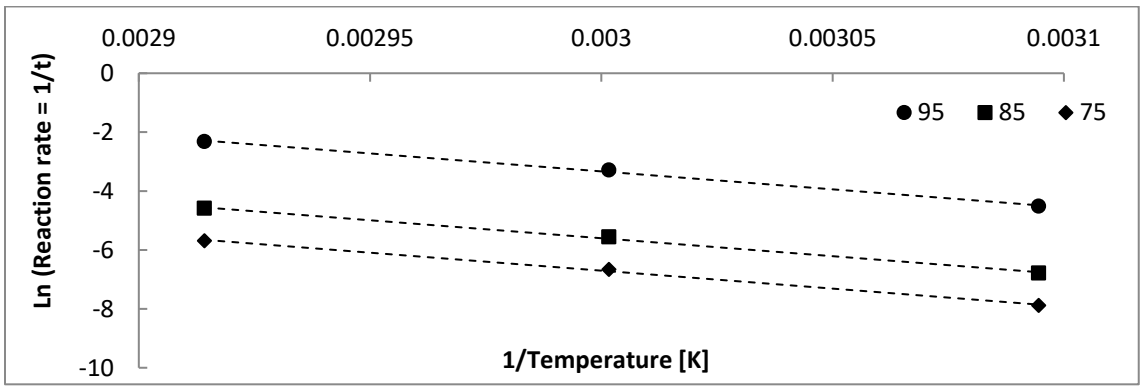

Fig. A9.25 – Arrhenius plot for a) M12 and b) M16 SB bars

a)

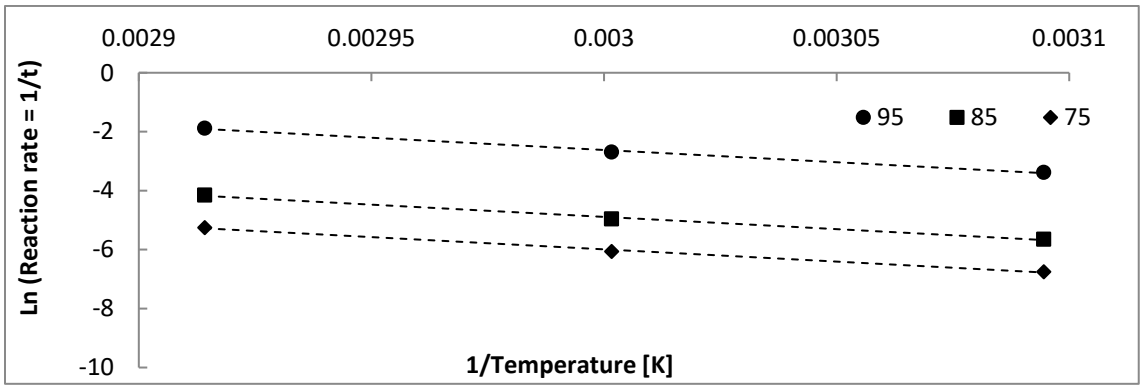

b)

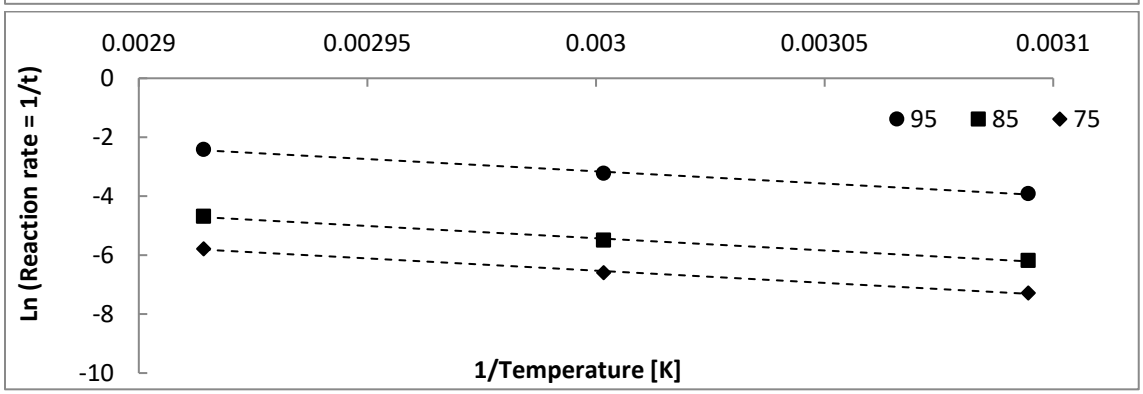

Fig. A9.26 – Arrhenius plot for a) M12 and b) M16 BB bars

Table A9.38 – Regression coefficient $\left(\frac{E_a}{R}\right)$ and correlation coefficient for SB bars

Temperature	$\left(\frac{E_a}{R}\right)$ for M12	R^2 for M12	$\left(\frac{E_a}{R}\right)$ for M16	R^2 for M16
50˚C	12182	0.99	12182	0.99
60˚C	12182	0.99	12182	0.99
70˚C	12182	0.99	12182	0.99

Table A9.39 – Regression coefficient $\left(\frac{E_a}{R}\right)$ and correlation coefficient for BB bars

Temperature	$\left(\frac{E_a}{R}\right)$ for M12	R^2 for M12	$\left(\frac{E_a}{R}\right)$ for M16	R^2 for M16
50˚C	8319	0.99	0.99	0.99
60˚C	8320	0.99	0.99	0.99
70˚C	8320	0.99	0.99	0.99

- **Step 4**

Table A9.40 – Acceleration Factors for SB bars

Temperature	AF
50˚C	47.37
60˚C	146.87
70˚C	426.33

Table A9.41 – Acceleration Factors for BB bars

Temperature	AF
50˚C	13.94
60˚C	30.19
70˚C	65.52

- **Step 5**

a)

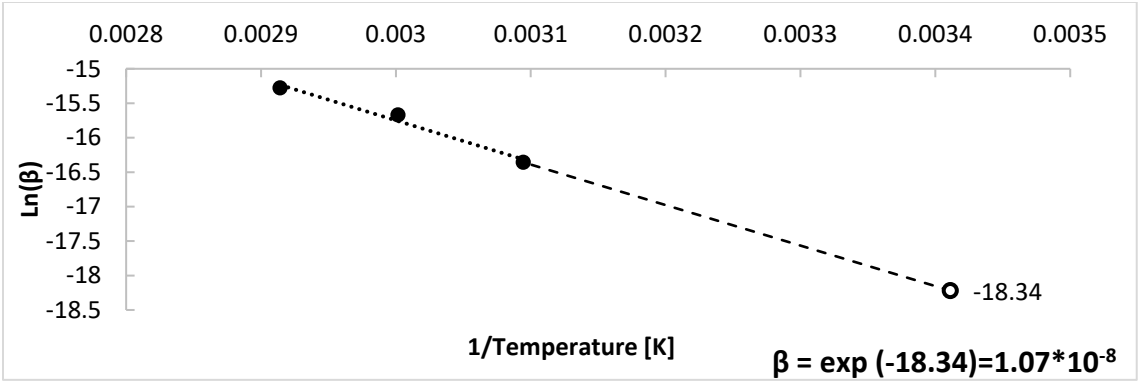

b)

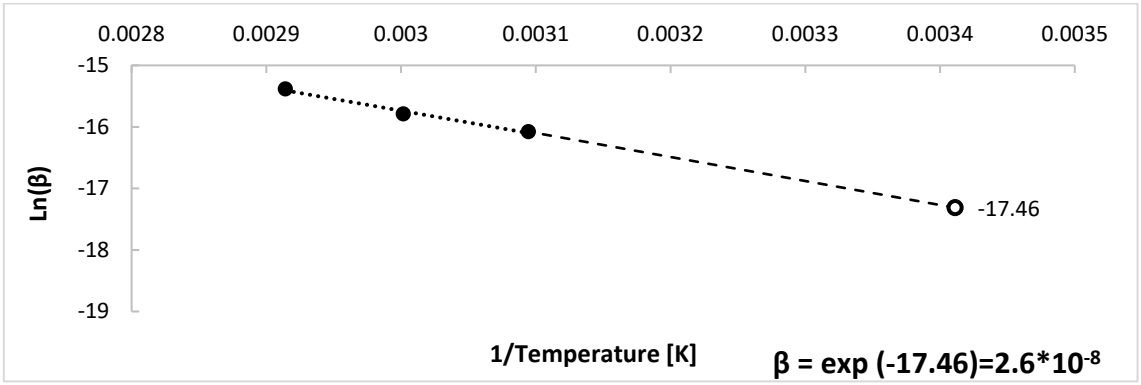

Fig. A9.27 – Arrhenius plot for rate parameter "β" including 20˚C for a) SB and b) BB bars

Table A9.42 – Rate constant "β" for SB and BB bars from Company II at 20˚C

Temperature	β[mm/s]	R^2 for M12	R^2 for M16
SB	1.07 * (10^{-8})	0.97	0.98
BB	2.6 * (10^{-8})	0.96	0.93

Table A9.43 – Long term flexure strength retention for SB bars

Flexure strength retention			
Time in Bath	Time in Construction	SB M12 [%]	SB M16 [%]
[days]	[years]	50˚C	
30	3.9	96.06	97.55
90	11.7	94.35	95.68
150	19.5	92.33	93.97
[days]	[years]	60˚C	
30	12.1	93.22	94.61
90	36.2	88.7	91.10
150	60.4	86.42	89.78
[days]	[years]	70˚C	
30	35	89.27	90.77
90	105.1	83.37	84.62
150	175.2	78.80	81.19

Table A9.44 – Long term flexure strength retention for BB bars

Flexure strength retention			
Time in Bath	Time in Construction	BB M12 [%]	BB M16 [%]
[days]	[years]	50˚C	
30	1.1	95.21	96.86
90	3.4	92.85	93.90
150	5.7	90.07	91.84
[days]	[years]	60˚C	
30	2.5	93.40	94.43
90	7.4	88.99	91.11
150	12.4	84.95	88.73
[days]	[years]	70˚C	
30	5.1	88.88	90.88
90	15.4	80.71	83.80
150	25.7	78.16	80.90

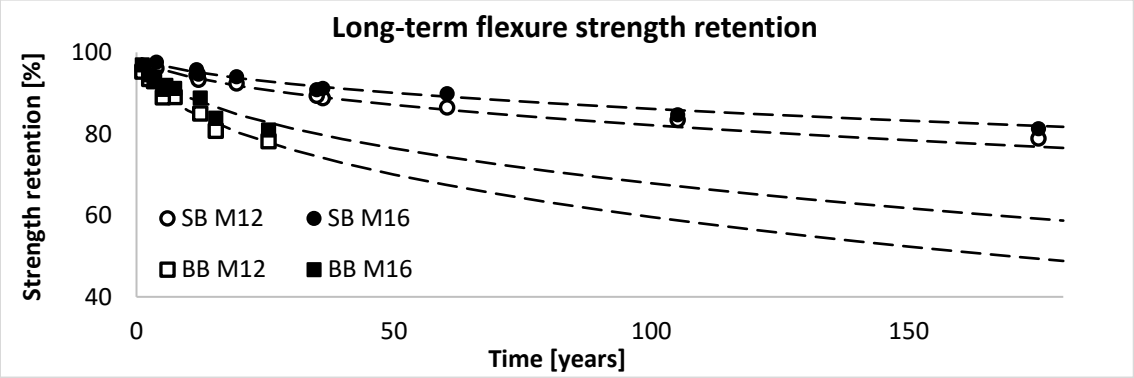

Fig. A9.28 – Long-term flexure strength retention at 20˚C for Model #4 – Company II

Appendix 10

FLEXURE STRENGTH DEGRADATION MODEL

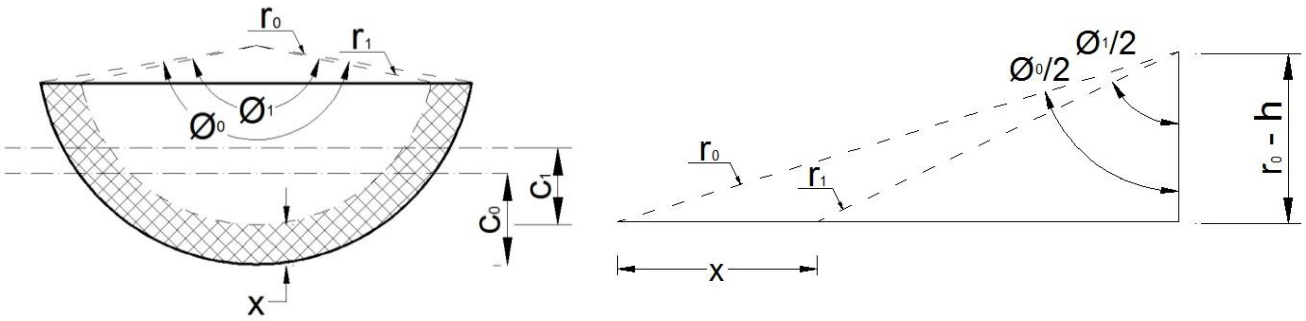

Fig. A10.1 – Graphical interpretation of degradation depth "x"

$$\sigma_0 = \frac{F_0 * L * c_0}{4I_0}$$

$$\sigma_1 = \frac{F_1 * L * c_1}{4I_1}$$

Where: F_0 and F_1 – force applied to sample; c_0 and c_1 – distance to the N.A.; I_0 and I_1 – moment of inertia; L – sample length, x – degradation depth

F_o, c_o, I_o – characteristics representing sample with diameter $\emptyset_0$

F_1, c_1, I_1– characteristics representing sample with diameter $\emptyset_0 - 2x$

$$\sigma_0 = \sigma_1 \rightarrow F_1 = \sigma_0 * \frac{4I_1}{L * c_1}$$

$$\sigma'_0 = \sigma_0 * \frac{I_1}{I_0} * \frac{c_0}{c_1}$$

Where: σ'_0 – strength of deteriorated sample.

Assuming that σ_0 is a 100% the strength retention can be written as:

$$Y = 100 * \frac{I_1}{I_0} * \frac{c_0}{c_1}$$

$$\cos\frac{\theta_0}{2}=\frac{r-h}{r}\rightarrow\theta_0=2\cos^{-1}\left(\frac{r-h}{r}\right)$$

$$\cos\frac{\theta_1}{2}=\frac{r-h}{r_1}\rightarrow\theta_1=2\cos^{-1}\left(\frac{r-h}{r_1}\right)=2\cos^{-1}\left(\frac{r-h}{r-x}\right)$$

$$\frac{I_1}{I_0}=\frac{\frac{{r_1}^4}{16}(2\theta_1-\sin\theta_1)-\frac{{r_1}^4}{9}\frac{(1-\cos\theta_1)^3}{\theta_1-\sin\theta_1}}{\frac{{r_0}^4}{16}(2\theta_0-\sin\theta_0)-\frac{{r_0}^4}{9}\frac{(1-\cos\theta_0)^3}{\theta_0-\sin\theta_0}}=\frac{{r_1}^4}{{r_0}^4}\left(\frac{\frac{1}{16}(2\theta_1-\sin\theta_1)-\frac{1}{9}\frac{(1-\cos\theta_1)^3}{\theta_1-\sin\theta_1}}{\frac{1}{16}(2\theta_0-\sin\theta_0)-\frac{1}{9}\frac{(1-\cos\theta_0)^3}{\theta_0-\sin\theta_0}}\right)$$

$$A=\left(\frac{\frac{1}{16}(2\theta_1-\sin\theta_1)-\frac{1}{9}\frac{(1-\cos\theta_1)^3}{\theta_1-\sin\theta_1}}{\frac{1}{16}(2\theta_0-\sin\theta_0)-\frac{1}{9}\frac{(1-\cos\theta_0)^3}{\theta_0-\sin\theta_0}}\right)$$

$$\frac{I_1}{I_0}=\frac{{r_1}^4}{{r_0}^4}*A=\left(\frac{r_0-x}{r_0}\right)^4*A=\left(1-\frac{x}{r_0}\right)^4*A$$

$$\frac{c_0}{c_1}=\frac{r_0-\left(\frac{4}{3}*r_0*\frac{\sin^3\frac{\theta_0}{2}}{\theta_0-\sin\theta_0}\right)}{r_1-\left(\frac{4}{3}*r_1*\frac{\sin^3\frac{\theta_1}{2}}{\theta_1-\sin\theta_1}\right)}=\frac{r_0}{r_1}*\left(\frac{1-\frac{4}{3}\frac{\sin^3\frac{\theta_0}{2}}{\theta_0-\sin\theta_0}}{1-\frac{4}{3}\frac{\sin^3\frac{\theta_1}{2}}{\theta_1-\sin\theta_1}}\right)$$

$$B=\left(\frac{1-\frac{4}{3}\frac{\sin^3\frac{\theta_0}{2}}{\theta_0-\sin\theta_0}}{1-\frac{4}{3}\frac{\sin^3\frac{\theta_1}{2}}{\theta_1-\sin\theta_1}}\right)$$

$$\frac{c_0}{c_1}=\frac{r_0}{r_1}*B=\left(\frac{r_0}{r_0-x}\right)*B=\left(\frac{1}{1-\frac{x}{r_0}}\right)*B$$

Flexure strength retention:

$$Y=100*\left(1-\frac{x}{r_0}\right)^4*A*\left(\frac{1}{1-\frac{x}{r_0}}\right)*B$$